Global Disruption Simulations and Lorentz Force Data for Passive Plates, PF support "Slings", Bellows, Heat Transfer Plates, TF and OH Coils.

Calculation No: NSTXU-CALC-10-07-0 # Revision No: #

Codes used:
ANSYS version 15.0 and 19.2
"hot plate disruption loads.xls" in my d:\divertor directory
DCPS Check True Basic program [5]

Purpose of Calculation:

The initial revision of this calculation is intended to support the Heat Transfer Plate (section 11.0) and Heat Transfer Tube (Section 17.0) FDR. Other components will be addressed in future revisions of the calculation

The purpose of this calculation is to provide loads and interface requirements on initial design and qualification of a variety of NSTXU components, including the passive plates, PF support "slings", bellows, heat transfer plates. Potential enhancements of NSTX are also included. Sections on the Non-Cylindrical Coils (NCC). And cryo-pump are included partly because similar modeling is used . ANSYS EMAG, version 15.0 and 19.2 are used for this series of analyses.

References

A full list of references may be found in Section 6.2 of the main body of the Calculation

Assumptions (Identify all assumptions made as part of this calculation.)

Disruption modeling is tailored to the component being addressed. For example, The passive plates loads are derived from an analysis that may not be ideal for quantifying the sling loads. It is assumed that the global disruption model can be optimized and simplified in this way

Calculation (Calculation is either documented here or attached)

Attached

Conclusion (Specify whether or not the purpose of the calculation was accomplished.)

Load files have been generated for the passive plates, inner pf support slings, centerstack casing. Heat transfer plate,

Eddy current loads have been assessed for the bellows, and found to be small . The bellows is more significantly stressed due to the halo current (see Calculation# NSTXU-CALC-10-8-0)

Cognizant Individual (or designee) printed name, signature, and date Dang Cai Digitally signed by Dang Cai DN: cn=Dang Cai, o=PPPL, ou=Engineering, email=dcai@pppl.gov, c=US Date: 2018.11.19 09:48:14 -05'00'

Preparer's printed name, signature and date Peter H. Titus Digitally signed by Peter H. Titus Date: 2018.11.12 11:46:54 -05'00'

I have reviewed this calculation and, to my professional satisfaction, it is properly performed and correct.

Checker's printed name, signature, and date Art Brooks Digitally signed by Art Brooks Date: 2018.11.13 16:18:57 -05'00'

Global Disruption Simulations and Lorentz Force Data for Passive Plates, PF support "Slings", Bellows, Heat Transfer Plates, TF and OH Coils.

Checks for Calculation No: __NSTXU-CALC-10-07- # #__ Revision No:

Component was checked against latest design

Yes. (This check is only for Section 11 to support the HTT/HTP FDR)

All required load cases are included and current

Yes

Discuss method used in the calculation

The analysis herein was done using an EM simulation in ANSYS based on the project requirements

Discuss how the calculation was checked

The results were compared to an independent analysis previously done for other purposes using the SPARK code and found to be in agreement.

List issue identified and how they were resolved

None

Checker: Art Brooks Digitally signed by Art Brooks Date: 2018.11.13 16:19:32 -05'00' ____________(sign and date)

Technical Authority: Andrei Khodak Digitally signed by Andrei Khodak Date: 2018.11.21 10:29:25 -05'00' ____________(sign and date)

NSTX Upgrade

Global Disruption Simulations and Lorentz Force Data for Passive Plates, PF support "Slings", Bellows, Heat Transfer Plates, TF and OH Coils.

NSTXU-CALC-10-07-0, October 2018

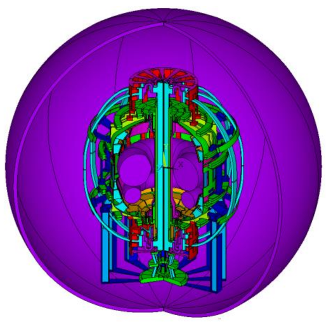

Prepared by P. Titus

Section 11.0 Reviewed by A. Brooks

2.0 Table of Contents

3.0 Revision Status Table

Rev 0	The initial revision of this calculation is intended to support the Heat Transfer Plate (section 11.0) and Heat Transfer Tube (Section 17.0) FDR. Other components will be addressed in future revisions of the calculation

4.0 Executive Summary

This calculation addresses a number of disruption simulations, all utilizing similar analysis approaches. The modeling uses the solid 97 element with AX,AY,and AZ degrees of freedom for the areas for which fields are to be calculated, and solid 97 with AX, AY, AZ, and volt degrees of freedom for areas where fields and eddy currents are to be calculated . Poloidal field coils are input with the element type that only solves AX, AU, and AZ - Not volt, so eddy currents are not calculated for the poloidal coils. One analysis allows currents to be driven in PF4 and 5 to answer a DVVR chit In all the models, the TF current is driven with currents entering and exiting the outer TF leg mid plane. This means that in the TF, eddy currents can be developed. Electromagnetic transient analyses other than disruptions analyses may be performed as well. Start up simulations are presented in [15] in which loads on various grounding straps may be calculated. In previous disruption simulations[1] the disruption simulation was performed in OPERA and maps of the axisymmetric vector potential solution were applied to 3D structural models . In this calculation the disruption simulation is done in ANSYS EMAG with enough detail that meaningful structural responses may be obtained from structural passes on the EMAG model.

Design requirements are outlined in the Systems Requirements Document SRD# NSTX-SRD-13-215 , Ref 1 The qualification needs to consider larger upgrade plasma currents, TF and PF fields, and Disruption specifications.

Passive Plate Loads and Cloud Data	Section 8
Helium Tubes in the Passive Plates	Section 9
Inner PF support "Slings",	Section 10
Divertor Heat transfer plates	Section 11
Bellows	Section 12
PF 4 and 5 Induced Currents	Section 13
Centerstack Casing VDE loads	Section 14
Casing Cooling Tubes	Section 17

4.8 Passive Plates

The passive plates were qualified back in 2012 for the upgrade loads. A few weaknesses were identified. Mounting hardware was poorly fit and produced sloppy mounts that could rattle during operation. A monitor and fix later approach was taken . For the recovery project, the as-build configuration was revisited. Weld deficiencies were identified. Repairs were recommended and planned. The loading on the plates needed to be re-evaluated and checked again and the possibilities of different loads addressed. The form of the loading also needed to be updated, because much more detailed structural models of the plates and their weld details have been used.

The passive plates are not conical sections, but instead are faceted. The CAD model that Andrei uses to build his model is faceted and to achieve a good transfer of loads the EMAG model must overlay his geometry precisely. The EMAG models used for most of the component qualifications in earlier analyses and in this calculation for other components are swept geometries. To build the faceted plates, the precise geometry of the plates in the detailed solid model was provided and a faceted model was created.

4.9 Helium Tubes in the Passive Plates

4.10 PF support "Slings",

The inside radius is 11.356", the outside radius is 14.330" is, the side thickness is .062", the top of the sides are 72.722" from the center plane, and the bottom of the sides is 53.698" from the center plane. The typical slide total included swept angle is 30 degrees.

The eight corners points of the cross section on plotted on the X-Y plane are:

11.356, 72.722
11.418, 72.722
14.268, 72.722
14.330, 72.722

11.356, 53.698
11.418, 53.698
14.268, 53.698
14.330, 53.698

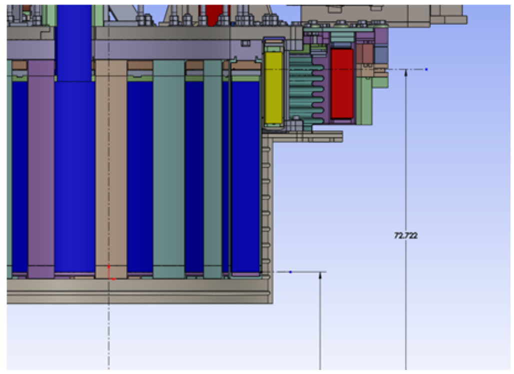

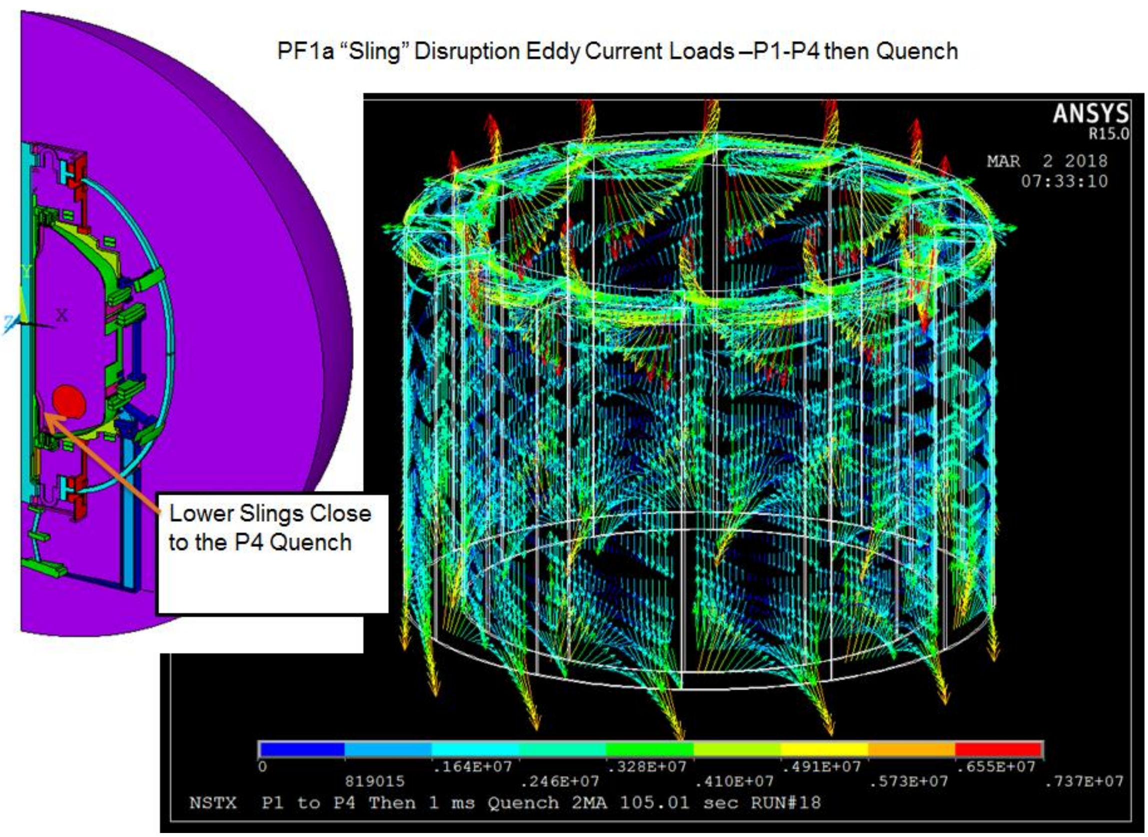

Figure 4.10-1 EMAG Model with the Flex or Sling Support Modeled Eddy Currents are Shown

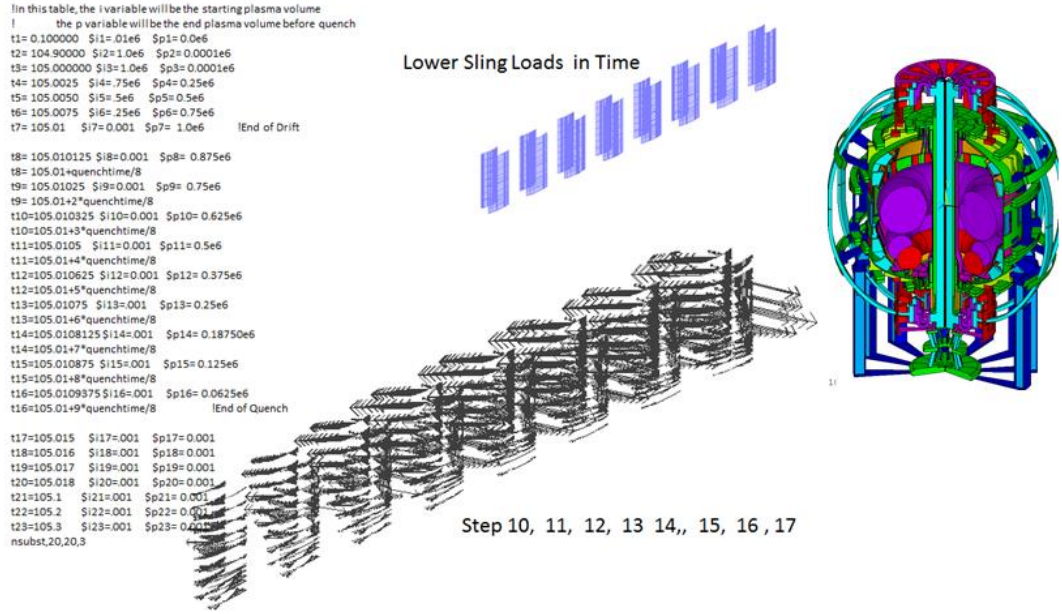

Figure 4.10-2 Plots of Sling Load Files

In figure 4.10-2, the plots of the load files are shown next to the time specifications for the transient analysis

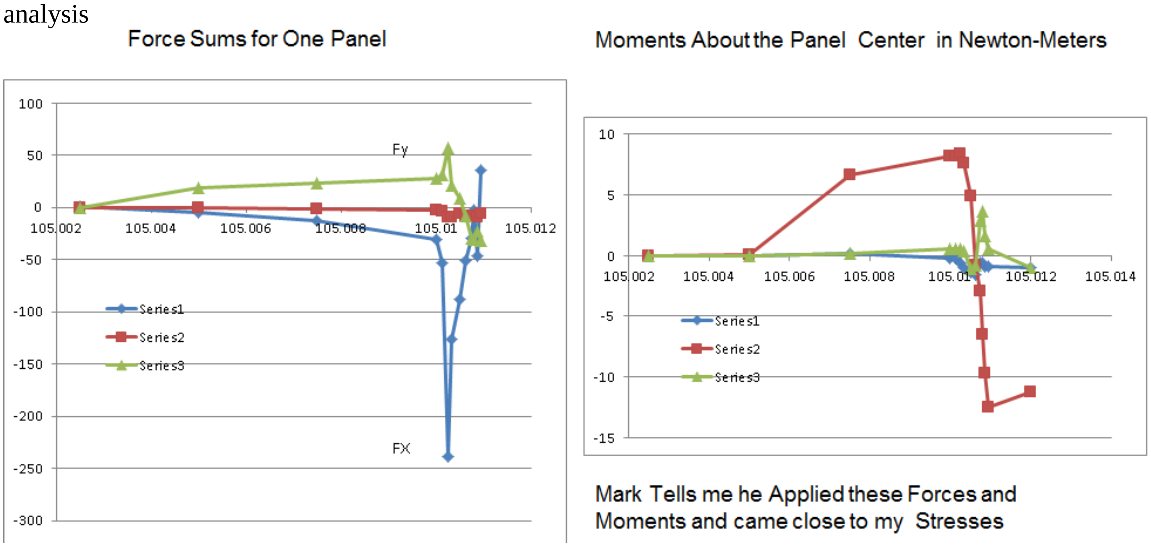

Figure 4.10-3 Force and Moment Sum for One Outer Panel

4.11 Heat Transfer Plate and Inner Divertical Vertical Section Cooling Tubes

The heat transfer plate is intended to provide local heating of the divertor tiles during bake-out to ensure achieving the required 350 C bake. The heat transfer plate is also used to remove heat during normal operation.

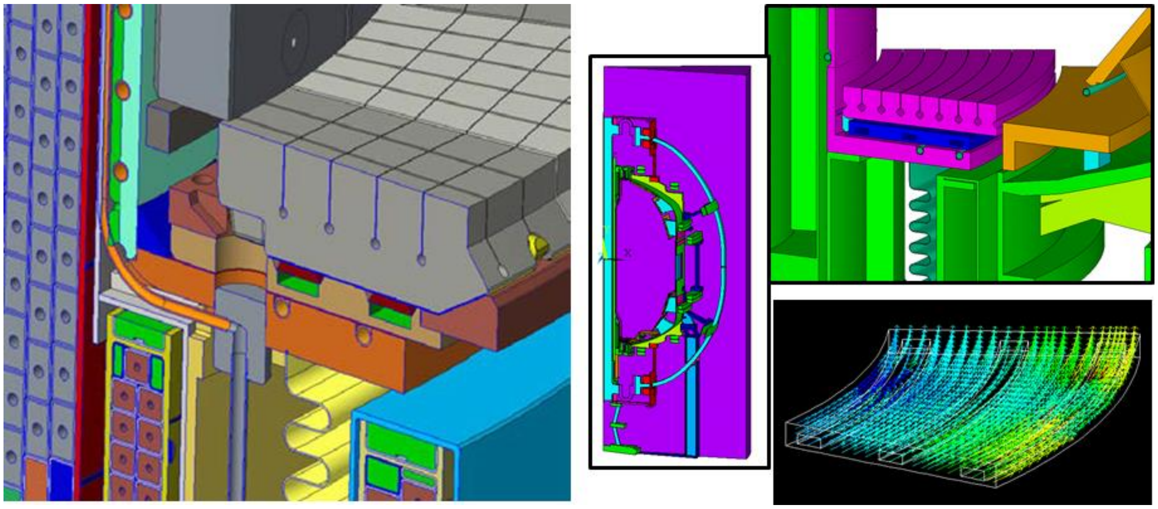

Figure 4.11-1 Hot Plate Disruption Currents (The HTP is Mat 32)

For the Halo currents, the poloidal fields are from a sweep of the 96 for a P1 to P4 plasma position. This is compared with Art's max tile B's and Bdots. The maximum magnitudes were used in a spreadsheet calculation and they were oriented to produce the largest tensile load on the studs. Art's calculation for the tile B's and Bdots is NSTXU-CALC-011-08-00 [17]. The loads on the heat transfer plate are included in section 11.

```
!mp,rsvx,22,2e-8  ! Ground Strap and cooling tubes   When they were copper
mp,rsvx,22,123e-8  ! Ground Strap and cooling tubes, Now Inconel 625
mp,rsvx,32,123e-8 ! Inconel 625      !     Divertor Hot plate
```

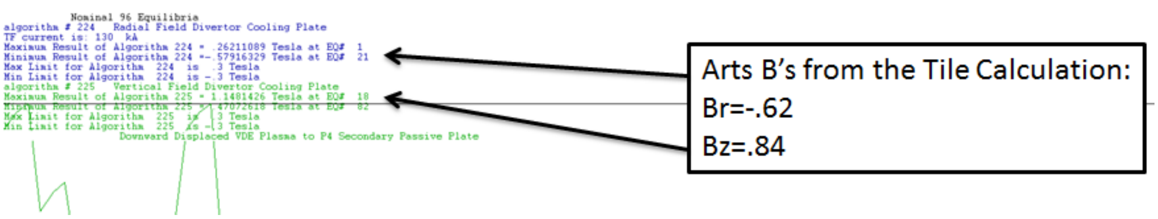

The plate is electrically, toroidally continuous – or made so by the connections to the casing divertor flange. Currents are primarily toroidal, although the interior cooling channels are more complex than the swept geometry shown in the model. . For both the eddy current and halo current loading, the poloidal fields were taken from a sweep of the 96 EQ and all disruption scenarios by Art Brooks, done for the high heat flux tiles on the divertor plate. I checked Art's calculation. Art used SPARK that included passive structure shielding, and I checked it with static field calculations with the plasma at P4. The halo loads were calculated by hand (spreadsheet) from the halo specs from Stefan. The eddy current EMAG analysis had a background field from EQ 79 but it basically wasn't used. Induced eddy currents based on P1 to P4 which was found to be the worst for the divertor area. I took the current densities - independent from the static background field and multiplied by the HTP cross sectional area - got a current, then crossed that with the max poloidal fields to get loads that were then applied to the HTP bolting. The spreadsheet calculations are in "hot plate disruption loads.xls" in my divertor directory, results from which are shown in figures 4.11-2 The loads are based on the worst poloidal fields of the 96 and all disruption specs. HTP eddy currents are worst in time for the P1 to P4 VDE disruption with 1 millisec quench, 10 millisec drift.

Halo loads are based on a halo fraction of .35 and a peaking factor of 2 from Stefans older halo spec, I think it might slightly lower now.

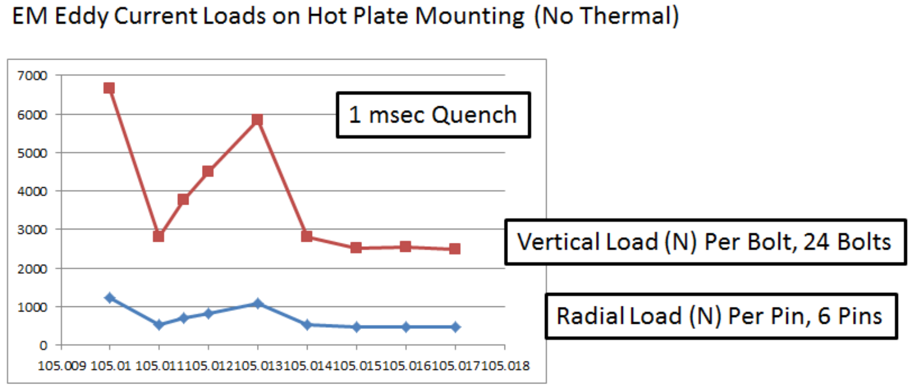

		Radius in	Ip	Hf	Peak Fact	Share Factor	Hot Plate width	Num Bolts	Btor				Halo Load per bolt N	Halo Load per bolt lbs
Halo Bolt Load:		19	2.00E+06	3.50E-01	2	0.384615	0.17780036	24	1.936175				7.72E+03	1.74E+03

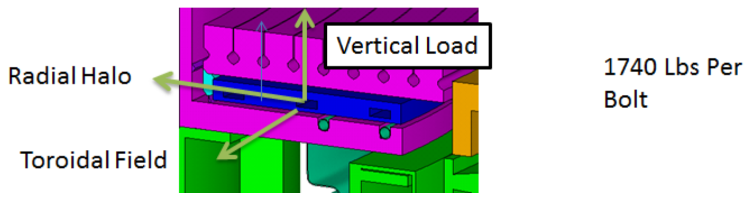

Figure 4.11-2 Hot Plate Loads

4.12 Bellows

Loading on the bellows due to eddy currents induced in the bellows is minimal. The Bdots below the . the toroidal field.

4.13 PF 4 and 5 Induced Currents

A DVVR CHIT (M5-6?) was entered that questioned the possibility of different and additional loads on PF4 and 5 due to a disruption. The intent of the question was to address the possibility of current changes incuced in the coils from the plasma motion and quench. Mid plane disruption effects have been extensively considered in the design point spreadsheet (DPSS) and more rigorously by Woolley, considering the effects of passive structures [18]. In Woolley's simulation, the current changes are minor and don't occur until after the vessel currents have decayed. Woolley did not consider a VDE. The coils are designed for post disruption currents and loads in the DCPS conservatively derived by ignoring passive structures. VDE's are not considered in the DCPS. VDE loads have been a part of qualification of vessel internal components (tiles, passive plates) during the Upgrade project and were only recently included in assessments of coil loads. In this assessment, the inner PF coils and OH coils were addressed (SEI-2018 03-18PHT/AB01) [20] which does not include passive structure shielding and also by A. Brooks including passive structures.

To address current changes in PF4 and 5, and EMAG run was performed in which the PF4 and 5 coils were converted to calculated conducting elements rather than prescribed current elements. This analysis produced opposing currents in the upper and lower pairs of PF4 and PF5. This is physically impossible because the upper and lower PF4 coils are connected in series and the upper and lower PF5 coils are connected in series and must have the same current in them. To simulate this accurately , the external series connection and circuit through the power supplies need to be modeled. As of this writing, this hasn't been done and it is less important than the loading imposed by unchanging currents reacting to the plasma shift from the equatorial plane. These net loads on PF4 and 5 due to the VDE can be bounded by the static field calculations based on the VDE coil positions. The method is the same as for the inner PF coils discussed in memo [21], included in the DCPS Check calculation [5] and results are discussed in section 13.0 and the main loading change is presented below.

Table 13.0-1 VDE Loads for (PF4U+PF5U)+(PF4L+PF5L) Compared with Design Point Spreadsheet (DPSS) with Plasma

	Max Vertical	Min Vertical
Upward VDE to P4 (All 96)	0 (DPSS 0.0)	-261,033 (DPSS -82,173)
Downward VDE to P4 (All 96)	220,756 (DPSS 0.0)	-106967 (DPSS -82,173)
Downward VDE to P5 (all 96)	1774	-81092
EMAG Downward VDE to P5 (EQ79)	50000	-20000

4.14 VDE Loading on the Centerstack

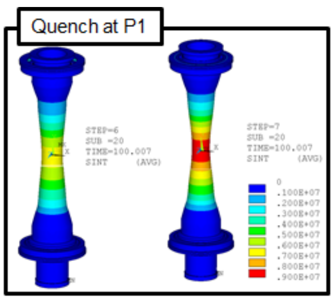

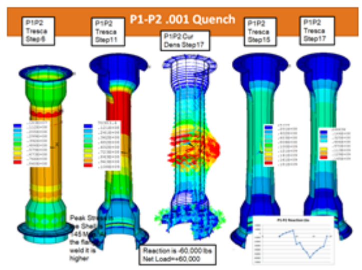

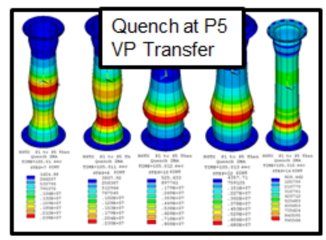

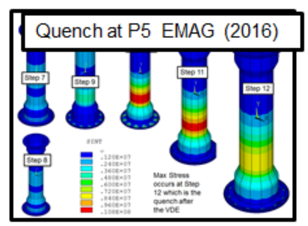

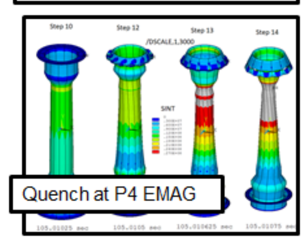

	Drift	Quench	Peak Stress	Peak Vertical Load	Ref
P1	0 sec	.002 sec	9 MPa		[1] (Vector Potential Transfer)
P1	0	.001	Not Run		
P1-P2	.01	.001	108	TBD	[2]
P1-P4	.01	.002	Not Run		
P1-P4	.01	.001	~50 MPa		[2]
P1-P5	.01	.002	8. MPa	8,000 lbs	[1] (Vector Potential Transfer)
P1-P5	.01	.001	10.8MPa		[1] (EMAG)
P1-P6	.01	.001	86	-50,000 Lbs	[2]

[1] NSTXU-CALC-133-03-01 Rev 0: Feb 10 2012 Rev 1, 2016
[2] NSTXU-CALC-10-07-0 Global Disruption Simulations and Lorentz Force Data for Passive Plates, PF support "Slings", Bellows, Heat Transfer Plates, TF and OH Coils.

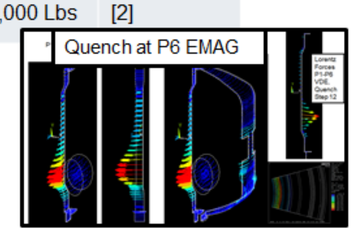

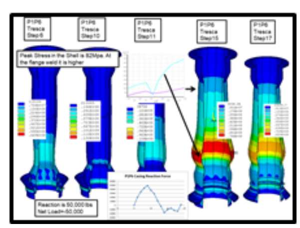

Dynamic load factors (DLF's) typically are around 1.0 – No amplification and no relief from static loads

4.15 TF Eddy Current VDE loading

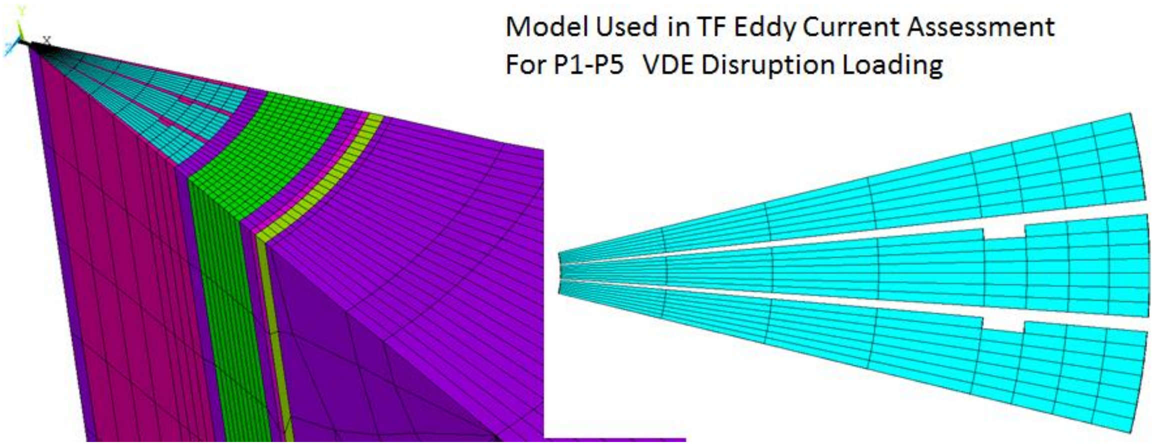

The TF developed eddy currents when the use of OH AC excitation was investigated for the bake out. The plasma current transients are further away than the OH transients. But still, the 36 eddys in the outer radius of TF conductors sum to a net toroidal current that crosses with the vertical field of the OH to produce hoop loads and the radial fields of the OH and plasma to produce vertical loads.

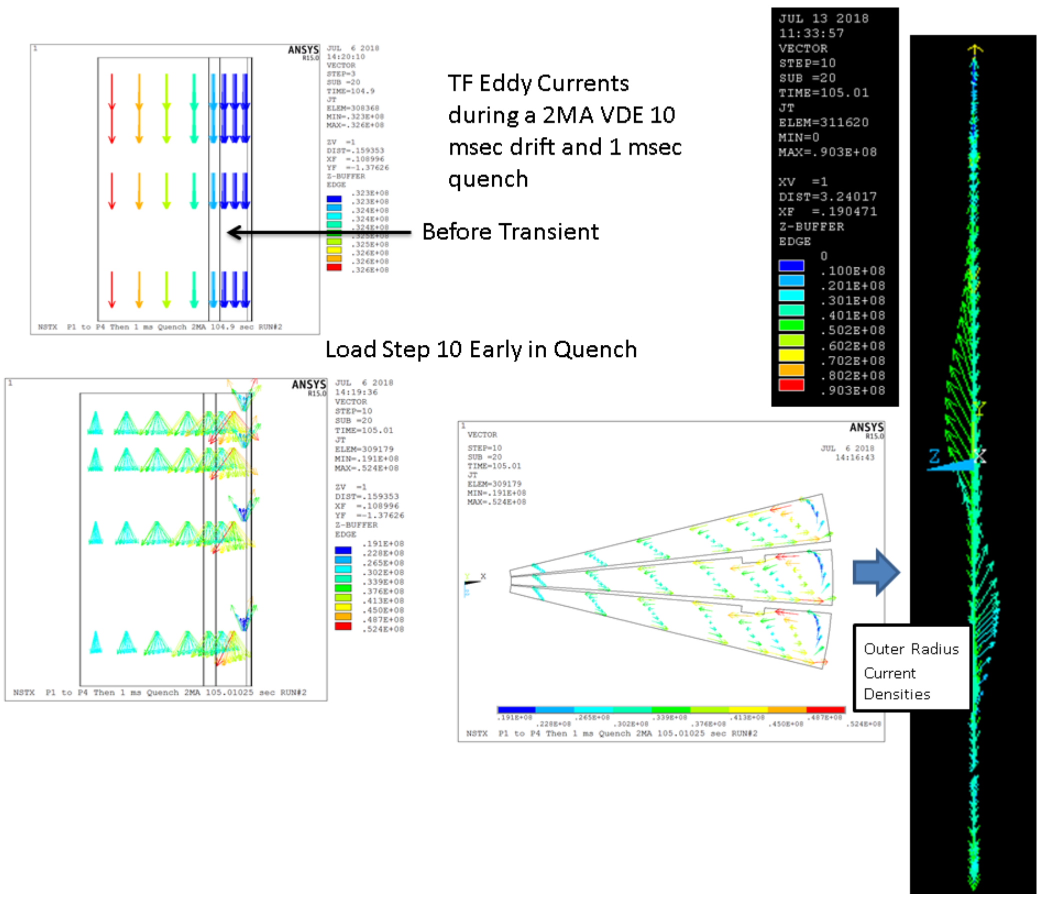

The net vertical load is 40,000 lbs on the TF inner leg. This load does not involve the casing and skirt, but does involve loads on the pedestal and the TF flag extension bolting to the pedestal. A dynamic simulation did not reduce this. The TF inner leg sees torsion and hoop tension and compressive loads resulting from the toroidal current. The net toroidal current is about 100kA at the outer radius of the TF or 5% of the Ip- Art estimated this from the areas.

Currents are higher locally. The tensile hoop stress may be a problem. I am still evaluating this. The problem is that the toroidal TF current crosses with the +/- 7 T field in the OH bore. It potentially can offset the compressive self wedge pressure in the TF. I started this work to investigate the net vertical load on the OH due to the VDE, but in this simulation I don't get much load - It may be a consequence of the reaction to the TF toroidal current. This is going to take more work. OH hoop stress can be effected too. There can be an effect on the start-up but I didn't see much in my startup simulation, Is the TF toroidal eddy current included in the start-up simulation?

4.16 VDE Loads on the OH and Inner PF Coils

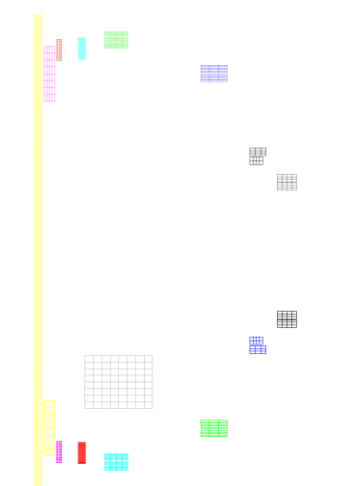
Influence Coefficient Model for VDE to P4 Down

Tile background fields and Bdots have been computed for the VDE cases. We are catching up with estimates of additional vertical loads on the inner PF coils with the plasma at the end of a VDE drift phase or P4 position for a downward drift and an equivalent negated position for an upward drift. So far we have only investigated the vertical loading. Max Loads on PF1aU, PF1bU&L,PF1cU&L are about 50% higher than nominal based on a static field calculation, mitigated by the vessel shielding . PF1aL remains about the same. This is a consequence of EQ 51 not being up-down symmetric with respect to PF1a currents. The increased loads will have an impact on the polar region design. Net loads on the OH and Centerstack components will change. Radial load effects also need to be included – especially if there is a hoop stress effect on the OH. The inner PFs have a large margin in hoop stress but the extra vertical loads will challenge the slings and polar region flanges and bolting. As the plasma approaches the divertor the inner PF coils that have currents in the same direction as the plasma are being attracted to the plasma, coils with reversed currents will be repulsed. The vessel shields the coils, but the slow drift and Inconel 625 structures reduce the shielding effect. Art ran a disruption simulation with EQ 16, and the 10ms drift adds 122 kN to the loads. Based on a static field analysis the difference for EQ16, is 61850N (VDE Down) – (-214999) N =276849N So for EQ 16 the static field prediction is about twice the prediction from an electromagnetic transient simulation. Only one transient simulation has been done but all the EQ's can be evaluated for static field effects with updates of the influence coefficients. The vertical load influence coefficient corrections for VDE Up and Down are included in the memo SEI-2018 03-18PHT/AB01

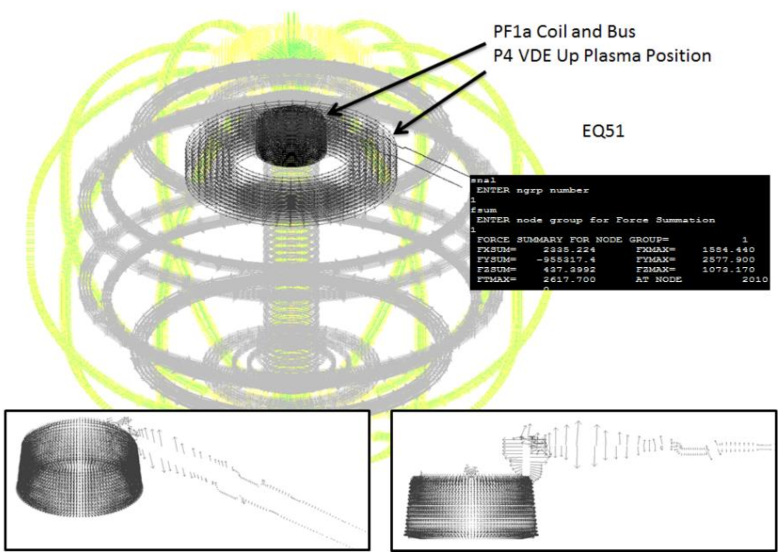

Figure 4.16-1 Loading of PF1aU leads due to and Upward VDE

4.17 Casing Cooling tubes

One of the major failures in the Upgrade project was the near failure of the copper cooling tubes on the inboard vertical divertor section of the centerstack casing. These picked up induced currents from start up and disruptions. This loaded the tubes significantly and the consequences of the loading on the copper tube was assessed in calculation ___ Ref ___. Section 17. Addresses the electromagnetic loads onreplacement Inconel cooling tubes which have much lower EM loads that the copper tubes they replace.

4.18 CDR Non Circular Coil Design

Figure 4.0-4 Model of the NCC Mounted on the Primary Passive Plate

The model shown in figure 4.0-4 is used in multiple analyses, including normal load stress analysis, modal analysis (below) disruption eddy current, thermal and normal operating Lorentz and thermal stresses.

5.0 Digital Coil Protection System, and Non DCPS Instrumentation

There is no input to the DCPS planned for disruption loading of components or for thermal response of components caused by plasma heat loads. Disruption loads on the passive plates with the added NCC coils will be monitored with the passive plate accelerometers. In order to keep the passive plate loads within the originally qualified attachment bolt capacity, accelerations should be maintained below those qualified for the Upgrade passive plate loads, corrected for the added mass of the NCC and new tiles.

6.0 Design Input

6.1 Requirements and Acceptance Criteria

6.1.1 Requirements

Requirements for the NCC coils and related alterations of the passive plates are found in the Systems Requirement Document [1]. Some of the contents of the requirements document are repeated here.

Table 5.2.3-1 from ref [1] NCC Coil Operational Modes

The number of full thermal ratcheted thermal cycles will be based on an estimated 20 full power pulses per day. Or 20,000/20 =1000 cycles.

6.1.2 Criteria

Stress Criteria are found in the NSTX Structural Criteria Document. Disruption and thermal specifications are outlined in the GRD -Ref [7] and are discussed in more detail in section 6.5. Cyclic requirements for the NCC Coils shall be 20,000 full power operating pulses.

The NSTX CSU is design to meet the NSTX Structural Design Criteria. However the existing criteria is silent on brittle materials. A revision to the criteria has been proposed specifically to address graphite tiles:

“This section describes the design criteria for carbon and carbon fiber composite (CFC) tiles. For static stresses, the design allowable stress of critical components (as defined by the GRD) shall be limited to 1/2 of the ultimate tensile and compressive stresses at temperature. Note that these materials generally have much lower tensile limits than compressive limits. This must be taken into consideration when defining allowable stresses. Non-critical components (as defined by the GRD) shall be limited to 3/4 of the ultimate tensile and compressive stresses at temperature. There shall be no relief for secondary stresses.

For other potentially brittle materials (e.g., ceramics), with an established lack of ductility, for static stresses, the design allowable stress shall be limited to 1/3 of the ultimate tensile and compressive stresses at temperature. These materials also generally have much lower tensile limits than compressive limits which must be taken into consideration when defining allowable stresses. There shall be no relief for secondary stresses.”

6.2 References

[1] NSTX Upgrade DISRUPTION ANALYSIS OF PASSIVE PLATES, VACUUM VESSEL AND COMPONENTS NSTXU-CALC-12-01-01 Rev 2 February , 2012 , P. Titus, and Yuhu Zhai

[2] NSTX-U Design Point Spreadsheet, **NSTXU-CALC-10-03-00** C. Neumeyer, http://w3.pppl.gov/~neumeyer/NSTX_CSU/Design_Point.html Recovery DPSS: https://sites.google.com/pppl.gov/systemengineering/design-point-spreadsheet?authuser=0

[3] Disruption specification J. Menard spreadsheet: disruption_scenario_currents_v2.xls, July 2010. NSTX Project correspondence, input to Reference [1]

[4] "Characterization of the Plasma Current quench during Disruptions in the National Spherical Torus Experiment" S.P. Gerhardt, J.E. Menard and the NSTX Team Princeton Plasma Physics Laboratory, Plainsboro, NJ, USA Nucl. Fusion 49 (2009) 025005 (12pp) doi:10.1088/0029-5515/49/2/025005

[5] “DCPS Check Calculations” NSTXU-CALC-13-07-00 P. Titus

[6] NSTX Structural Design Criteria Document, NSTX_DesCrit_IZ_080103.doc I. Zatz

[7] Recovery Project Update of the GRD, NSTX-U-RQMT-GRD-001-00, Dec 1 2017, Stefan Gerhardt, Superseding NSTX Upgrade General Requirements Document, NSTX_CSU-RQMTS-GRD Revision 0, C. Neumeyer, March 30, 2009,

[8] Inductive and Resistive Halo Current s in the NSTX Centerstack, A.Brooks, Calc # NSTX-103-05-00

[9] OPERA 2D Disruption Analyses, R. Hatcher, NSTX upgrade calculation #NSTXU-CALC- NSTXU-CALC-12-03-00

[10] Inner PF Coils (1a, 1b & 1c), Center Stack Upgrade NSTXU-CALC-133-01-02 May, 2014 Rev 2 by Len Myatt. Rev 2 by A Zolfaghari and A Brooks

[11] NSTXU Disruption Analysis Requirements NSTXU RQMT RD-003-00

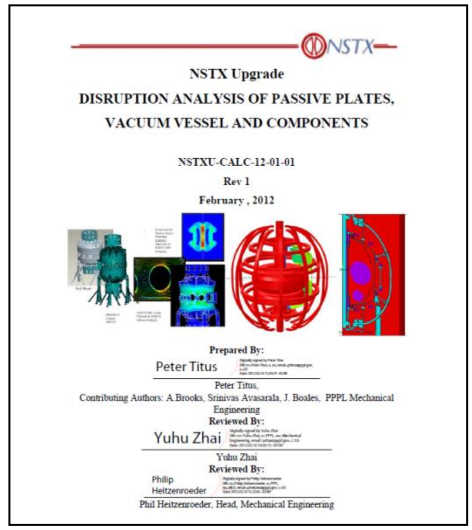
NSTX Upgrade

DISRUPTION ANALYSIS OF PASSIVE PLATES, VACUUM VESSEL AND COMPONENTS

NSTXU-CALC-12-01-01

Rev 1

February , 2012

Prepared By:

Peter Titus

Peter Titus,

Contributing Authors: A.Brooks, Srinivas Avasarala, J. Boales, PPPL Mechanical Engineering

Reviewed By:

Yuhu Zhai

Yuhu Zhai

Reviewed By:

Philip Heitzenroeder

Phil Heitzenroeder, Head, Mechanical Engineering

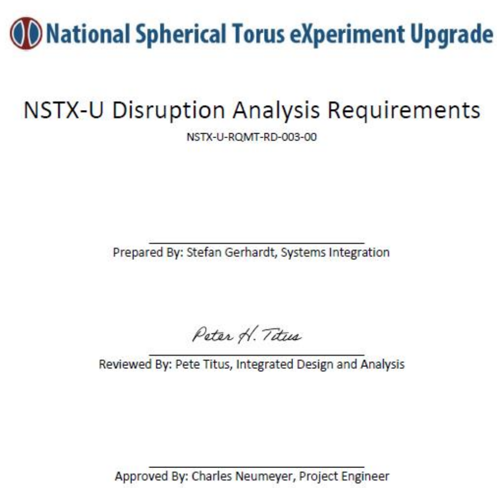
National Spherical Torus eXperiment Upgrade

NSTX-U Disruption Analysis Requirements

NSTX-U-RQMT-RD-003-00

Prepared By: Stefan Gerhardt, Systems Integration

Peter H. Titus

Reviewed By: Pete Titus, Integrated Design and Analysis

Approved By: Charles Neumeyer, Project Engineer

[12] Modeling of the Toroidal Asymmetry of Poloidal Halo Currents in Conducting Structures
N. Pomphrey, J.M. Bialek_, W. Park Princeton Plasma Physics Laboratory,
[13] "OH Stress and Segmented OH Influence Coefficients for the DCPS" P. Titus NSTXU-CALC-133-14-00
[14] ITER material properties handbook, ITER document No. G 74 MA 15, file code: ITER-AK02-22401.
[15] OH Grounding Strap and Centerstack Casing Copper Cooling Tube Evaluations NSTXU-CALC-133-20-0 Date October 28 2016
NSTX Upgrade
[16] Centerstack Casing and Lower Skirt Stress Summary, Rev1 NSTXU-CALC-133-03-01, Rev 0: Feb 10 2012 P. Titus Rev 1, 2016
[17] Tile B's and Bdots , NSTXU-CALC-011-08-00. A. Brooks September 2018
[18] DIGITAL COIL PROTECTION SYSTEM (DCPS) ALGORITHMS FOR THE NSTX ENTERSTACK UPGRADE R. D. Woolley, P. H. Titus, c.L. Neumeyer, R. E. Hatcher, 2011 IEEE/NPSS 24th Symposium on Fusion Engineering, Chicago Illinois
[19] VDE PLASMA POSITION ADDITIONAL LOADS ON OH AND INNER PF COILS SEI-2018 03-18PHT/AB01 Memo from P. Titus
[20] Email from Stefan Gerhart
>> > 2) I suspect that the toroidal symmetry should be fairly good...better
>> > than
>> > the symmetry (or lack thereof) for the halo current entrance points. I
>> > think
>> > that a peaking factor of 1.5 could be assumed for a first analysis
>> > (max/average = 1.5). If this poses a problem, please let me know and we
can revisit. Note that there are no measurements of this peaking, so it will
be a guess no matter what.
>> >
[21] MEMO TO: STEFAN GERHARDT JON MENARD,CHARLES NEUMEYER, FROM: PETER TITUS, ART BROOKS SUBJECT: VDE PLASMA POSITION ADDITIONAL LOADS ON OH AND INNER PF COILS SEI-2018 03-18PHT/AB01
[22] OH-PF1a/b Magnetic Stability NSTXU-CALC-133-11-00 Rev 0 P. Titus, Checked by A. Zolfaghari, March 2 2010
[23] "Molybdenum" Metallwerk Plansee GhmbH A-6600 Reuttee, http://www.plansee.com/english/
[26] Non-Axisymmetric Control Coils (NCC) Systems Design Requirements, NSTX-SRD-13-215 P. Titus et.al, Project Engineer N. Atnafu
[27] Systems Requirements Document for the Non-Axisymmetric Control Coils Design Analysis and Construction Including Switching Junction Box, WP #2027
[29] NSTX Disruption Simulations of Detailed Divertor and Passive Plate Models by Vector Potential Transfer from OPERA Global Analysis Results P. H. Titus, S. Avasaralla, A.Brooks, R. Hatcher 2010 SOFT Conference, Porto Portugal October 2010

6.4 Drawing Excerpts and Photos

6.4 Materials Properties

```
!Default Settings for Stainless Steel Components
*do,imat,1,100
mp,dens,imat,8950
mp,murx,imat,1.0
mp,rsvx,imat,74e-8      !Generic Stainless Steel
mp,c,imat,100
*enddo
```

6.4.1 Copper Allowable

```
!        CuCrZr Passive Plates
mp,rsvx,7,.85*2.443e-8 ! @400K
!   TF Joint Strap
mp,rsvx,2,2e-8
```

6.4.1.2 Copper Fatigue Allowable

```
!    Cryo Pump
mp,rsvx,55,60e-8 !Cryo Pump   !SST at 80K
mp,rsvx,57,123e-8 !Cryo Pump Helium Tube Inconel 625 at 4K
!    BES Aluminum Cylinder
mp,rsvx,21,2.65e-8     ! Aluminum
!    Graphite Tiles
mp,rsvx,30,117e-7 ! ATJ at  300C Set the same as graphite
mp,dens,30,1760
mp,rsvx,8,123e-8 ! Inconel 625    !      Centerstack Casing
!mp,rsvx,22,2e-8  ! Ground Strap and cooling tubes   When they were copper
mp,rsvx,22,123e-8  ! Ground Strap and cooling tubes
mp,rsvx,32,123e-8 ! Inconel 625      !     Divertor Hot plate
```

6.4.2 Magnesium Oxide Insulation Properties

At this generation of the design (June 2014). Molybdenum is not being used, but in anticipation of the possibility of the stainless steel shield being switched out for molybdenum, the Molybdenum properties are retained here.

Molybdenum Properties

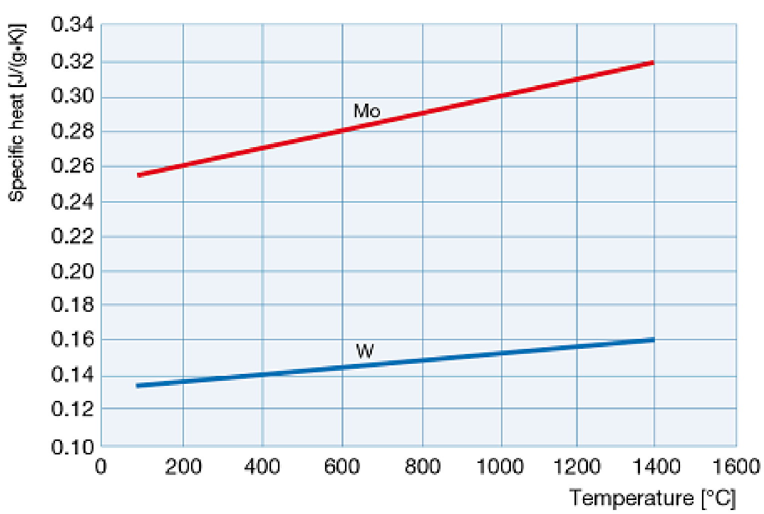

138 W/(m K) at room temp, about 100 at 1000C
Properties of TZM

Elongation : < 20 %
Modulus of Elasticity : 320 GPa
Tensile Strength : 560 - 1150 MPa (81 ksi to 167 ksi)

6.6 Design Currents and Max Fields

6.6.1 Normal Operating Fields at the Passive Plates

	1	2	3	4	5	6	7	8
	OH	PF1AU	PF1bU	PF1cU	PF2U	PF3U	PF4U	PF5U
79	-24.0000	6.8200	.0000	.0000	-6.1100	.6084	.0000	-33.1948
80	.0000	8.4313	.0000	.0000	1.8735	2.5310	.0000	-32.7086
81	13.0237	9.2903	.0000	.0000	6.1842	3.5571	.0000	-32.4390

9	10	11	12	13	14			
PF1AL	PF1bL	PF1cL	PF2L	PF3L	PF4L	PF5L	ip	
6.8199	.0000	.0000	-6.1100	.6084	.0000	-33.1948	2000.0000	130.0000
8.4313	.0000	.0000	1.8735	2.5310	.0000	-32.7086	2000.0000	130.0000
9.2895	.0000	.0000	6.1846	3.5571	.0000	-32.4379	2000.0000	130.0000

Input of EQ 79 in the EMAG Model

```
!Terminal Current   Number of turns      Area m^2     Coil   Real Constant
TerCur2=  -24   $numturns2=  884  $Area2=  .2778247       !OH     ,    2
TerCur3=   6.2  $numturns3=    64 $Area3=  .0333619      !PF1aU  ,    3
TerCur4=  0.0   $numturns4=    32 $Area4=  .00608698      !PF1bU  ,    4
TerCur5=  0.0   $numturns5=    20 $Area5=  .00818269      !Pf1cU  ,    5
TerCur6=-5.555  $numturns6=    28 $Area6=  .022127185     !PF2U   ,    6
TerCur7=  .553  $numturns7=    30 $Area7=  .02535049      !PF3U   ,    7
TerCur8=  0.0   $numturns8=    17 $Area8=  .014062411     !PF4    '    8
TerCur9=-30.177 $numturns9=    24 $Area9=  .01861829      !PF5    ,    9
TerCur10=  .553 $numturns10=   30 $Area10=  .02535049     !PF3L   ,   10
TerCur11=-5.555 $numturns11=   28 $Area11=  .022127185    !PF2L   ,   11
TerCur12= 0   $numturns12=   20 $Area12=  .00818269     !PF1cL  ,   12    Nominal EQ 79 PF1cL
!TerCur12= -16.0 $numturns12=   20 $Area12=  .00818269     !PF1cL  ,   12    Max Current in PF1cL
TerCur13=  0.0  $numturns13=   32 $Area13=  .00608698     !PF1bL  ,   13
TerCur14=  6.2  $numturns14=   64 $Area14=  .0333619      !PF1aL  ,   14
```

The background fields at the primary passive plate for normal – non-disrupted operation are shown in figures 6.6.1-1, and 6.6-2. These results come from the DCPS “Simulator” used to check the DCPS algorithms. Disruption values are also shown in the figures for comparison. The radial field maximum is

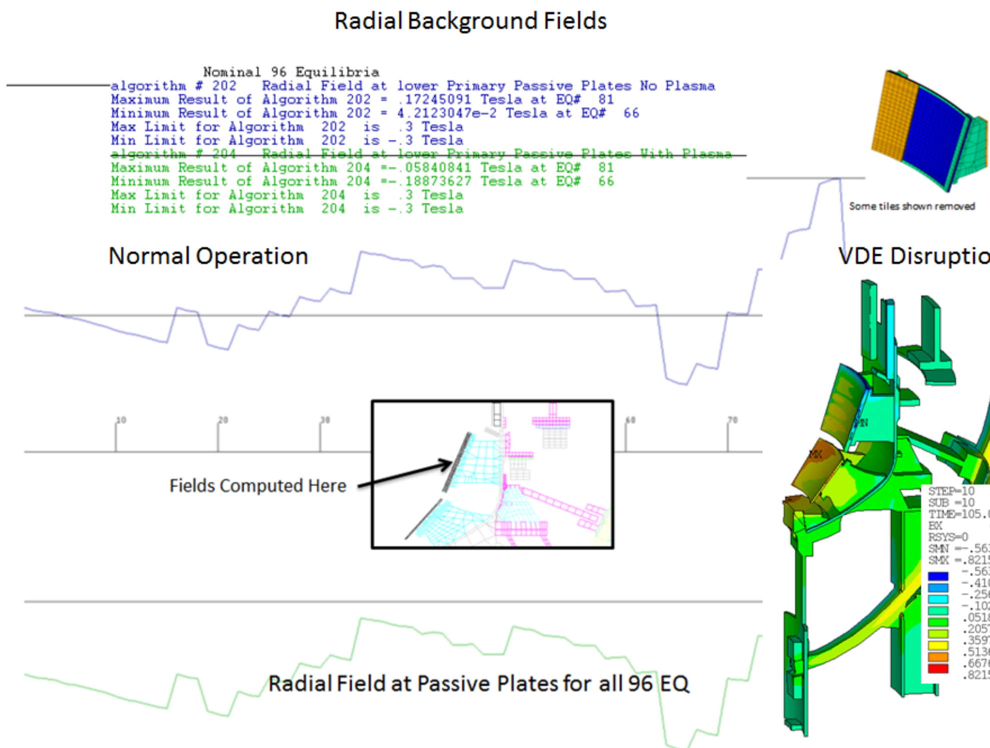

Figure 6.6.1-1 Radial Fields at the Primary Passive Plates, All 96 Equlibria

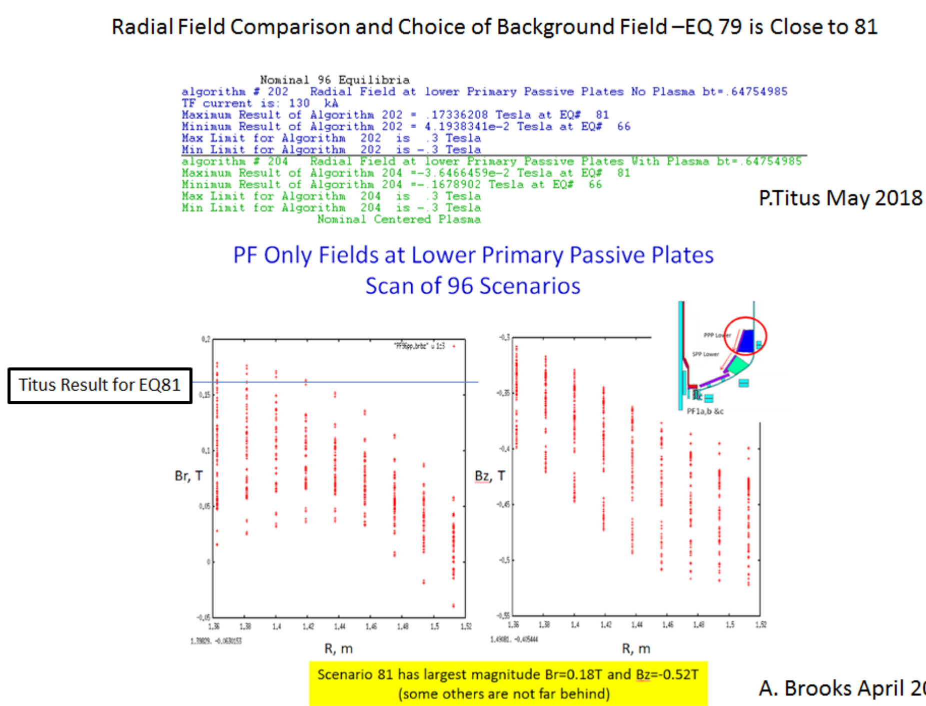

Figure 6.6.1-2 Radial Fields at the Primary Passive Plates, All 96 Equlibria VDE P5 Plasma Position

Vertical Field at Passive Plates for all 96 EQ

```
           Nominal 96 Equilibria
algorithm # 201   Vertical Field at lower Primary Passive Plates No Plasma
Maximum Result of Algorithm 201 =-.42599493 Tesla at EQ#  66
Minimum Result of Algorithm 201 =-.57741115 Tesla at EQ#  49
Max Limit for Algorithm  201  is  .3 Tesla
Min Limit for Algorithm  201  is  0 Tesla
algorithm # 203   Vertical Field at lower Primary Passive Plates With Plasma
Maximum Result of Algorithm 203 =-.43341506 Tesla at EQ#  66
Minimum Result of Algorithm 203 =-.58483128 Tesla at EQ#  49
Max Limit for Algorithm  203  is  .3 Tesla
Min Limit for Algorithm  203  is -.3 Tesla
```

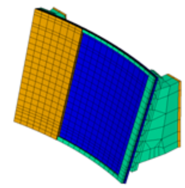

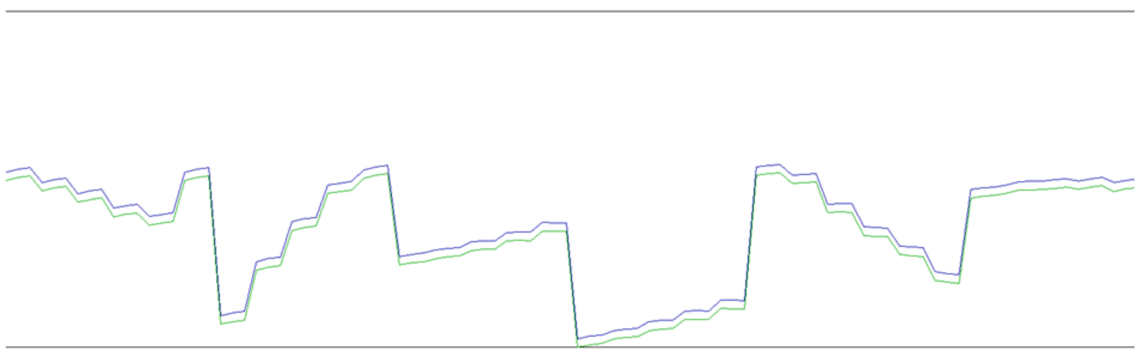

Vertical Field Comparison

```
           Nominal 96 Equilibria
algorithm # 201   Vertical Field at lower Primary Passive Plates No Plasma bt=.64754985
TF current is: 130  kA
Maximum Result of Algorithm 201 =-.4235894 Tesla at EQ#  66
Minimum Result of Algorithm 201 =-.57917479 Tesla at EQ#  49
Max Limit for Algorithm  201  is  .3 Tesla
Min Limit for Algorithm  201  is  0 Tesla
algorithm # 203   Vertical Field at lower Primary Passive Plates With Plasma bt=.64754985
Maximum Result of Algorithm 203 =-.43148201 Tesla at EQ#  66
Minimum Result of Algorithm 203 =-.58706741 Tesla at EQ#  49
Max Limit for Algorithm  203  is  .3 Tesla
Min Limit for Algorithm  203  is -.3 Tesla
                    Nominal Centered Plasma
```

P.Titus May 2018

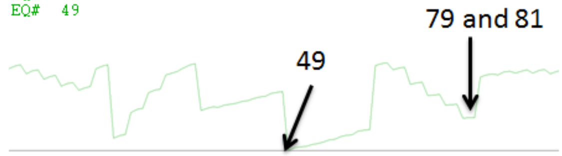

PF Only Fields at Lower Primary Passive Plates
Scan of 96 Scenarios

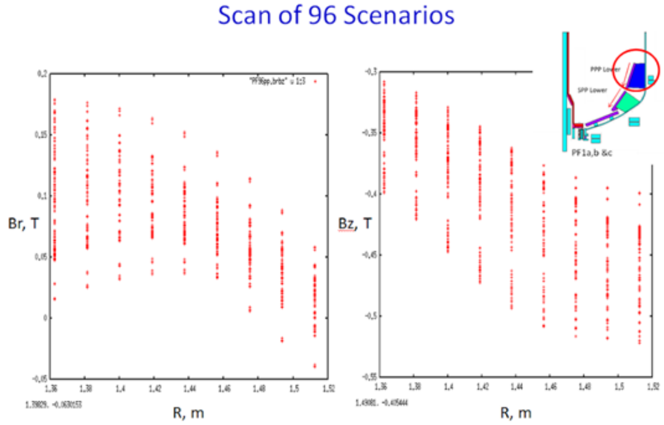

Scenario 81 has largest magnitude Br=0.18T and Bz=-0.52T
(some others are not far behind)

A. Brooks April 2018

EQ 49 might be a better choice but there only a small difference, and Art found 81 limiting – I stayed with 79

Figure 6.6.1-2 Vertical Fields at the Primary Passive Plate for All 96 Equilibria]

6.6.2 Normal Operating Fields at the NCC Terminals

6.6.2 Fields at the Passive Plates/ NCC During a Disruptions

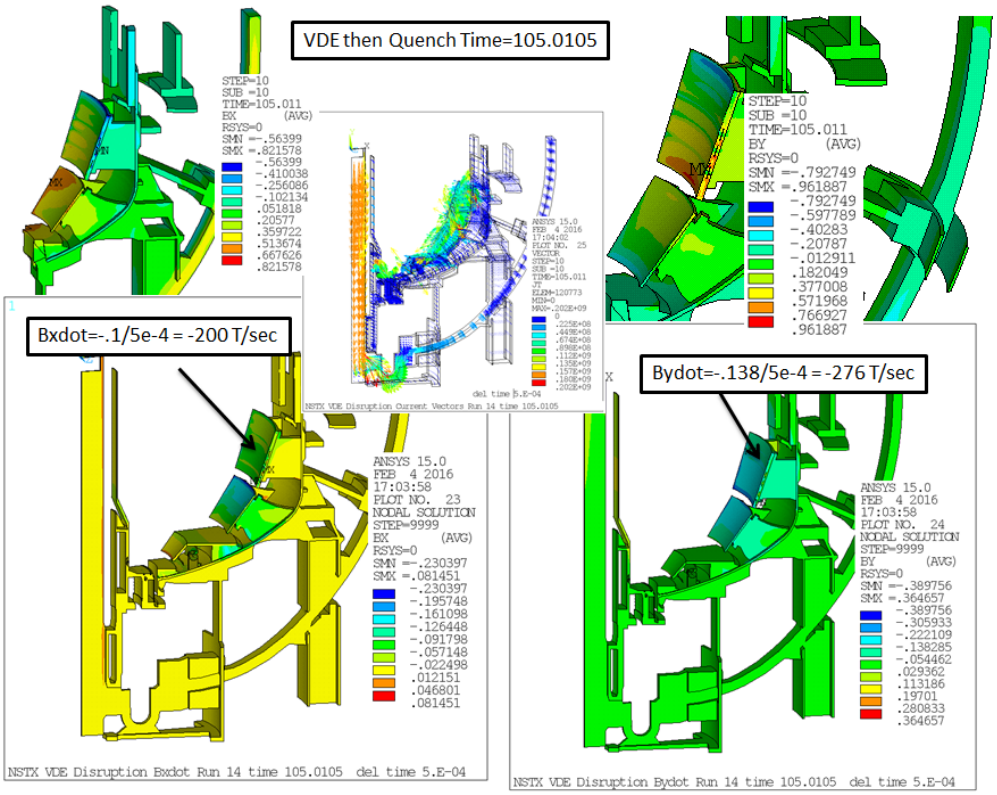

Figure 6.6-3 Background fields and Bdots

Note that the background fields at the passive plates in the disruption simulation are higher than the normal operating 96 EQ fields in figures 6.6.1-1, and 2

6.7 Self Fields and Forces

Figure 6.7-2 Self Field Loads Coherent Current (Above) and Reversed Current (Below

Self loads are plotted in figure 6.6-2. Effects of background fields has been removed. The effects of coherent and reversed coil currents are compared The peak field is .115T in both cases. Only three coils are modeled. The coil in the center is loaded in a representative manner to the full array of 24 coils arrayed above and below the equatorial plane around the machine. The immediate neighboring coils will have the most effect on the coil loads. In the figure, the left-right asymmetry in loads in the lower plot shows the effects of reversing currents in the neighboring coils. The asymmetry produces a net lateral load on the center coil of 12 Newtons or 2.7 lbs. This can be neglected in subsequent calculations. Interactions with the background field are by far more significant.

6.7 Disruption Loads, Field Transients (Bdot's) and Halo Currents

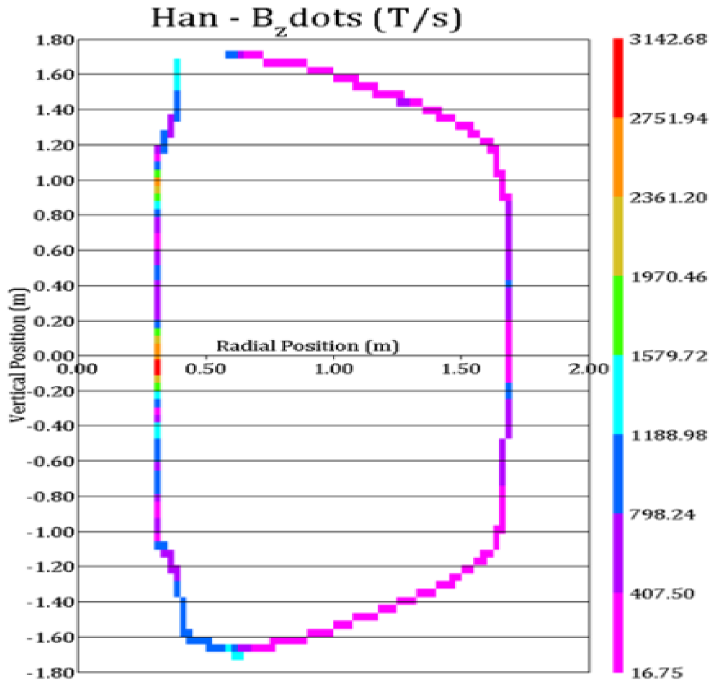

Figure 6.7-1 Bdots plotted around the vessel

Halo currents have not been postulated for the Primary Passive Plate. The behavior of the Upgrade configuration may behave differently and future operations might experience halo currents in the case. NSTX operation did experience halo currents crossing the CHI gap, so it is conceivable that halo loading might be a concern for the PF1c case, in the future. The requirements for disruption analysis are outlined in the NSTX Upgrade General Requirements Document [7]. The latest (August 2010) disruption specification were provided by Jon Menard as a spreadsheet: disruption_scenario_currents_v2.xls.[3] This reference includes a suggested time phasing of the inductively driven currents and the halo currents. A disruption analysis of the pro

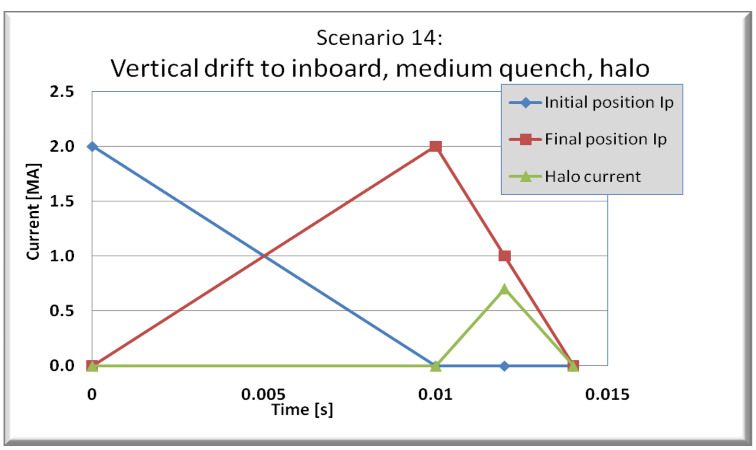

Figure 6.7-1Time phasing of the plasma current changes that induce currents in the vessel and vessel components, and the halo currents. From J. Menard

Criteria from the GRD[7]:

Current and field directions (referring to Figure 2.2-2) shall be as follows: Plasma current Ip into the page (counter-clockwise in the toroidal direction, viewed from above) Halo current exits plasma and enters the structure at the entry point, exits the structure and re-enters the plasma at the exit point (counter-clockwise poloidal current, in the view of the figure) Toroidal field into the page (clockwise in the toroidal direction, viewed from above)

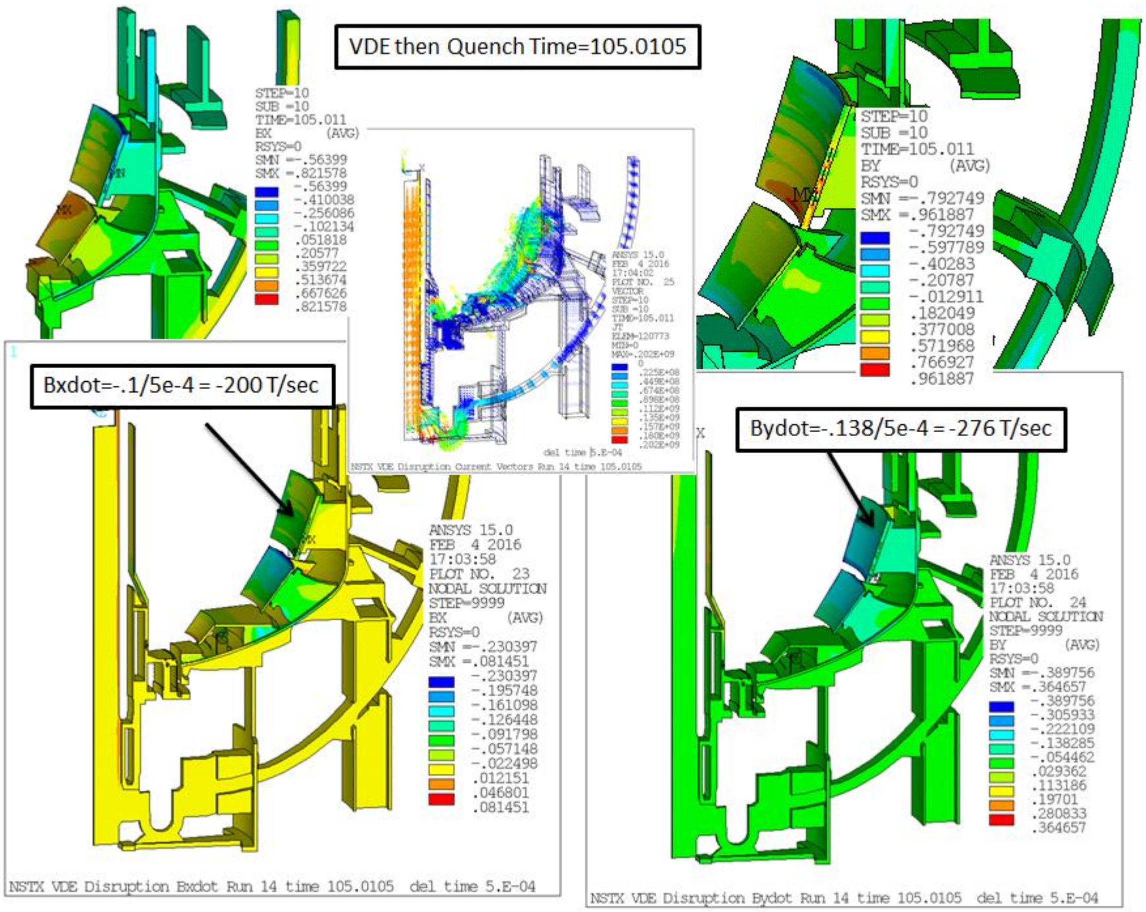

7.0 Models

The primary model used in this calculation is a 3D, 30 degree cyclic symmetry series of models , One of which is shown in figure 7.0-1. These are swept from 2D meshes, one of which is shown in Figures 7.0-2. Modifications are made to the 2D mesh to tailor the analysis to a specific component. Figure 7.0-1 is the model used to evaluate the Non-Circular Coils (NCC) that were to be mounted on the passive plates. The NCC enhancement to NSTXU been put off indefinitely.

Structural evaluations, both static and transient, are performed on subsets of the EMAG analysis. Loads are transferred to the structural models via LDREAD commands. Node numbering and element definitions are identical in the EMAG model and the selected elements in the structural models. When "Cloud" force density data is required for more detailed structural models using WORKBENCH, the FLIST command is used in the EMAG postprocessor to save load files in nodal forces. The ELIST and NLIST commands are used to list out the node coordinates and element definition. An external program (Written in TRUE BASIC) is used to convert the nodal data to coordinates and force densities.

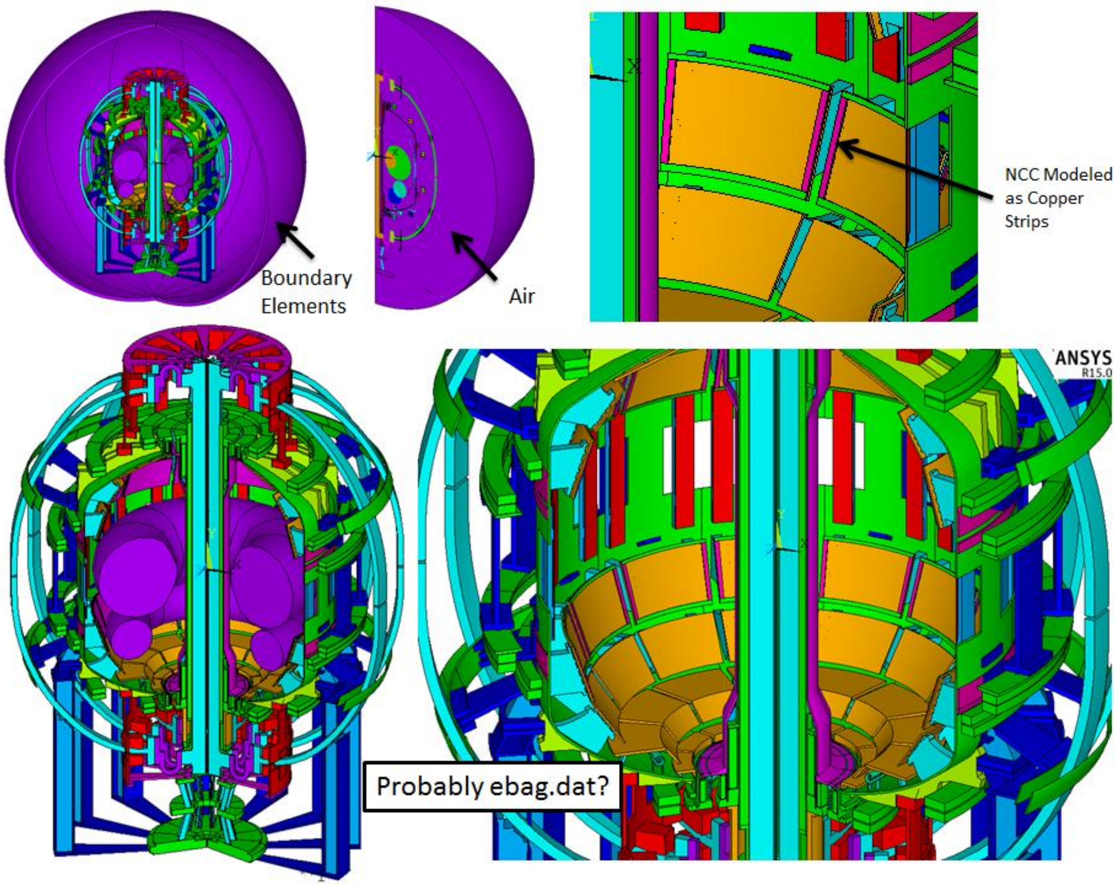
Boundary Elements
Air
NCC Modeled as Copper Strips
ANSYS
R15.0
Probably ebag.dat?

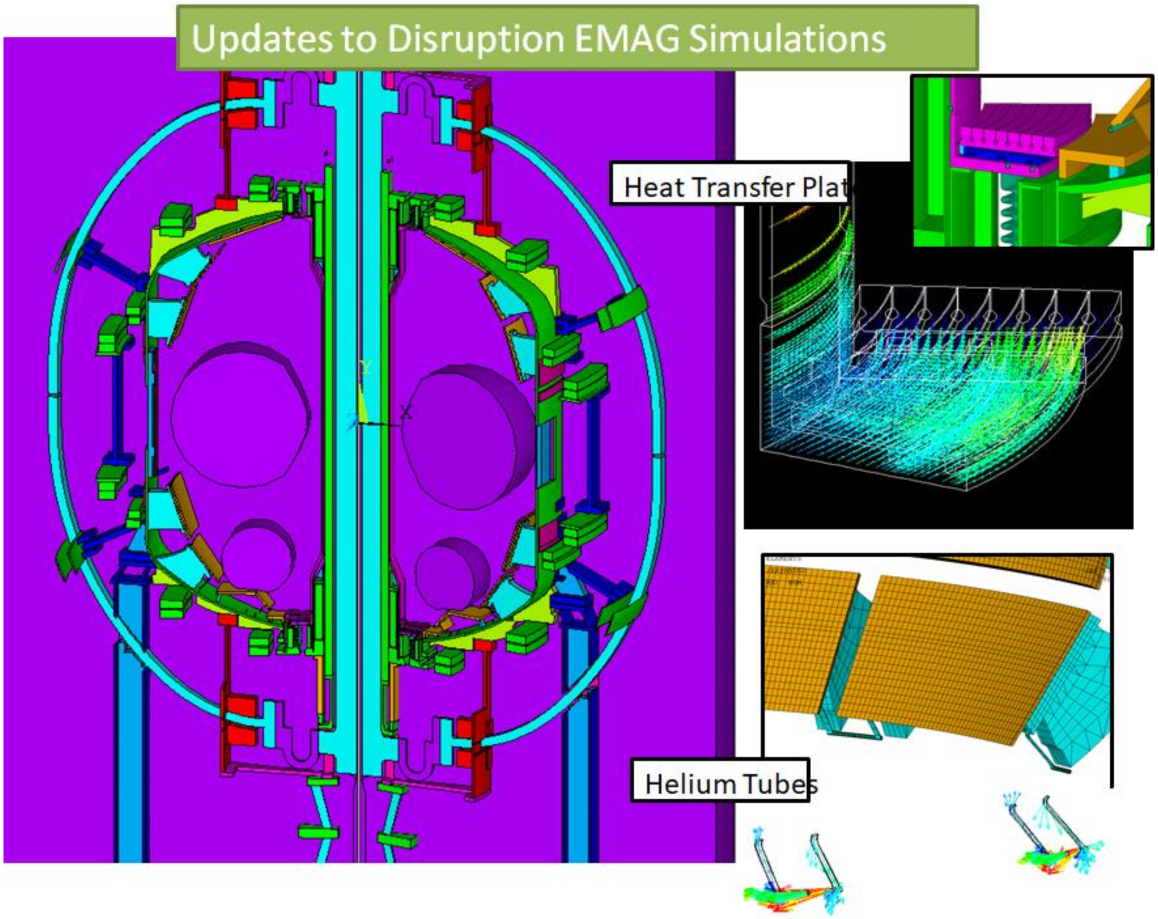

Figure 7.0-1 Global EMAG Disruption Model with Simplified Modeling of NCC

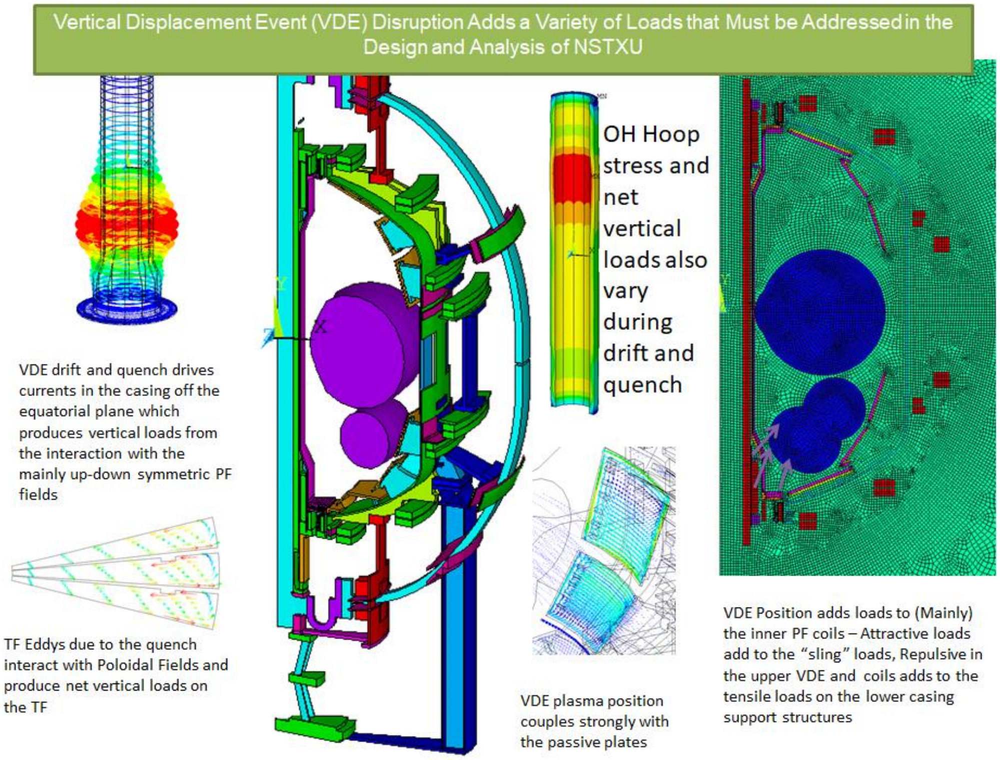

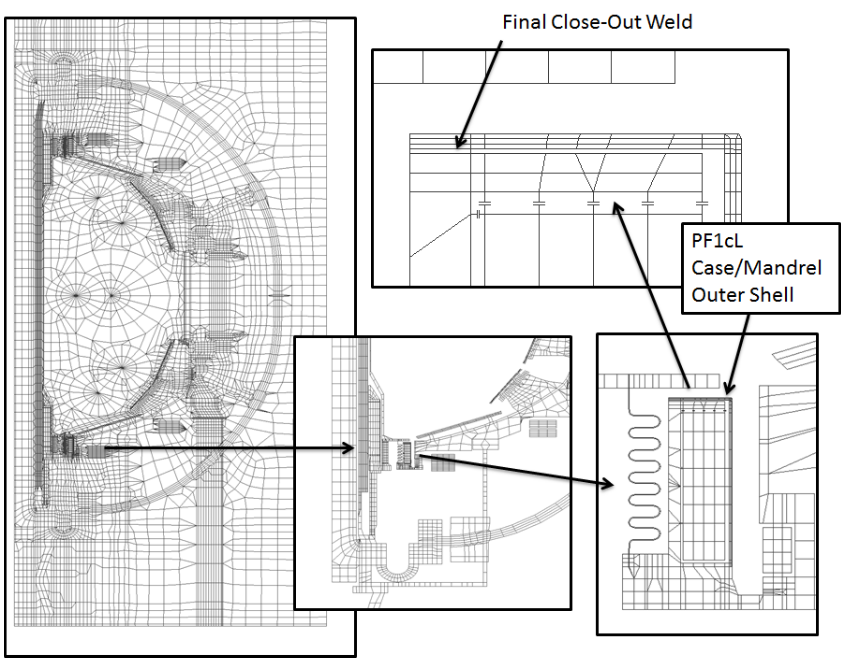

Figure 7.0-2 2D model used for the Swept Mesh

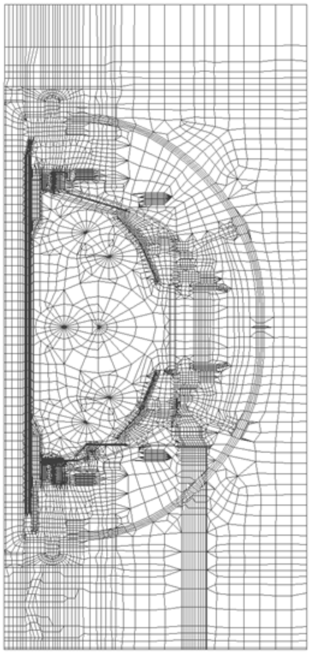

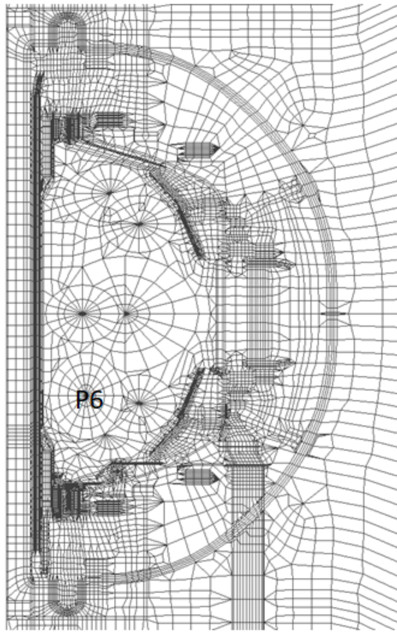

P1 to P4 VDE

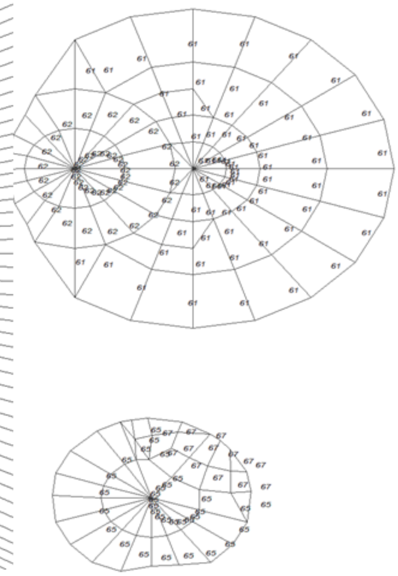

p1area=.962278 !Plasma 1 Real 61, 62
p2area=.25051 !Plasma 2 Real 62, 63
p3area= 1 !Plasma 3 Real 64
p4area=.2494 !Plasma 4 Real 65, 67
p5area=.2498 !plasma 5 Real 66
p6area=.37451 !plasma 6 Real 68

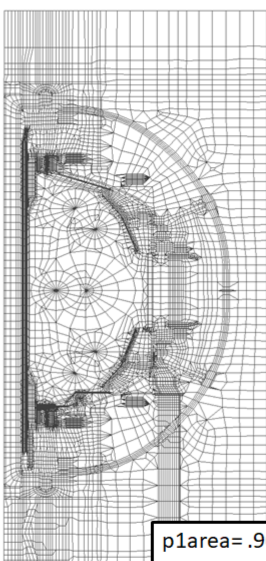

P1 to P5 VDE

```
type,2
mat,90
real,66
esel,real,66
emodif,all
real,67
esel,real,67
emodif,all
real,61
esel,real,61
emodif,all
real,62
esel,real,62
emodif,all
```

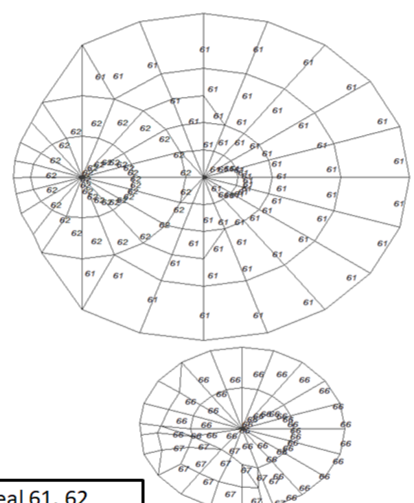

p1area=.962278 !Plasma 1 Real 61, 62
p2area=.25051 !Plasma 2 Real 62,63
p3area= 1 !Plasma 3 Real 64
p4area=.2494 !Plasma 4 Real 65, 67
p5area=.2498 !plasma 5 Real 66,67
P6 area= !Plasma 6 Real 68

Real 66 Area =1.94684
Real 67 Area= .0548
P5=.2498

7.1 Run Log and Files

	*.mod			Directory
Start01.txt		12/07/2015	09:00 AM	D:\nstx\csu\emag
Start02.txt		10/24/2016	02:08 PM	D:\nstx\csu\emag
Start03.txt		03/23/2017	04:25 PM	D:\nstx\csu\emag
Start04.txt		04/28/2017	10:29 AM	D:\nstx\csu\emag
Start05.txt	ebau	05/24/2017	10:47 AM	D:\nstx\csu\emag
Start06.txt	nocr	11/26/2017	02:02 PM	D:\nstx\csu\emag

	*.mod			Directory
moly01.txt		10/31/2014	08:26 AM	D:\nstx\csu\emag
moly02.txt		12/03/2014	05:41 PM	D:\nstx\csu\emag
moly03.txt		03/05/2015	04:05 PM	D:\nstx\csu\emag
moly04.txt		05/18/2015	07:03 AM	D:\nstx\csu\emag
moly07.txt		05/18/2015	04:40 PM	D:\nstx\csu\emag
moly08.txt		05/20/2015	05:07 PM	D:\nstx\csu\emag
moly09.txt		05/20/2015	11:07 PM	D:\nstx\csu\emag
moly10.txt		06/18/2015	09:07 AM	D:\nstx\csu\emag
moly11.txt		06/18/2015	04:56 PM	D:\nstx\csu\emag
moly12.txt		07/02/2015	01:46 PM	D:\nstx\csu\emag
moly13.txt		12/04/2015	03:41 PM	D:\nstx\csu\emag
moly14.txt		02/22/2017	03:03 PM	D:\nstx\csu\emag
moly15.txt		07/17/2017	12:19 PM	D:\nstx\csu\emag
moly16.txt		03/09/2017	09:14 AM	D:\nstx\csu\emag
moly17.txt		10/13/2017	12:06 PM	D:\nstx\csu\emag
moly18.txt		02/12/2018	10:02 PM	D:\nstx\csu\emag
moly19.txt		03/05/2018	03:00 PM	D:\nstx\csu\emag
Moly20Q1.txt				F:\nstx\csu\emag\sling

tube.txt	10/25/2016 04:00 PM	180	
tube01.txt	10/25/2016 09:58 PM	452	
tube02.txt	10/26/2016 11:19 AM	1	510

2D Model Files Used to Generate the 3D Models

ebaj .dat	Cryodivertor
ebak .dat	cryo divertor with baffle
ebaq .dat	incomplete adding divertor tubes
Ebar.dat	

7.2 EMAG Disruption Models

The recovery project includes repairs to the passive plates and investigations of disruption loads on a number of new designs used in the new polar region configuration. A more precise treatment of the loading on the passive plates is needed beyond the one filed in 2012 [1]. Repairs of the poorly fitting support bolts and clevises. Disruption loads on sensitive polar region components like the coil support slings are needed. Time dependent disruption loads that can be applied to more complicated models of the casing and support hardware are also needed. Simple disruption electromagnetic models are needed to generate loads for the more detailed structural models.

In the future, the configuration of NSTX-U will evolve as enhancements to the upgrade are investigated. The global disruption analysis is based on an earlier machine cross section but with upgrades representing the NCC coils and cryo divertor. This model has reasonably accurate representation of the passive plates. To allow a meaningful assessment of the stresses in the details of the NCC, an approximate sub-structuring procedure is used along with extracting the NCC coil loads and behavior directly from the global EMAG model.. The transient solution of the VDE disruption is used as a source of B's and Bdots to impose on the detailed vessel model. Vector potential boundary conditions are imposed in a transient electromagnetic model.

The NSTX-U disruption analysis used for the NCC assessment is a VDE with drift then a current quench based on NSTX-U disruption parameters [1] of At this time only the VDE has been simulated, as this case includes a quench in front of the primary passive plate. This was chosen because it potentially applied large net loads on the structures and local loads on the NCC. The assumed disruption specifications taken from [1]data are 10 millisec for the drift and 1 and 2 millisec for the quench.

The modeling of NSTX-U components in this simulation of the VDE is very simple but it provides a basis for quantifying the B's and Bdots experienced by the NCC during the disruption. These could be mapped to the detailed model of the vessel via imposed vector potential boundary conditions. This has been done for NSTX U and for the C-Mod advanced divertor project, but requires some effort to build the data tables for the full region of the vessel and all the time steps. A simplification is to impose the vertical B dot as enveloped for the vessel and also impose the appropriate vector potential distribution to get the toroidal field. The procedure maps the background vertical field, and the background toroidal field with currents in the vessel driven by the change in vertical field. This is a an approximation, The accuracy of this approach was tested in the analysis of the passive plates. And thisa analysis will be used as a benchmark for corrections in the vector potential imposition analysis.

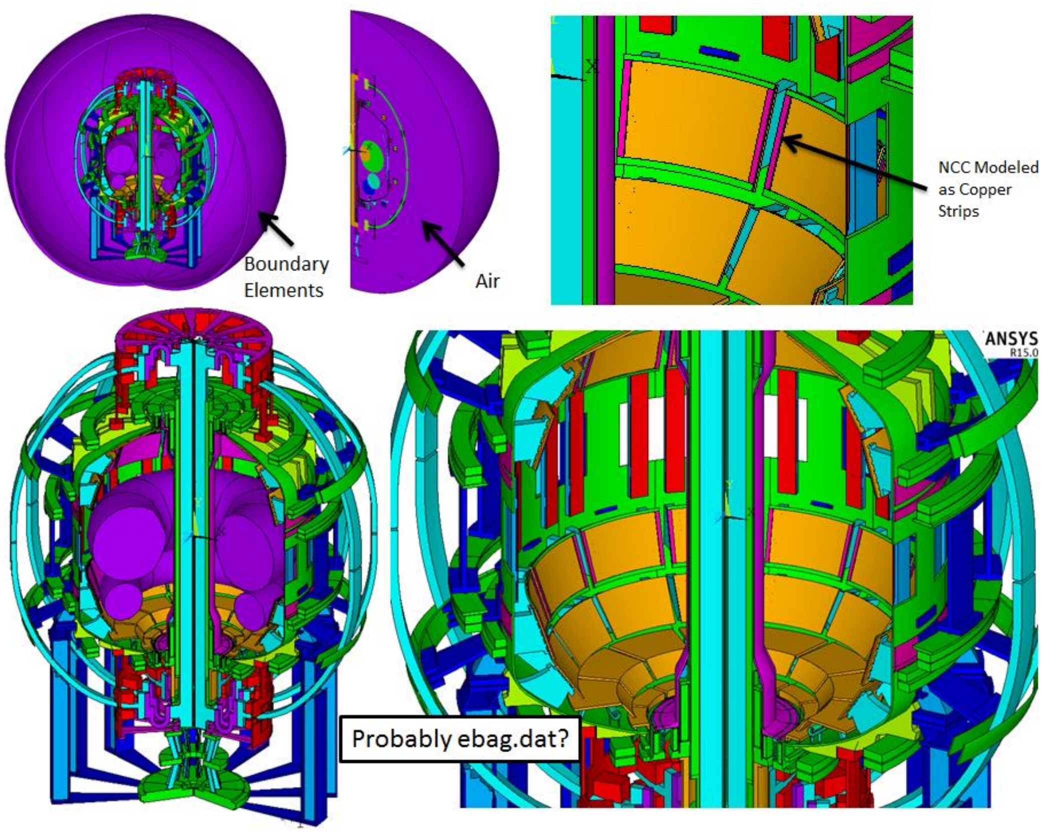

Figure 7.2-2 ANSYS Electromagnet (Disruption) Model

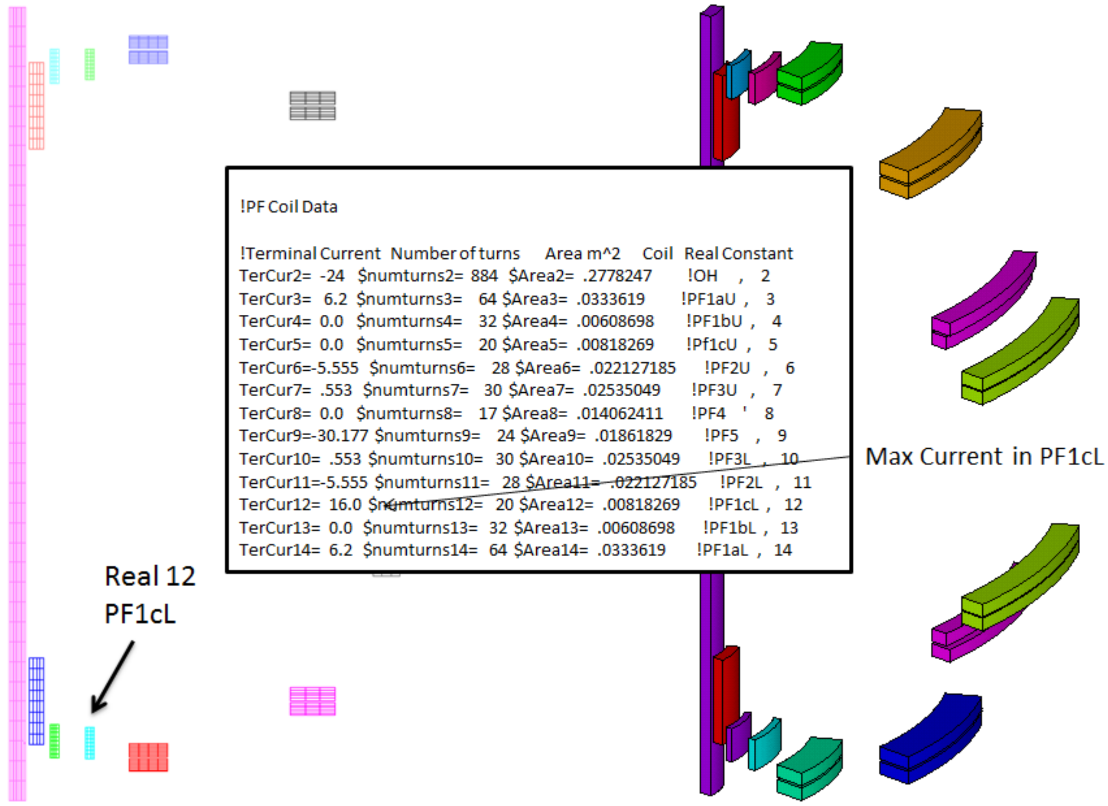

Figure 7.2-3 ANSYS Electromagnet (Disruption) Model PF Coil Input

Input of EQ 79

!Terminal Current Number of turns Area m^2 Coil Real Constant
TerCur2= -24 $numturns2= 884 $Area2= .2778247 !OH , 2
TerCur3= 6.2 $numturns3= 64 $Area3= .0333619 !PF1aU , 3
TerCur4= 0.0 $numturns4= 32 $Area4= .00608698 !PF1bU , 4
TerCur5= 0.0 $numturns5= 20 $Area5= .00818269 !Pf1cU , 5
TerCur6=-5.555 $numturns6= 28 $Area6= .022127185 !PF2U , 6
TerCur7= .553 $numturns7= 30 $Area7= .02535049 !PF3U , 7
TerCur8= 0.0 $numturns8= 17 $Area8= .014062411 !PF4 ' 8
TerCur9=-30.177 $numturns9= 24 $Area9= .01861829 !PF5 , 9
TerCur10= .553 $numturns10= 30 $Area10= .02535049 !PF3L , 10
TerCur11=-5.555 $numturns11= 28 $Area11= .022127185 !PF2L , 11 Max Current in PF1cL
TerCur12= -16.0 $numturns12= 20 $Area12= .00818269 !PF1cL , 12
TerCur13= 0.0 $numturns13= 32 $Area13= .00608698 !PF1bL , 13
TerCur14= 6.2 $numturns14= 64 $Area14= .0333619 !PF1aL , 14

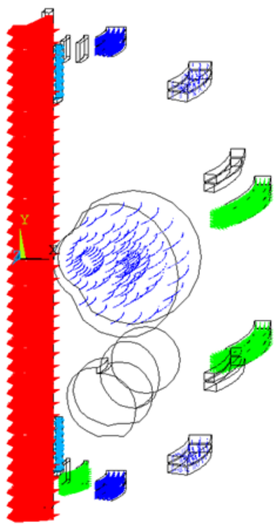

```
LOCAL,12,1,0,0,0,0,-90.0,0.0
CSYS,0
esys,12
/input,fac1,mod
/input,fac2,mod

!P1-P4
curd= Ipmax*p%ls%/p4area
esel,type,2
ersel,real, 65,67,2
bfe,all,js,1,0,curd,0
```

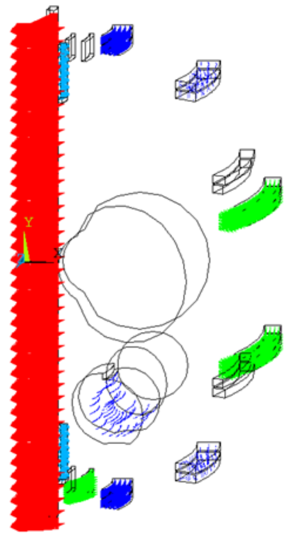

```
csys,12
*do,ipf,2,14
esel,mat,17
ersel,real,ipf
!bfe,all,js,1,0, 32740820. ,0
bfe,all,js,1,0,
tercur%ipf%*1000*numturns%ipf%/area%ipf%,0
*enddo
```

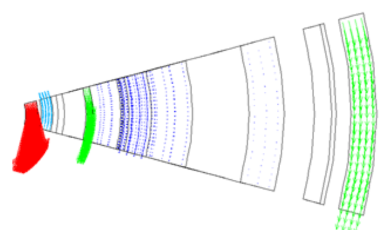

Input Poloidal Field Coil Currents, Showing Proper Theta Direction of the Currents

TF Current Density

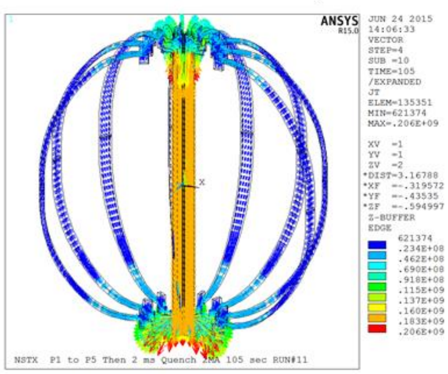

Nominal PF and Ip Current Density

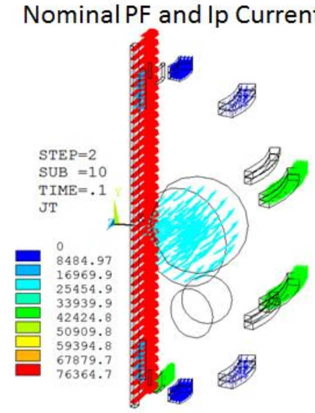

PF and Ip Current Density After Drift

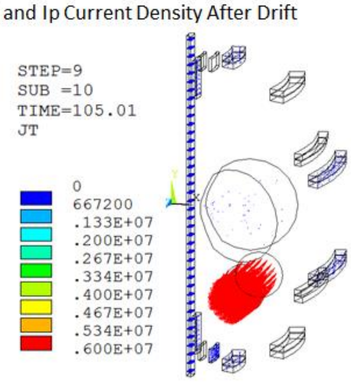

PF and Ip Current Density After Quench

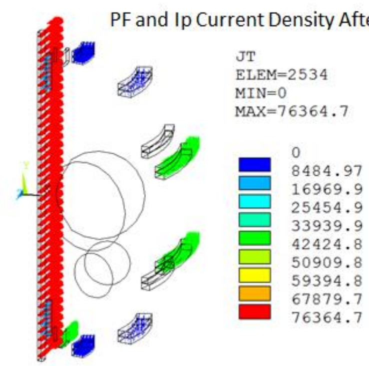

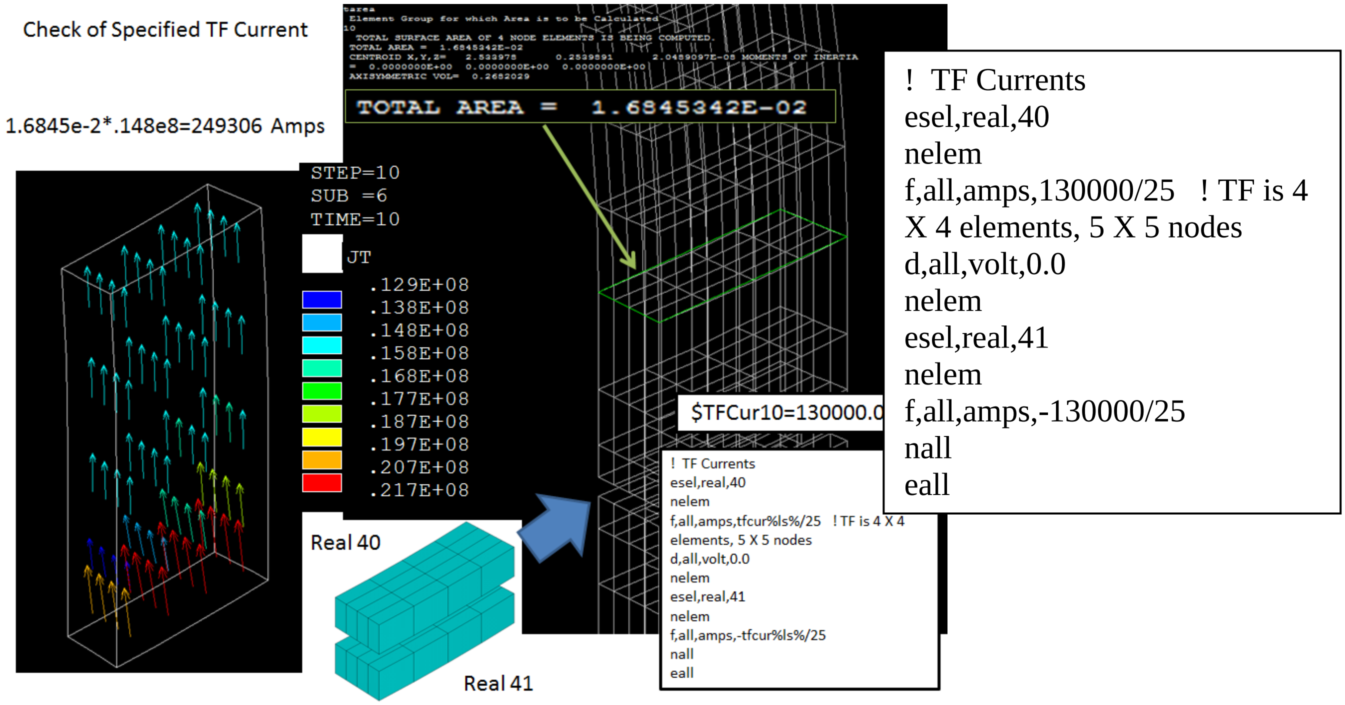

Calculation of the TF Current

Evaluating equilibria with a large vertical field produces the largest “pulling” force from the induced quench current. In earlier calculations, EQ 79 was used. A. Brooks recommends EQ 81 with a Br=.18T and Bz=.52T. EQ 79 has values close to these.

```
type,2
mat,90
real,66
esel,real,66
emodif,all
real,67
esel,real,67
emodif,all
real,61
esel,real,61
emodif,all
real,62
esel,real,62
emodif,all
real,68
esel,real,68
emodif,all
```

```
!Commands needed to input
!local element coordinate for
!imposed currents
LOCAL,12,1,0,0,0,0,-90.0,0.0
CSYS,0
esys,12
!/input,ebaj,mod
/input,ebaz,mod
```

```
csys,12     ! this is is needed
!instead of CSYS,5   I also
!deleted ifs that relate to
!allowing PF4and5 to freewheel
*do,ipf,2,14
esel,mat,17
ersel,real,ipf
!bfe,all,js,1,0,0, 32740820.
bfe,all,js,1,0,
tercur%ipf%*1000*numturns%
ipf%/area%ipf%,0
*enddo
```

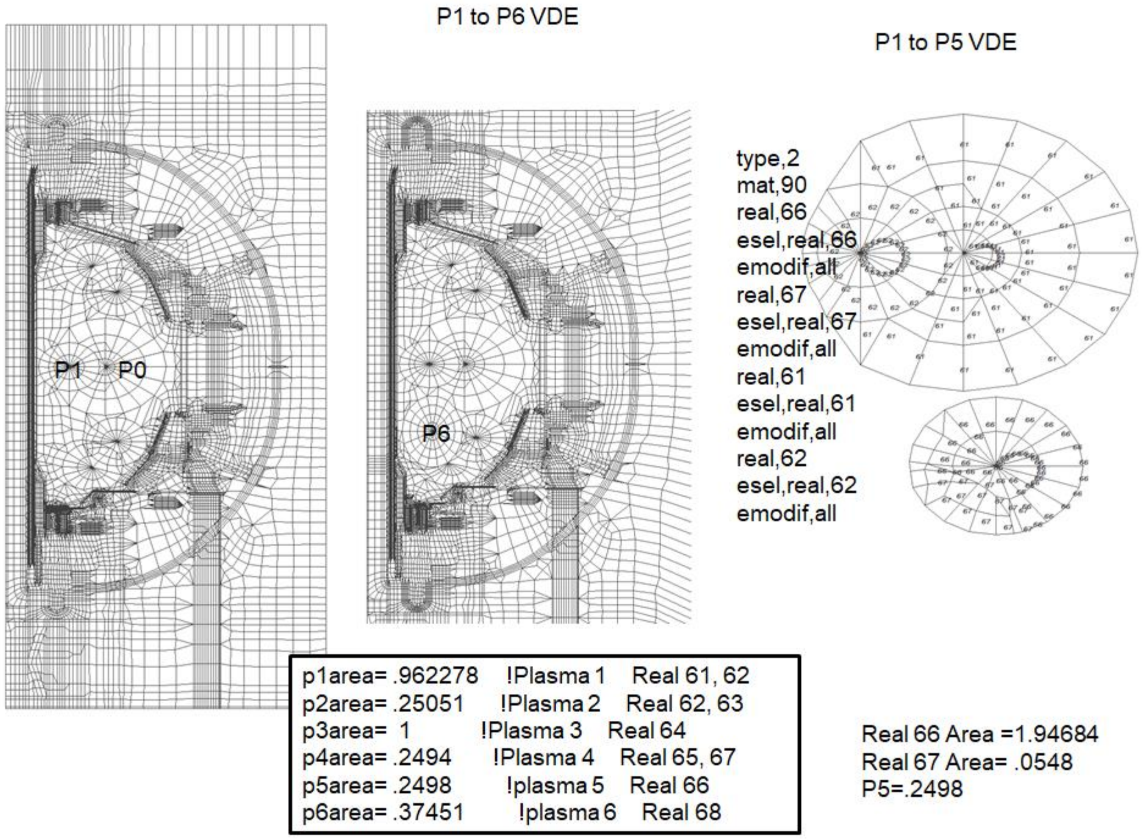

Figure 7.2-Passive Plate Model Features

Figure 7.3-Heat Transfer Plate and Tube Model Features

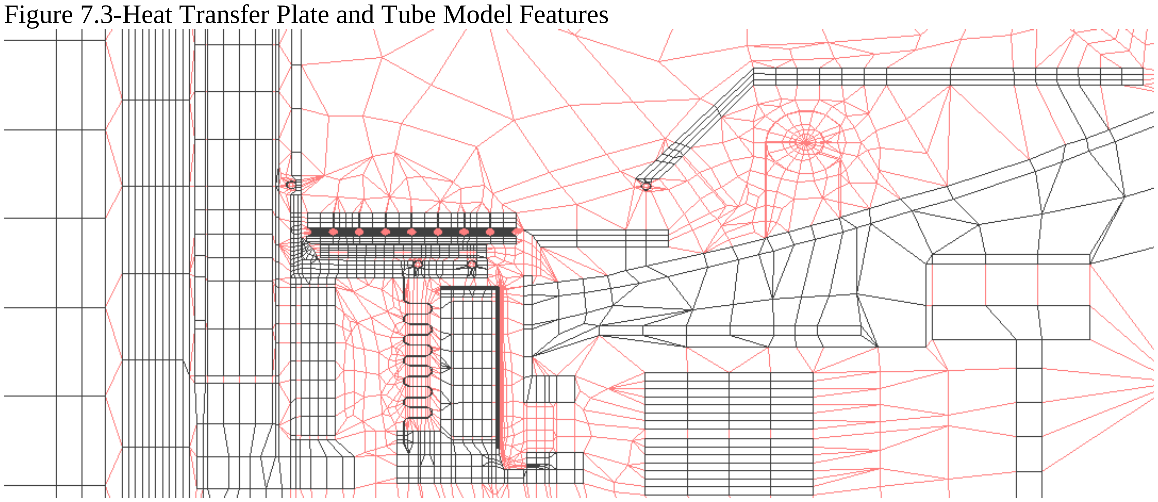

Note the air mesh includes the remnants of the cryo-divertor, but the elements were converted to air. The divertor cavity remains . It is representing the outboard divertor tile support in this run

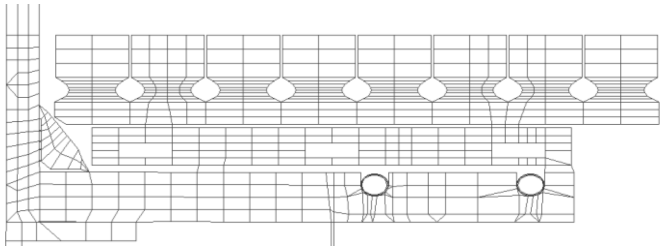

!mp,rsvx,22,2e-8 ! Ground Strap and cooling tubes   When they were copper
mp,rsvx,22,123e-8 ! Ground Strap and cooling tubes
mp,rsvx,32,123e-8 ! Inconel 625   !   Divertor Hot plate

Figure 7.3-Polar Region “Sling” Model Features

Gap elements in the double conductor model. – Similar gaps are used to model the interface between the single round conductor and clamps.

Figure 7.0-2 Model with Cyclic Symmetry Expansion

Figure 7.1-1 July 2014 Model with Added Annular Plate. Crack Tip Elements Added in December 2014

The primary model used in this calculation is a 3D, 360 degree model shown in figure 7.1-3. This was swept from 2D meshes shown in Figures 7.1-1 and-2..

Figure 7.1-2 Circular Conductor with a Two Turn Layout
Figure 7.1-3 June 27 2014 Model With flex Shell Centering Mechanism

8.0 Passive Plates

The passive plates were qualified back in 2012 for the higher upgrade loads. A few weaknesses were identified. Mounting hardware was poorly fit and produced sloppy mounts that could rattle during operation. A monitor and fix later approach was taken . For the recovery project, the as-build configuration was revisited. Weld deficiencies were identified. Repairs were recommended and planned. The loading on the plates needed to be re-evaluated and checked again and the possibilities of different loads addressed. The form of the loading also needed to be updated, because much more detailed structural models of the plates and their weld details have been used.

8.1 Faceted Model for Load Transfer to Andrei's Model

The passive plates are not conical sections, but instead are faceted. The CAD model that Andrei uses to build his model is faceted and to achieve a good transfer of loads the EMAG model must overlay his geometry precisely.

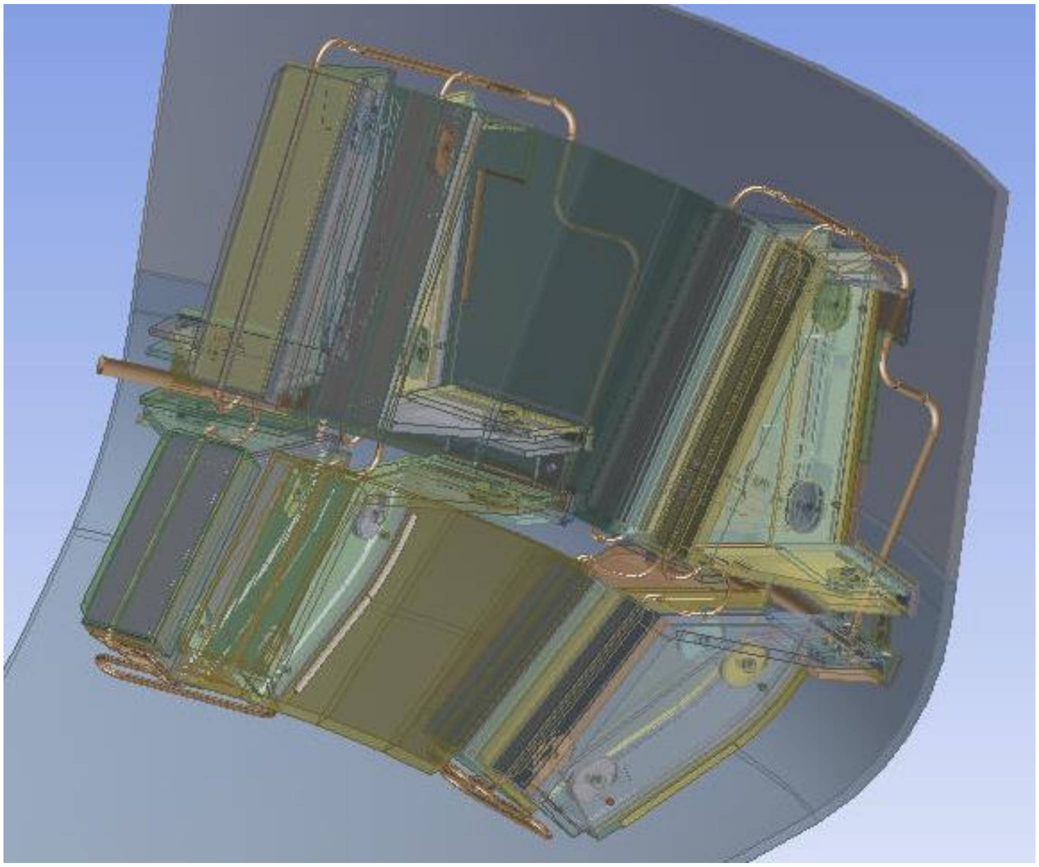

Figure 8.1-1 CAD model With Faceted Plates, Input to the Structural Model

The EMAG models used for most of the component qualifications in earlier analyses and in this calculation for other components are swept geometries. To build the faceted plates, the precise geometry of the plates in the detailed solid model was provided and a faceted model was created. This was done by a coarse 4 angle sweep to get a 30 degree cyclic symmetry model and then the elements were linearly divided to a fine enough mesh to provide appropriate precision of the loads being applied to the structural model.

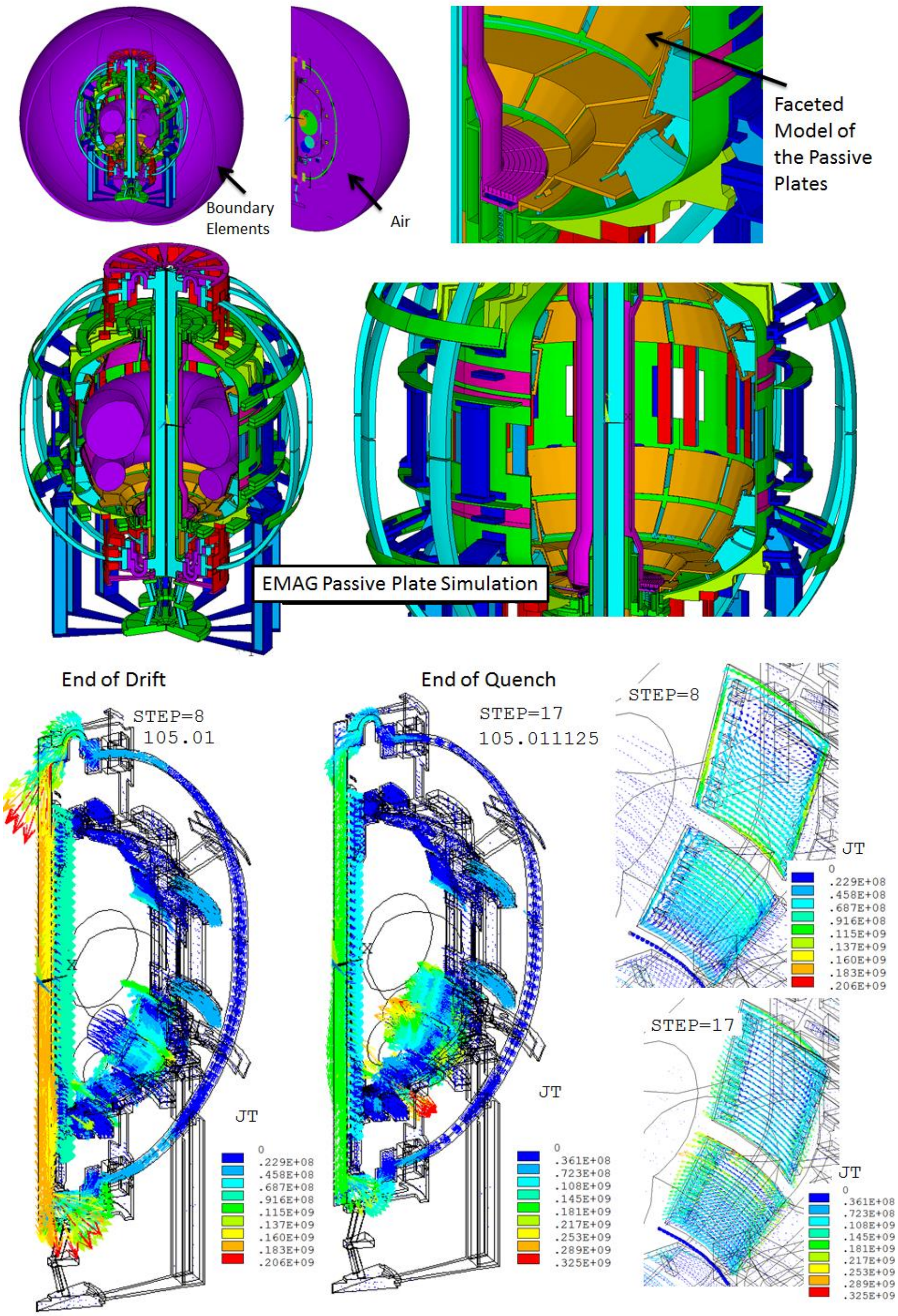

New files are at: P:\public\Snap-srv\Titus\NSTX\CSU\PassivePlates\Facet

There are 24 load files. These have corrected PF5 currents - I had converted PF5 to a coil driven by the EM transients rather than having an imposed current. This eliminated most of the vertical field. Art still has larger loads in his sweep of the 96. So we will have to reconcile the differences and I will have to pick one of his worst and re-run. In the vintage of Yuhu's and my disruption calculations, we were using either 41 or 79. The excel plot below is for the lower primary passive plate with a VDE down and a 1 millisec quench

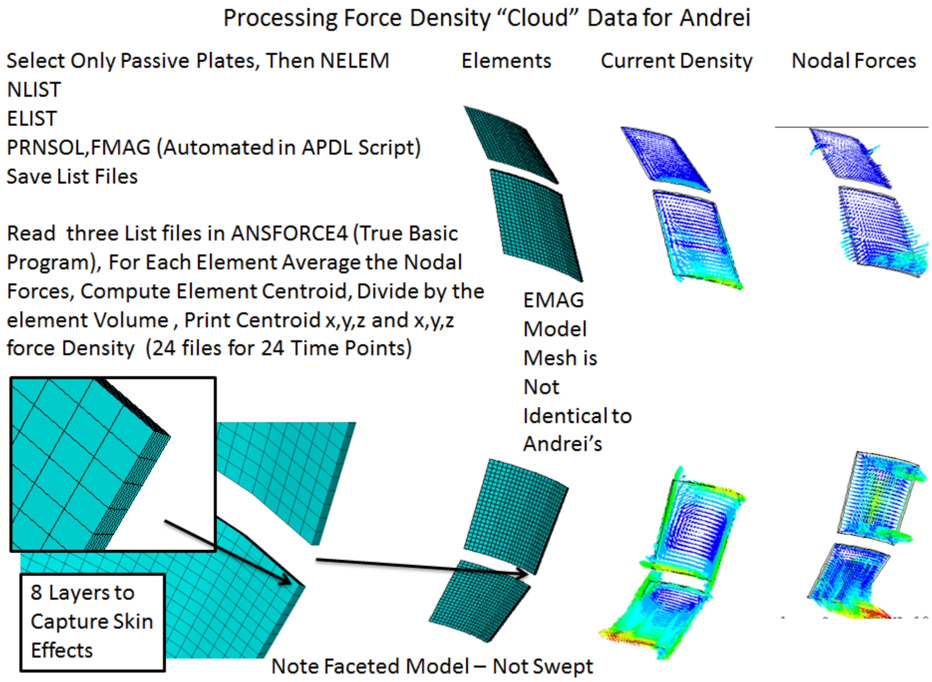

Processing the Force Density "Cloud" Data

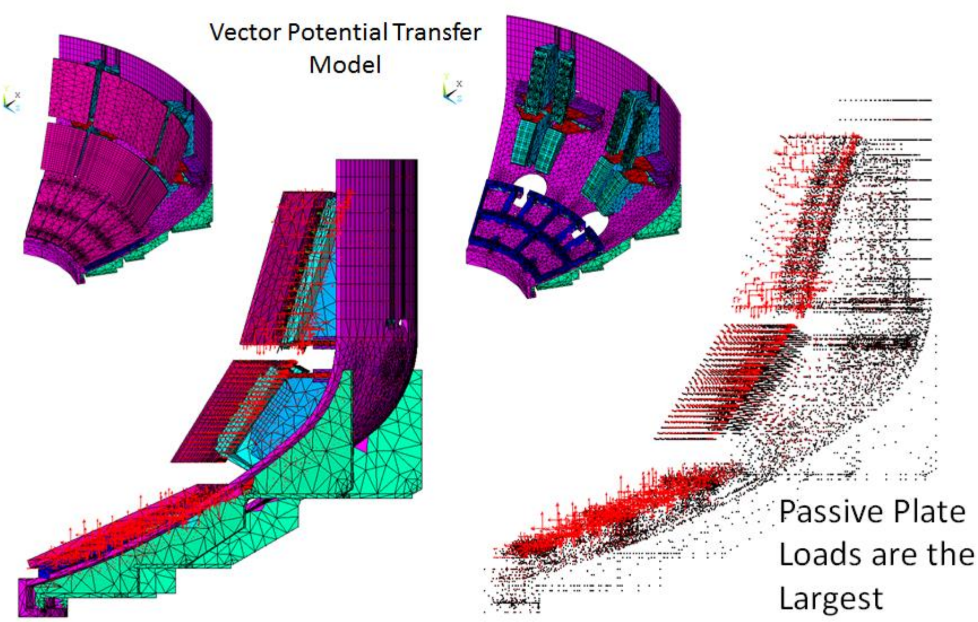

Plots of the Nodal Forces for Passive Plates and Backing Structures

Only loads on the passive plates were transferred to Andrei's model. Results of analyses which included the backing structures are available from [1] and [29] and these show that the bulk of the loading is on the copper passive plates vs. the stainless steel structures behind them.

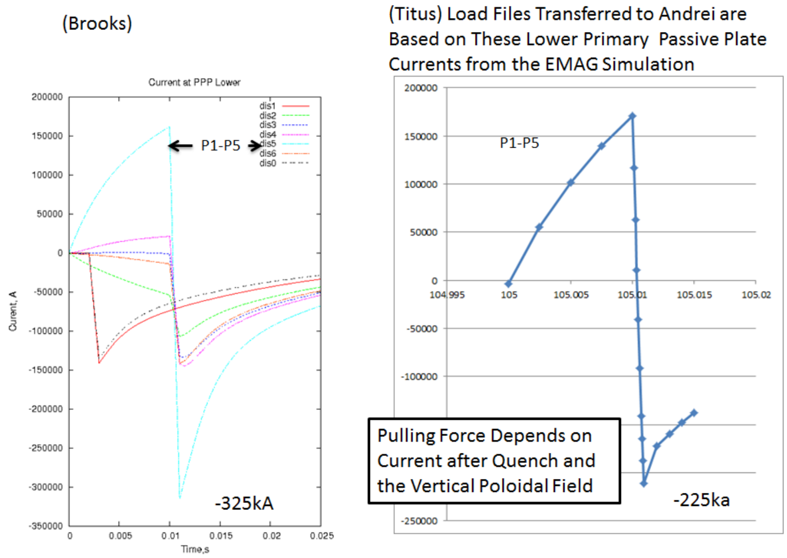

The difference between A. Brooks results and the P. Titus results is substantial, but in subsequent analyses to quantify Helium tube loads, Art found a strong dependency on resistance in the plate-vessel toroidal loop. Since the Helium tubes share in this, the resistance of the vessel-plate loop can change the Helium tube currents substantially.

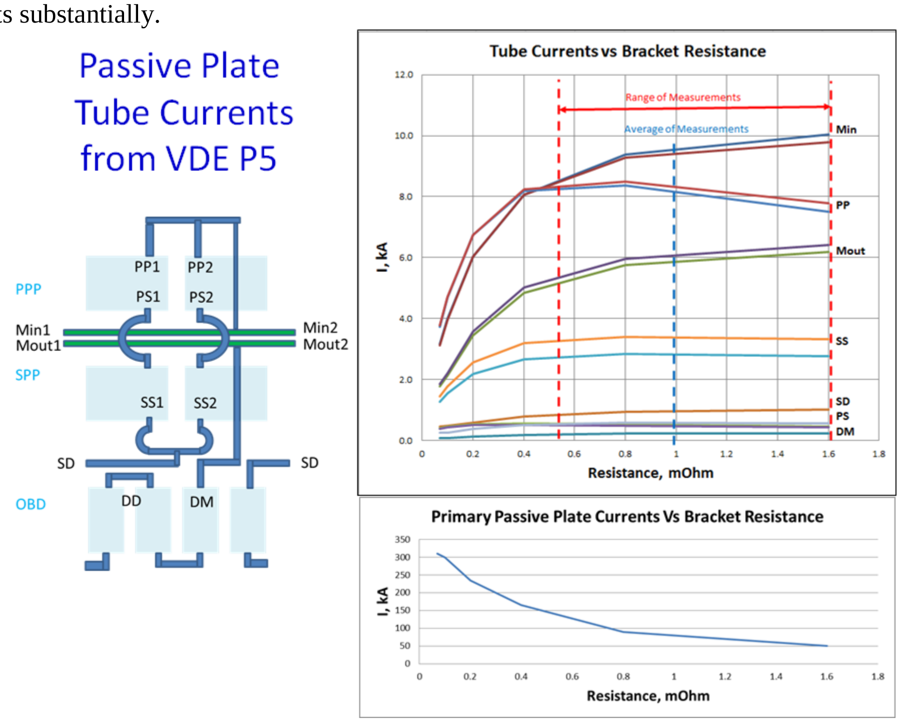

Tube Currents and Passive Plate Currents vs. Bracket resistance

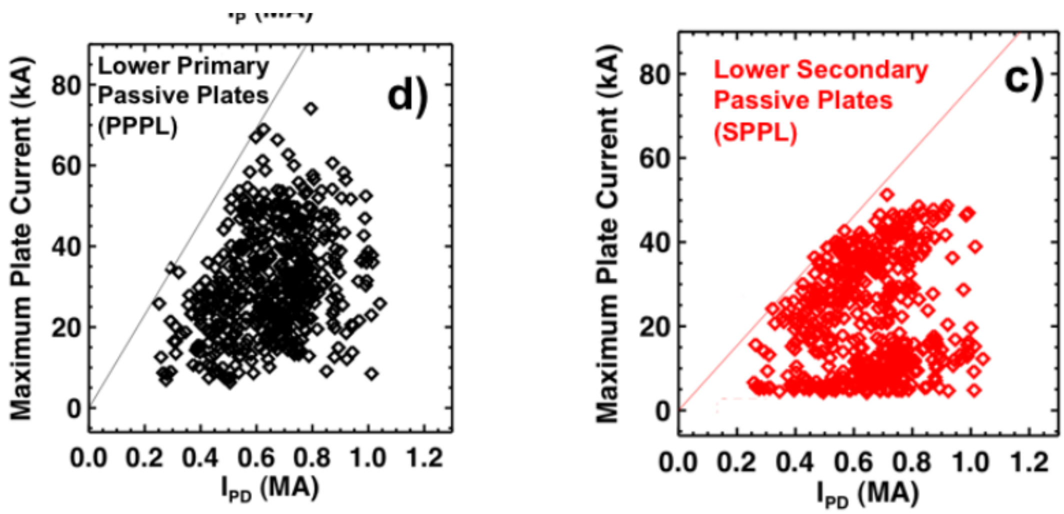

[4] "Characterization of the Plasma Current quench during Disruptions in the National Spherical Torus Experiment" S.P. Gerhardt, J.E. Menard and the NSTX Team Princeton Plasma Physics Laboratory, Plainsboro, NJ, USA Nucl. Fusion 49 (2009) 025005 (12pp) doi:10.1088/0029-5515/49/2/025005

The plot on the upper left shows an upper bound on the toroidal currents of 10% of Ip, so for a 2MA Ip the toroidal Current would be 200kA for the lower primary passive plates or 400kA total for the upper and lower plates.

Passive Plate Currents Measured during the NSTX Run Period

Measured passive plate currents during the NSTX run period produced currents enveloped by a 10% limit with most of the disruptions below this. For a 2MA Ip the passive plate current would be 200,000 amps

For a bracket resistance of between 4 and 6 milliohms, the plate current is about 150 kA – or less than both the Brooks, and Titus analyses represented in figure __. Loads provided to Andrei for the structural analysis of the plates and brackets, are based on a toroidal current of 225 kA which will produce a higher load than for the 150kA predicted for the measured resistances, but is consistent wit the NSTX experience..

Art used my database file and carved out half a primary passive plate with one support (cut at the VV) and ran a simple dc current model - ground the PP midplane cut and couple the bracket/VV cut and apply a 1 amps force. The max voltage then gives the resistance.

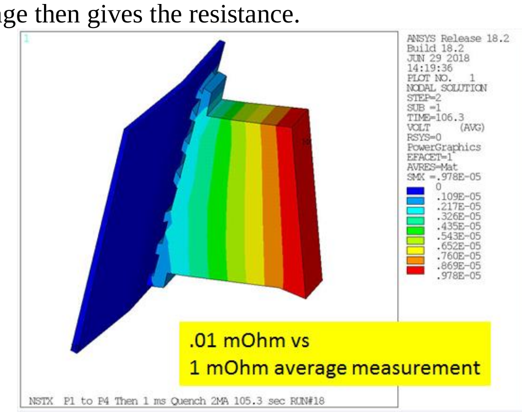

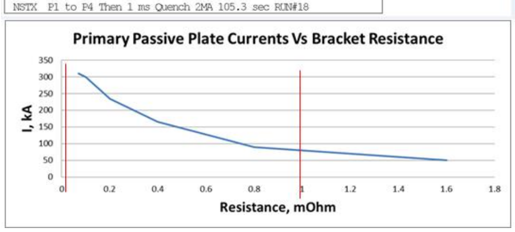

Art got a very low resistance from the (Titus) model - .01 mOhm vs 1.0 mOhm average measurement - which would suggest the PPP currents are very conservative.

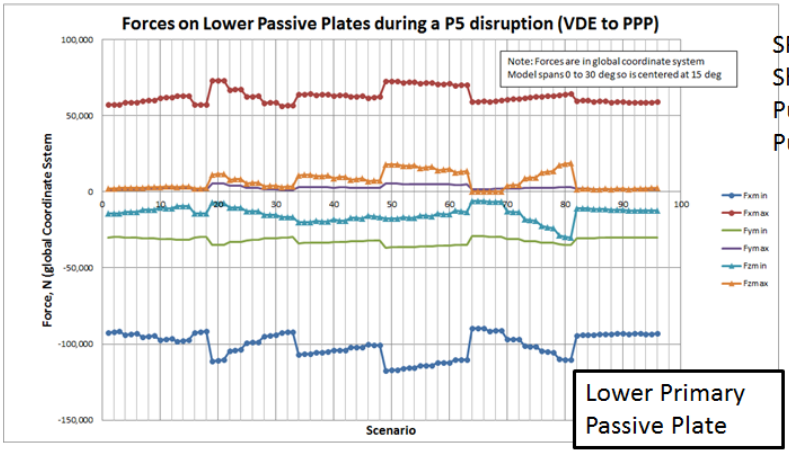

SPARK Results Show Shifted Pushing and Pulling

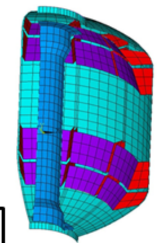

Lower Primary Passive Plate

A. Brooks and P. Titus EMAG Agree Pretty Well

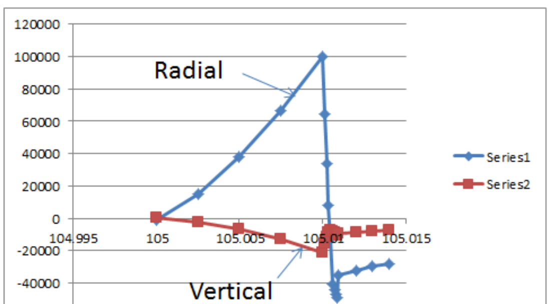

P. Titus EMAG Results Using EQ 79

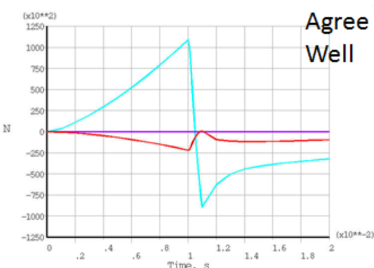

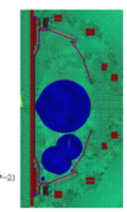

A. Brooks EMAG Results Using EQ 79

Disruption Forces on One Lower Primary Passive Plate
EQ 79

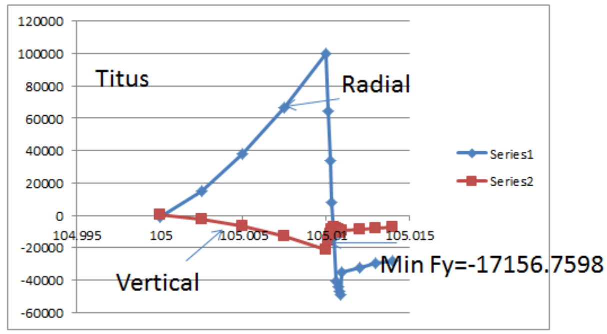

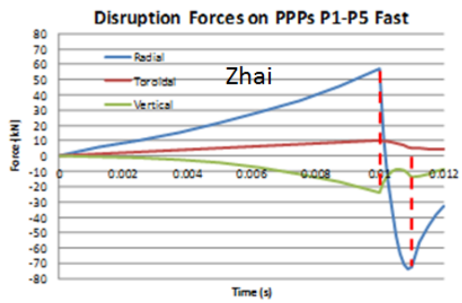


```
          Nominal 96 Equilibria
algorithm # 202   Radial Field at lower Primary Passive Plates No Plasma bt=.64754985
TF current is: 130  kA
Maximum Result of Algorithm 202 = .17336208 Tesla at EQ#  81
Minimum Result of Algorithm 202 = 4.1938341e-2 Tesla at EQ#  66
Max Limit for Algorithm  202  is  .3 Tesla
Min Limit for Algorithm  202  is -.3 Tesla
algorithm # 204   Radial Field at lower Primary Passive Plates With Plasma bt=.64754985
Maximum Result of Algorithm 204 = .36501142 Tesla at EQ#  81
Minimum Result of Algorithm 204 = .23358768 Tesla at EQ#  66
Max Limit for Algorithm  204  is  .3 Tesla
Min Limit for Algorithm  204  is -.3 Tesla
                   Downward Displaced VDE Plasma at P5 Primary Passive Plate
```

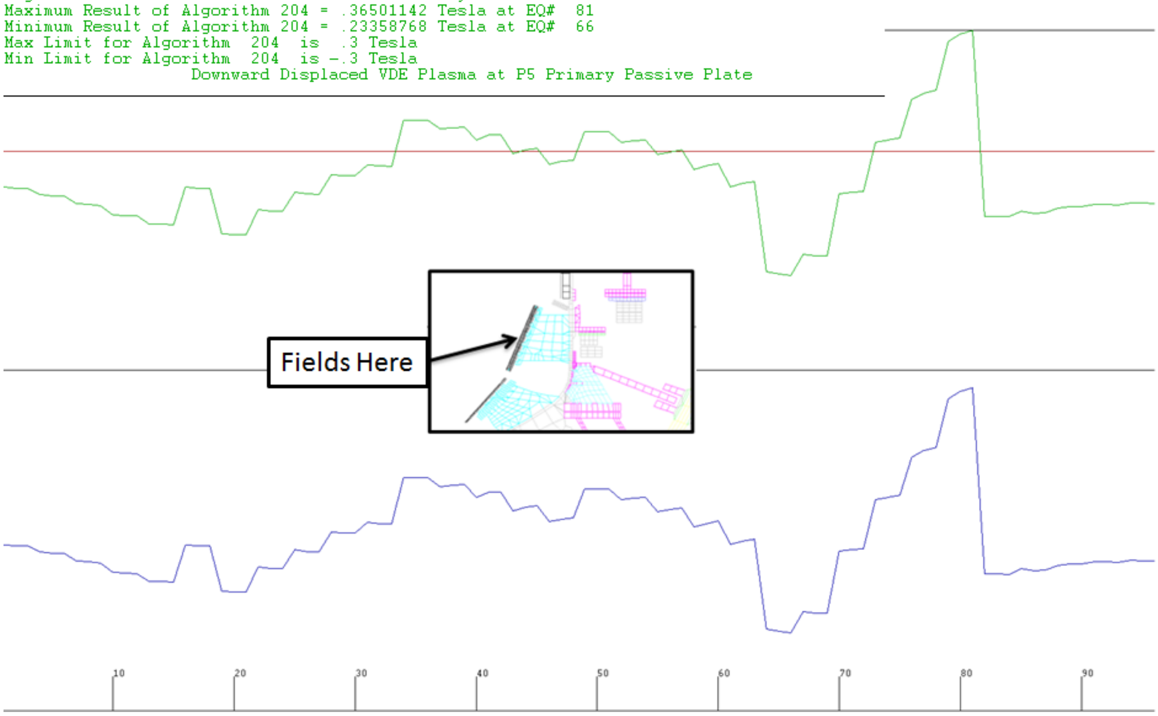

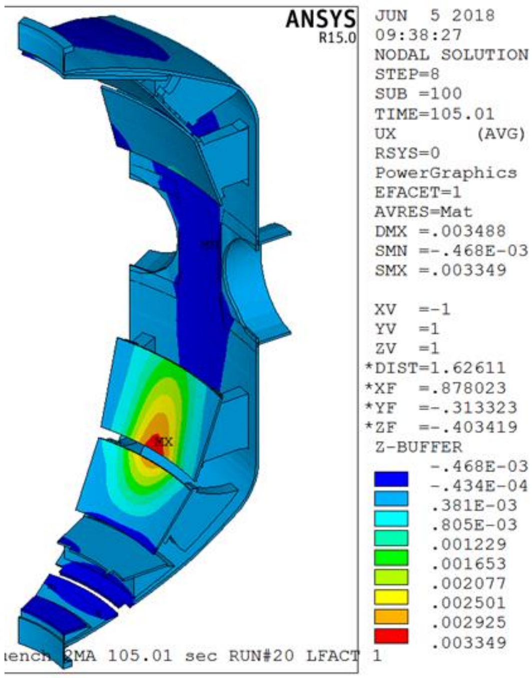
ANSYS
R15.0
JUN 5 2018
09:38:27
NODAL SOLUTION
STEP=8
SUB =100
TIME=105.01
UX (AVG)
RSYS=0
PowerGraphics
EFACET=1
AVRES=Mat
DMX =.003488
SMN =-.468E-03
SMX =.003349
XV =-1
YV =1
ZV =1
*DIST=1.62611
*XF =.878023
*YF =-.313323
*ZF =-.403419
Z-BUFFER
-.468E-03
-.434E-04
.381E-03
.805E-03
.001229
.001653
.002077
.002501
.002925
.003349
MX
2MA 105.01 sec RUN#20 LFACT 1

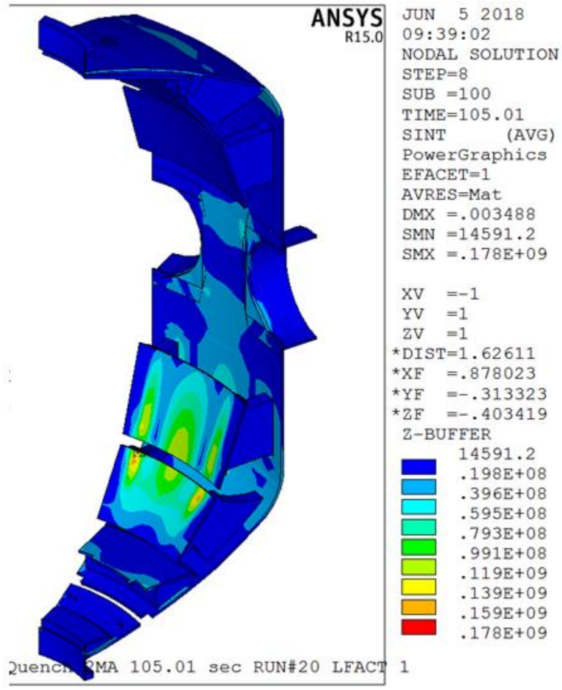
ANSYS
R15.0
JUN 5 2018
09:39:02
NODAL SOLUTION
STEP=8
SUB =100
TIME=105.01
SINT (AVG)
PowerGraphics
EFACET=1
AVRES=Mat
DMX =.003488
SMN =14591.2
SMX =.178E+09
XV =-1
YV =1
ZV =1
*DIST=1.62611
*XF =.878023
*YF =-.313323
*ZF =-.403419
Z-BUFFER
14591.2
.198E+08
.396E+08
.595E+08
.793E+08
.991E+08
.119E+09
.139E+09
.159E+09
.178E+09
2MA 105.01 sec RUN#20 LFACT 1

9.0 Helium Tube Analysis

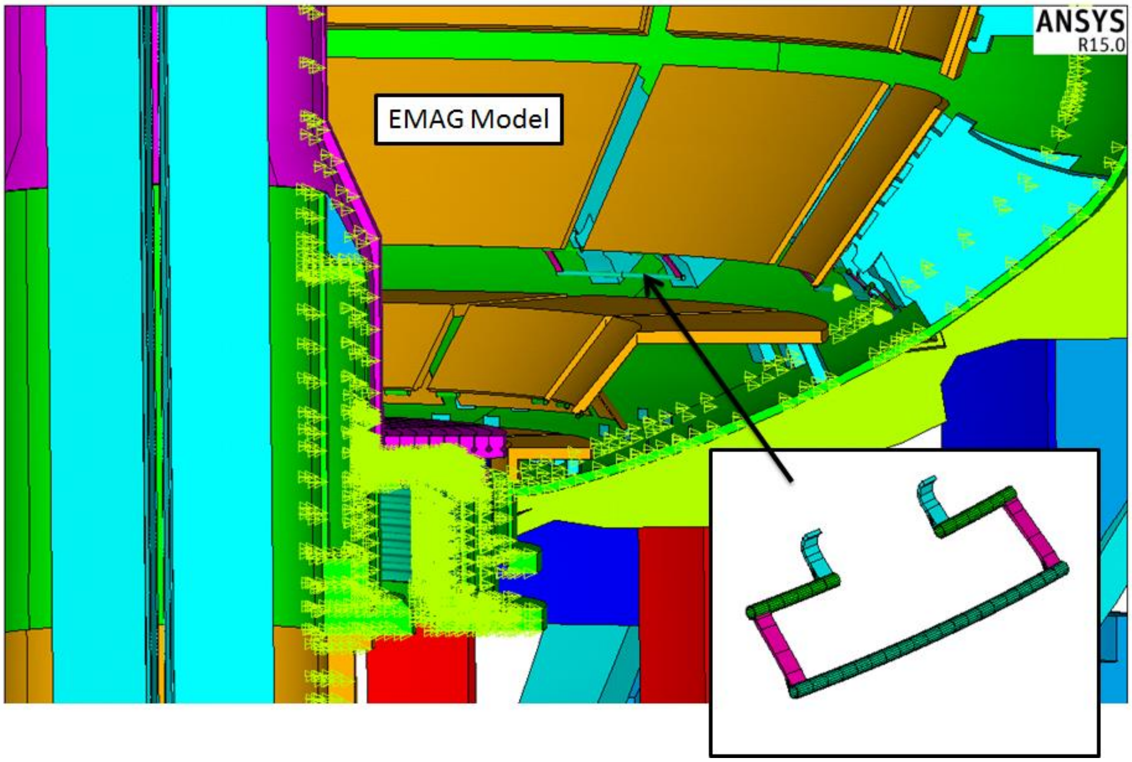

A.Brooks Tube Model with Simplified PP & VV

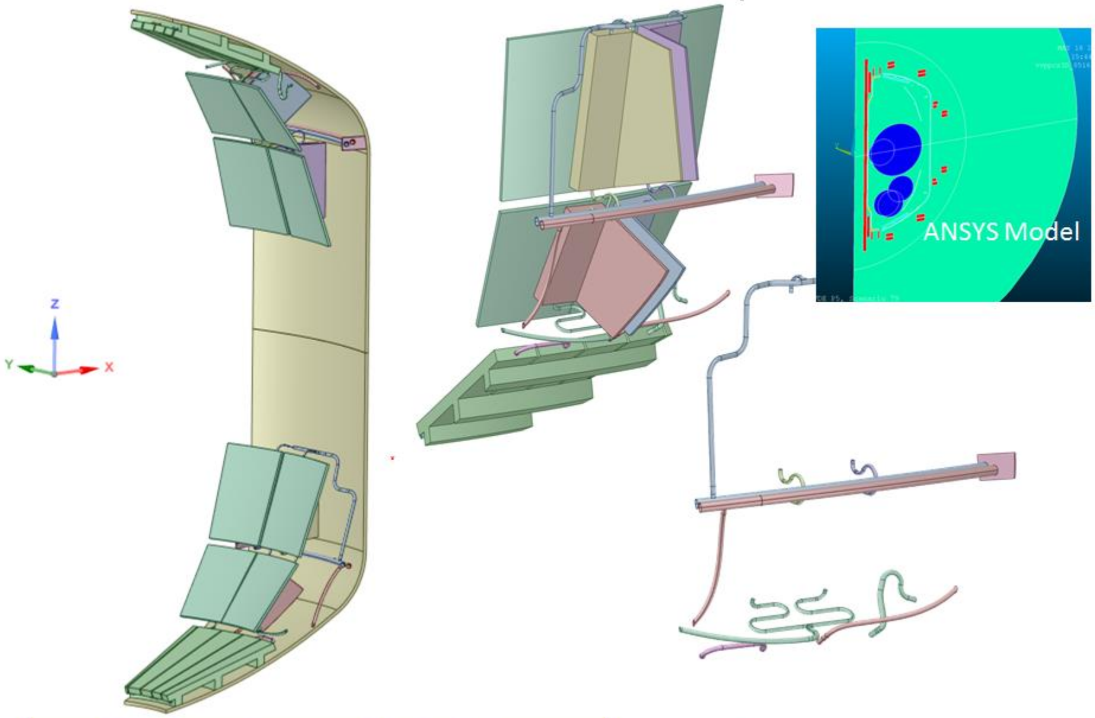

e-ed1439-08_art Courtesy of Richard Upcavage

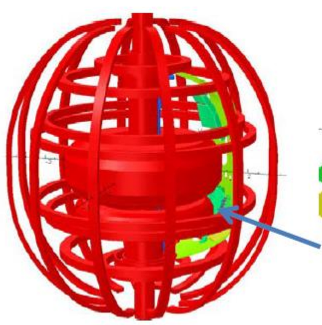

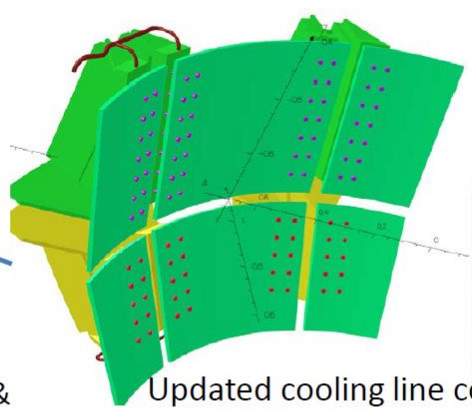

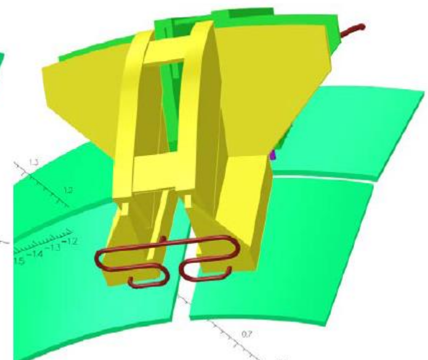

Updated cooling line connection - EM loads

- Real tube geometry & route layout used (P1-P5)
- Current on He tubes at ***the kA level but w/ uncertainty***
- ill-condition in FEA model (>30% uncertainty – error bar) - CAD geometry issues
- *To update with latest clean CAD geometry from RU&AK*

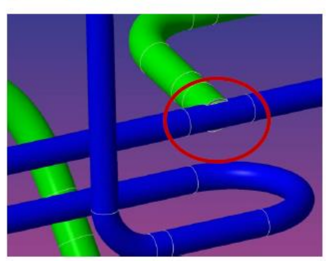

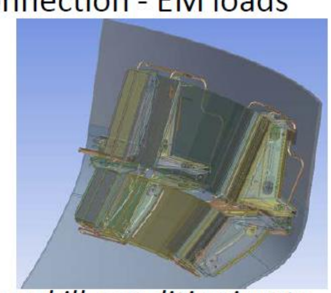

Need to resolve CAD induced ill-conditioning to reduce uncertainty in calculations

A. Brooks Results Summary

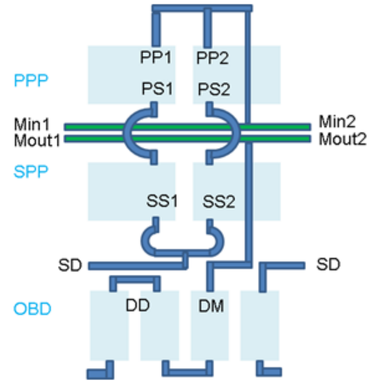

- Results shows a high resistance bracket - that could results from poor contact - will limit the total toroidal current thru the Primary Passive Plates **but drive more currents thru the tubes** that short them

- The Secondary Passive Plates will be similarly effected but to a lesser degree
- Manifold currents will also be higher though the manifold connected to the OBD sees less current

- Resistance Measurements are needed to better assess where we are

Zhai 5kA

Titus 1.1kAS
Zhai 2.2 kA

Currents, kA, in Lower PPP and Tubes

	Bracket Resistance, mOhm		
Part	0.1	0.2	0.4
PPP	300	310	165
PP1	4.8	3.7	8.1
PP2	4.8	3.7	8.1
PS1	0.4	0.4	0.5
PS2	0.4	0.4	0.5
SS1	1.6	1.3	2.6
SS2	1.8	1.5	3.0
SD	0.2	0.2	0.5
Min1	4	3.2	8.1
Min2	4	3.2	8.1
Mout1	2.1	1.6	4.9
Mout2	2.1	1.6	4.9
DM1	0.4	0.4	0.1
DM2	0.4	0.4	0.1

Symmetry Expansion of the Loop

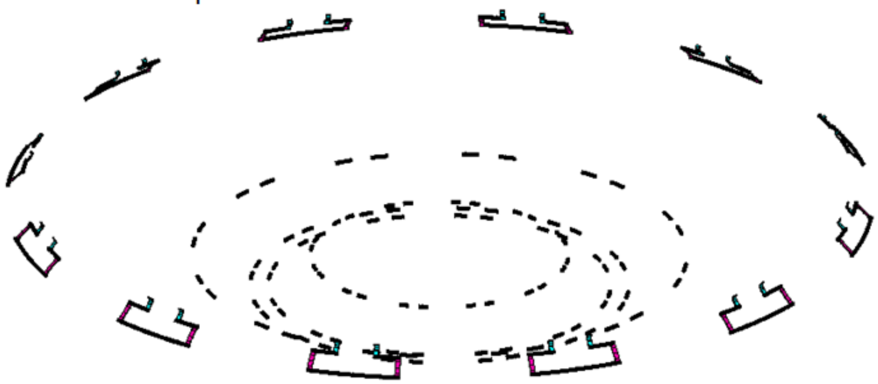

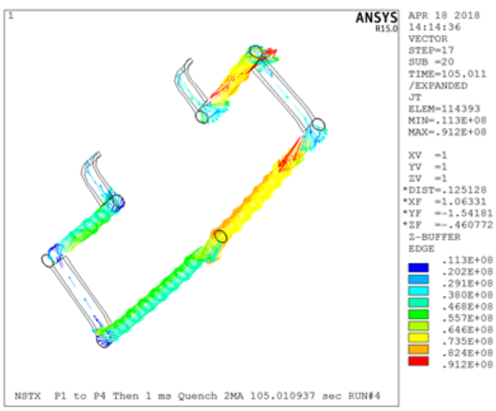

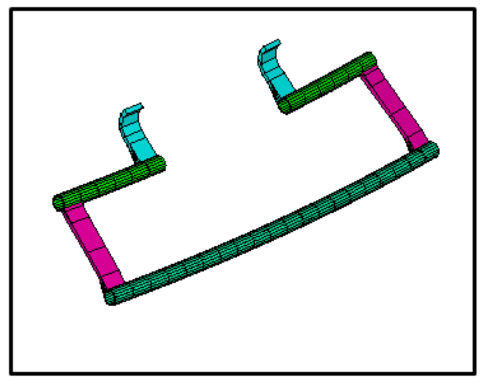

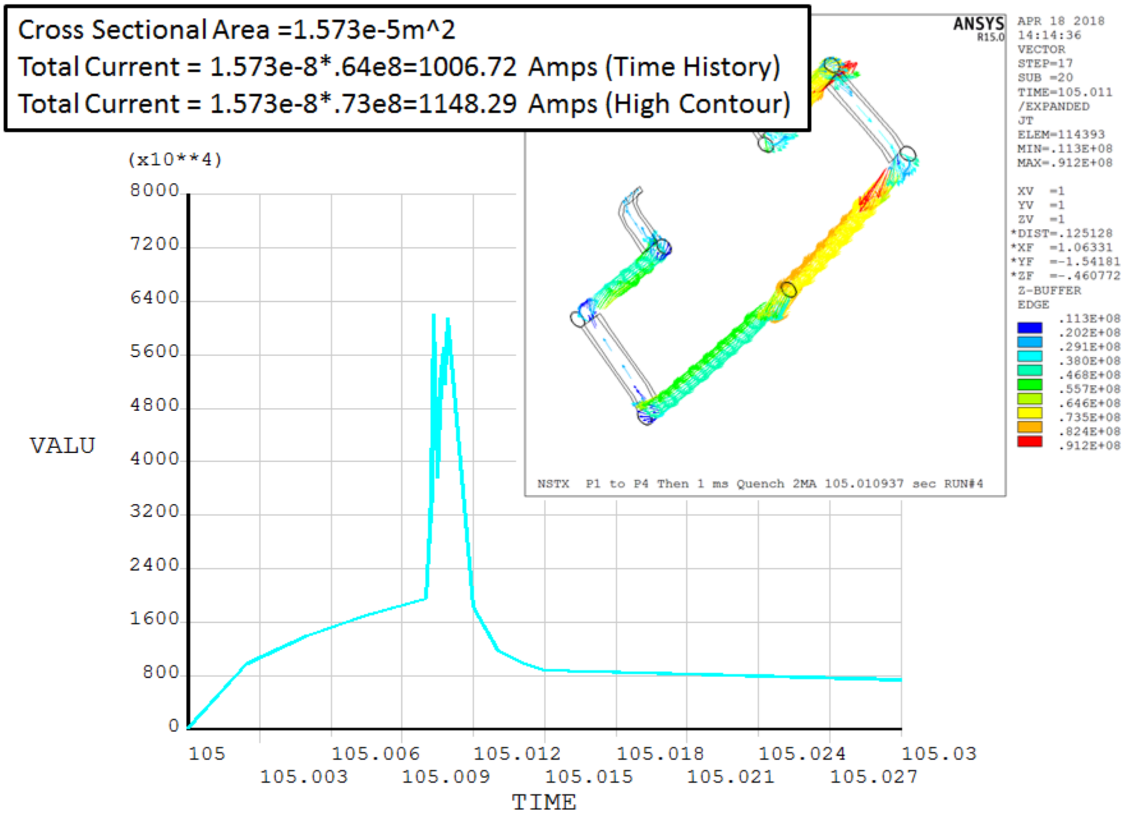
Cross Sectional Area =1.573e-5m^2
Total Current = 1.573e-8*.64e8=1006.72 Amps (Time History)
Total Current = 1.573e-8*.73e8=1148.29 Amps (High Contour)
ANSYS
R15.0
APR 18 2018
14:14:36
VECTOR
STEP=17
SUB =20
TIME=105.011
/EXPANDED
JT
ELEM=114393
MIN=.113E+08
MAX=.912E+08
XV =1
YV =1
ZV =1
*DIST=.125128
*XF =1.06331
*YF =-1.54181
*ZF =-.460772
Z-BUFFER
EDGE
.113E+08
.202E+08
.291E+08
.380E+08
.468E+08
.557E+08
.646E+08
.735E+08
.824E+08
.912E+08
NSTX P1 to P4 Then 1 ms Quench 2MA 105.010937 sec RUN#4
(x10**4)
VALU
8000
7200
6400
5600
4800
4000
3200
2400
1600
800
0
105
105.003
105.006
105.009
105.012
105.015
105.018
105.021
105.024
105.027
105.03
TIME

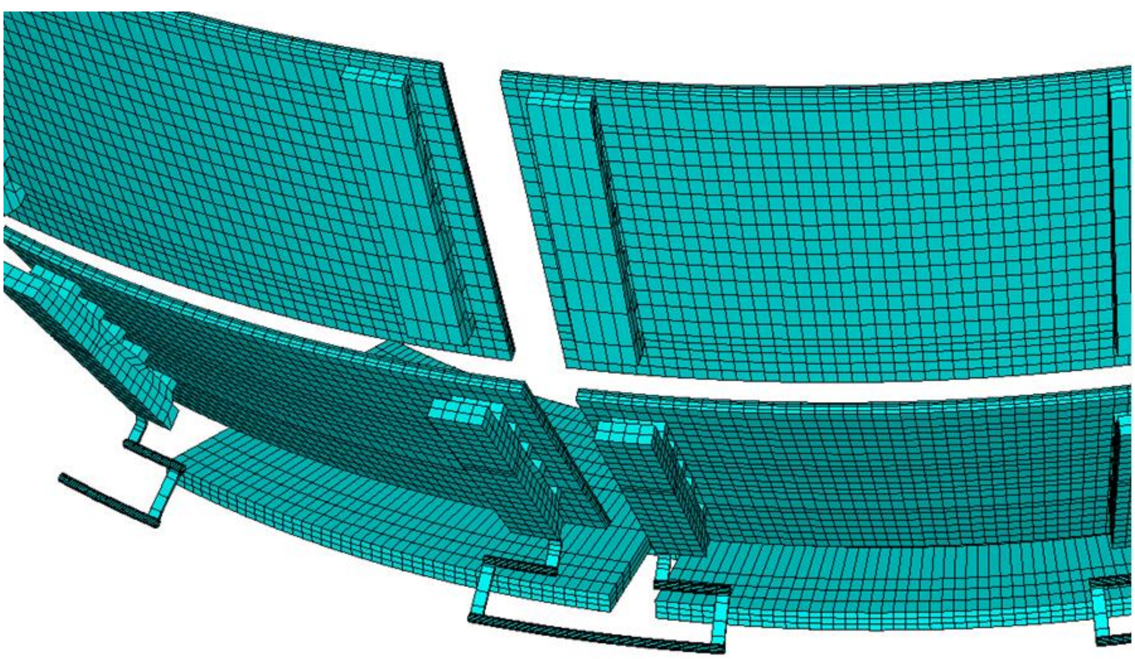

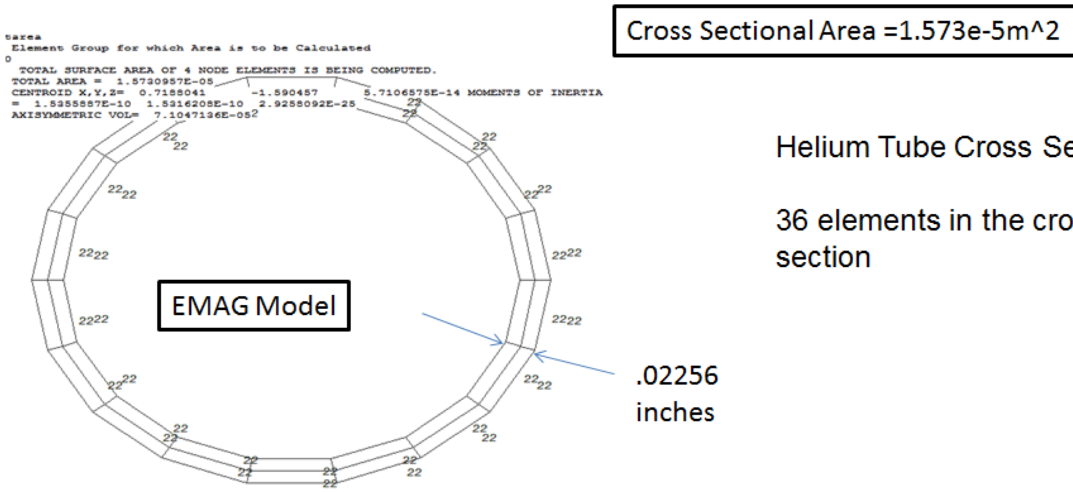

Helium Tube Cross Section

36 elements in the cross section

dB/dt Results Behind the Passive Plates

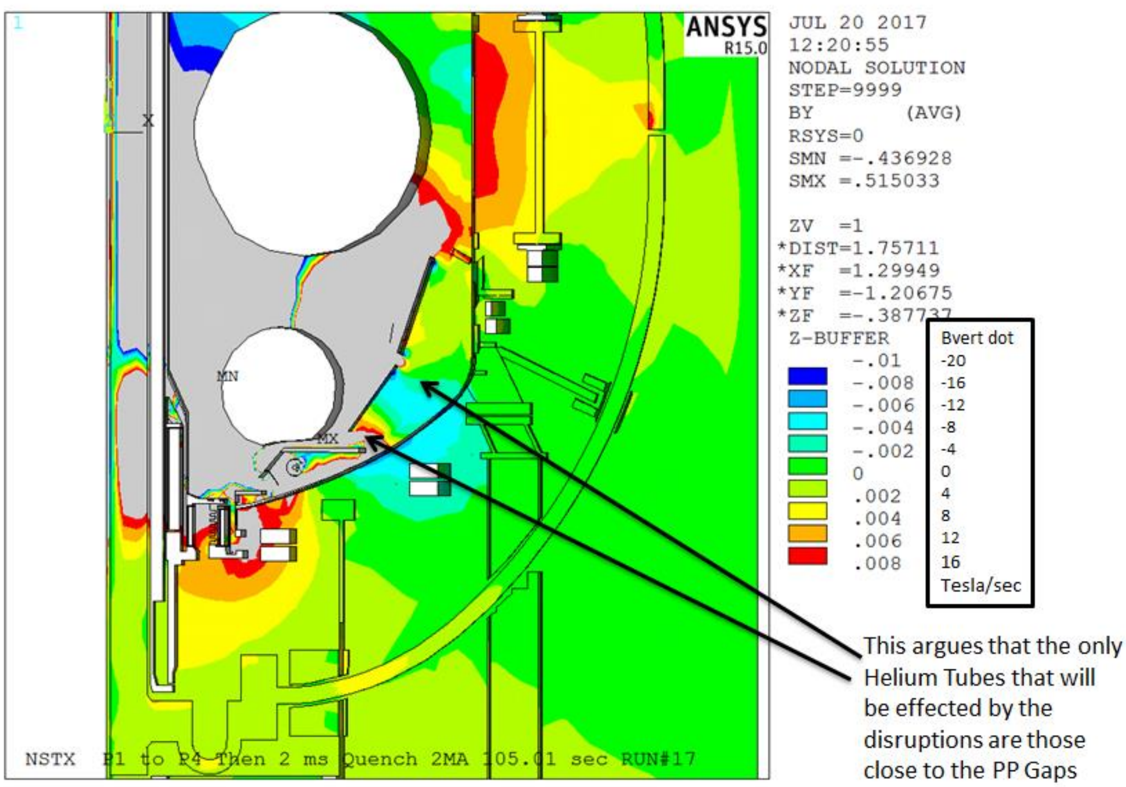

dB/dt Results Behind the Passive Plates

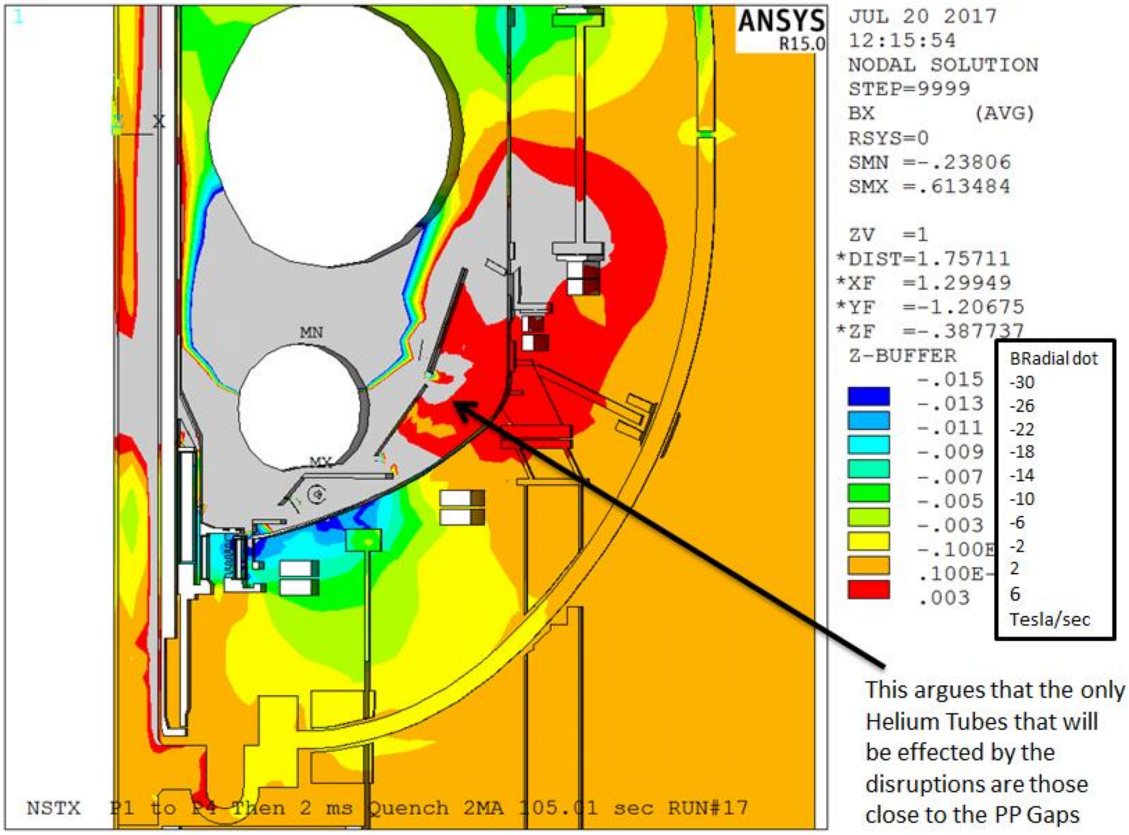

10.0 Inner PF "Sling" Eddy Currents,Lorentz Forces and Cloud Data

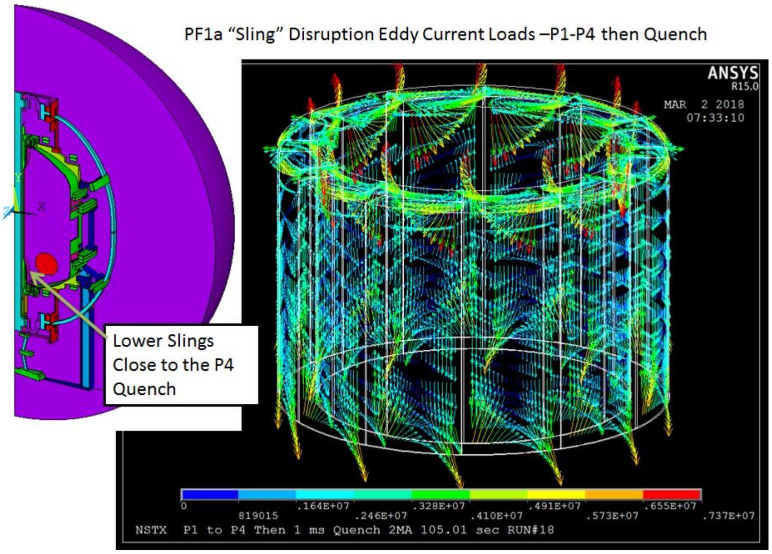

Figure 10.0-1 Sling Eddy Current Introductory Slide

The inside radius is 11.356", the outside radius is 14.330" is, the side thickness is .062", the top of the sides are 72.722" from the center plane, and the bottom of the sides is 53.698" from the center plane. The typical slide total included swept angle is 30 degrees.

The eight corners points of the cross section on plotted on the X-Y plane are:

11.356, 72.722
11.418, 72.722
14.268, 72.722
14.330, 72.722

11.356, 53.698
11.418, 53.698
14.268, 53.698
14.330, 53.698

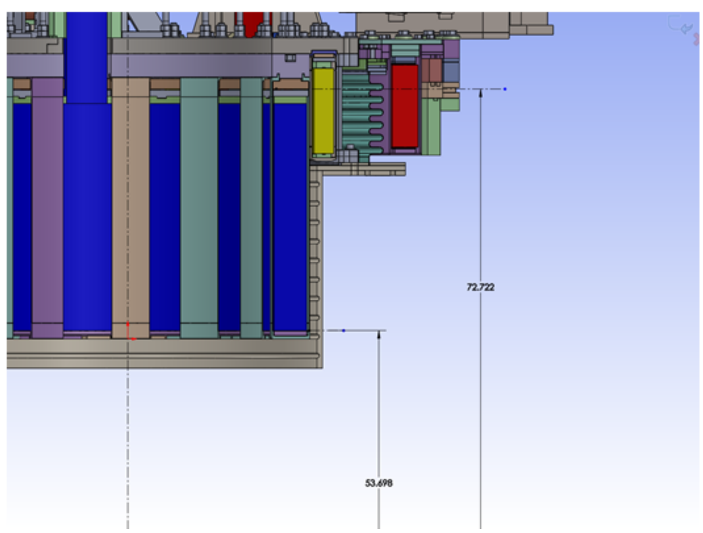

Figure 10.0-2 PF1a Sling Dimensions

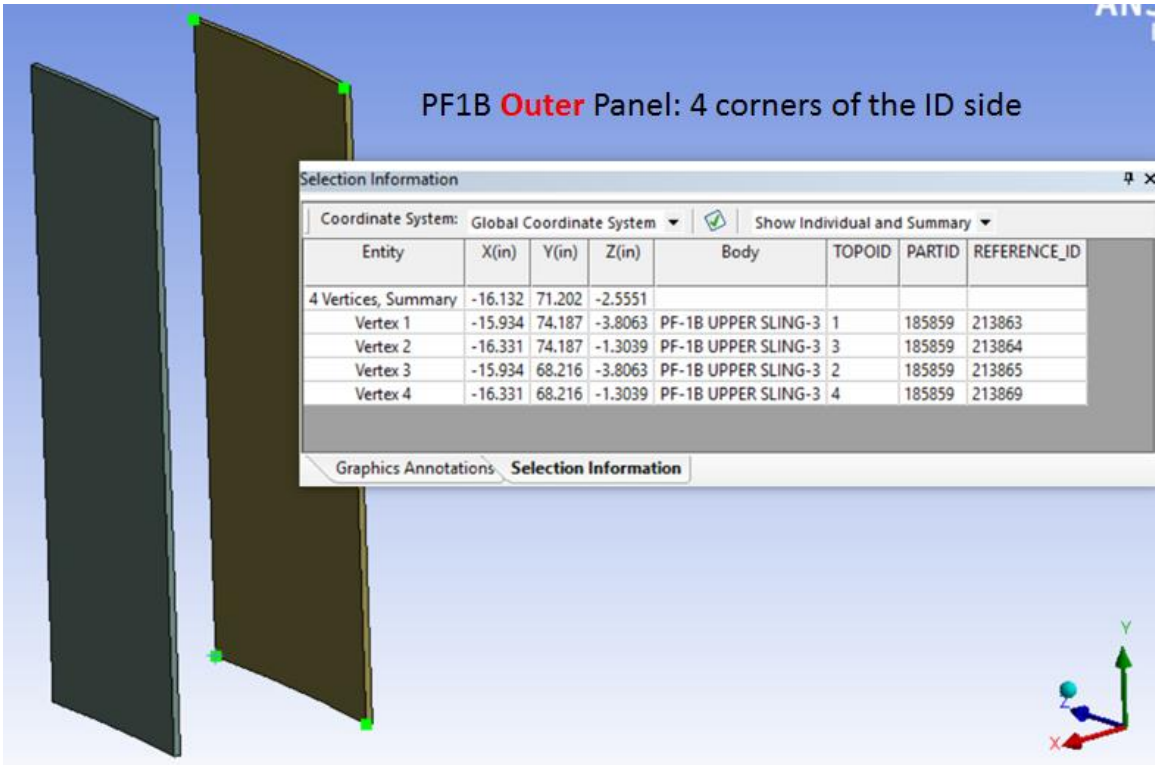

Entity	X(in)	Y(in)	Z(in)	Body	TOPOID	PARTID	REFERENCE_ID
4 Vertices, Summary	-16.132	71.202	-2.5551				
Vertex 1	-15.934	74.187	-3.8063	PF-1B UPPER SLING-3	1	185859	213863
Vertex 2	-16.331	74.187	-1.3039	PF-1B UPPER SLING-3	3	185859	213864
Vertex 3	-15.934	68.216	-3.8063	PF-1B UPPER SLING-3	2	185859	213865
Vertex 4	-16.331	68.216	-1.3039	PF-1B UPPER SLING-3	4	185859	213869

Figure 10.0-3 PF1a Sling Outer Panel Coordinates

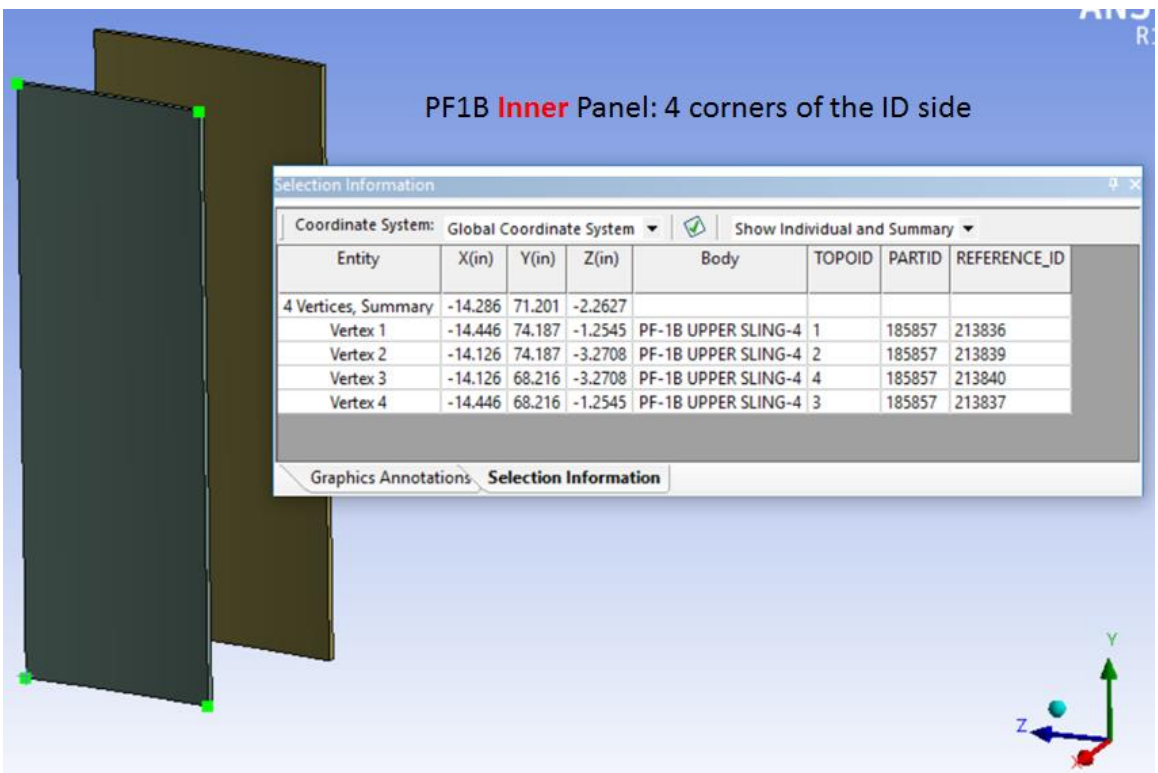

Entity	X(in)	Y(in)	Z(in)	Body	TOPOID	PARTID	REFERENCE_ID
4 Vertices, Summary	-14.286	71.201	-2.2627				
Vertex 1	-14.446	74.187	-1.2545	PF-1B UPPER SLING-4	1	185857	213836
Vertex 2	-14.126	74.187	-3.2708	PF-1B UPPER SLING-4	2	185857	213839
Vertex 3	-14.126	68.216	-3.2708	PF-1B UPPER SLING-4	4	185857	213840
Vertex 4	-14.446	68.216	-1.2545	PF-1B UPPER SLING-4	3	185857	213837

Figure 10.0-4 PF1aSling Inner Panel Coordinates

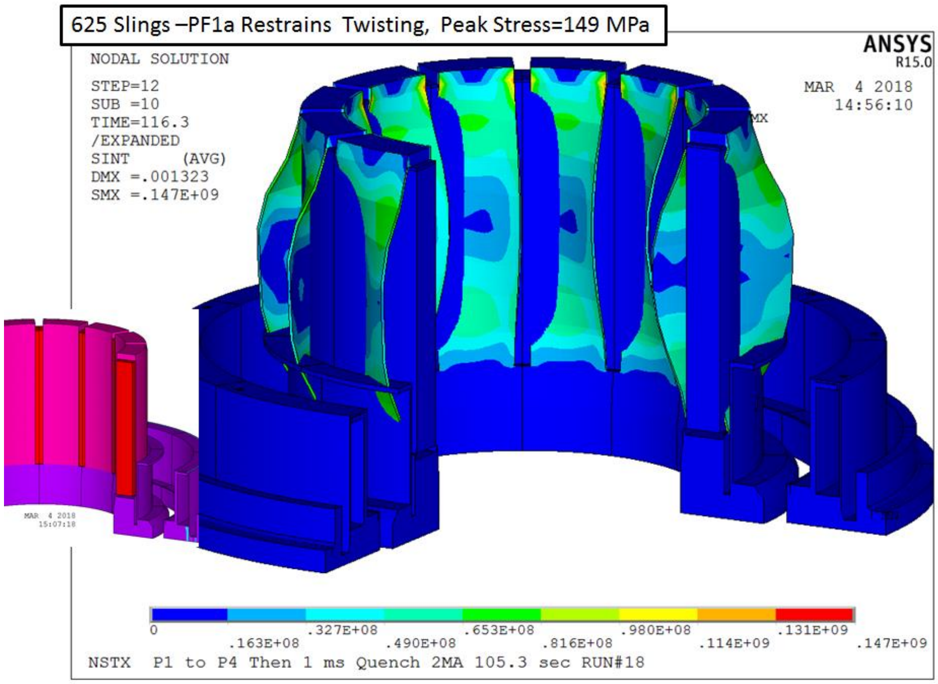
625 Slings –PF1a Restrains Twisting, Peak Stress=149 MPa
ANSYS
R15.0
NODAL SOLUTION
STEP=12
SUB =10
TIME=116.3
/EXPANDED
SINT (AVG)
DMX =.001323
SMX =.147E+09
MAR 4 2018
14:56:10
MX
0
.163E+08
.327E+08
.490E+08
.653E+08
.816E+08
.980E+08
.114E+09
.131E+09
.147E+09
NSTX P1 to P4 Then 1 ms Quench 2MA 105.3 sec RUN#18

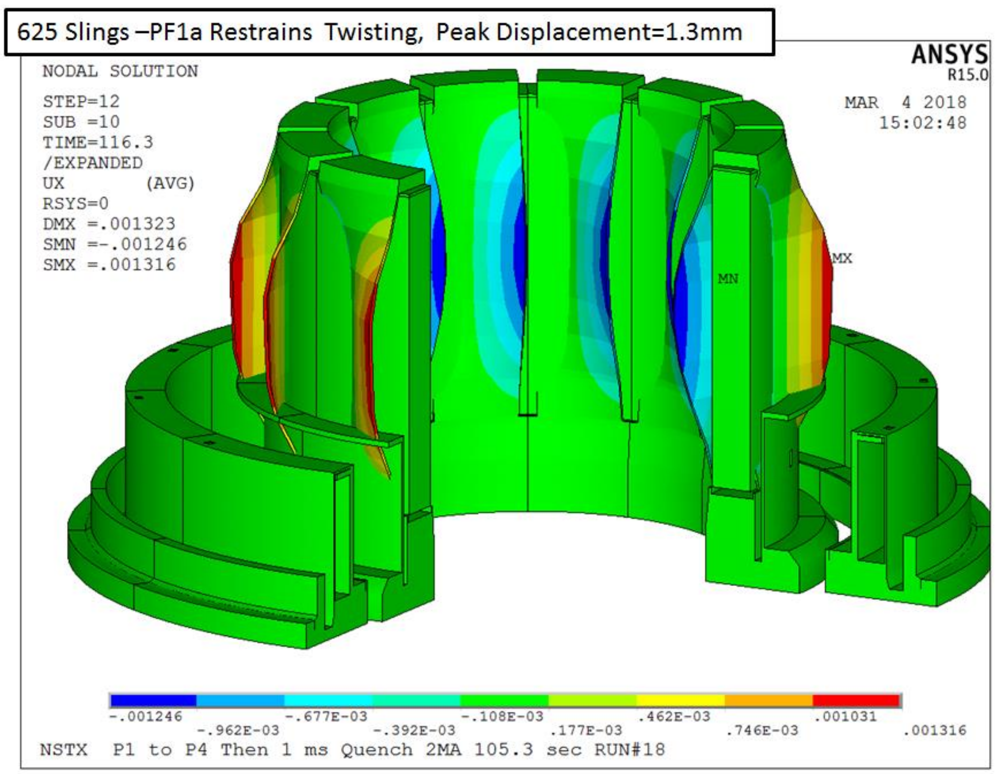
625 Slings –PF1a Restrains Twisting, Peak Displacement=1.3mm
ANSYS
R15.0
NODAL SOLUTION
STEP=12
SUB =10
TIME=116.3
/EXPANDED
UX (AVG)
RSYS=0
DMX =.001323
SMN =-.001246
SMX =.001316
MAR 4 2018
15:02:48
MX
MN
-.001246
-.962E-03
-.677E-03
-.392E-03
-.108E-03
.177E-03
.462E-03
.746E-03
.001031
.001316
NSTX P1 to P4 Then 1 ms Quench 2MA 105.3 sec RUN#18

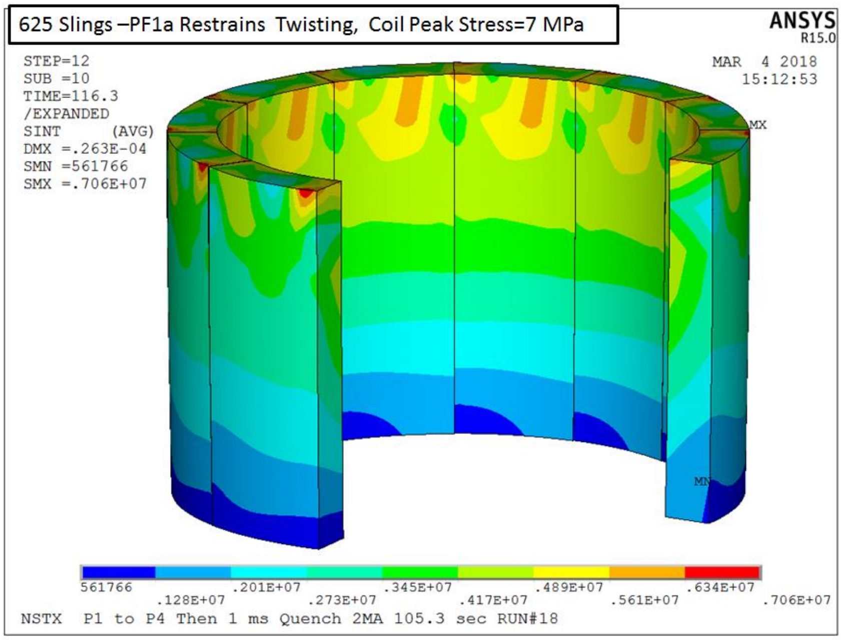
625 Slings –PF1a Restrains Twisting, Coil Peak Stress=7 MPa
ANSYS
R15.0
STEP=12
SUB =10
TIME=116.3
/EXPANDED
SINT (AVG)
DMX =.263E-04
SMN =561766
SMX =.706E+07
MAR 4 2018
15:12:53
MX
MN
561766
.128E+07
.201E+07
.273E+07
.345E+07
.417E+07
.489E+07
.561E+07
.634E+07
.706E+07
NSTX P1 to P4 Then 1 ms Quench 2MA 105.3 sec RUN#18

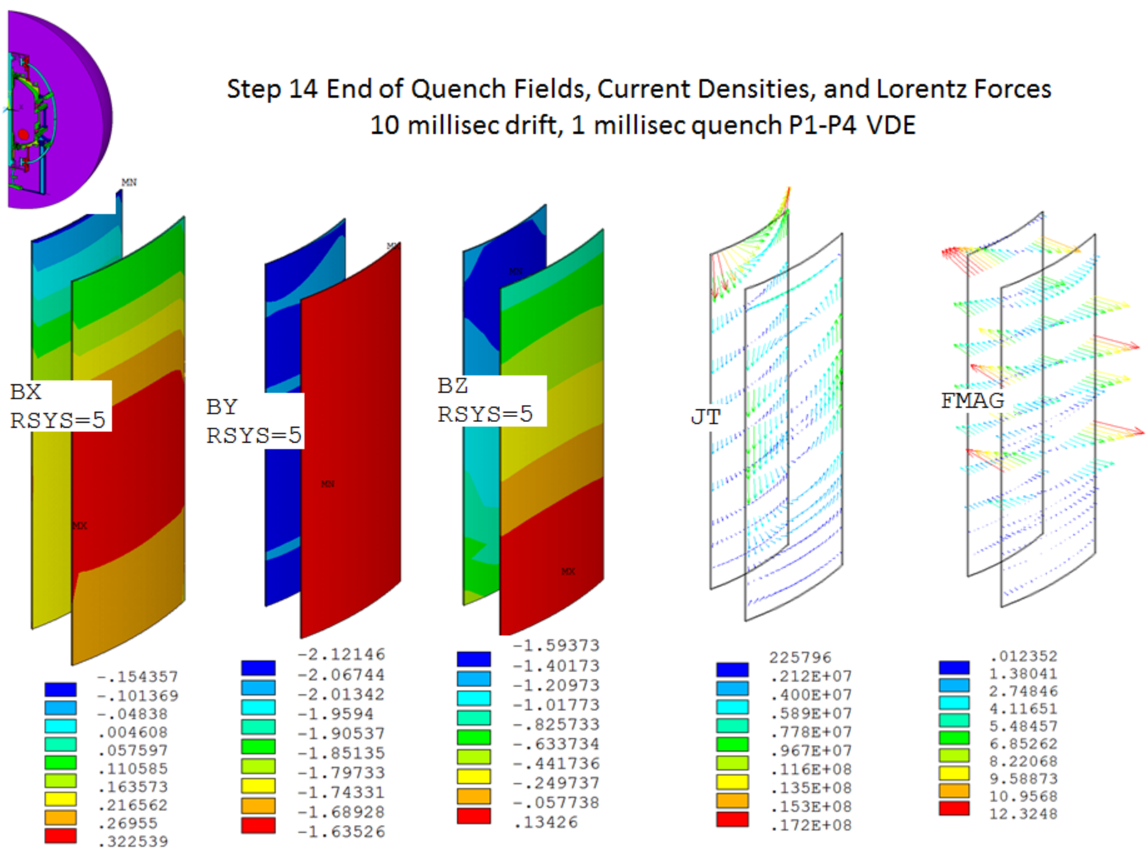
Step 14 End of Quench Fields, Current Densities, and Lorentz Forces
10 millisec drift, 1 millisec quench P1-P4 VDE
BX
RSYS=5
BY
RSYS=5
BZ
RSYS=5
JT
FMAG
-.154357
-.101369
-.04838
.004608
.057597
.110585
.163573
.216562
.26955
.322539
-2.12146
-2.06744
-2.01342
-1.9594
-1.90537
-1.85135
-1.79733
-1.74331
-1.68928
-1.63526
-1.59373
-1.40173
-1.20973
-1.01773
-.825733
-.633734
-.441736
-.249737
-.057738
.13426
225796
.212E+07
.400E+07
.589E+07
.778E+07
.967E+07
.116E+08
.135E+08
.153E+08
.172E+08
.012352
1.38041
2.74846
4.11651
5.48457
6.85262
8.22068
9.58873
10.9568
12.3248

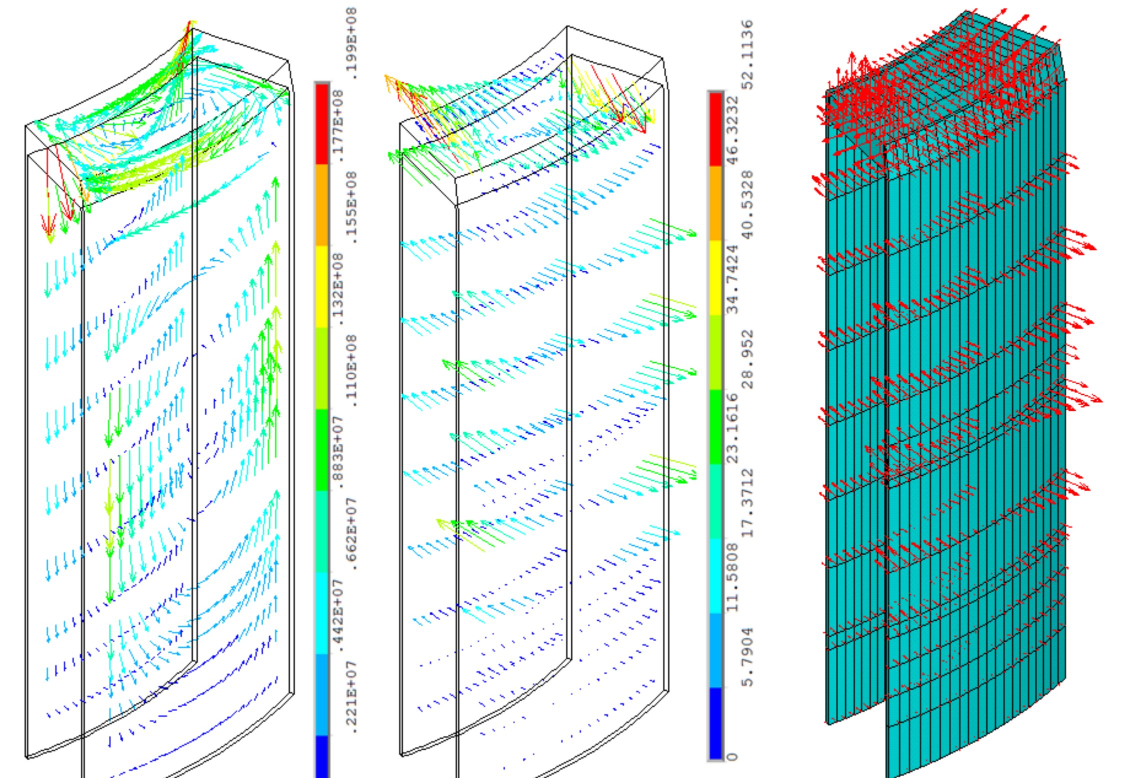

EMAG Cur Dens, Step 12

EMAG Forces, Step 12

Structural Pass Loads, Step 12

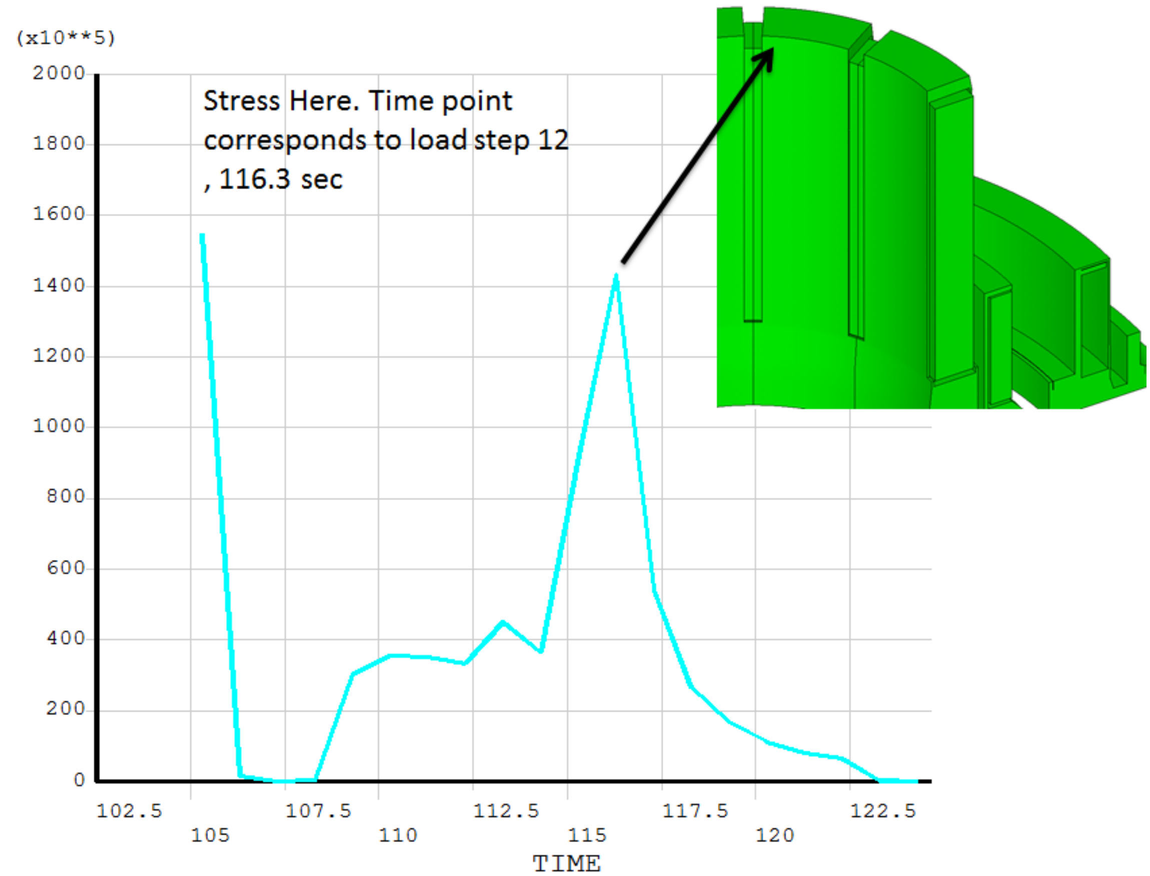


```
!In this table, the i variable will be the starting plasma volume
!           the p variable will be the end plasma volume before quench
t1= 0.100000   $i1=.01e6    $p1=0.0e6
t2= 104.90000  $i2=1.0e6    $p2=0.0001e6
t3= 105.000000 $i3=1.0e6    $p3=0.0001e6
t4= 105.0025   $i4=.75e6    $p4=0.25e6
t5= 105.0050   $i5=.5e6     $p5=0.5e6
t6= 105.0075   $i6=.25e6    $p6=0.75e6
t7= 105.01     $i7=0.001    $p7= 1.0e6        !End of Drift

t8= 105.010125 $i8=0.001    $p8= 0.875e6
t8= 105.01+quenchtime/8
t9= 105.01025  $i9=0.001    $p9= 0.75e6
t9= 105.01+2*quenchtime/8
t10=105.010325 $i10=0.001   $p10= 0.625e6
t10=105.01+3*quenchtime/8
t11=105.0105   $i11=0.001   $p11=0.5e6
t11=105.01+4*quenchtime/8
t12=105.010625 $i12=0.001   $p12= 0.375e6
t12=105.01+5*quenchtime/8
t13=105.01075  $i13=.001    $p13=0.25e6
t13=105.01+6*quenchtime/8
t14=105.0108125 $i14=.001   $p14= 0.18750e6
t14=105.01+7*quenchtime/8
t15=105.010875 $i15=.001    $p15=0.125e6
t15=105.01+8*quenchtime/8
t16=105.0109375 $i16=.001   $p16= 0.0625e6
t16=105.01+9*quenchtime/8             !End of Quench

t17=105.015    $i17=.001    $p17=0.001
t18=105.016    $i18=.001    $p18=0.001
t19=105.017    $i19=.001    $p19=0.001
t20=105.018    $i20=.001    $p20=0.001
t21=105.1      $i21=.001    $p21= 0.001
t22=105.2      $i22=.001    $p22= 0.001
t23=105.3      $i23=.001    $p23= 0.001
nsubst,20,20,3
```

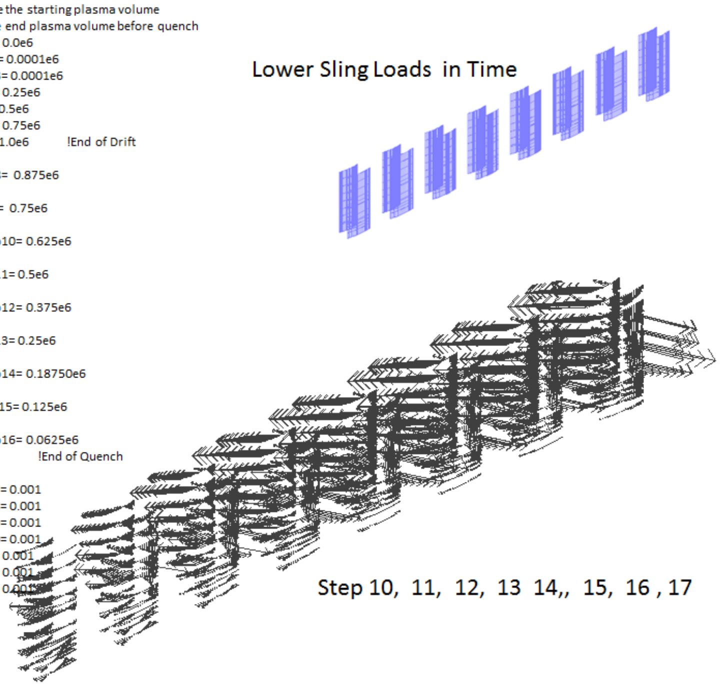

The files that were sent to Tom Willard were for the 30 degree cyclic symmetry model. My panel is actually +/- 12.5 degrees - not far from your 20 degree panel. The loads will map onto your 20 degree model and will "miss" the edges, but the loading should be pretty good for the larger panel.

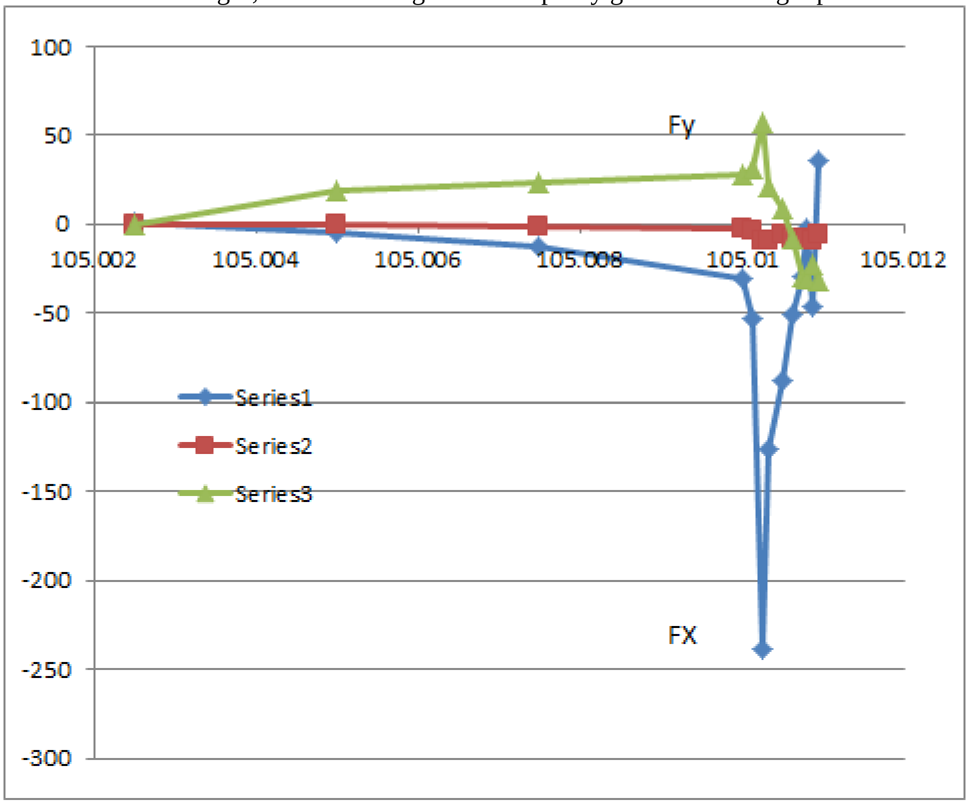

Outer Panel Force per Panel in Machine Global Cartesian System, FX Radial and FY Vertical in Newtons

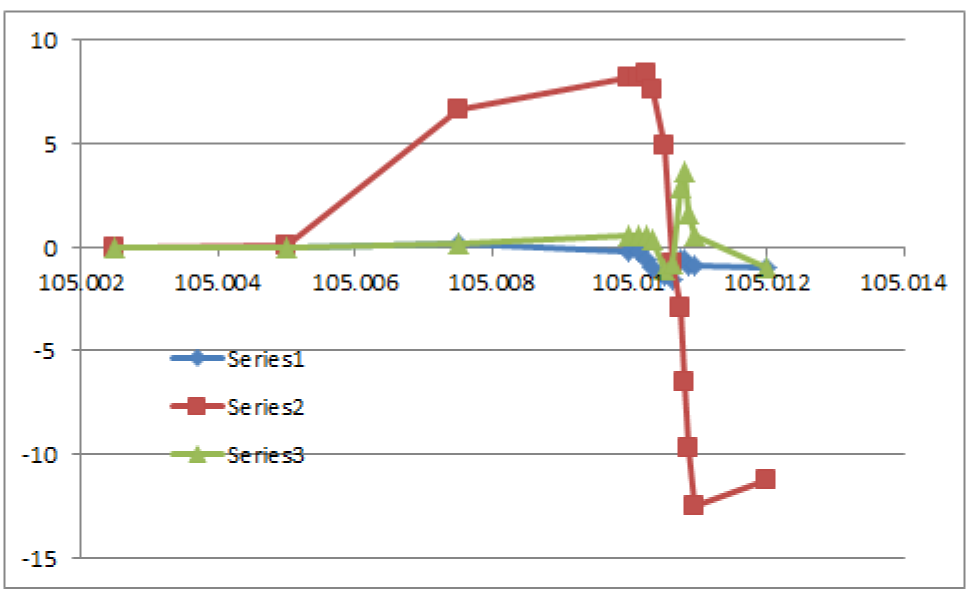

PFP1a Outer Panel Moments per panel in Machine Global Cartesian System Moments About the Centroid of the Outer Panel in Newton-meters

An EXCEL load summary for the lower PF1a outer sling panel was provided to Mark. l. If we can show proper mapping of loads to the outer panel , for the PDR we could assume the mapping is good for all the panels. Moments have been calculated at the panel center and the global moments are also included. The time history has 24 load steps. I haven't given you all of them. If you are doing a time transient you may want more load files. The simulation is done self consistently in EMAG - no vector potential transfer. a 10 millisec drift, 1 millisec quench P1-P4 VDE is simulated. I am not sure that the load distributions lend themselves to be applied as a "smeared" force and moment in Workbench. Let me know if you want the inner panel - the cloud data previously sent has inner and outer panels of the PF1aL sling support

The biggest effect is the vertical currents in the eddy currents in the sling panel crossing the toroidal field Most of the toroidal currents that would cross the poloidal field occur in the thick end flanges. It is a similar situation with the bellows. The load with the toroidal field was 6000 lbs and the load with toroidal field and poloidal field was 7000 lbs with eq 79. The problem with the slings and bellows is that they are very thin and easily stressed by even small eddy currents.

PF1b Slings

The PF1b slings were included in the EMAG model. The 30 degree cyclic symmetry model has one 25 degree PF1a sling and two 11.25 degree PF1b slings. This is assumed from pictures I have seen of the PF1b slings and is representative of the larger pf1a panel in your design. Shown below is a symmetry expansion. The stresses in the PF1b slings are a small fraction of those experienced by the PF1a slings. The reasons are obvious from the plot. The b panels are much much smaller in both angular extent and height and pick up much less flux change. Their bending stress is a function of the square of the dimensions and thus is smaller by a large factor. As long as the width of the PF1b panel is not substantially different than what I modeled, I think PF1b sling disruption eddy currents can be neglected. I can produce cloud data for PF1b slings. Rather, I would encourage the PF1a sling data be used on your model. -Peter

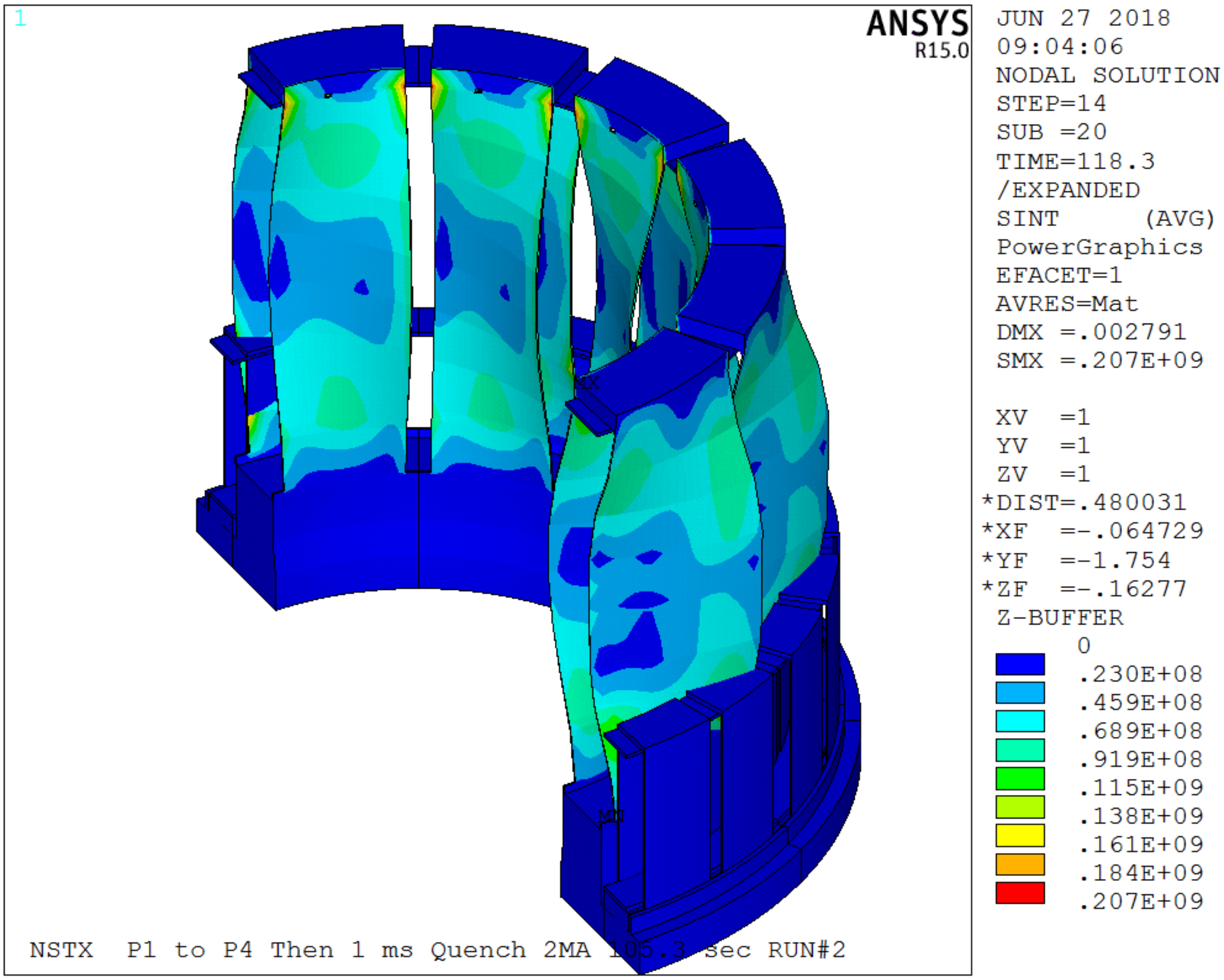
1
ANSYS
R15.0
JUN 27 2018
09:04:06
NODAL SOLUTION
STEP=14
SUB =20
TIME=118.3
/EXPANDED
SINT (AVG)
PowerGraphics
EFACET=1
AVRES=Mat
DMX =.002791
SMX =.207E+09
XV =1
YV =1
ZV =1
*DIST=.480031
*XF =-.064729
*YF =-1.754
*ZF =-.16277
Z-BUFFER
0
.230E+08
.459E+08
.689E+08
.919E+08
.115E+09
.138E+09
.161E+09
.184E+09
.207E+09
NSTX P1 to P4 Then 1 ms Quench 2MA 105.3 sec RUN#2

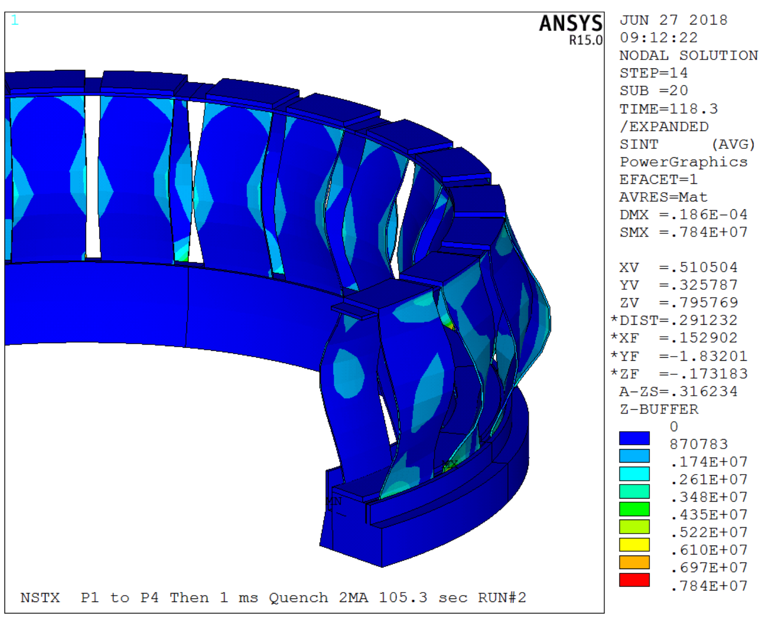
1
ANSYS
R15.0
JUN 27 2018
09:12:22
NODAL SOLUTION
STEP=14
SUB =20
TIME=118.3
/EXPANDED
SINT (AVG)
PowerGraphics
EFACET=1
AVRES=Mat
DMX =.186E-04
SMX =.784E+07
XV =.510504
YV =.325787
ZV =.795769
*DIST=.291232
*XF =.152902
*YF =-1.83201
*ZF =-.173183
A-ZS=.316234
Z-BUFFER
0
870783
.174E+07
.261E+07
.348E+07
.435E+07
.522E+07
.610E+07
.697E+07
.784E+07
NSTX P1 to P4 Then 1 ms Quench 2MA 105.3 sec RUN#2

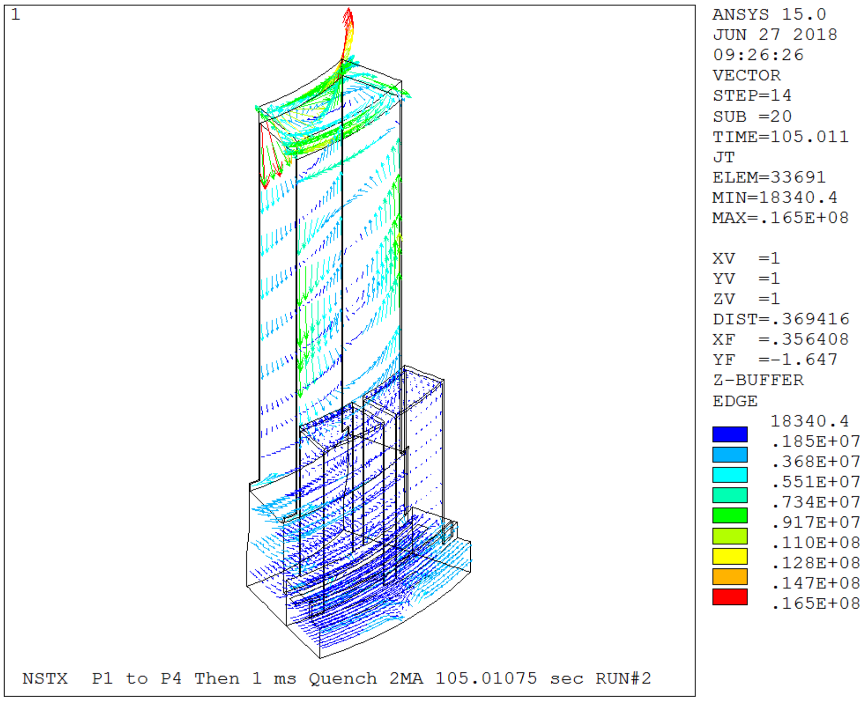

11.0 Heat Transfer Plates

The heat transfer plate is intended to provide local heating of the divertor tiles during bake-out to ensure achieving the required 350 C bake. The heat transfer plate is also used to remove heat during normal operation.

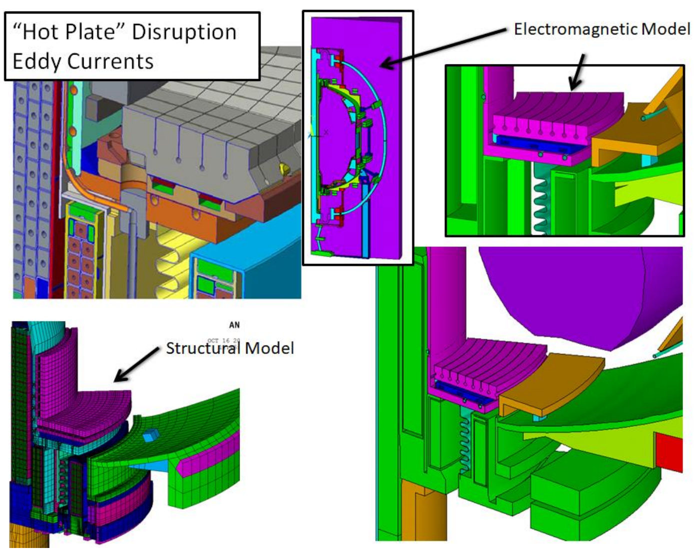

Figure 11.0-1 Heat Transfer Plate Models – Solid top left EMAG Top Right, Structural Lower Left, and an EMAG detail Lower Right

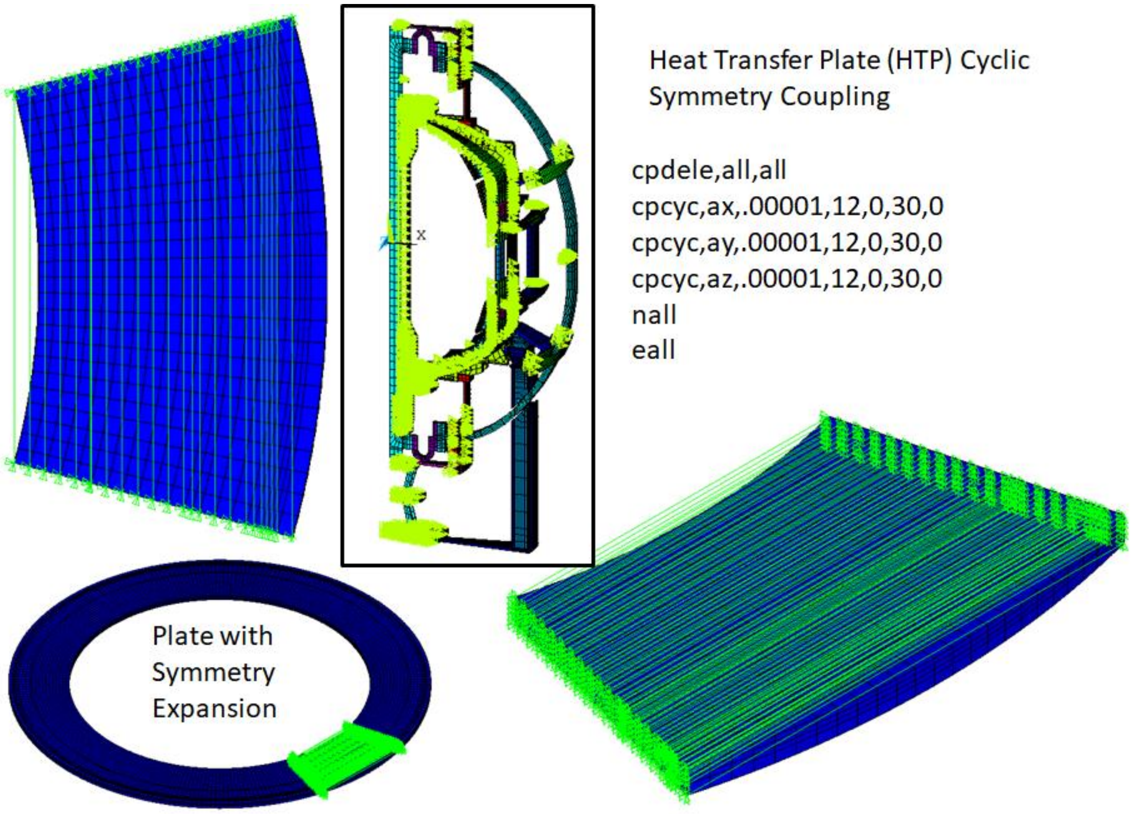

Figure 11.0-2 AX,AY,AZ Coupled Sets

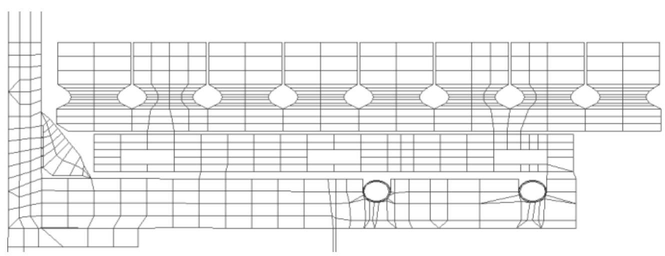

Figure 11.0-3 2D Cross Section of the HTP from the EMAG Model

The plate is electrically, toroidally continuous – or made so by the connections to the casing divertor flange. Eddy currents are primarily toroidal, although the interior cooling channels are more complex than the swept geometry shown in the model. . For both the eddy current and halo current loading, the poloidal fields were taken from a sweep of the 96 EQ and all disruption scenarios by Art Brooks, done for the high heat flux tiles on the divertor plate. This is compared with Art's max tile B's and Bdots. The maximum magnitudes were used in a spreadsheet calculation and they were oriented to produce the largest tensile load on the studs. Art's calculation for the tile B’s and Bdots is NSTXU-CALC-011-08-00 [17]. Art used SPARK in an analysis that included passive structure shielding, and I checked it with static field calculations with the plasma at P4. The halo loads were calculated by hand (spreadsheet) from the halo specs from Stefan. The eddy current EMAG analysis had a background field from EQ 79 but it basically wasn't used. Induced eddy currents were based on P1 to P4 which was found to be the worst for the divertor area. I took the current densities - independent from the static background field and multiplied by the HTP cross sectional area - got a current, then crossed that with the max poloidal fields to get loads that were then applied to the HTP bolting. The spreadsheet calculations are in “hot plate disruption loads.xls” in my divertor directory, results from which are shown in figures 11.0-3 and 4

A 1 millisecond quench is implemented in the input of the time parameters and the parameters that inpuit the fractions of current in the P1 position and the P4 positions

t3= 105.000000 $i3= 1.0e6 $p3= 0.0001e6
t4= 105.0025 $i4= .75e6 $p4= 0.25e6
t5= 105.0050 $i5= .5e6 $p5= .5e6
t6= 105.0075 $i6= .25e6 $p6= .75e6
t7= 105.01 $i7= 0.001e6 $p7= 1.0e6
t8= 105.01025 $i8= 0.001e6 $p8= 0.75e6
t9= 105.0105 $i9= 0.001e6 $p9= 0.5e6
t10=105.01075 $i10=.001 $p10= 0.25e6
t11=105.011 $i11=.001 $p11= 0.001

So the loads are based on the worst poloidal fields of the 96 and all disruption specs. HTP eddy currents are worst in time for the P1 to P4 VDE disruption with 1 millisec quench, 10 millisec drift.

Halo loads are based on a halo fraction of .35 and a peaking factor of 2 from Stefans older halo spec, I think it might slightly lower now. Halo loads have been updated and treated in a calculation by Han Zhang

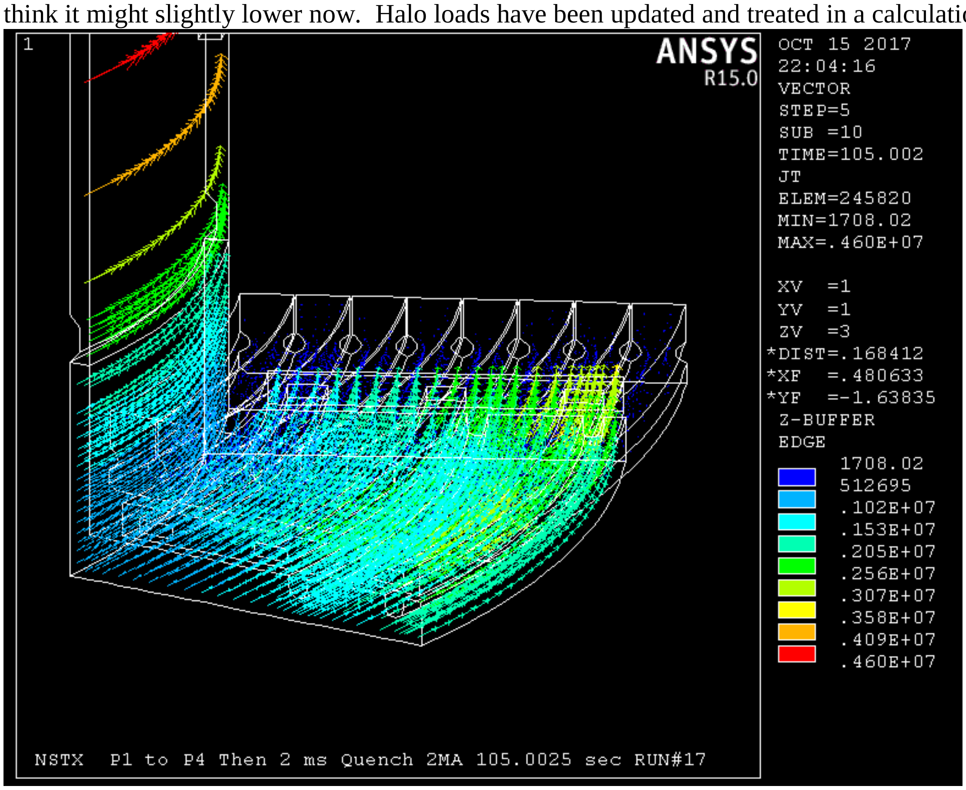

Figure 11.0-2 Heat Transfer Plate Current Density

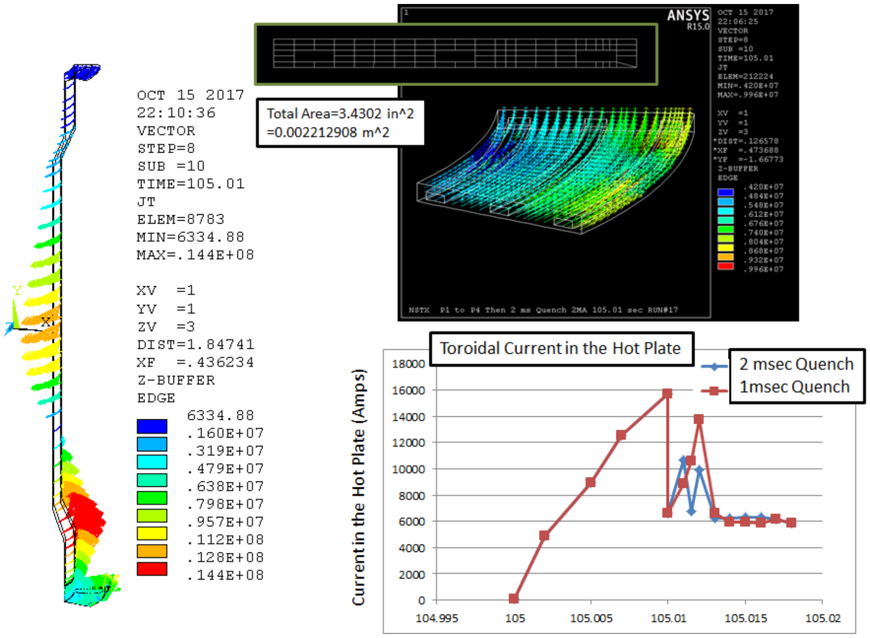

Figure 11.0-3 Model Details and Toroidal (Absolute) Current Time History

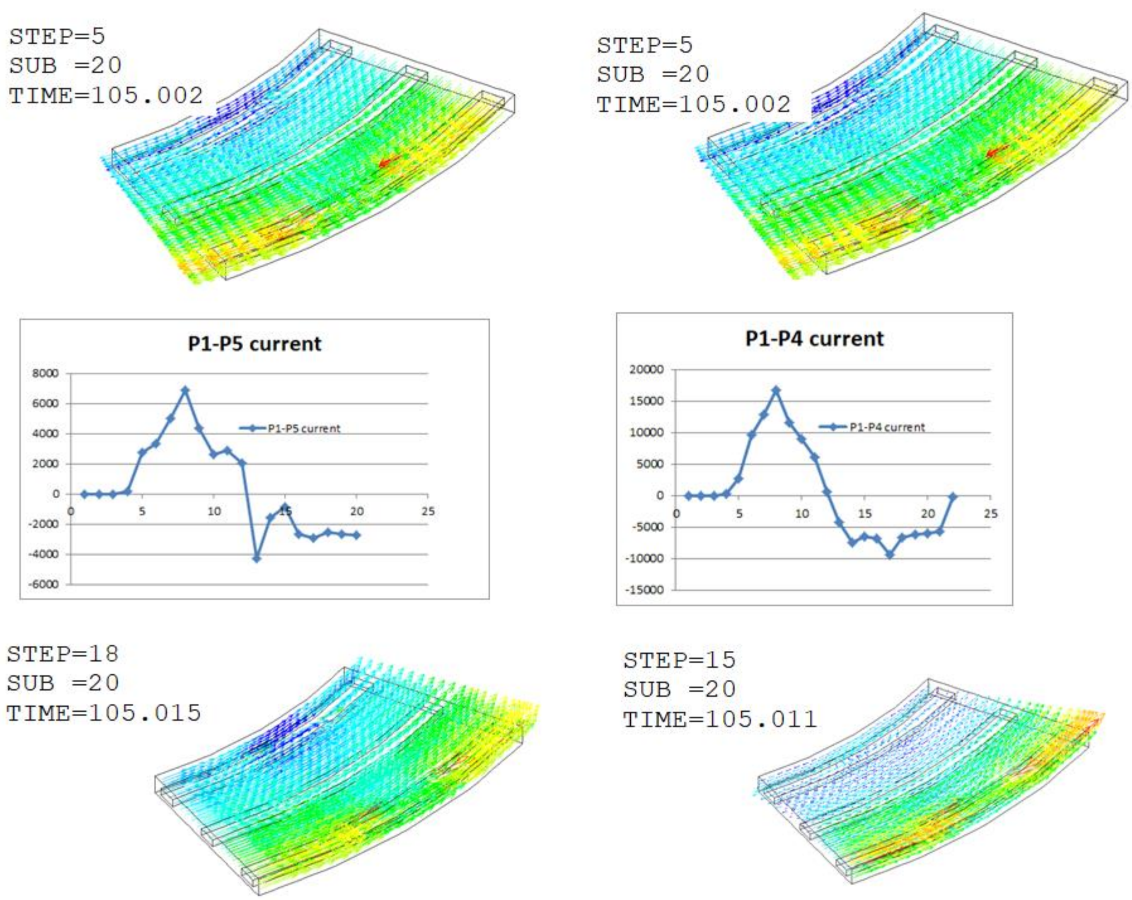

Figure 11.0-4 Toroidal Currents in the Heat Transfer Plate

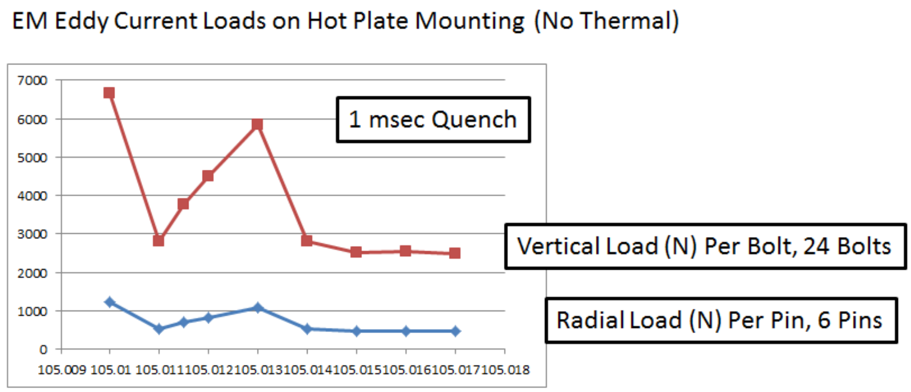

	Radius in	Ip	Hf	Peak Fact	Share Factor	Hot Plate width	Num Bolts	Btor				Halo Load per bolt N	Halo Load per bolt lbs
Halo Bolt Load:	19	2.00E+06	3.50E-01	2	0.384615	0.17780036	24	1.936175				7.72E+03	1.74E+03

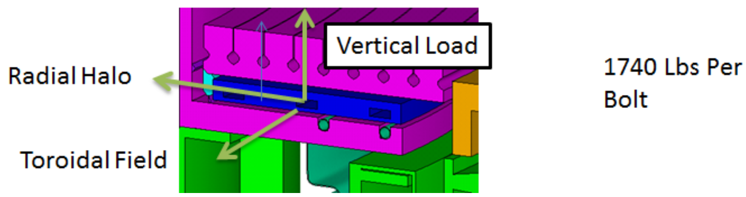

Figure 11.0-5 Radial and Vertical Load Time History

Total number of bolts is 96 for 360 degree 12 shear pins for 360 degree - check the peaking factor. Halo loads have been re-calculated by Dang Cai and Han Zhang , so this section of the calculation is being retained only for comparison and checking.

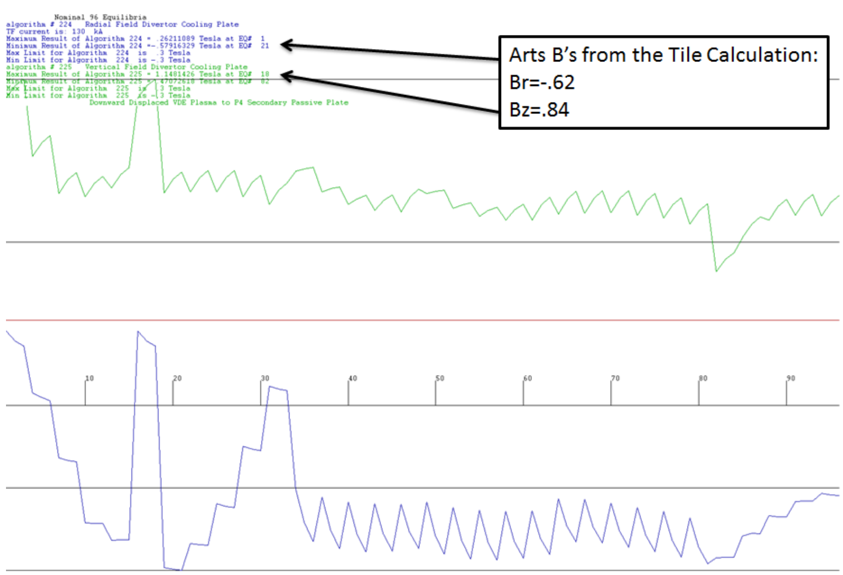

Figure 11.0-6 Worst Radial and Vertical Field Magnitudes for the HTP. The plot is from a program developed in [5] and the field values noted "from Art's Calculation are from [17]

12.0 Bellows

Loading on the bellows due to eddy currents induced in the bellows is minimal. The Bdots below the vessel near the bellows are relatively small. Currents induced in the bellows are toroidal and do not cross with the toroidal field.

Bdot for VDE and Quench at P4

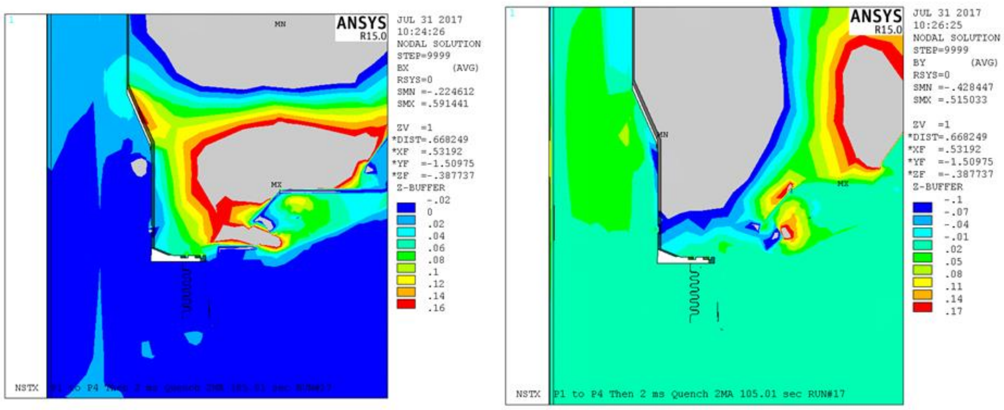

Bradial Difference, For Bdot Divide by .0005 Bvertical Difference, For Bdot Divide by .0005

Figure 12.0-1 Field Transients near the Bellows

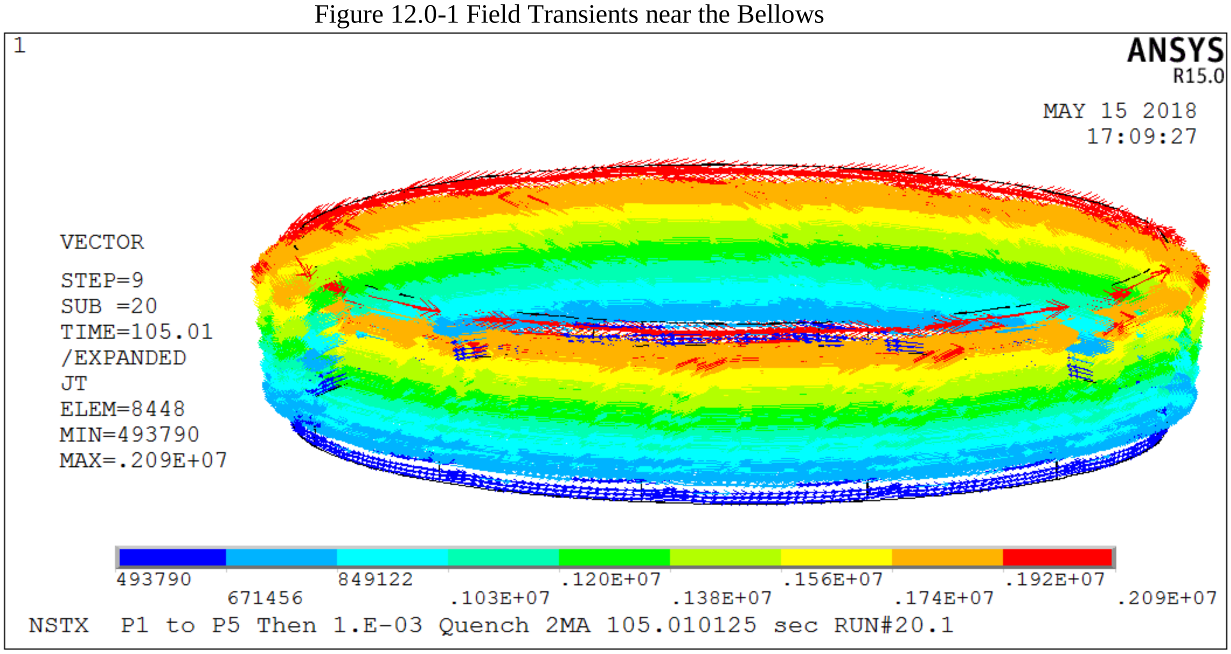

Figure 12.0-2 Results from This Calculation of Disruption Loading Using a Full EMAG Model

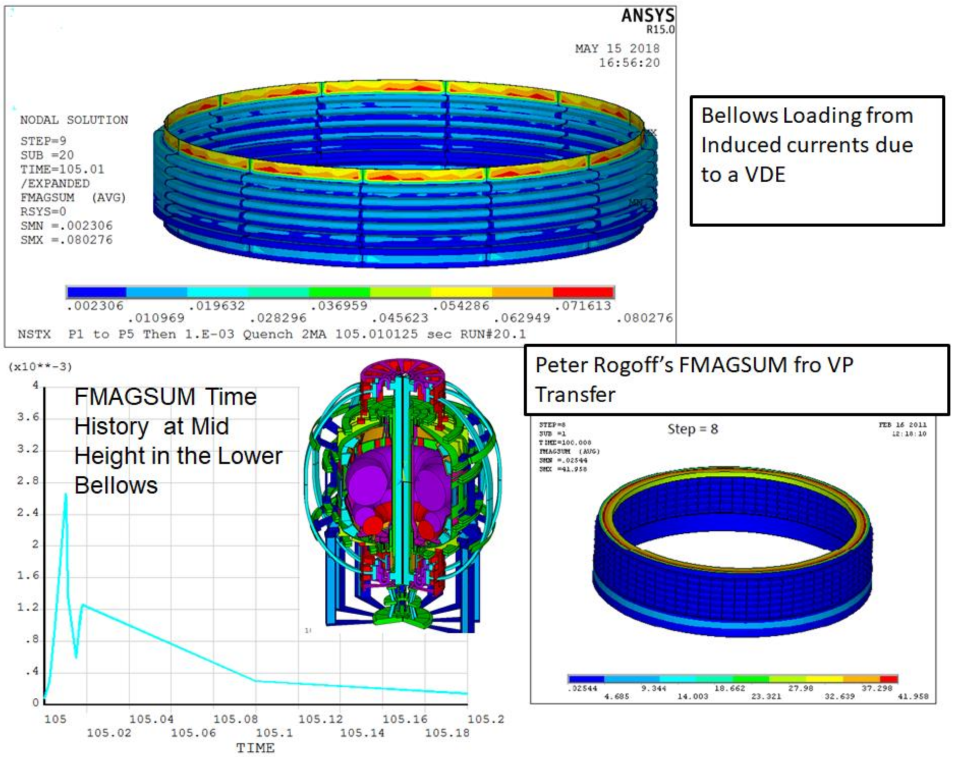

Results from P.Rogoff's Calculation of Disruption Loading Using the Vector Potential Transfer Approach

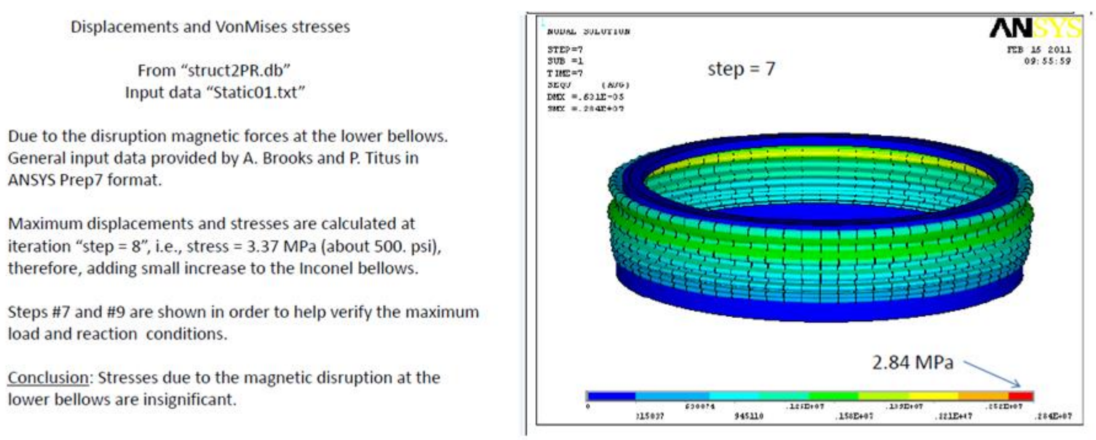

13.0 PF 4 and 5 Induced Currents and VDE Loads

A DVVR CHIT (M5-6?) was entered that questioned the possibility of different and additional loads on PF4 and 5 due to a disruption. The results of this assessment shows that the currents in PF 4 and 5 canot be altered by the VDE motion because the up-down paired coils are in series and the induced currents in the upper coil would be countered by the lower coil. However loading on PF4 and 5 U&L is increased by the VDE disruption in a manner similar to the effects on the inner PF coils caused by the plasma center shifting off the equatorial plane[19]. .

The intent of the DVVR question was to address the possibility of current changes induced in the coils from the plasma motion and quench. Mid plane disruption effects have been extensively considered in the design point spreadsheet (DPSS) and more rigorously by Woolley, considering the effects of passive structures [18]. In Woolley's simulation, the coil current changes are minor and don't occur until after the vessel currents have decayed. Woolley did not consider a VDE. The coils are designed for post disruption currents and loads in the DCPS conservatively derived by ignoring passive structures. VDE's are not considered in the DCPS. VDE loads have been a part of qualification of vessel internal components (tiles, passive plates) during the Upgrade project and were only recently included in assessments of coil loads. In this assessment, the inner PF coils and OH coils were addressed (SEI-2018 03-18PHT/AB01) [20]. An assessment of the VDE coil loads is done with static field calculations and an example by A. Brooks that considers the passive structure effects

```
*create,PF45Modify
  ! This is used to make PF4 and 5 Driven by Disruption
type,1
mat,17
real,8
esel,type,2
ersel,mat,17
ersel,real,8
emodif,all

type,1
mat,17
real,9
esel,type,2
ersel,mat,17
ersel,real,9
emodif,all
eall
nall
*end
```

In the first analysis performed to address effects on PF4 and 5, the PF4 and 5 upper and lower coils are modeled as Type 1 solid 97 elements with AX,AY,and AZ degrees of freedom. The currents in the PF 4 and 5 coils are calculated rather than being prescribed by a specific equilibria. In order to make the behavior of PF 4 and 5 optional, a macro was created that makes the conversion to Type 1 97 elements. This is implemented with the command *use,PF45Modify (See right). This analysis produced opposing currents in the upper and lower pairs of PF4 and PF5. This is physically impossible because the upper and lower PF4 coils are connected in series and the upper and lower PF5 coils are connected in series and must have the same current in them. To simulate this accurately , the external series connection and circuit through the power supplies need to be modeled. As of this writing, this hasn't been done in the EMAG simulation, but it is considered in the DCPS to some degree as a part of the DCPS post disruption current estimations. It is expected that the primary effect will be loads on the PF4 and 5 coils similar to the effects considered for the inner PF coils. There are net loads on PF4 and 5 due to the VDE which can be bounded by the static field calculations based on the VDE coil positions. This is discussed in memo SEI-2018 03-18PHT/AB01, included in the DCPS Check calculation [5] . Loads on PF4 and 5 U&L are also computed here with the EMAG disruption model with prescribed currents in the coils. This is shown in Figure 13.0-1. Figure 13.0-2 shows the results of the EMAG model with the PF4 and 5 coils changed to current regions with the VOLT degree of freedom turned on. The up-down reversal of current is apparent. Because of the non physical behavior of this, subsequent analyses went back to the prescribed currents in PF4 and 5, based on EQ 79 to get loading on the coils during the VDE. For EQ 79 only PF5 U&L are energized. This will serve as a benchmark for the static field calculations performed.

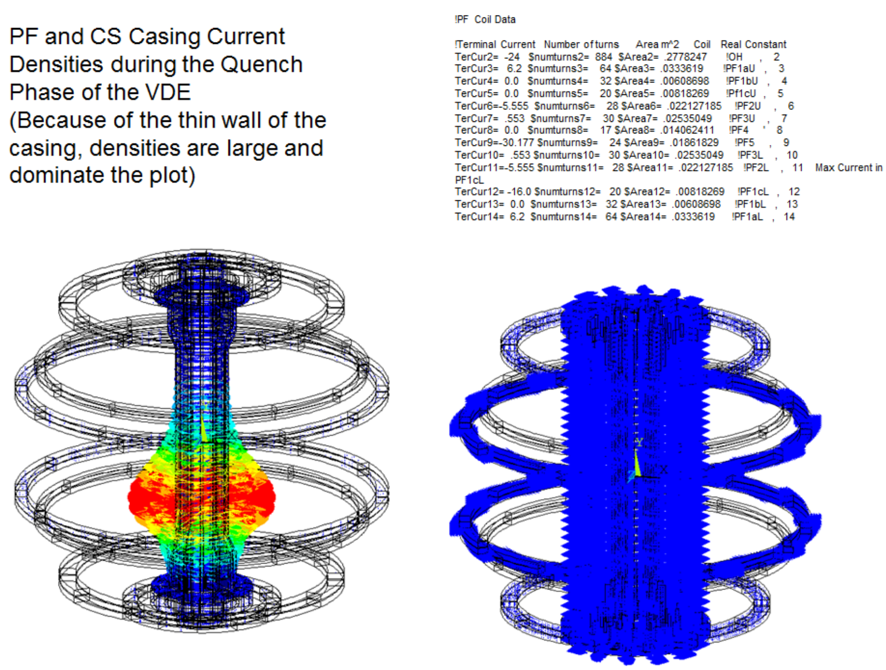

Figure 13.0-1 PF Coil Current Data (Upper Right), Plot of Input Current (Lower Right)
And Induced Casing Currents (Left)

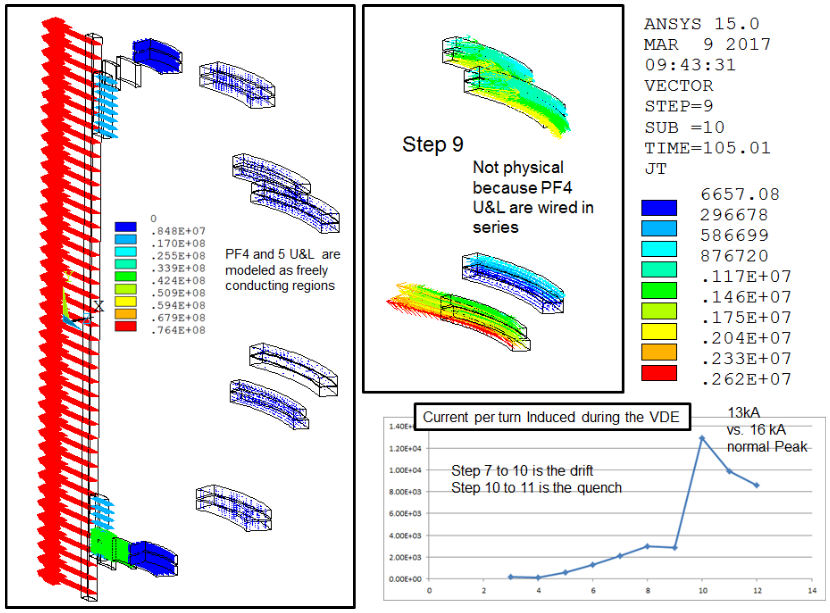

Figure 13.0-2 Results of the Analysis in which Currents are Driven in PF 4 and 5 U&L

PF5U and L are connected in series. They always attract due to their self loads. PF4 U&L also are in series and always attract to each other. It can get more complicated if PF4 and 5 are reversed in current or local interactions between upper coil pairs dominate or local interactions of the coil pairs dominate.

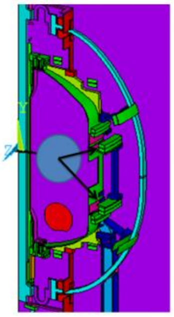

Figure 13.0-3

The Plasma and PF5 U&L have opposed currents and there is a repulsive force between them. When the plasma is at the mid plane, it pushes on PF5 U and L and increases their hoop stress and decreases the attractive force between the two coils.

The PF4,5,U&L coil group can be thought of as having a current center at the equatorial plane. Because of the opposed currents, an upward displaced plasma will push the coil group down and a downward displaced plasma will push the coil group up. With the EQ 79 background fields, these forces are +/-176,000 lbs on the coil group based on static field influence coefficients (shown in figure 13.0-5). With the plasma at the mid-plane, the vertical load on the coil group for EQ 79 is ~zero.

Based on the EMAG analysis of a downward VDE with a 10 millisecond drift, based on EQ79, with the vessel shielding effects, after the drift and before the quench, the net load is 50,000 lbs . This is shown in Figure 13.0-6. This result is similar to Art Brooks assessment of the net load on PF1a that showed the vessel currents shielded the loading substantially with respect to the static field loading.

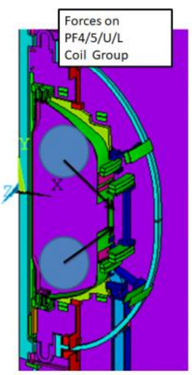

Figure 13.0-4

With a mid plane plasma position the maximum magnitude net load on the PF4/5/U/L coil group is -82,173 lbs downward for all 96 EQ. This occurs at EQ50 . This load is what the coil group vessel connections were qualified for. There are 6 PF4/5 coil support brackets connected to the vessel vs. 12 columns reacting the upper and lower coil attractions. So to include the effect of the VDE we need to add 50,000 lbs to this.

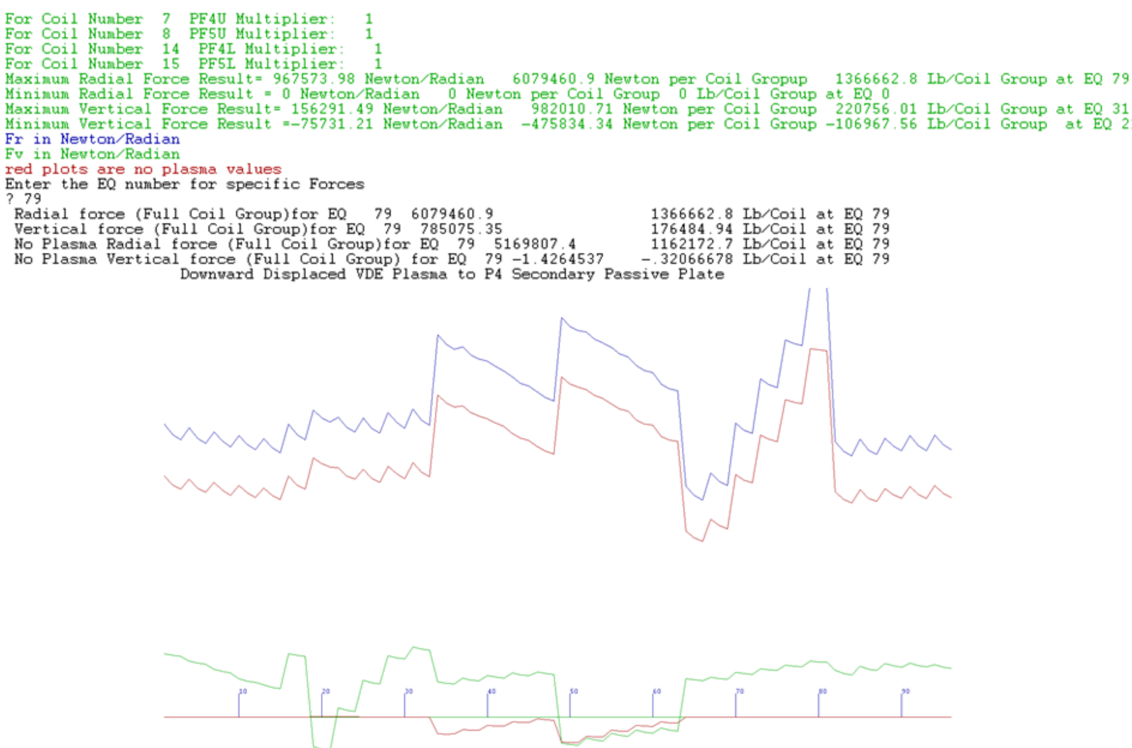

Figure 13.0-5 Coil Group PF4,5,U,L Max and Min of the 96 and EQ 79 results

Table 13.0-1 VDE to P4 Loads for (PF4U+PF5U)+(PF4L+PF5L) All 96 EQ Compared with Design Point Spreadsheet (DPSS) with Plasma

	Max Vertical	Min Vertical
Upward VDE to P4	0	-261,033
Mid Plane	1774 (DPSS Mid Plane 0.0)	-81092 (EQ50) (DPSS -82,173)
Downward VDE	220,756 (DPSS 0.0)	-106967

Table 13.0-1 VDE to P4 Loads for (PF4U+PF5U)+(PF4L+PF5L) EQ79 Compared with Design Point Spreadsheet (DPSS) with Plasma

	Max Vertical	Min Vertical
Upward VDE EQ79		-176506
MidPlane	1 (DPSS 0.0)	
Downward VDE EQ 79	176484 EMAG 50,000	EMAG -20000

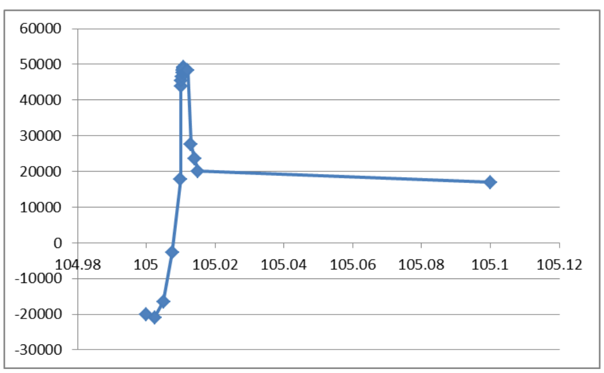

Figure 13.0-6 Net Loads on Coil Group PF4,5 U&L

The net load on the coil group PF4,5,U&L is transferred to the vessel by the 6 pairs of welded brackets. VDE loads will be increased by 50,000 lbs. with vessel shielding based on a 10 millisecond drift. It is important to note that slower drift times not specified in the GRD[7] but possible during machine operation, could allow the loading to approach the static field calculated value. Which would be up to 176506 lbs for very slow VDE drifts that do not develop vessel shielding. The GRD[7] does not require consideration of anything but the 10 millisec drift used to calculate the 50,000 lb increase, but longer drift times are likely.

These results raise the concern that the welds of the six support brackets could possibly be over-stressed. The net load is 1.6 times larger with shielding, and 3.18 times larger, without shielding, than the DPSS net load that was used to qualify the bracket weld. Note that the mid-plane vertical loads for both the DPSS and the force influence coefficients from [5] agree.

```
!   Select of PF4,5,U,L Coil Group
esel,mat,17
nelem
ersel,real,8,9
nelem

/output,nlist,lis
nlist
/output,elist,lis
elist
set,1
/output,PF45flist01,lis
PRNSOL,FMAG,COMP
set,2
/output,PF45flist02,lis
PRNSOL,FMAG,COMP
```

```
! Select of PF5Upper
esel,mat,17
nelem
ersel,real,9
nelem
nrsel,y,0,1000
enode,1

/output,nlist,lis
nlist
/output,elist,lis
elist
set,1
/output,PF5flist01,lis
PRNSOL,FMAG,COMP
set,2
/output,PF5flist02,lis
PRNSOL,FMAG,COMP
```

The next couple of figures are copied from the PF 4 and 5 support calculation[ ]. The "hand calculation" results are shown because the finite element calculations shows peak stresses in the corners that are not a static stress concern, and are unlikely to be a fatigue concern because of the low number of cycles the VDE load will be combined with the worst of the 96 EQ loads. The weld corners are included in the inspection regimen planned for the machine.

Weld Stresses Calculated From Weld Section Properties

psi	Worst Net PF4,5,U,L	Moment Sum for 6 Supports (12 U&L), 10.5" Lever	Section Modulus (in^3)	Bending Stress (psi)
Type A or B Bracket	-81953	-71708.875	13.22	-7672.237534
Type A Pad	-81953	-71708.875	47.87	-2118.800505
Type B Pad	-81953	-71708.875	36.7	-2763.677935

From Charlie's Design Point Spreadsheet

Fz(lbf)	(PF4U+PF5U)+(PF4L+PF5L)
Min w/o Plasma	-81947
Min w/ Plasma	-81953
Min Post-Disrupt	-58992
Min	-81953
Worst Case Min	-513255
Max w/o Plasma	0
Max w/ Plasma	17
Max Post-Disrupt	15
Max	17
Worst Case Max	513255

Conservatively uses PF5 moment arm and .707 factor on ¼ in weld

Figure 13.0-7 Bracket Weld Summary

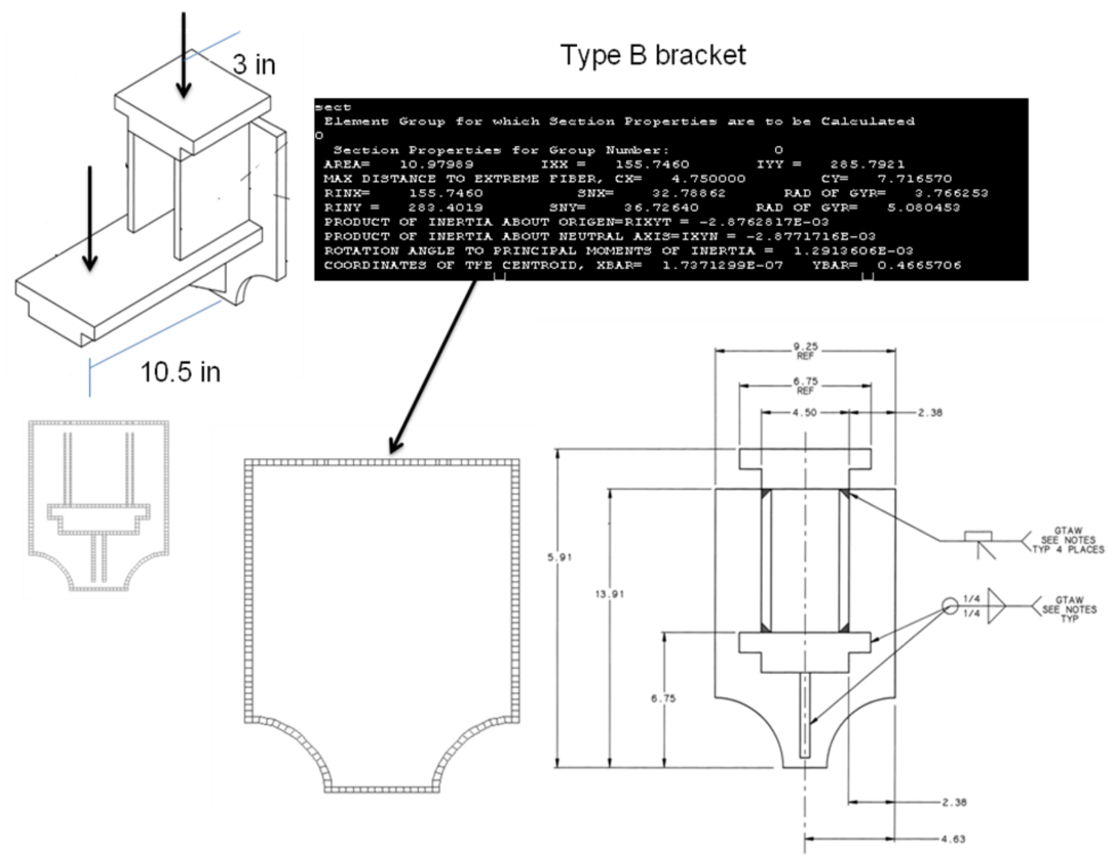

Figure 13.0-8 Weld Section Calculation from [1]

A likely operating scenario is running an up-down symmetric scenario, then having a VDE with a 10 millisec drift. This will produce a 50,000 lb load on the PF4 and 5 U&L coil group, which is less than the DPSS max load magnitude of 81953 lbs (81092 lbs from my influence coefficients)

A more troublesome situation occurs when running an up-down asymmetric scenario that has a slow drift and approaches the static field solution. The net VDE loads could go from -82173 lbs to -261,033 lbs for the upward VDE. This is an increase of 3.18 times larger vertical load . The bracket stress will be 7672*3.1 = 23783.2psi and the pad stresses go up to 6566 psi and 8565.3psi. These are still acceptable for static loading, but will aggravate fatigue life at local weld details and sharp geometries, further justifying the planned inspection regimen.

The net loads on the PF4 and 5 support hardware go up substantially. The individual coil loads also go up but less so – but still significantly. The magnitude of the vertical load (+ or -) on PF4 is -203,125lbs for the mid plane plasma position which increases in magnitude to -313,031 for the VDE Up position, or a 51% increase. For PF5 -239984 becomes -338,261 or a 41% increase.

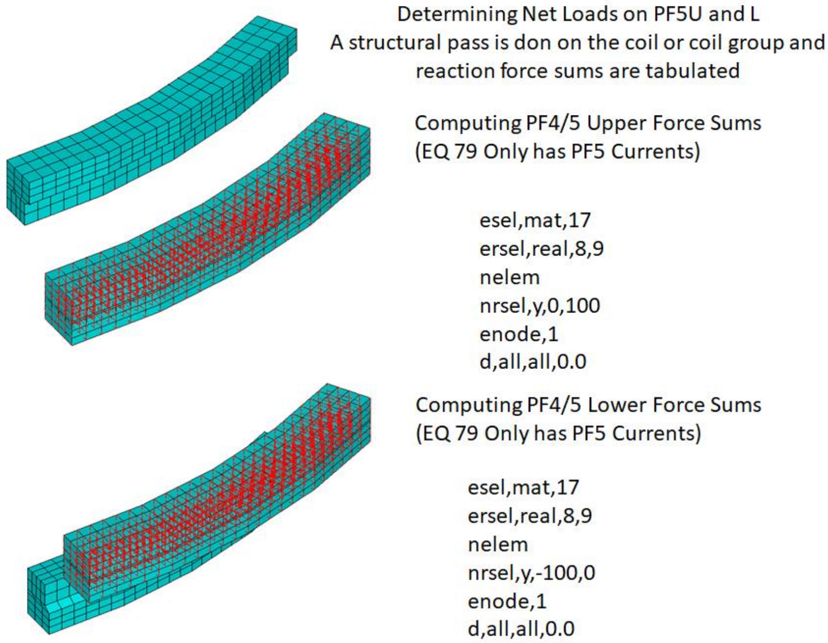

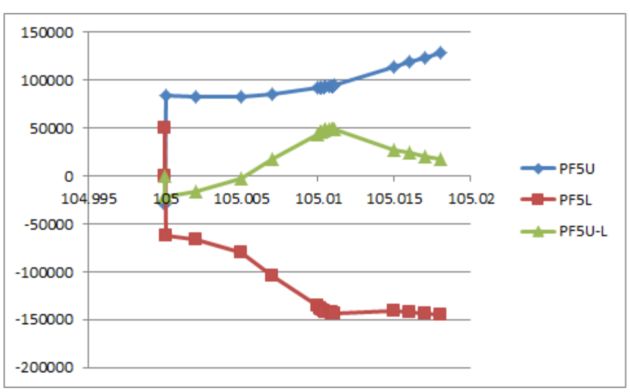

PF 5 U & L Reaction sums for EQ 79
(Negate for the load on the Coil)
P1 to P5
10 millisec drift and 1 millisec quench

The vertical load on PF5U for EQ79 is -89004 lbs with a centered plasma and the load on PF5L is 89004 lbs. The scenario is symmetric. The EMAG solution does not have the 10% headroom in it – so we should compare the net load with 80,000 In the EMAG simulation, during the disruption, the PF5U coil load goes from ~85,000 lbs to 125,000lbs, or 40000 lbs extra and the PF5L coil load goes from ~ -65000 to -145 000 or about 80,000 lbs extra

Table 13.0-2 Upward VDE to P4 Loads Compared with Design Point Spreadsheet (DPSS) with Plasma for all 96 EQ

	Max Radial (lbs)	Min Radial (lbs)	Max Vert (lbs)	Min Vert (lbs)
PF4U	286,123 (DPSS 260,144)	33,388 (DPSS -105,829)	**123,731** **(DPSS 63,458)**	**-313,031** **(DPSS -203,125)**
PF5U	683332 (DPSS 625,160)	0 (DPSS 153489)	3218 (DPSS 145,158)	-338,261 (DPSS -239,984)
PF5L	683329 (DPSS 625,247)	0 (DPSS 153522)	**338,244** **(DPSS 150,401)**	-3,227 (DPSS -49,657)
PF4L	286173 (DPSS 289,442)	-8384 (DPSS -152,181)	96,165 (DPSS 148,418)	-40,018 (DPSS -78008)

Table 13.0-2 Mid Plane With Plasma Loads Compared with Design Point Spreadsheet (DPSS) , for all 96 EQ

	Max Radial (lbs)	Min Radial (lbs)	Max Vert (lbs)	Min Vert (lbs)
PF4U	286173 (DPSS 260,144)	23626 (96) (DPSS -105,829)	90991 (31) (DPSS 63,458)	-230115 (49) (DPSS -203,125)
PF5U	637621 581086 (No Ip) (DPSS 625,160)	0 -167925 (No Ip) (DPSS 153491)	143337 60766 (no Ip) (DPSS 145,158)	-89004 -233009 (No Ip) (DPSS -150401)
PF5L	683329 581086 (DPSS 625,247)	0 -58055 (DPSS 153522)	89005 233009 (DPSS 150,401)	-143282 (19) -60767 (DPSS -145159)
PF4L	286173 (DPSS 289,442)	-84371 (DPSS -152,181)	**215583** **(DPSS 148,418)**	-91236 (DPSS -78008)

Table 13.0-3 Downward VDE to P4 Loads Compared with Design Point Spreadsheet (DPSS) with Plasma for all 96 EQ

	Max Radial (lbs)	Min Radial (lbs)	Max Vert (lbs)	Min Vert (lbs)
PF4U	286,173 (DPSS 260,144)	28030 (DPSS -105,829)	105,781 (DPSS 63,458)	-262465 (DPSS -203,125)
PF5U	683332 (DPSS 625,160)	0 (DPSS 153489)	100,277 145000(EMAG) (DPSS 145,158)	-161759 -125,000 (EMAG) (DPSS -150401)
PF5L	683329 (DPSS 625,247)	0 (DPSS 153522)	**338,244** **(DPSS 150,401)**	-3,227 (DPSS -145,159)
PF4L	286173 (DPSS 289,442)	-8384 (DPSS -152,181)	96,165 (DPSS 148,418)	-40,018 (DPSS -78008)

The coils were qualified for combinations of their max currents. The PF4 coil was qualified for a load of 174, 000 N *2 = 348000n or 70,000 lbs

PF5 is qualified for 348749N*2=697500 N or 156797 lbs

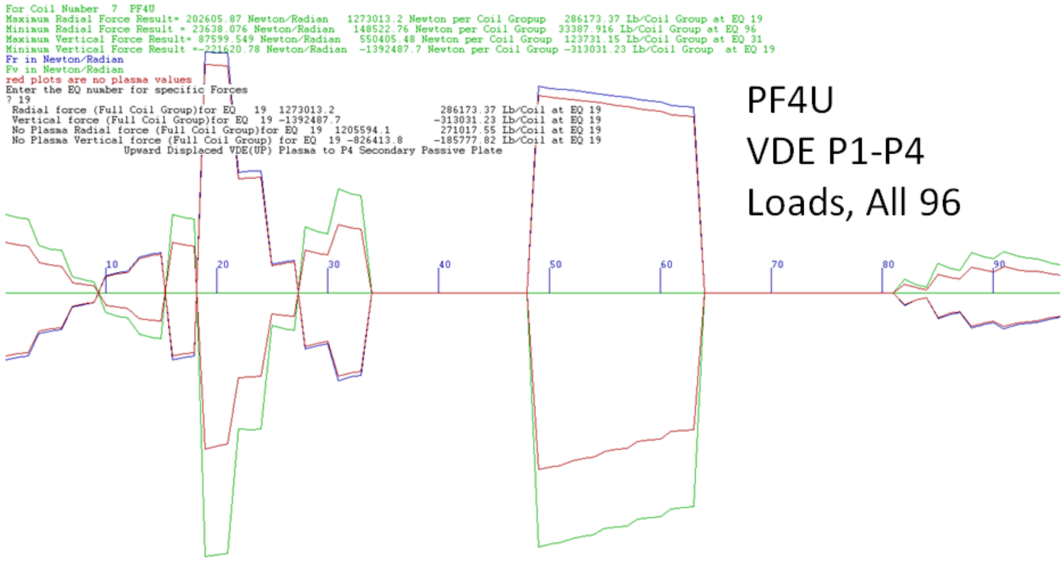

Results from the Program Described in [5]

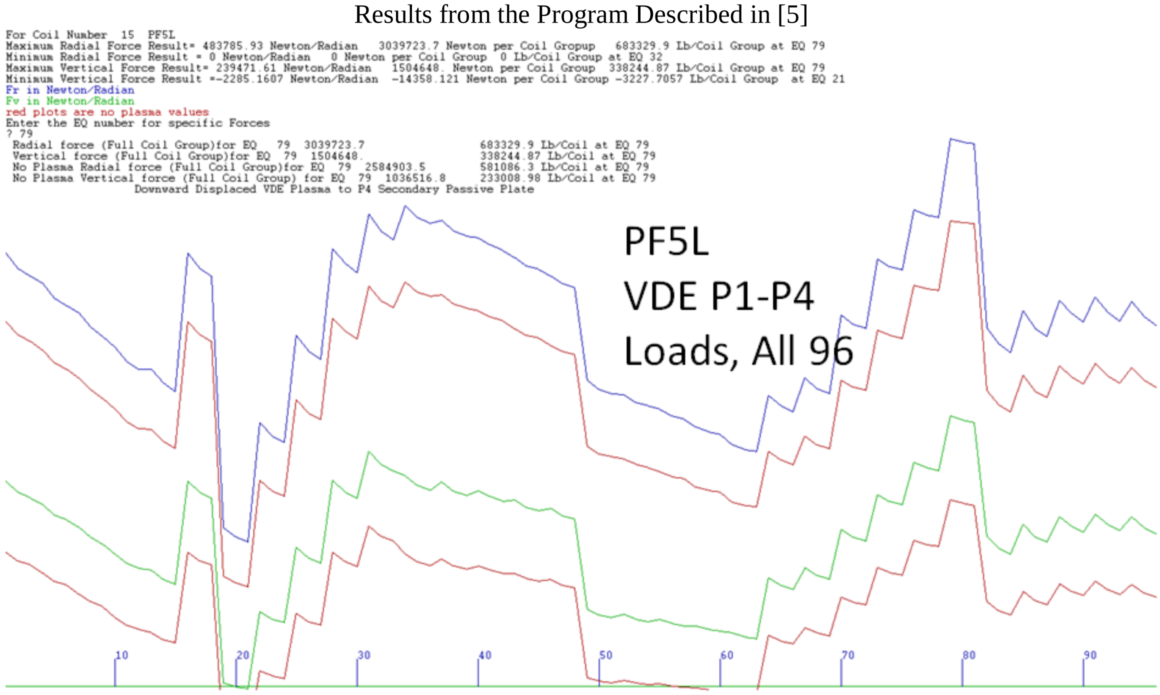

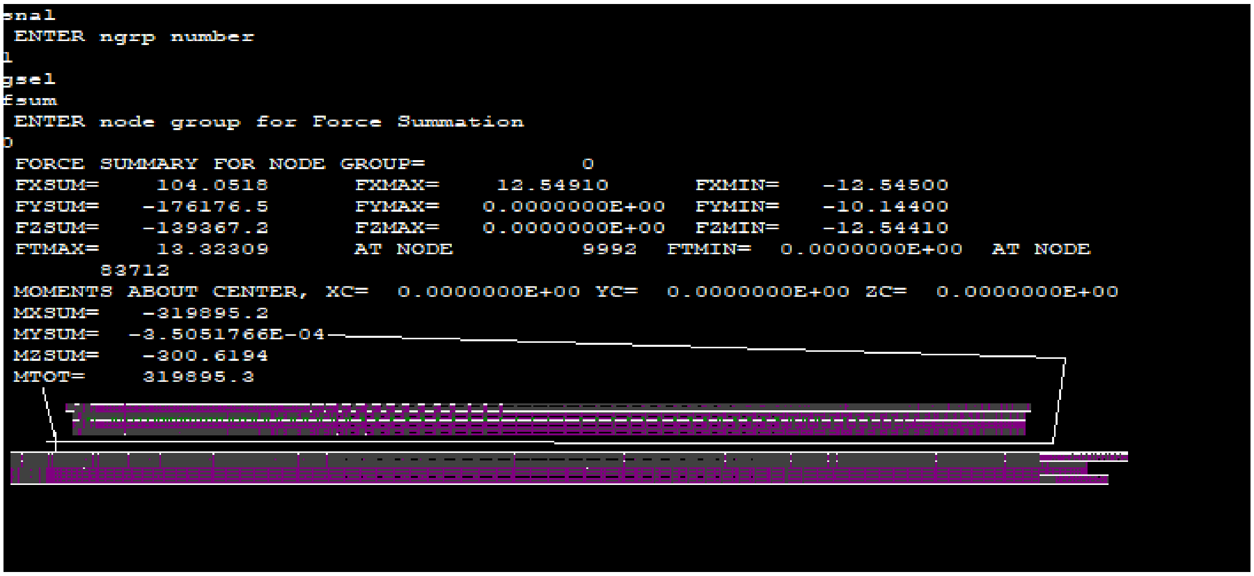

```
snal
 ENTER ngrp number
1
gsel
fsum
 ENTER node group for Force Summation
0
 FORCE SUMMARY FOR NODE GROUP=          0
 FXSUM=    104.0518       FXMAX=    12.54910       FXMIN=   -12.54500
 FYSUM=   -176176.5       FYMAX=   0.0000000E+00   FYMIN=   -10.14400
 FZSUM=   -139367.2       FZMAX=   0.0000000E+00   FZMIN=   -12.54410
 FTMAX=    13.32309       AT NODE          9992  FTMIN=  0.0000000E+00   AT NODE
       83712
 MOMENTS ABOUT CENTER, XC=  0.0000000E+00 YC=  0.0000000E+00 ZC=  0.0000000E+00
 MXSUM=   -319895.2
 MYSUM=  -3.5051766E-04
 MZSUM=   -300.6194
 MTOT=    319895.3
```

PF 4 Net Load (180 Degree Sector), PF4 16kA, PF5 31.84kA
Net Vertical Load= -176176N for half or 79108lbs per coil

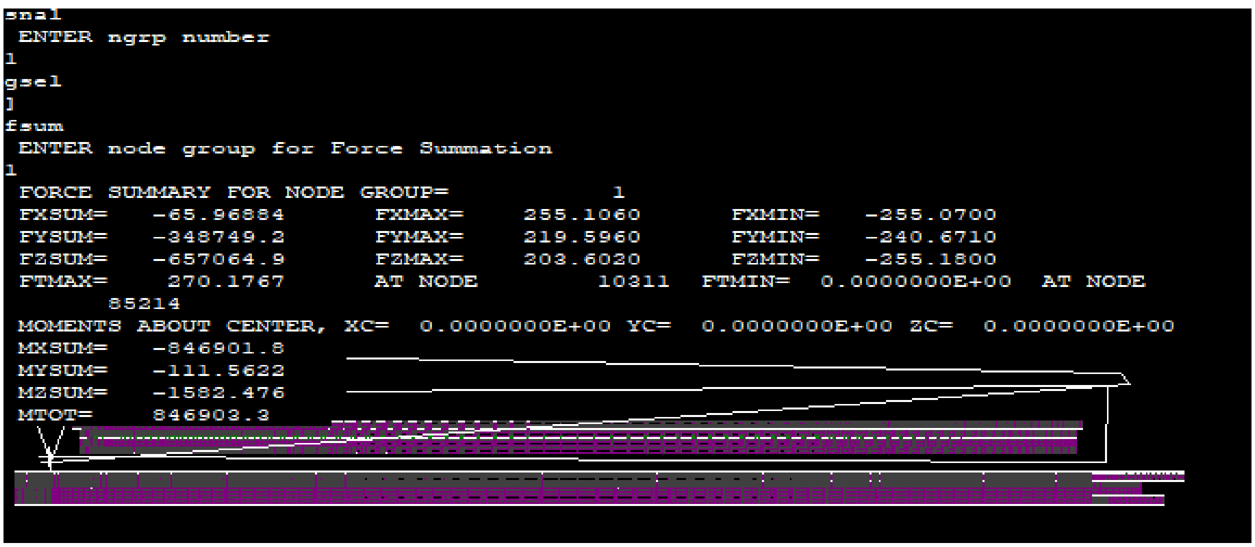

```
snal
 ENTER ngrp number
1
gsel
1
fsum
 ENTER node group for Force Summation
1
 FORCE SUMMARY FOR NODE GROUP=           1
 FXSUM=   -65.96884       FXMAX=    255.1060       FXMIN=   -255.0700
 FYSUM=   -348749.2       FYMAX=    219.5960       FYMIN=   -240.6710
 FZSUM=   -657064.9       FZMAX=    203.6020       FZMIN=   -255.1800
 FTMAX=    270.1767       AT NODE         10311  FTMIN=  0.0000000E+00   AT NODE
       85214
 MOMENTS ABOUT CENTER, XC=  0.0000000E+00 YC=  0.0000000E+00 ZC=  0.0000000E+00
 MXSUM=   -846901.8
 MYSUM=   -111.5622
 MZSUM=   -1582.476
 MTOT=    846903.3
```

PF5 Net Load (180 Degree Sector) PF4 16kA, PF5 31.84kA
Net Vertical Load= -348749 N for half or 156,797 lbs per coil

14.0 Disruption and VDE loads on the Centerstack Casing

Disruption loading on the casing was addressed in [1] The disruption calculation and [16], the casing loading calculation. The analysis approach was to use vector potential transfer from Ron Hatcher’s axisymmetric OPERA analysis. In this calculation, the disruption is simulated in ANSYS EMAG and the loads are passed to a structural analysis that selects the casing elements from the EMAG model .

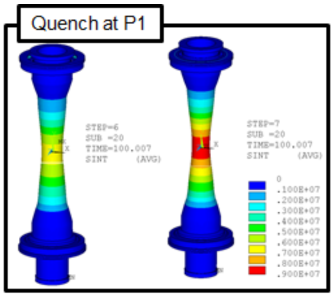

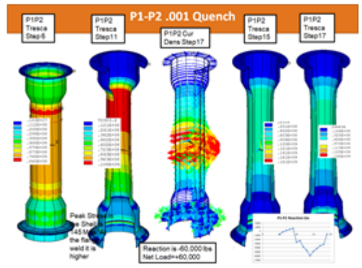

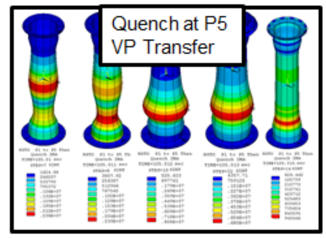

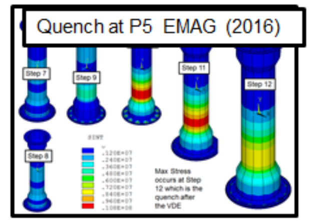

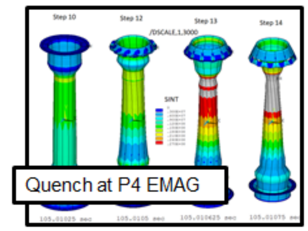

	Drift	Quench	Peak Stress	Peak Vertical Load	Ref
P1	0 sec	.002 sec	9 MPa		[1] (Vector Potential Transfer)
P1	0	.001	Not Run		
P1-P2	.01	.001	108	TBD	[2]
P1-P4	.01	.002	Not Run		
P1-P4	.01	.001	~50 MPa		[2]
P1-P5	.01	.002	8. MPa	8,000 lbs	[1] (Vector Potential Transfer)
P1-P5	.01	.001	10.8MPa		[1] (EMAG)
P1-P6	.01	.001	86	-50,000 Lbs	[2]

[1] NSTXU-CALC-133-03-01 Rev 0: Feb 10 2012 Rev 1, 2016
[2] NSTXU-CALC-10-07-0 Global Disruption Simulations and Lorentz Force Data for Passive Plates, PF support "Slings", Bellows, Heat Transfer Plates, TF and OH Coils.

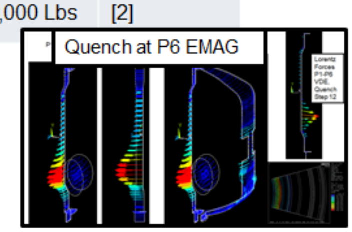

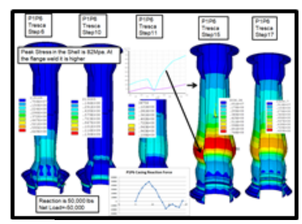

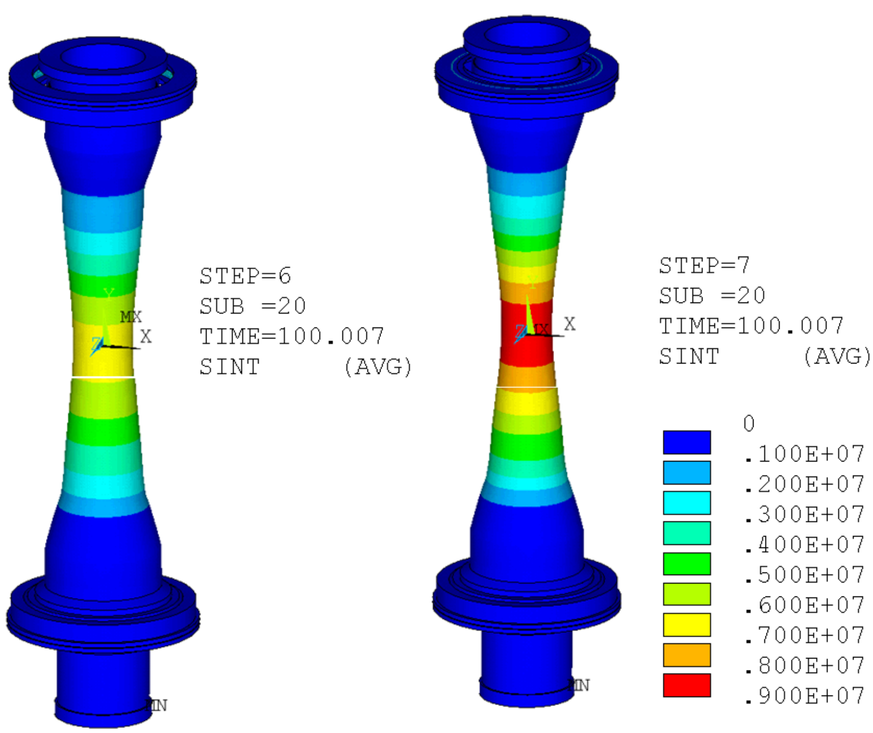

Figure 14.0-1Casing Stress from [16] for the mid-plane disruption – Based on Vector Potential Transfer Ref [16] Figure 11.1-1 CS Casing Stresses for Translation and Quench (2 Millisecond Quench)

14.1 Mid-Plane P1-P2 Disruption Loads on the Centerstack Casing

P1-P2 disruption loads are based on 10 Millisec radial drift to a circular P2 and a 1 millisec quench

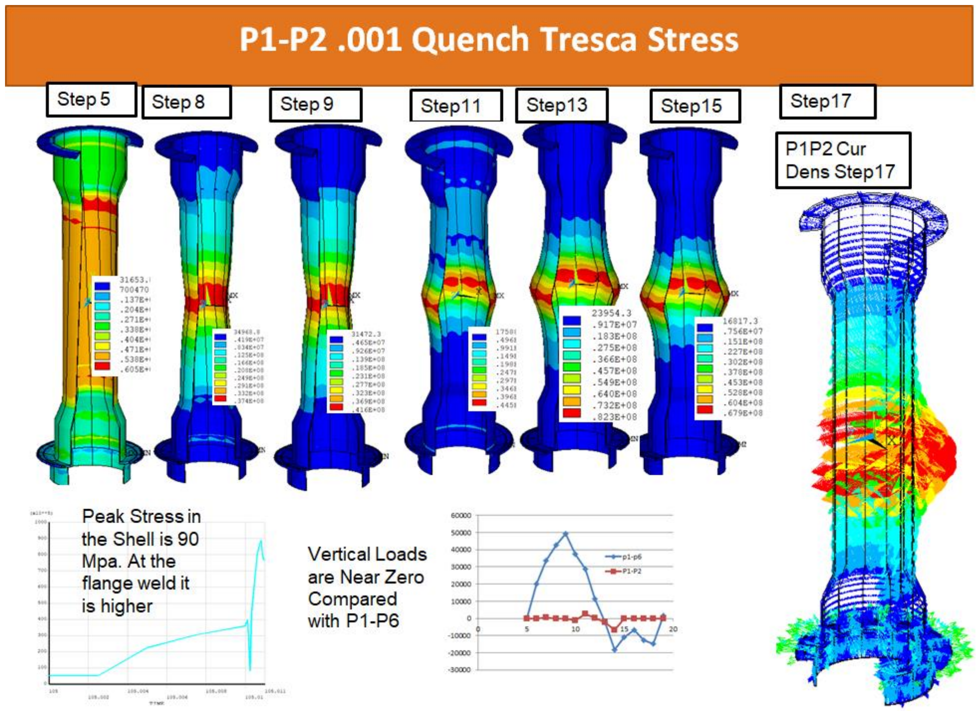

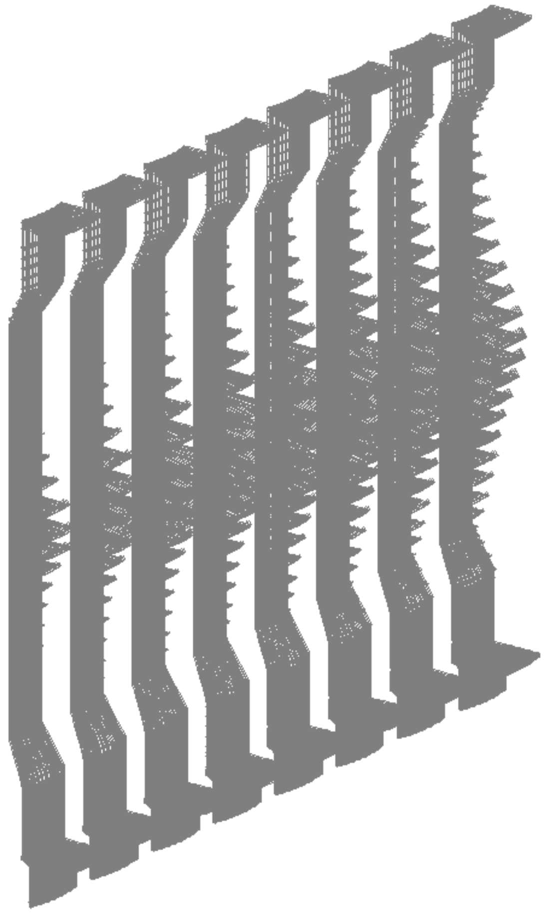

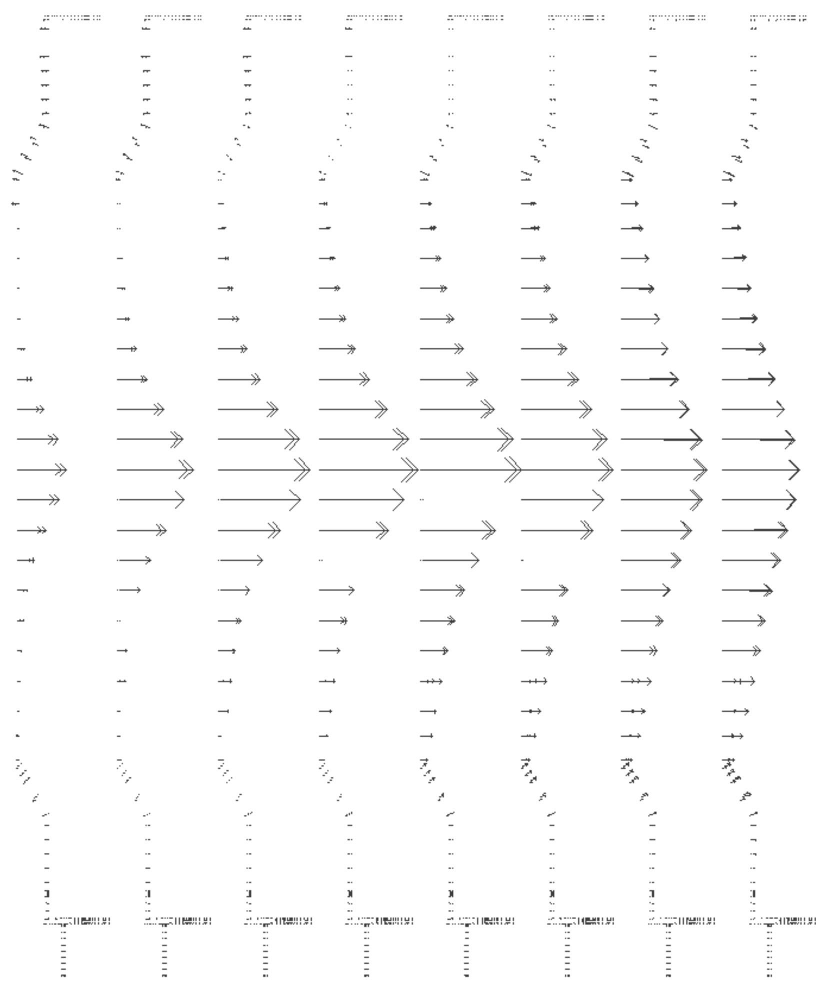

Filenames of “cloud” data are: P2Cloud04 through P2Cloud18

14.2 VDE P1 to P5 loads on the Centerstack Casing

In the VDE disruption, the plasma first shifts down (or up) toward the divertor without losing plasma current – then at the lower extremity of the chamber the currents collapse. Eddy currents are induced in the walls of neighboring structures such as the passive plates and centerstack casing. Currents develop in the centerstack casing in a non-up-down symmetric manner . These interact with the (mainly) the Up-Down symmetric poloidal field and produce net vertical loads on the casing. This analysis is also presented in [16]

Appendix I of reference [10] introduces another disruption simulation. Simulation of the passive plate disruptions also includes other structures including the centerstack casing.

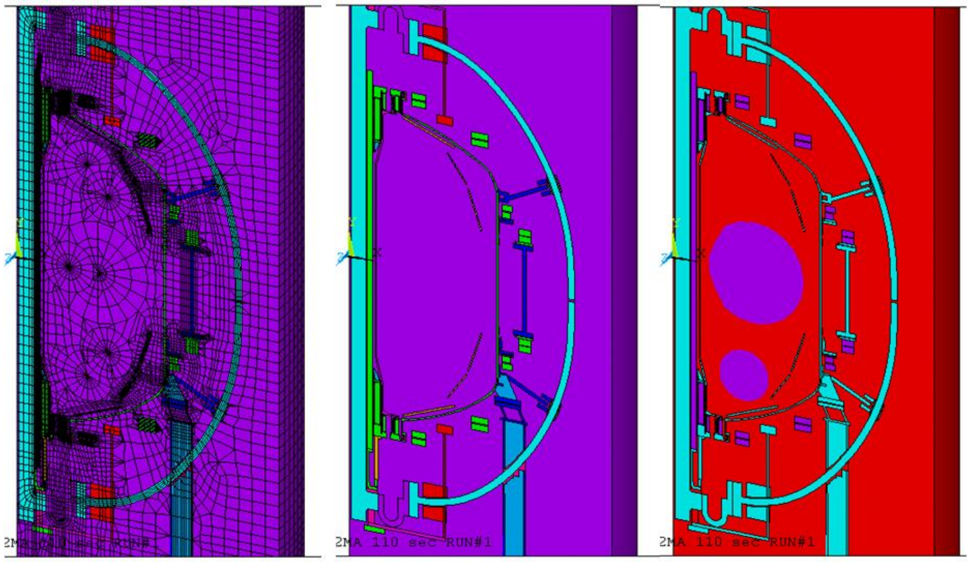

Mesh, Including Air   Materials   Solid 97 Type

Figure 14.2-1 Appendix I of Reference 10 Electromagnetic model

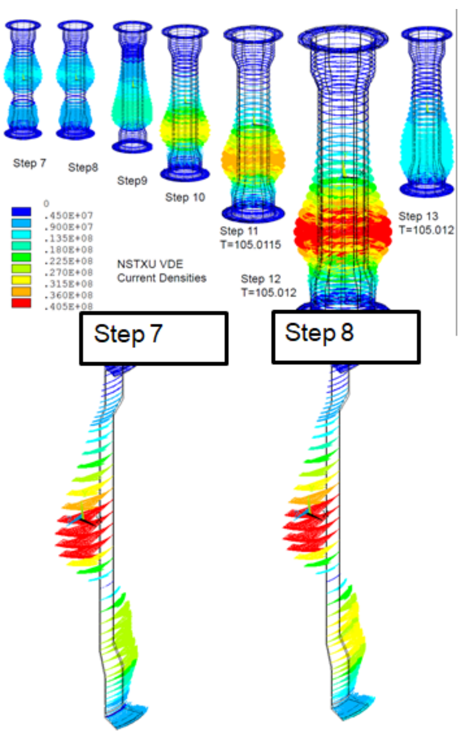

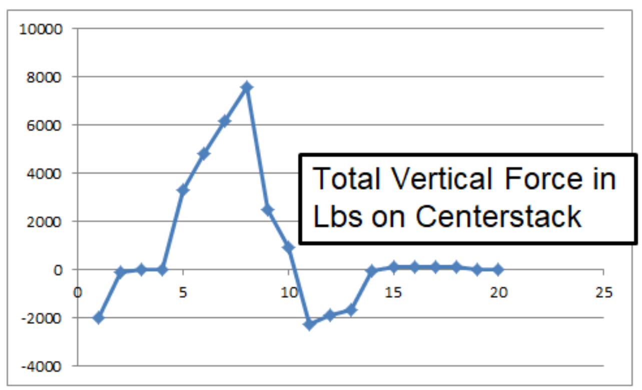

Max reaction force of 8000 lbs total occurs at step 8, which is the end of the vertical translation and not during the large current densities induced during the subsequent quench. What appears to happen is that the reversed currents above and below the equatorial plane both react to the background PF field adding net forces vertically.

Figure 14.2-2

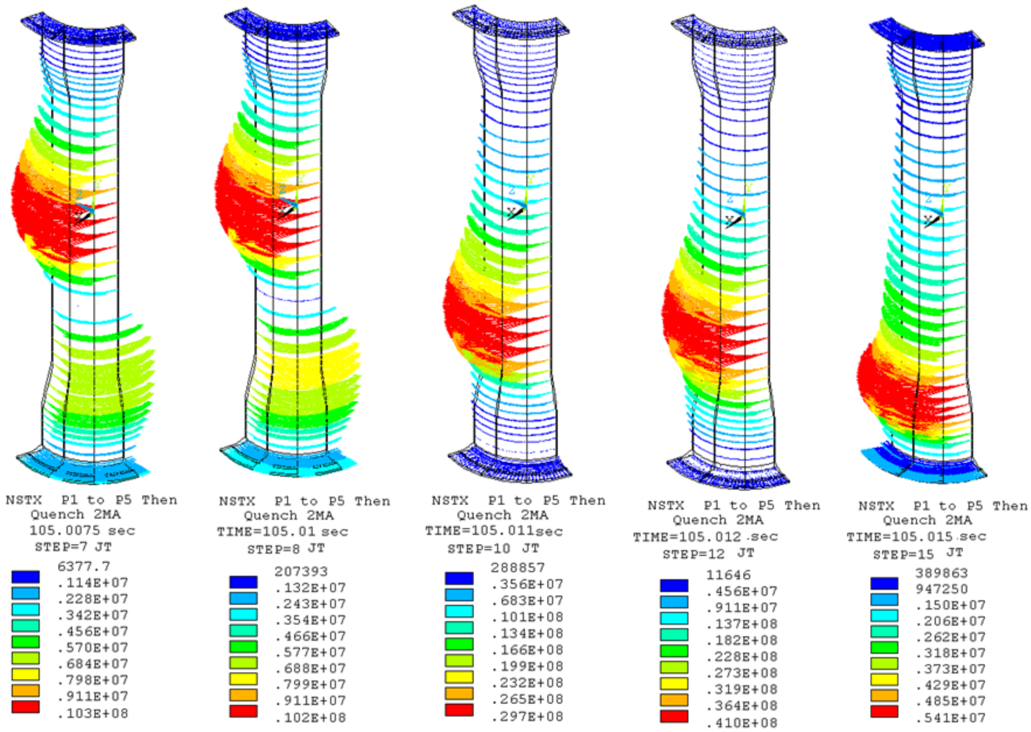

Figure 14.2-2 Current Densities, P1-P5, 10ms VDE (ends at Step 8) and Quench at P5

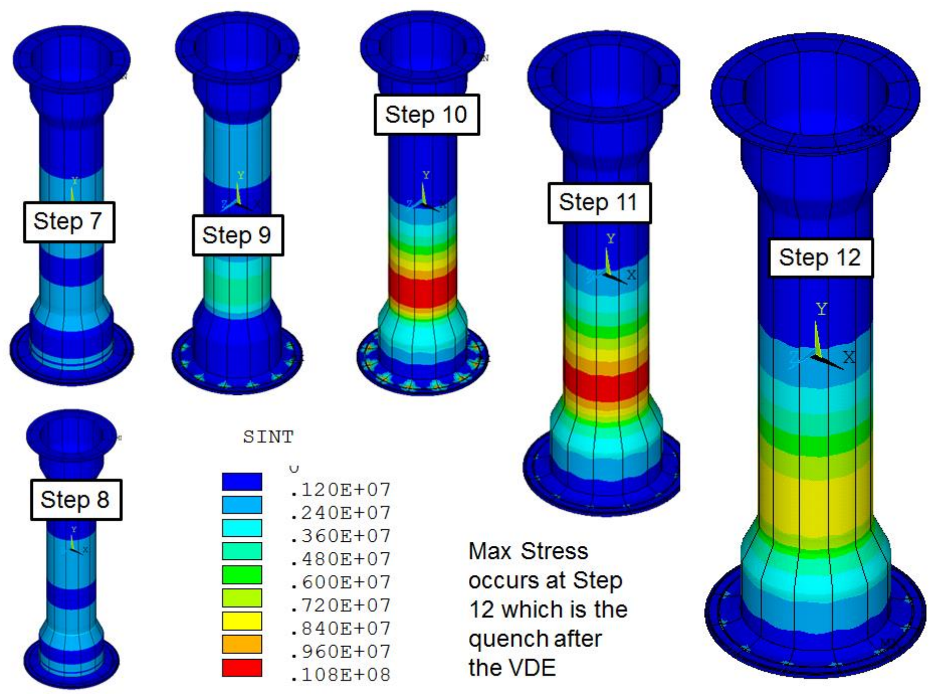

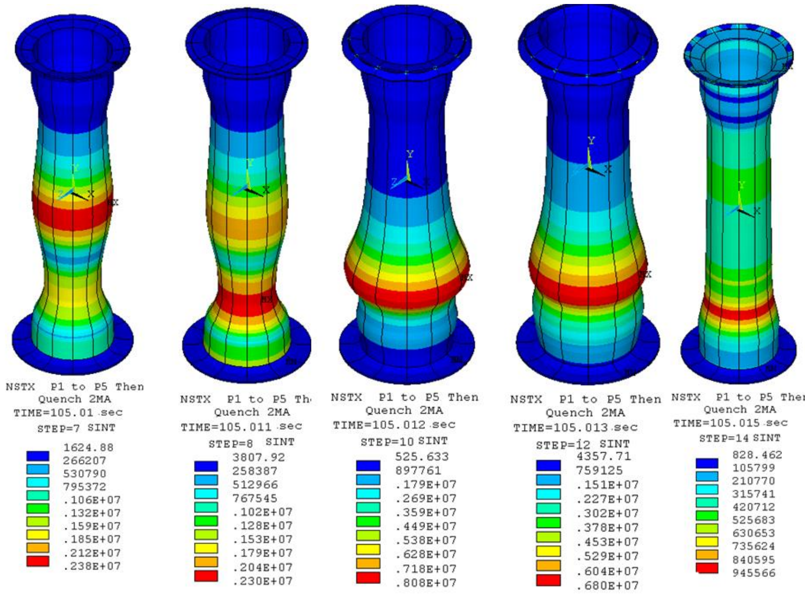

Figure 14.2-2 Tresca Stress, P1-P5, 10ms VDE (ends at step 8) and Quench at P5

This disruption simulation produces nothing more than 8.08 MPa.

14.3 Casing P1-P4 VDE and "Cloud" Data

14.3.1 P1-P4 EMAG Solution

The sling disruption analysis for P1 to P4 was postprocessed. This is for a 1 millisec quench, and 10 millisec drift. Load files for the case were extracted. There are 24 load files which represent the disruption electromagnetic loads at: P:\public\Snap-srv\Titus\NSTX\CSU\emag\Casing P1 P4. Deformed shapes look dramatic below because of the multiplier, The shell stresses are ~50 MPa. Step 10 is during the drift, 13 and 14 are during the quench.

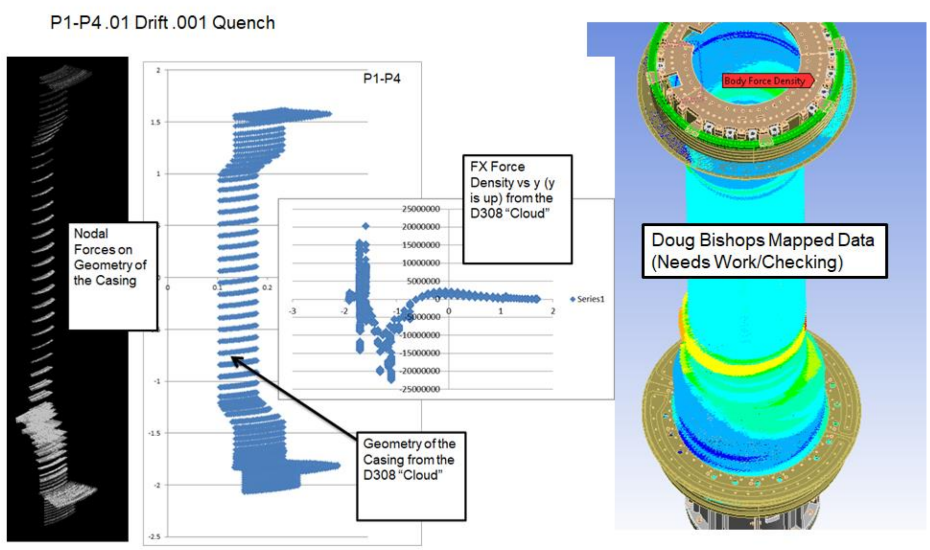

Figure 14.3.1-1

Force Sums (N) for each of the load files, computed from the nodal data, plotted and tabulated

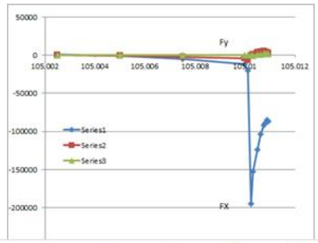

Time	Fx	Fy	Fz	Mx	My	Mz	
c302	104.9	4252.82	818.739	128.69	-194.78	-19.663	-547.98
c303	105	602.794	7.0878	52.3468	-35.809	1.0123	3.4969
c304	105.003	697.748	21.4905	58.331	-26.14	2.57	26.4686
c305	105.005	-1080.9	-644.4	119.256	130.056	-28.893	-6157.2
c306	105.008	-5060.9	-2348.3	79.4719	51.7689	-14.601	-14292
c307	105.01	-11881	-4183.1	64.0433	22.4536	-6.9467	-23083
c308	105.01	-19806	-6250.8	29.153	22.503	-2.7195	-32772
c309	105.01	-194613	-600.42	57.6852	4564.92	-241.7	40768.6
c310	105.01	-152358	624.35	-361.48	7137.36	-42.656	82914.5
c311	105.011	-123634	3419.52	663.411	7183.01	-379.56	104119
c312	105.011	-103380	4725.79	1304.94	7180.41	-594.55	116477
c314	105.011	-92141	4938.48	1895.48	6956.13	-810.14	112657
c315	105.011	-89511	4110.32	1925.91	7097.89	-820.82	106853
c316	105.011	-84962	3420.15	2008.35	7038.71	-843.14	100862
c317	105.011	-86565	2746.15	2086.8	7006.26	-868.78	94600.8
c318	105.012	19973.9	-511.85	-323.53	-1011.5	157.563	-5265.5
c319	105.013	2579.04	267.3	35.4463	-154.63	17.4385	692.757
c320	105.014	2081.18	289.858	97.0234	-75.913	10.8357	150.299
c321	105.015	1586.51	278.278	76.2561	-56.022	11.243	-153.75
c322	105.1	615.355	16.8546	49.0083	-28.653	3.557	-8.9457
c323	105.2	0	0	0	0	0	0

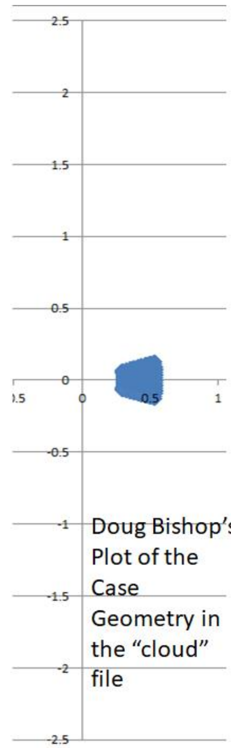

Doug Bishop's Plot of the Case Geometry in the "cloud" file

Figure 14.3.1-3

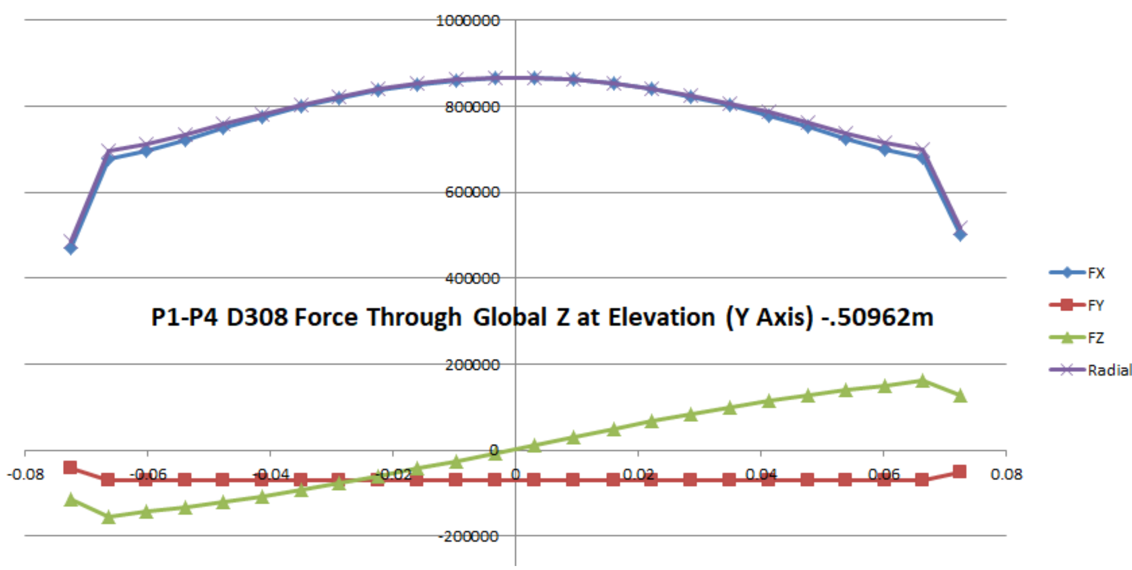

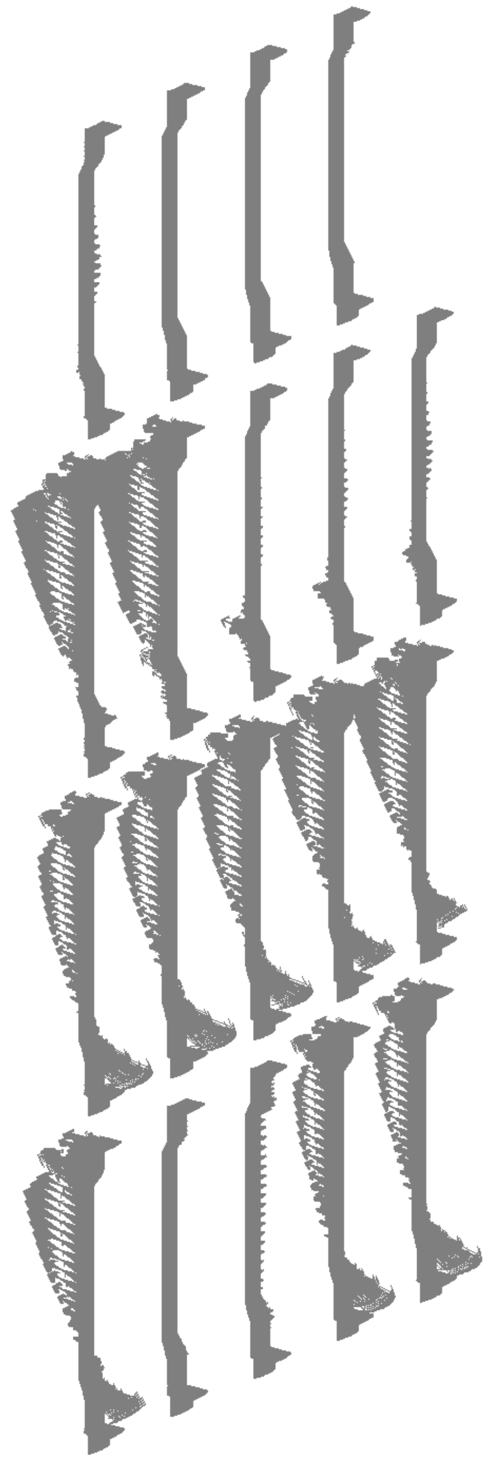

Figure 14.3-4

14.3.2 P1-P4 Static Stress Analysis

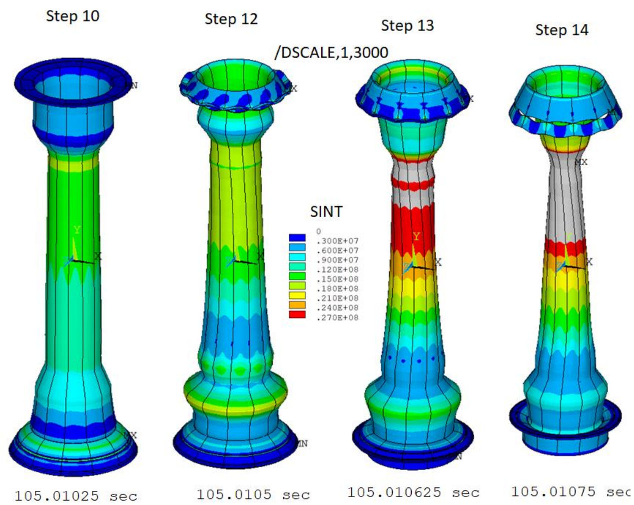

14.6 Casing P1-P6 Disruption and "Cloud" Data

14.6.1 EMAG Simulation

P6 was added to the GRD disruption spec. It has the potential of loading the centerstack differently that the P1 to P4 or P5 disruptions – those were intended to load the passive plates more severely. The definition of the P6 plasma was taken from the Recovery GRD The P1-P6 Eddy current (not Halo) Cloud data was transmitted to Mark Smith and Doug Bishop, after the pictures. This is P1-P6 down. The data is from a 30 degree cyclic symmetry model and needs to be repeated and rotated 12 times. The P1-P6 Up will be almost identical but flipped vertically.

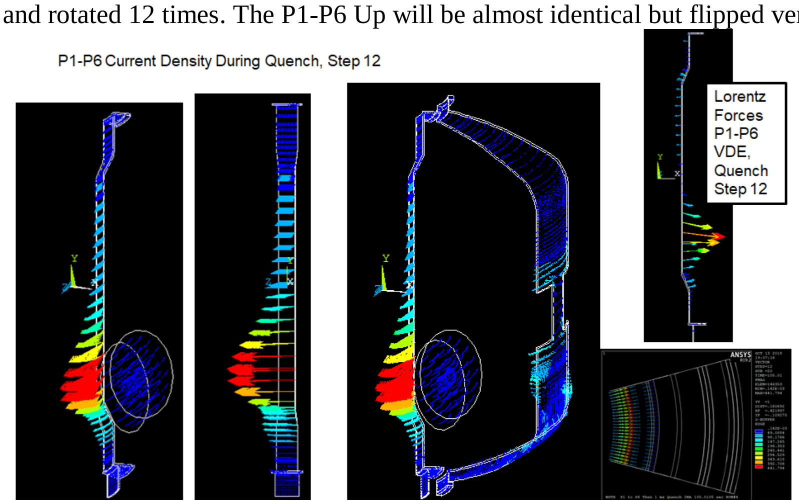

Figure 14.6.1-1

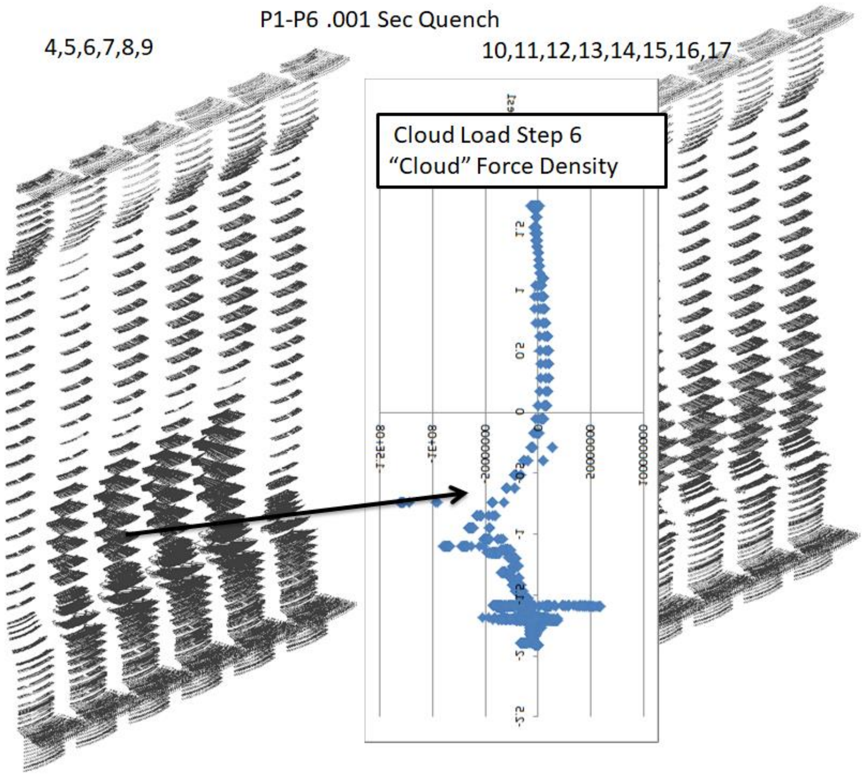

Figure 14.6.1-3 Comparison of Cloud load Step 6 Nodal Data and force Density Data

Casing 30 Degree Sector Force and Moment Sums

Casing Nodal Force (N) Sums vs Time

Casing Moment (N-m) Sums vs Time

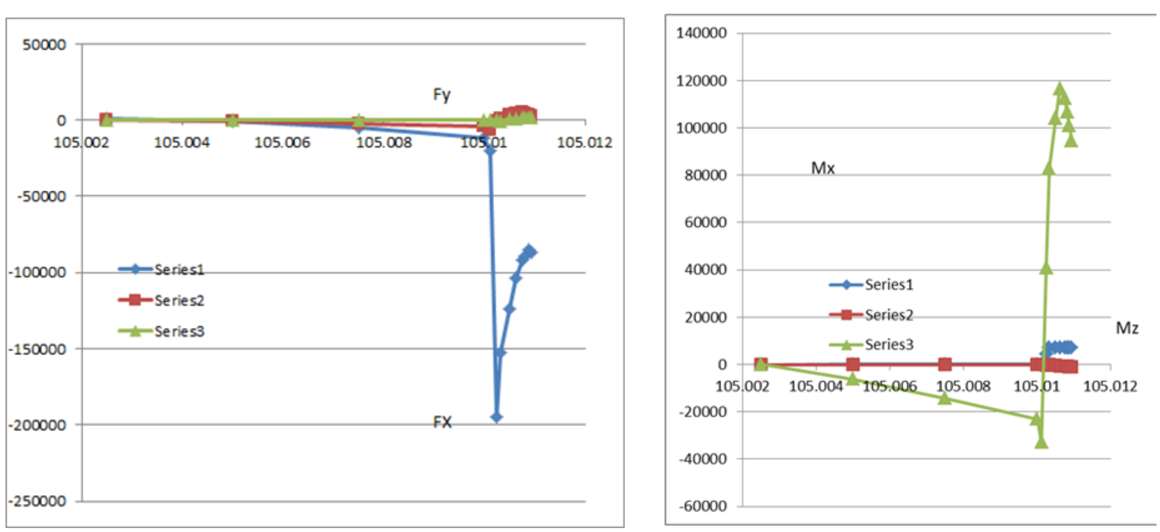

Figure 14.3-5

14.6.2 Static Stress Analysis

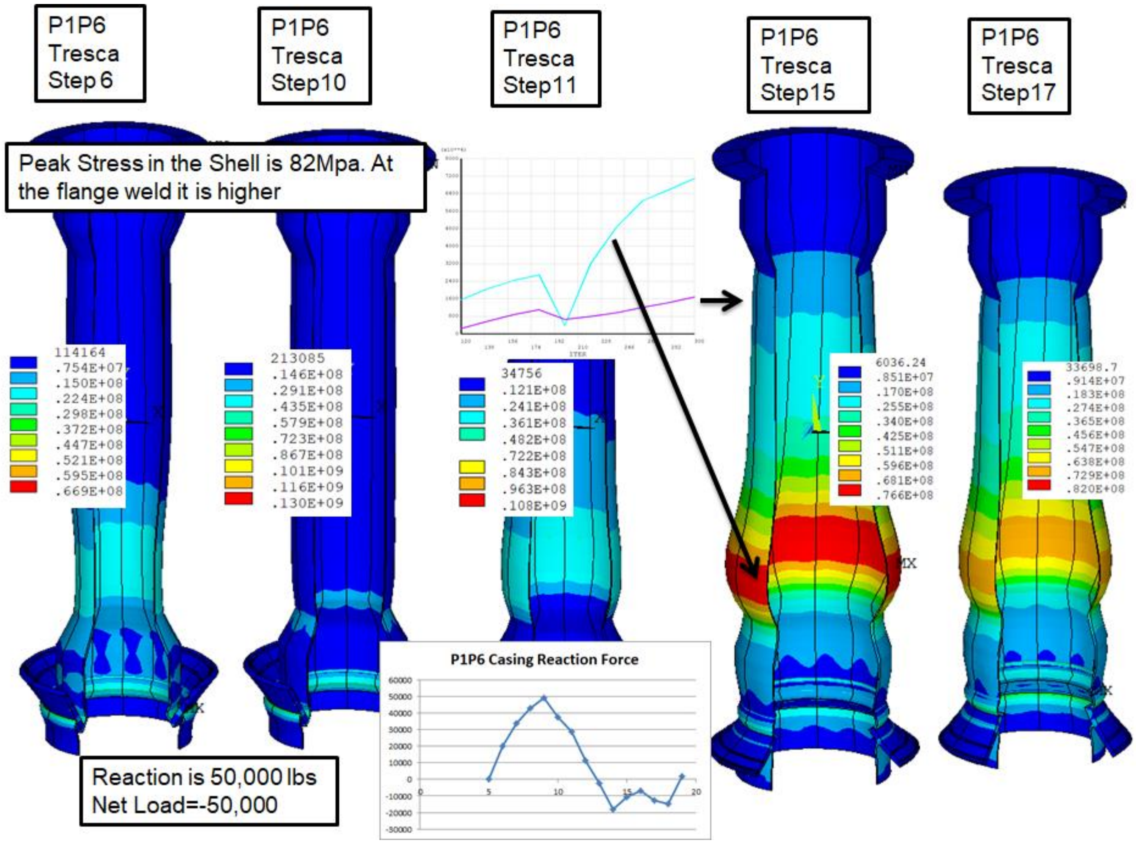

14.6.3 Disruption Dynamic Load Factor

Dynamic Load Factor for the casing response to a P1-P6 10 millisec drift then 1 millisec quench.
ANTYPE,TRANS rerun of the static loads from the EMAG disruption simulation

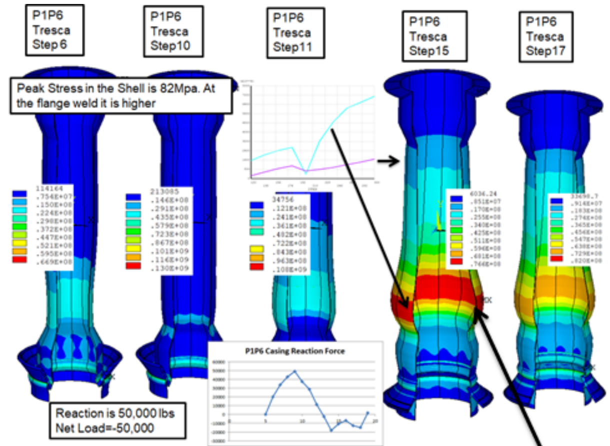

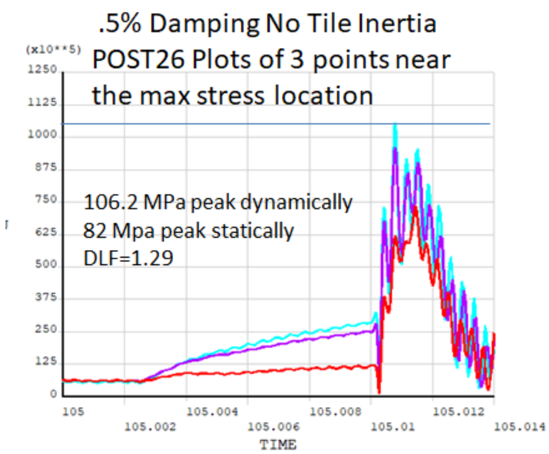

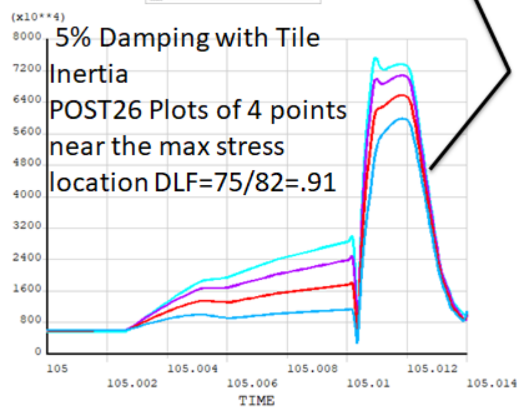


```
percentdamp=.05
Frequency=150
bdamp=2*percentdamp/(Frequency*2*3.1416)
betad,bdamp        !Damping
adamp=
2*percentdamp*frequency*2*3.1416
alphd,adamp        !Damping
```

```
DensATJ=1769      !kg/m^3
dens,8,8440+DensATJ*1/.25   !8440 density of Inconel 625
```

The tiles will increase the damping and add to the inertia . With damping and tile inertia added, a DLF of a little less than one results A DLF of 1.0 is recommended.

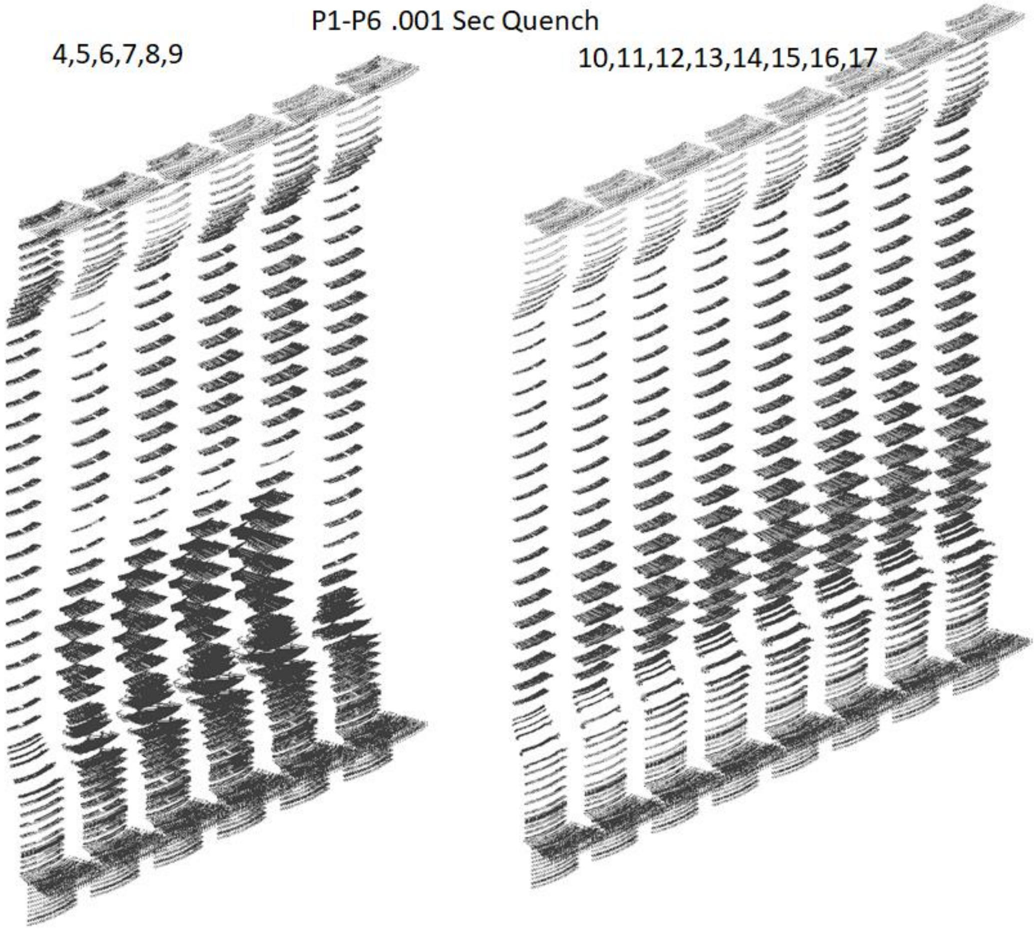
P1-P6 .001 Sec Quench
4,5,6,7,8,9
10,11,12,13,14,15,16,17

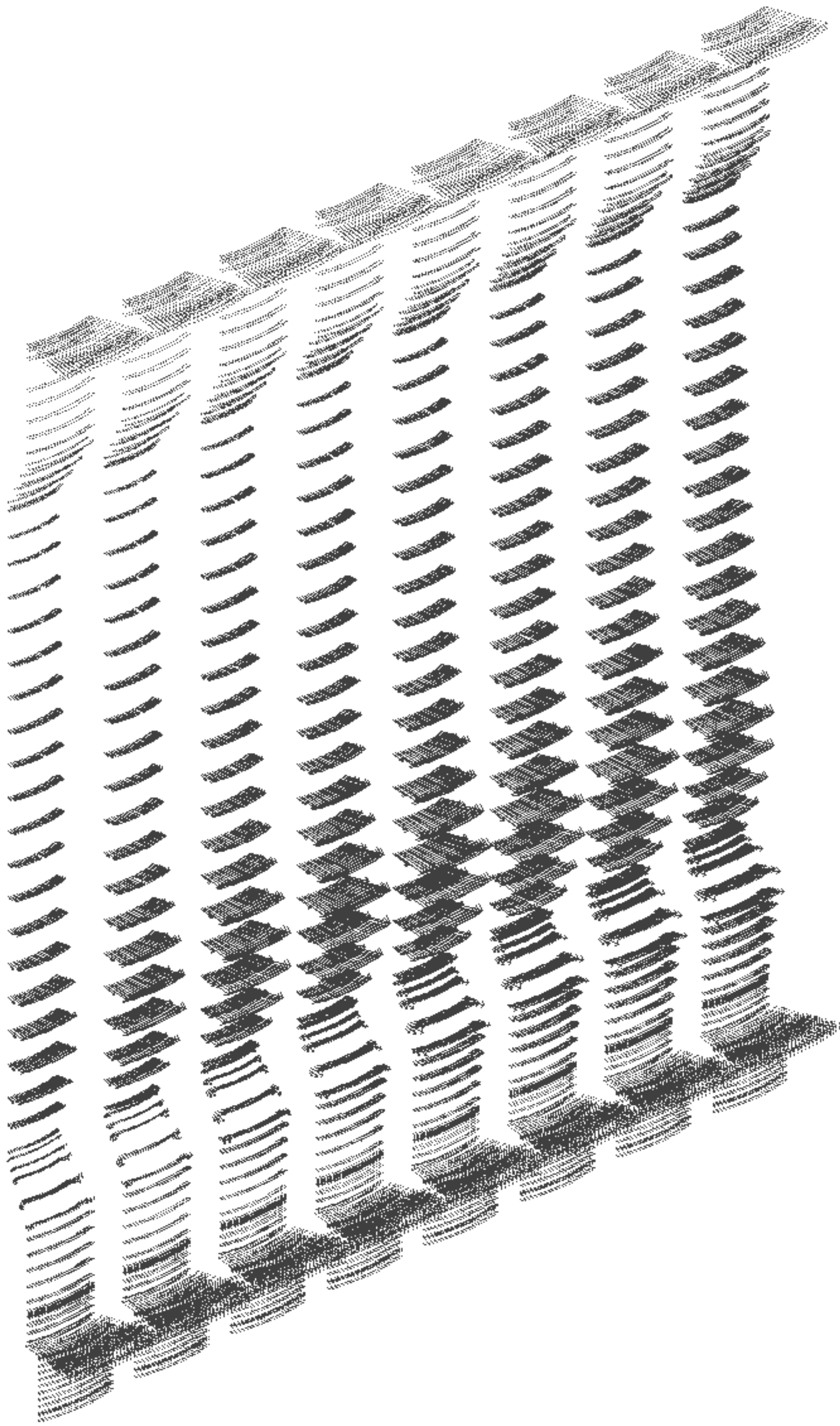

15.0 TF Eddy Current Loads VDE Loading

The TF developed eddy currents when we investigated use of OH AC excitation for the bake out. The TF eddy current assessment for P1-P5 VDE disruption loading uses a model developed to investigate OH AC excitation for bake out. As of August 2018, these analyses are included in the directory e:\nstx\csu\emag\tfeddy. The latest run is tfeddy03.txt

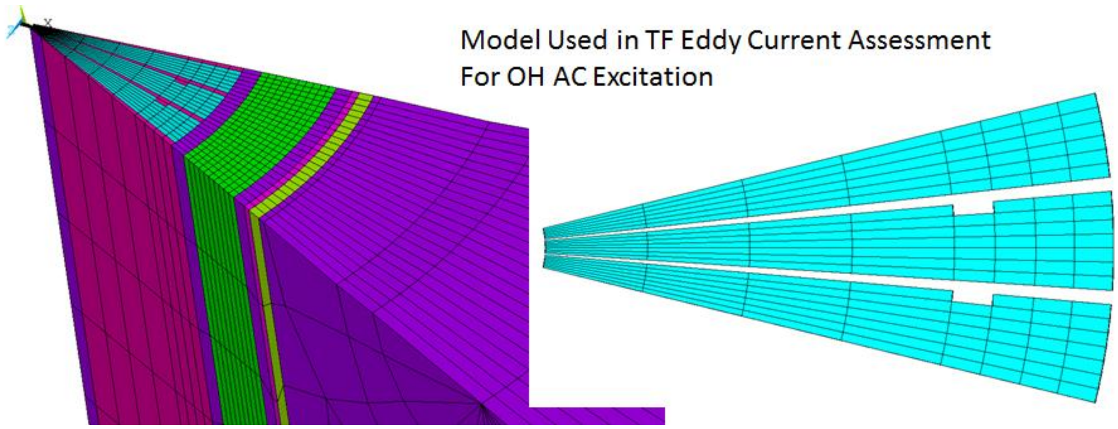

Figure 15.0-1

The plasma current transients are further away than the OH transients. But still, the 36 eddys in the outer radius of TF conductors sum to a net toroidal current that crosses with the vertical field of the OH to produce hoop loads and the radial fields of the OH and plasma to produce vertical loads.

15.1 Current Densities

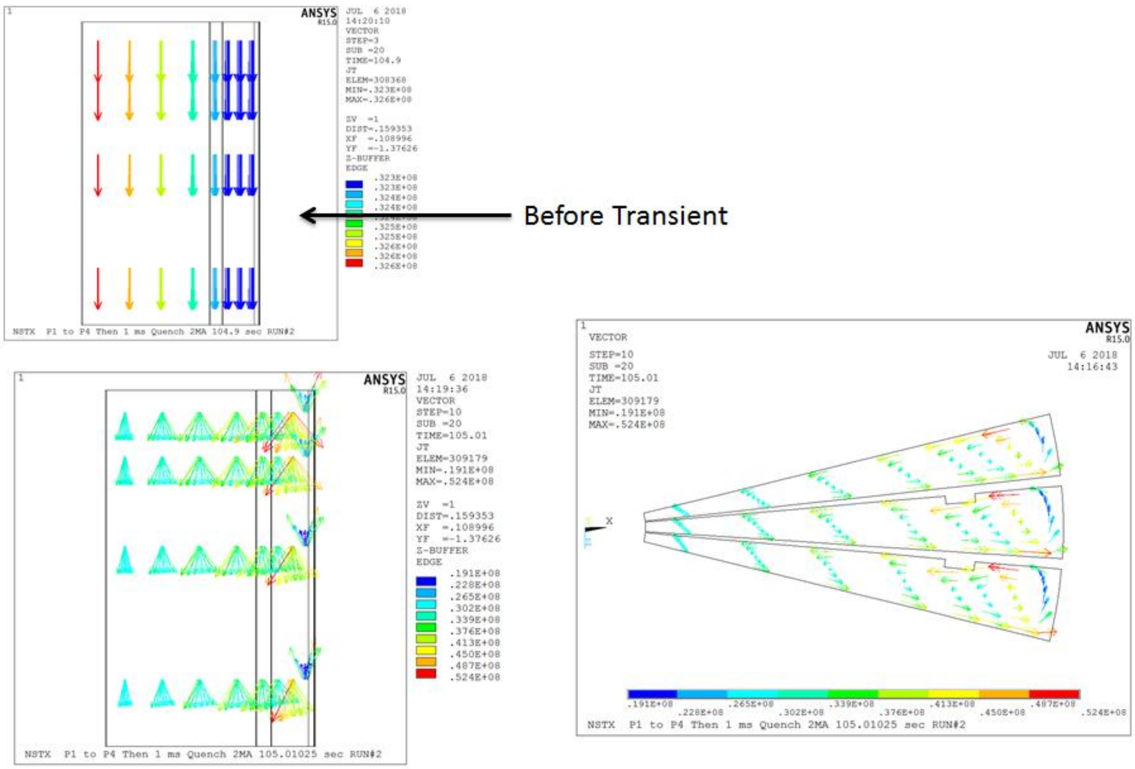

Load Step 10 Early in Quench

Figure 15.1-1

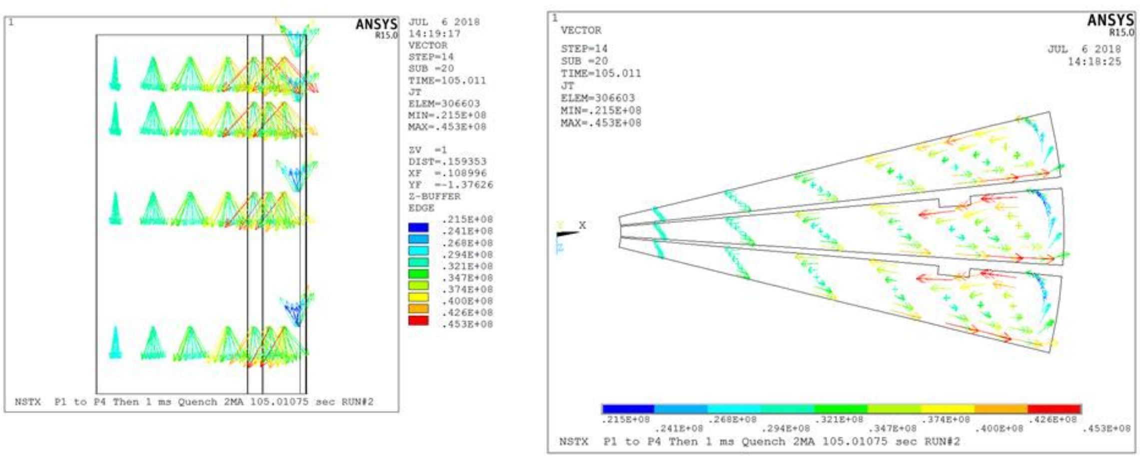

Figure 15.1-2 Load Step 14, Later in the Quench

15.2 Net Loads on the TF

The net vertical load is 40,000 lbs on the TF inner leg. This load does not involve the casing and skirt, but does involve loads on the pedestal and the TF flag extension bolting to the pedestal.

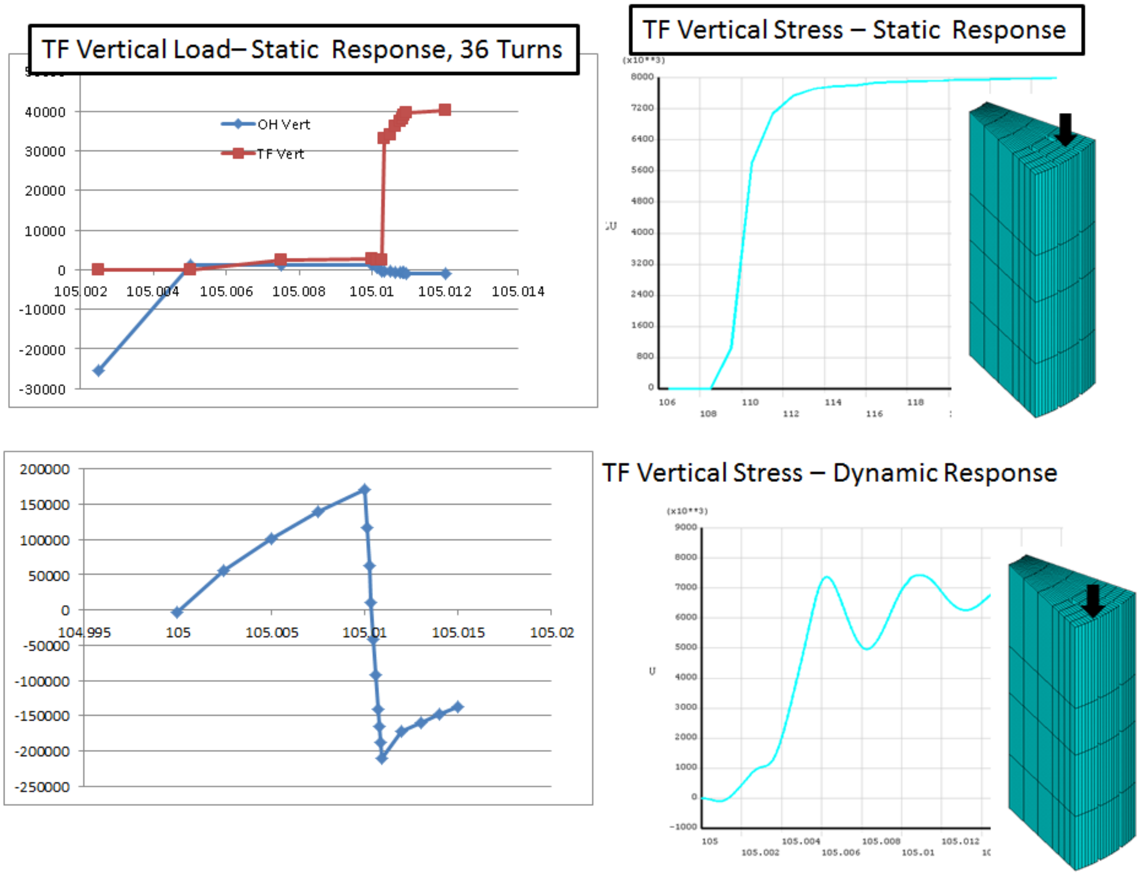

Figure 15.2-1 Comparison of Static and Dynamic Response of the TF Coil
(Passive Plate Currents are Plotted in Lower Left for Comparison)

A dynamic simulation did not reduce this. The TF inner leg sees torsion and hoop tension and compressive loads resulting from the toroidal current. The net toroidal current is about 100kA at the outer radius of the TF or 5% of the Ip- Art estimated this from the areas. Currents are higher locally. The tensile hoop stress may be a problem. I am still evaluating this. The problem is that the toroidal TF current crosses with the +/- 7 T field in the OH bore.

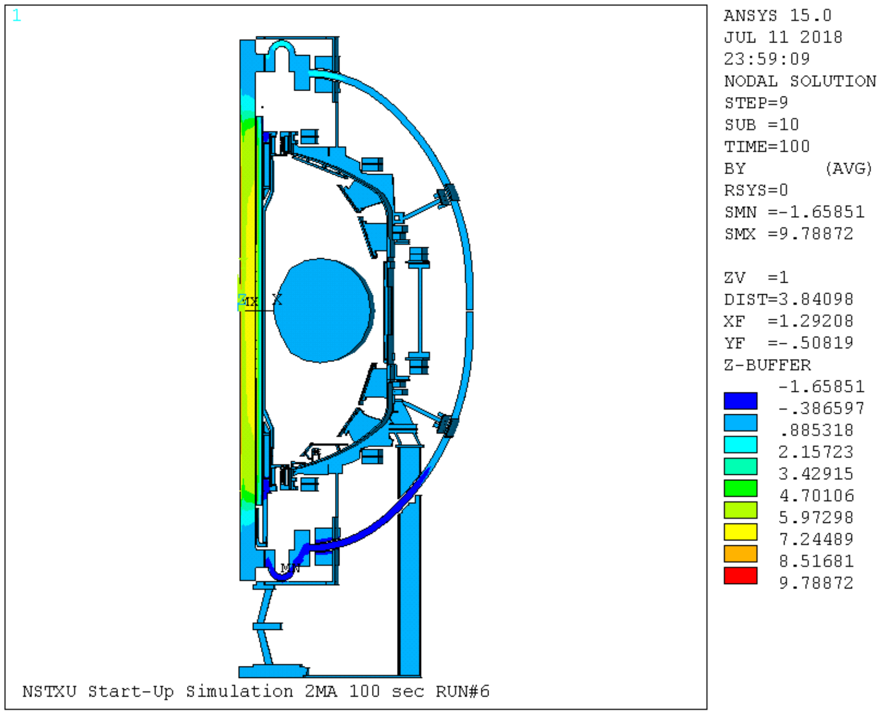

Figure 15.2-2 Vertical Field in the TF Coil Due to the OH Predominantly

It potentially can offset the compressive self wedge pressure in the TF. I started this work to investigate the net vertical load on the OH due to the VDE, but in this simulation not much load was obtained. It may be a consequence of the reaction to the TF toroidal current. This is going to take more work. OH hoop stress can be affected too. There can be an effect on the start-up but I didn't see much in my startup simulation,

15.3 TF Frequency Response

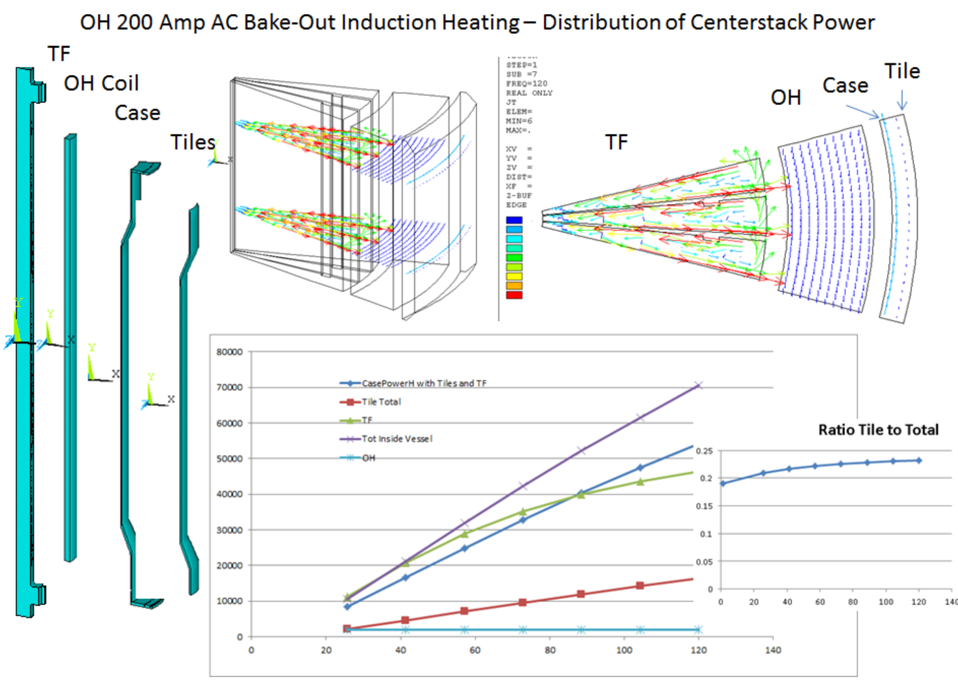

Figure 15.3-1 TF Frequency Response Due to an OH Excitation
A 1 millisec disruption corresponds to a frequency of 250 to 500 hz

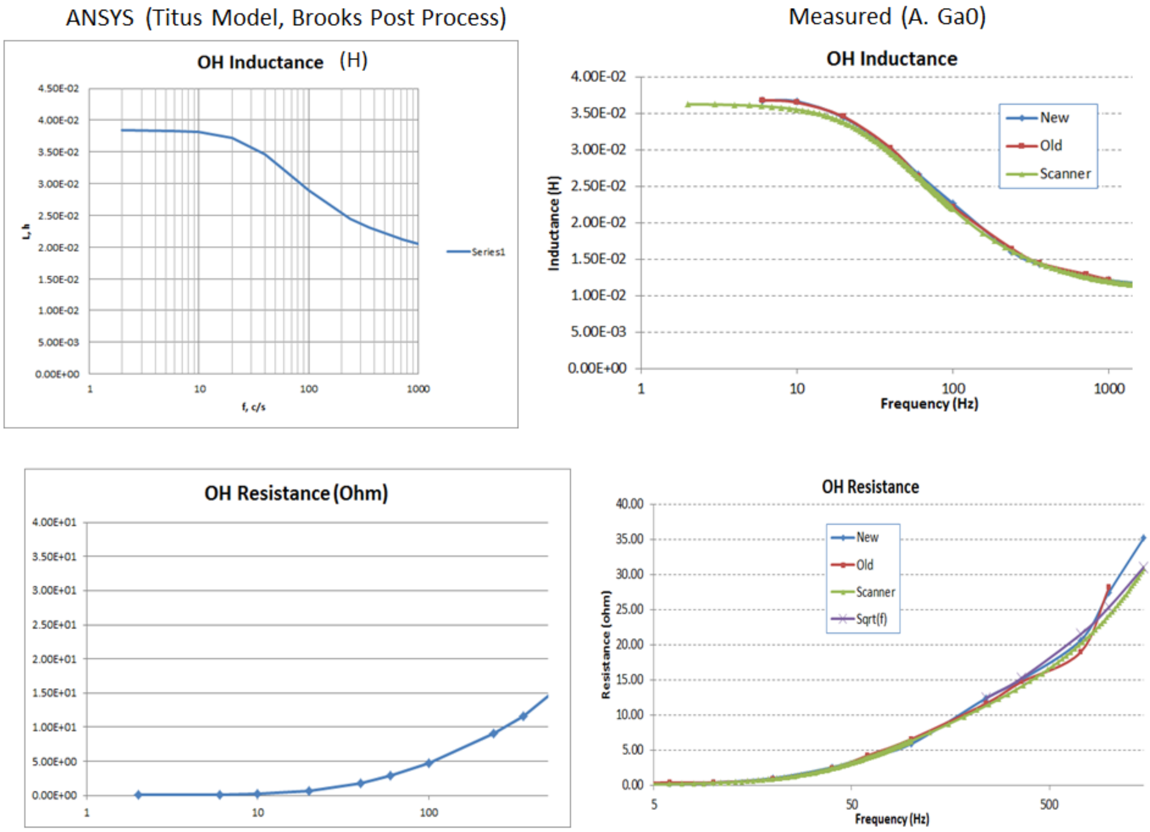

Figure 15.3-1Frequency Response Due to an OH AC Excitation

15.4 TF Toroidal Net Current due to VDE

The net eddy currents are effectively resolved to a toroidal current at the outer radius of the TF inner leg column,

15.4 TF Hoop Stress

The net eddy currents are effectively resolve to a toroidal current at the outer radius of the TF inner leg column, and an opposed current at the inner radius. This will cross with the OH field, and depending on the direction of the OH field and current, the resulting loading will either add to the TF centering force or add a radially outward load on the TF central column. In the disruption emag model, the -24 kA OH current produced an addition to the centering load and the +13kA EQ 81 produced outward loads. The effect in the structural pass was small.

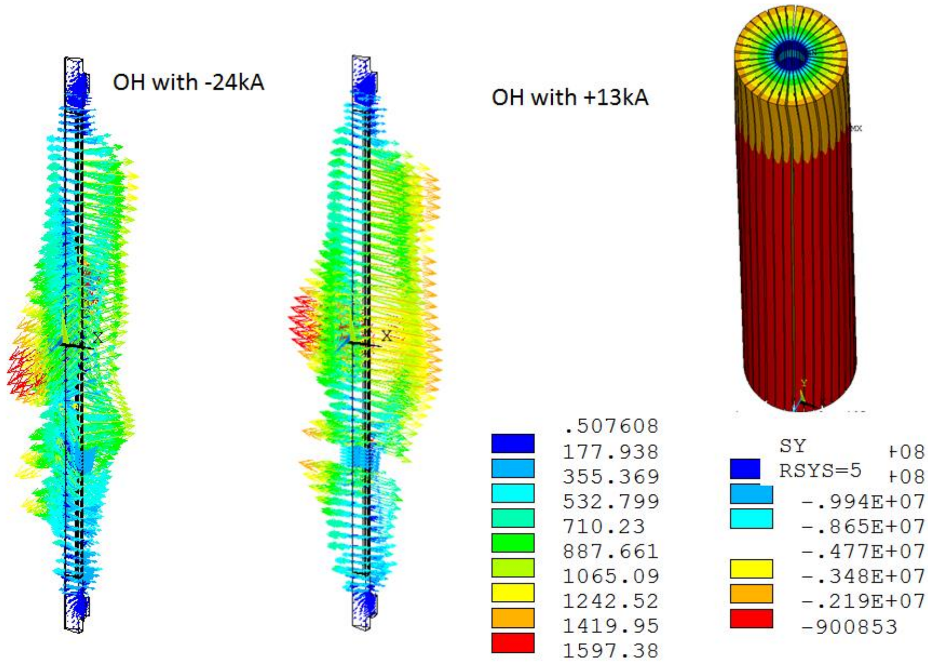

Figure 15.4-1 Loads on the TF

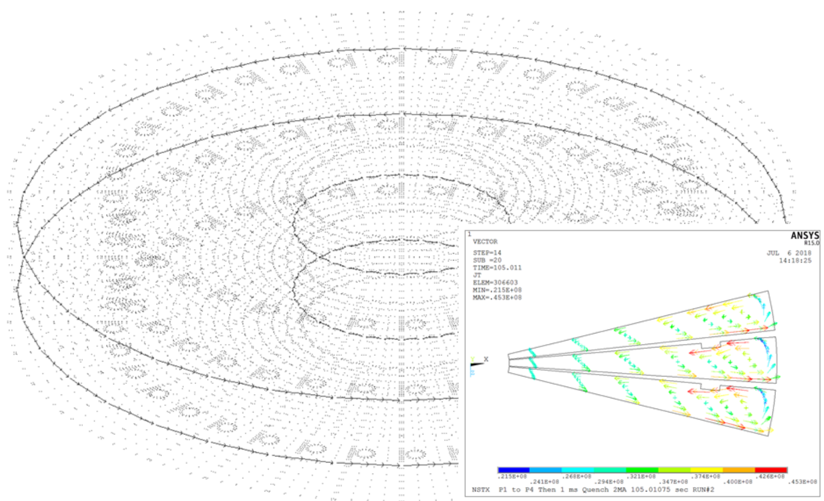

Figure 15.4-2 TF “Slice” Model with eddy currents Shown

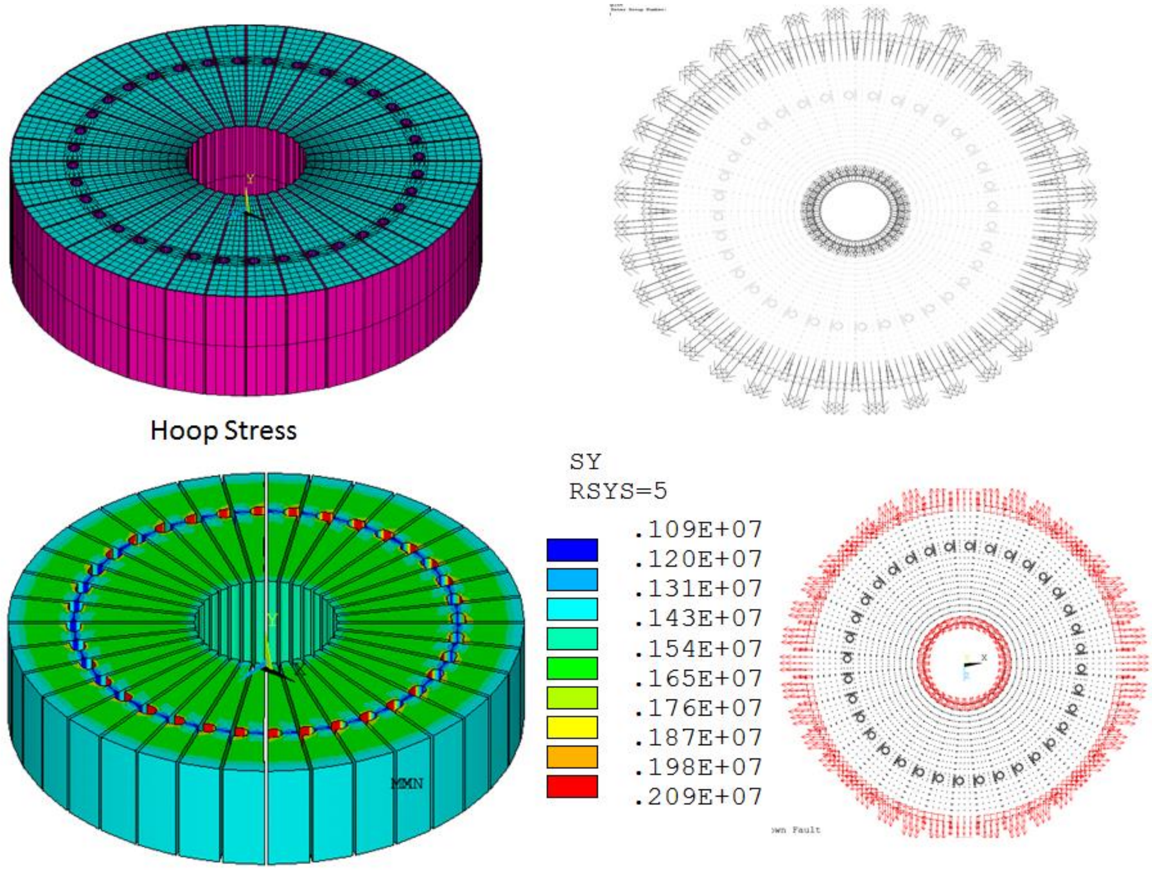

Figure 15.4-2 TF "Slice" Model with Lorentz Forces Shown

The results of the simplified "slice" model show only a 1.6 MPa hoop tensile stress

16.0 VDE Imposed Loads on the OH and Inner PF Coils
16.1 VDE Imposed Loads on the Inner PF Coils

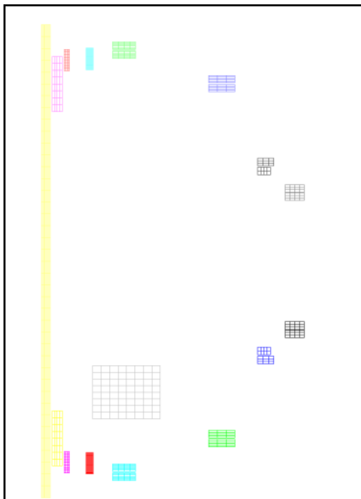

Influence Coefficient Model for VDE to P4 Down

From [21]: Tile background fields and Bdots have been computed for the VDE cases. We are catching up with estimates of additional vertical loads on the inner PF coils with the plasma at the end of a VDE drift phase or P4 position for a downward drift and an equivalent negated position for an upward drift. So far we have only investigated the vertical loading. Max Loads on PF1aU, PF1bU&L,PF1cU&L are about 50% higher than nominal based on a static field calculation, mitigated by the vessel shielding . PF1aL remains about the same. This is a consequence of EQ 51 not being up-down symmetric with respect to PF1a currents. The increased loads will have an impact on the polar region design. Net loads on the OH and Centerstack components will change. Radial load effects also need to be included – especially if there is a hoop stress effect on the OH. The inner PFs have a large margin in hoop stress but the extra vertical loads will challenge the slings and polar region flanges and bolting. As the plasma approaches the divertor the inner PF coils that have currents in the same direction as the plasma are being attracted to the plasma, coils with reversed currents will be repulsed. The vessel shields the coils, but the slow drift and Inconel 625 structures reduce the shielding effect. Art ran a disruption simulation with EQ 16, and the 10ms drift adds 122 kN to the loads. Based on a static field analysis the difference for EQ16, is 61850N (VDE Down) – (-214999) N =276849N So for EQ 16 the static field prediction is about twice the prediction from an electromagnetic transient simulation. Only one transient simulation has been done but all the EQ's can be evaluated for static field effects with updates of the influence coefficients. The vertical load influence coefficient corrections for VDEUp and Down are included at the end of memo SEI-2018 03-18PHT/AB01

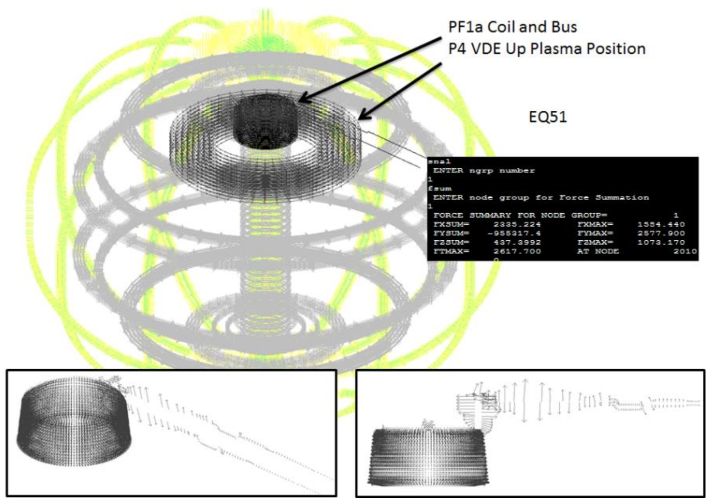

Max Loads for VDE vs. Nominal (Static Field)

Coil Number	Coil	VDE Up	DPSS Min	VDE Down	DPSS Max
2	PF1aU	-728528	-426023		
9	PF1aL			424044	426023
3	PF1bU	-426384	-218327		
10	PF1bL			417043	218327
4	PF1cU	-365785	-145062		
11	PF1cL			365916	145062

16.2 VDE Imposed Loads on the OH

Nominal	VDE Down	VDE Up
40477N	376285 N	183218 N
9099 Lb (8489 from the DPSS)	84,588 Lb	41187Lb

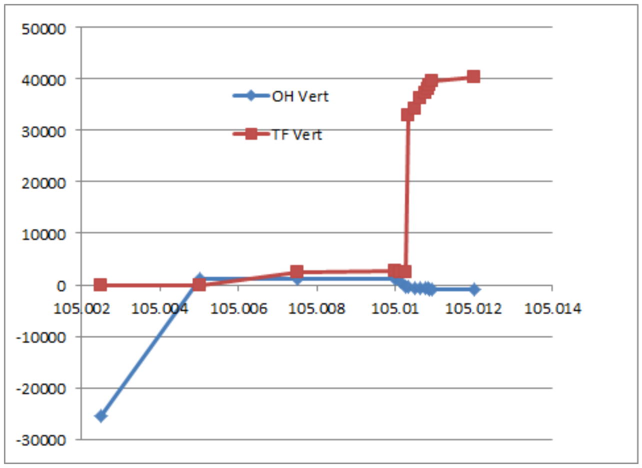

OH Hoop Stress During a VDE

The OH hoop stress is primarily determined from the self field of the coil, but there is an interaction with the plasma and other coils, principally PF1a [13]

Like the vertical loading, the hoop stress depends on the magnitude of the current in the OH and the direction of the current with respect to the plasma. In the case where the OH current is in the opposite direction from the plasma current, the loading resulting from the plasma is inward and reduces the hoop stress.

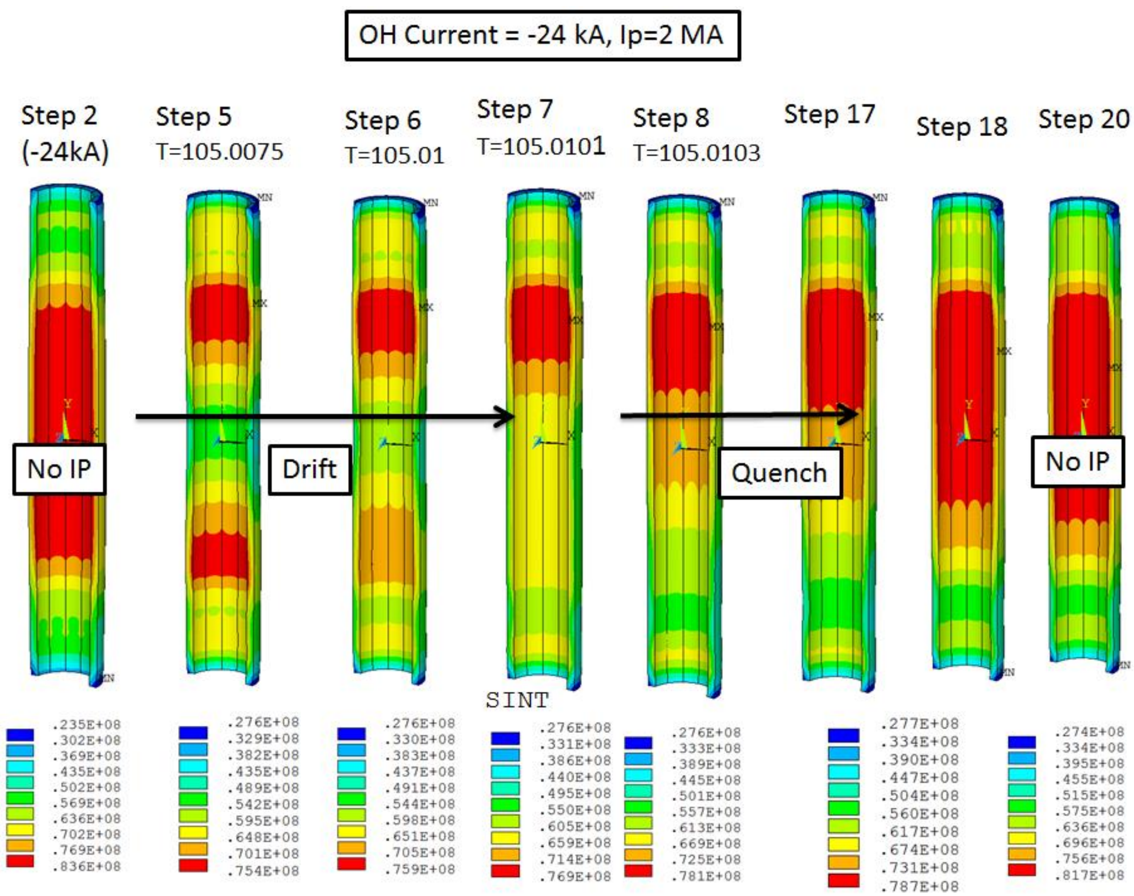

In the case where the current in the OH is in the same direction as the plasma, the coil is attracted to the plasma and the hoop stress is increased. In the results shown below, the hoop stress maximum is 125 MPa, smeared. With

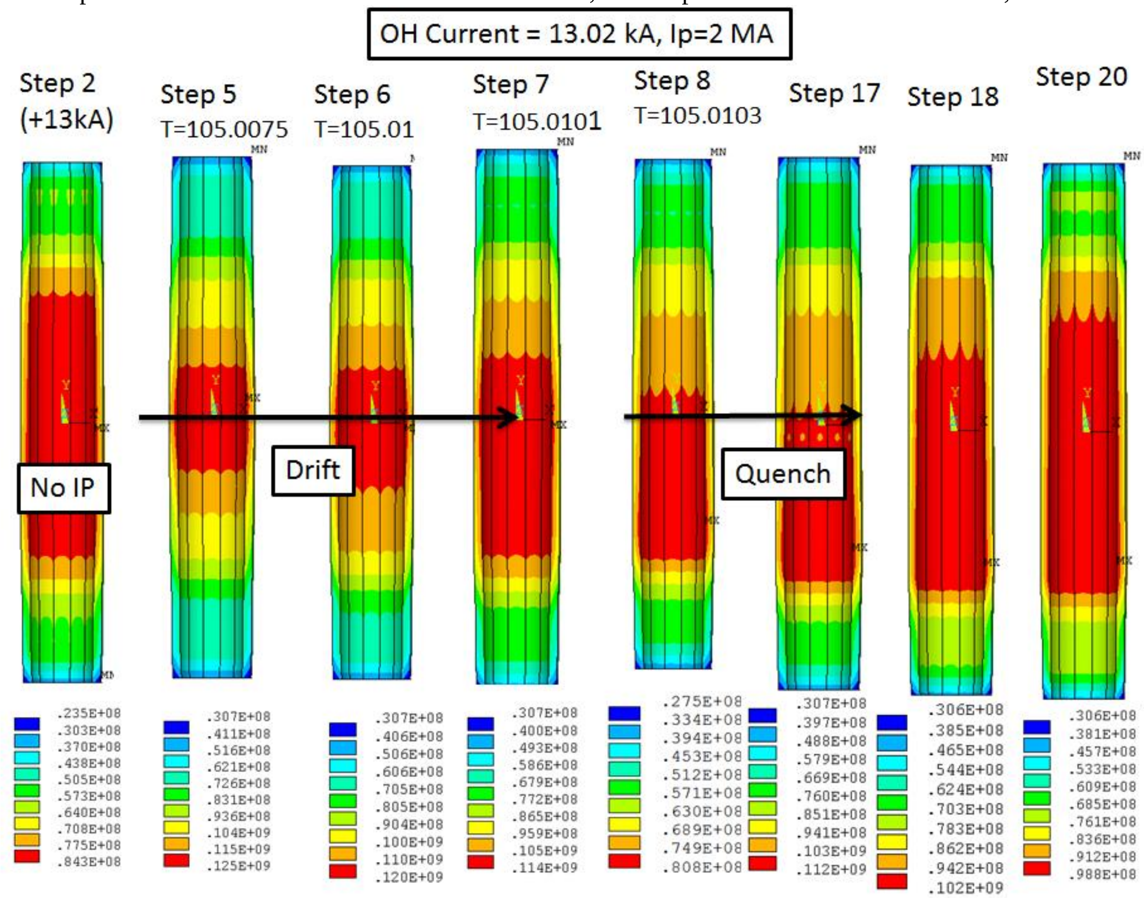

From the Design Point Spreadsheet:

	NSTX	NSTXU
OH Packing fraction	0.7455	0.7012

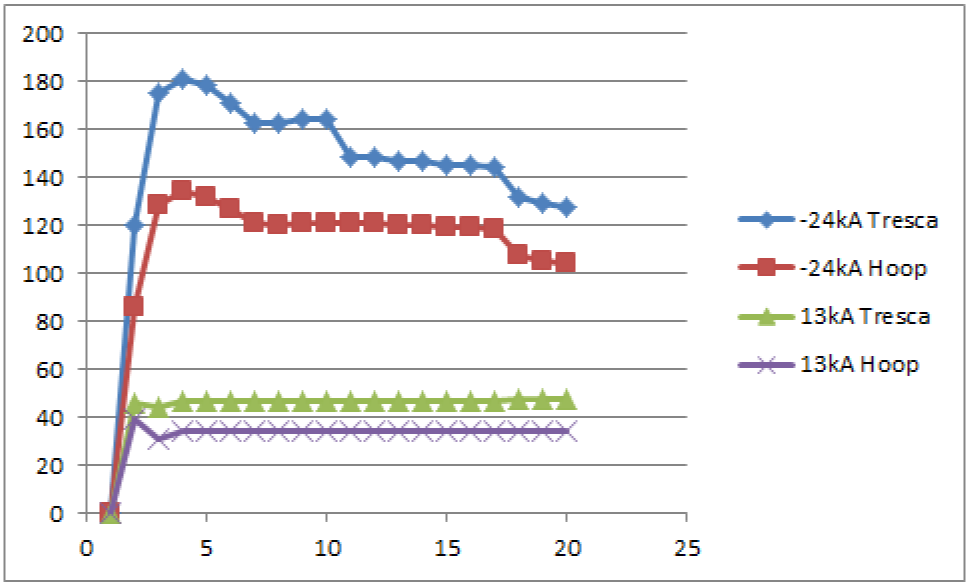
200
180
160
140
120
100
80
60
40
20
0
0
5
10
15
20
25
-24kA Tresca
-24kA Hoop
13kA Tresca
13kA Hoop

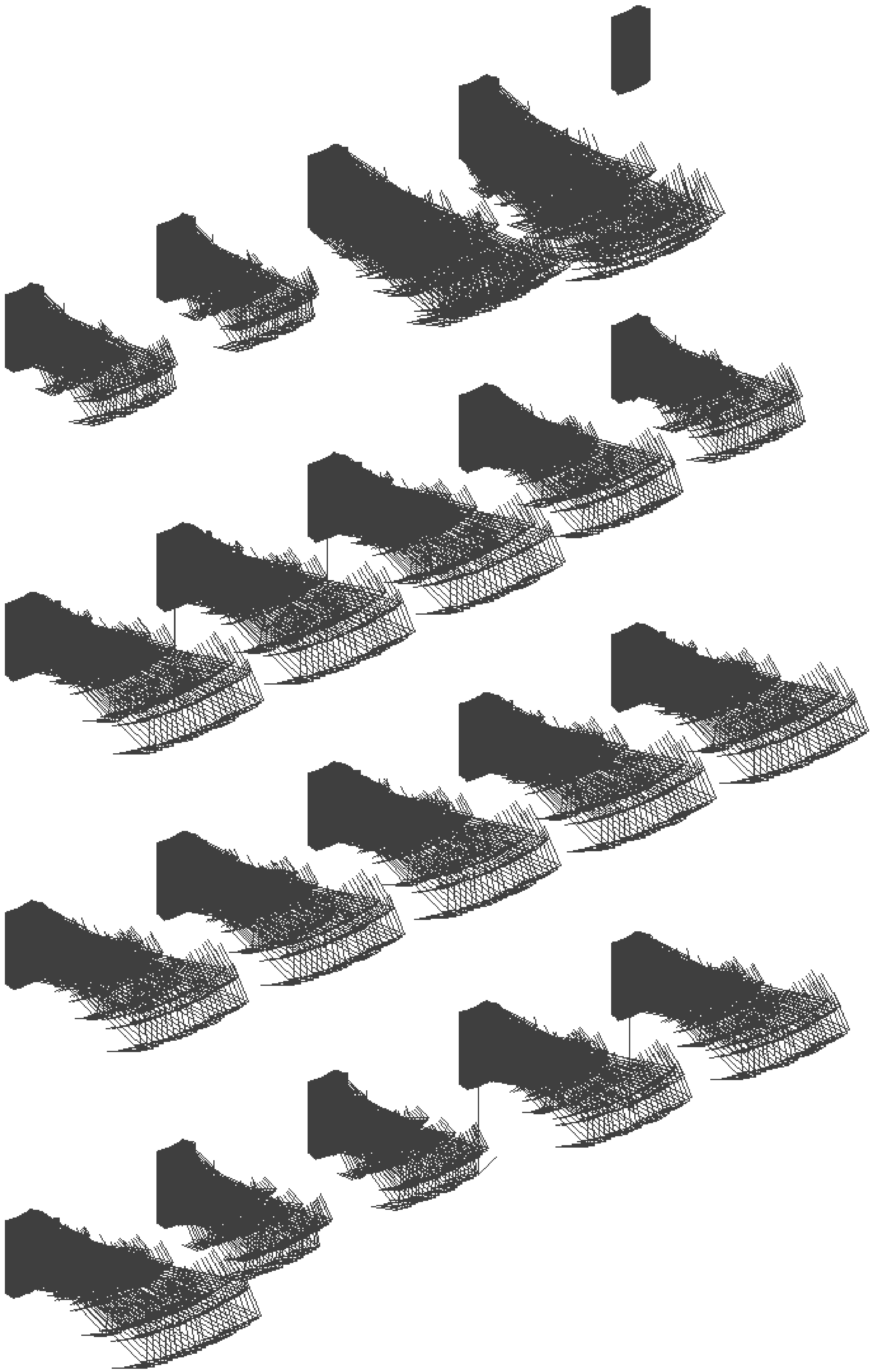

17.0 Disruption Loads on the Casing Cooling Tubes.

One of the major failures in the Upgrade project was the near failure of the copper cooling tubes on the inboard vertical divertor section of the centerstack casing. These picked up induced currents

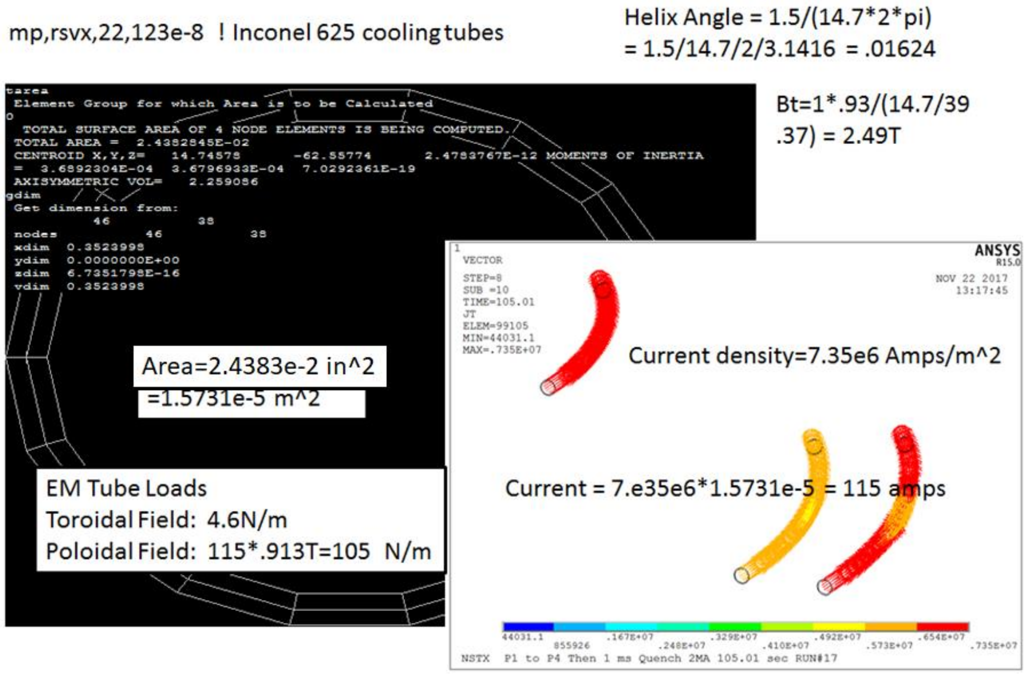

Figure 17.0-1 Loads on the Inconel 625 Tubes

In checking the results, A. Brooks found higher currents in the tubes furthest from the divertor plate. The model used in this analysis does not have these tubes modeled. The casing current density was found to be very close to the tube density so to get an indication of the upper tubes, the casing current density

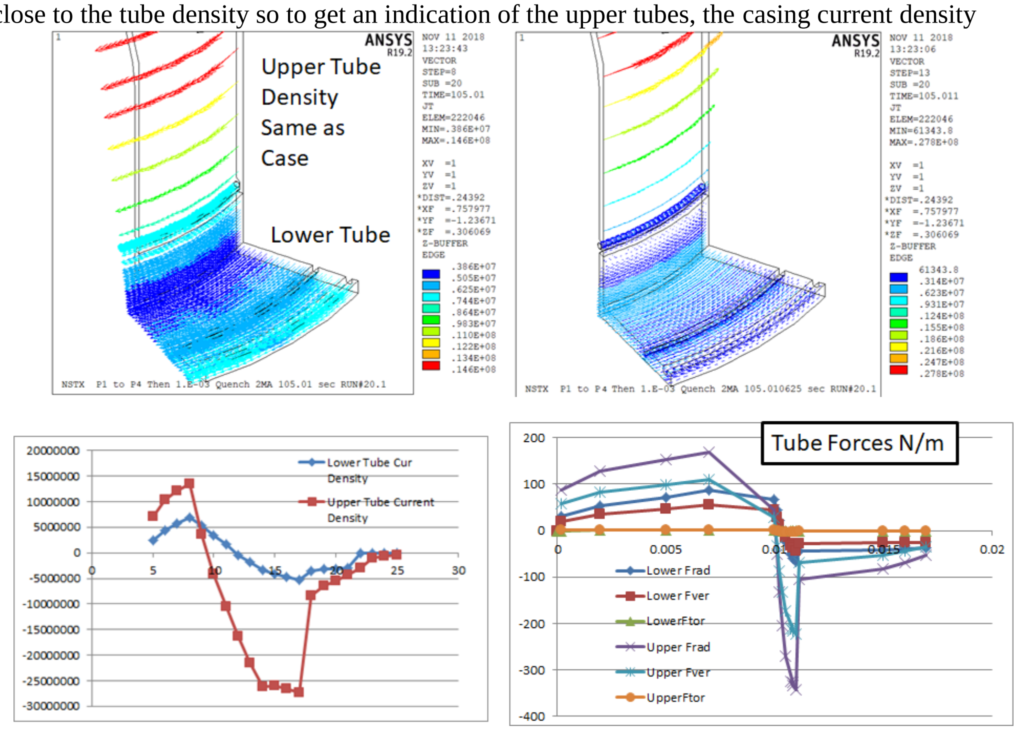

Figure 17.0-2 Current Density and Loads on the Inconel 625 Tubes P1-P4 (\emag\facet\run)

There are no Eddy Current Forces of any consequence on the new 625 cooling tubes. Art used larger values more consistent with the upper tube values in the above plot in his analysis of the tube retainers.

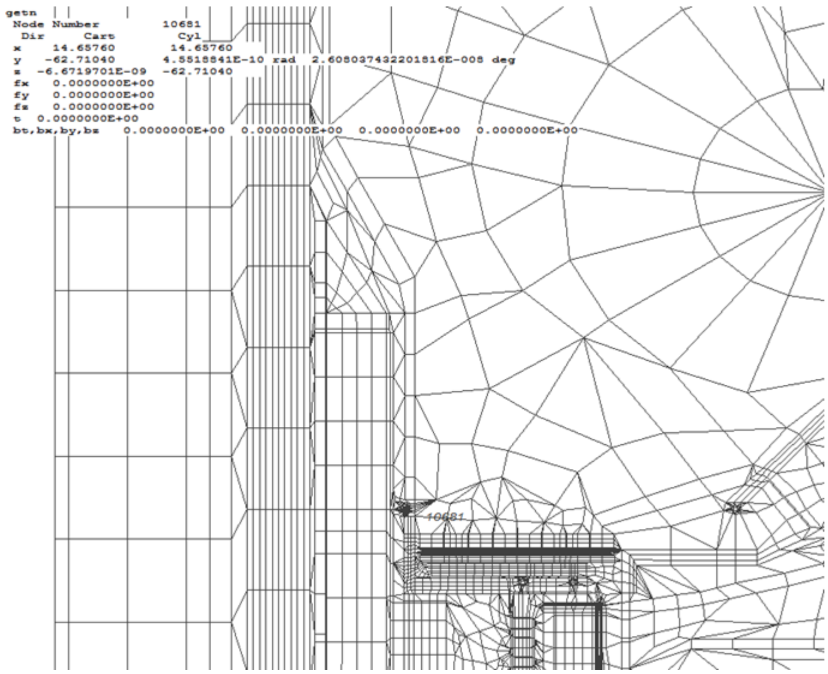

Figure 17.0-3 Coordinate Location of the tubes for Poloidal Field Calculation

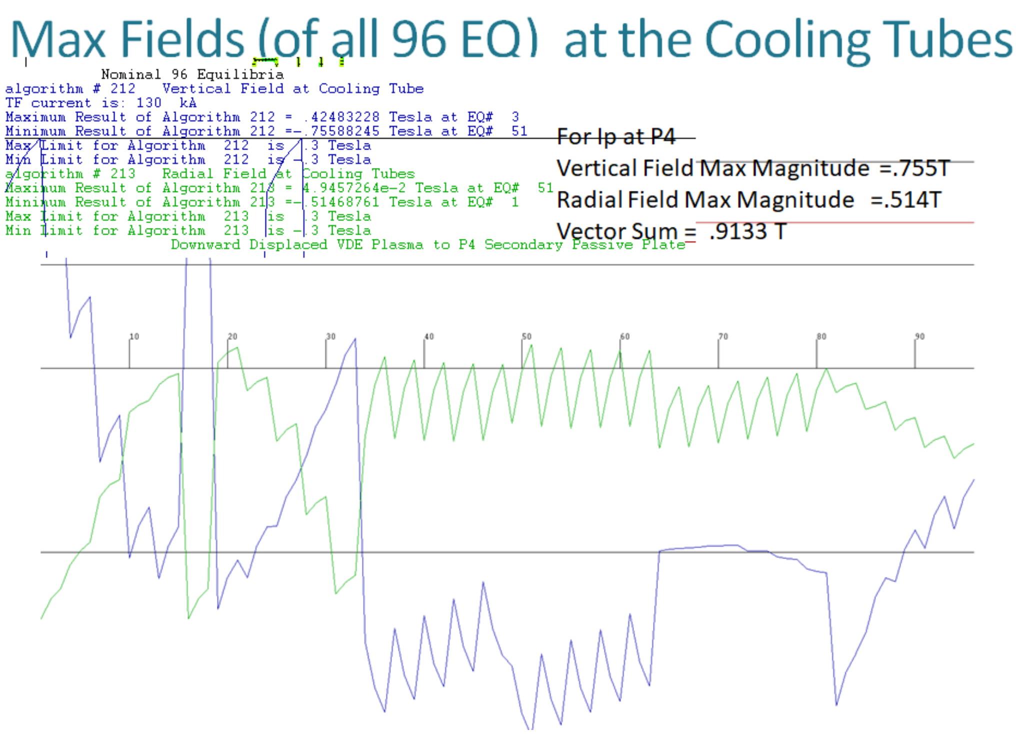

Figure 17.0-4 Max fields on the Inconel 625 Tubes for all 96 EQ for Ip at P4

18.0 Bay L Moly Shield

The objective of this analysis is to estimate and assess the stresses in a Moly shield being applied to the Bay L reinforcements caused by the plasma disruption.

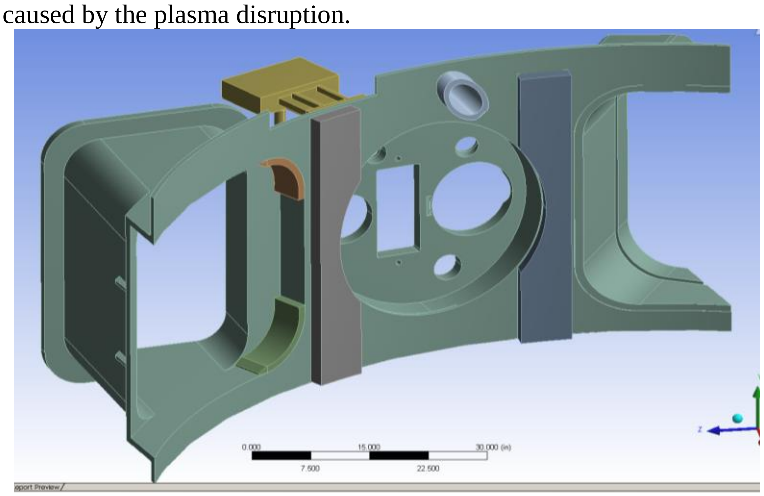

19.0 Non Circular Coils (NCC)

Job #1151****N110

19.1 Mission

The need for the non-axisymmetric control coils (NCC) is discussed in the 5 year plan [3] in section 1.4.2.2 "Utilization of non-axisymmetric (3D) magnetic fields "A small non-axisymmetric (3D) field almost always exists in tokamaks, due to imperfect primary magnets and surrounding conductors and machine components. Tokamaks are highly sensitive to 3D fields, which can cause unnecessary transport and instability and even lead to a disruption if not properly compensated. On the other hand, 3D fields can be greatly beneficial if properly controlled, by timely inducing new neoclassical process with non-ambipolar transport and by consequently modifying equilibrium profiles and macroscopic stability, as well known by edge localized mode (ELM) control using resonant magnetic fields and resistive wall mode (RWM) and tearing mode (TM) control using non-resonant magnetic fields. Therefore, it will be critical to achieve the controllability as well as the predictability of these 3D field applications, in order to improve plasma stability and performance in the next-step devices such as FNSF, ST Pilot, and ITER. To implement and augment NTSX-U capability to control 3D fields, (in vacuum) Non-Circular Coils (NCC) are being added to existing (external to the vacuum vessel) RWM coils. The new coils will be mounted on the plasma facing surface of the primary passive plates.

The objective of this calculation is to provide guidance on initial design and qualify the final design of the Non-Axisymmetric Control Coils (NCC).

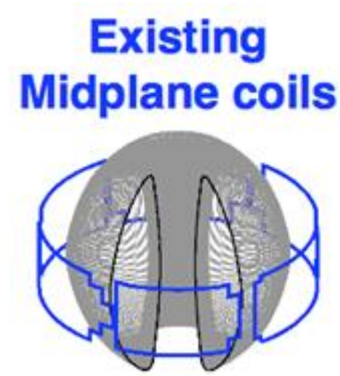

Figure 4.1-1 Resistive Wall Mode (RWM) coils

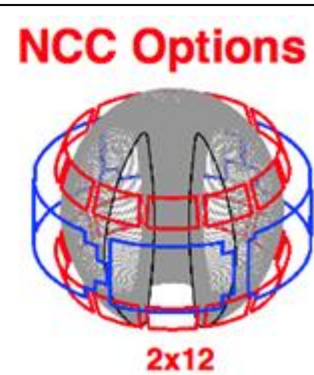

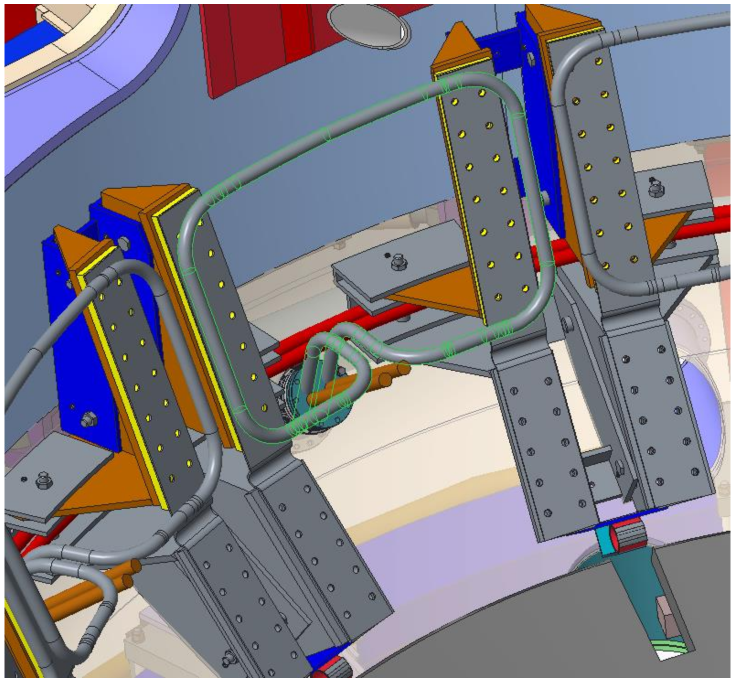

Figure 4.3-1 Coil Arrangement with Passive Plate Removed

19.1 All coils operating in 3kA DC Mode

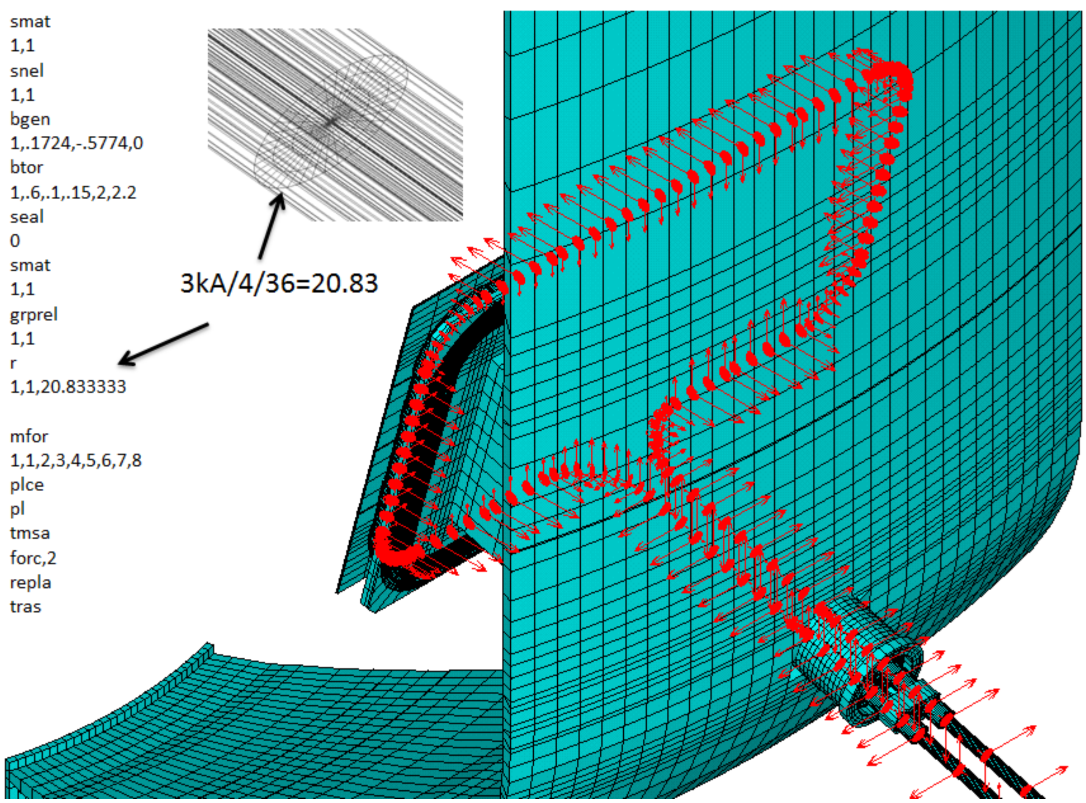

For the normal Lorentz force calculation the currents in the conductor are prescribed as 3kA total by implementing uniform currents in each element in the cross section. In this method the current density is not uniform. This is a reasonable approximation for determing Lorents loads on the conductor, but not Joule heat.

19.2.1 All Coils Operating at 3kA 60 Hz

AC operations have the potential of developing resonances.

```
/solu
antype,transient
outres,all,1     ! writes results every sub step.  Use smaller # for more resolution
nsubst,10        ! For more finer results use larger #.
psi=.005   !  Critical Damping
dfreq =150 ! Frequency at which the damping is computed
betad,2*psi/(dfreq*2*3.1416)      !beta Damping
alphd,2*psi*dfreq*2*3.1416      !alpha dampingDamping
kbc,0
fdele,all,all

tref,292
tunif,292
pi=3.1416
frequency=60
Period=1/frequency
dt=period/20
tottime=0
*do,ld,1 ,500
tottime=tottime+dt
/title,Max PF and TF on the NCC Coil %frequency% Hz %psi*100% pct damping
time,tottime
/input,forc,mod
fscale,sin(2*pi*tottime/period)
solve
save
*enddo
fini
/exit
```

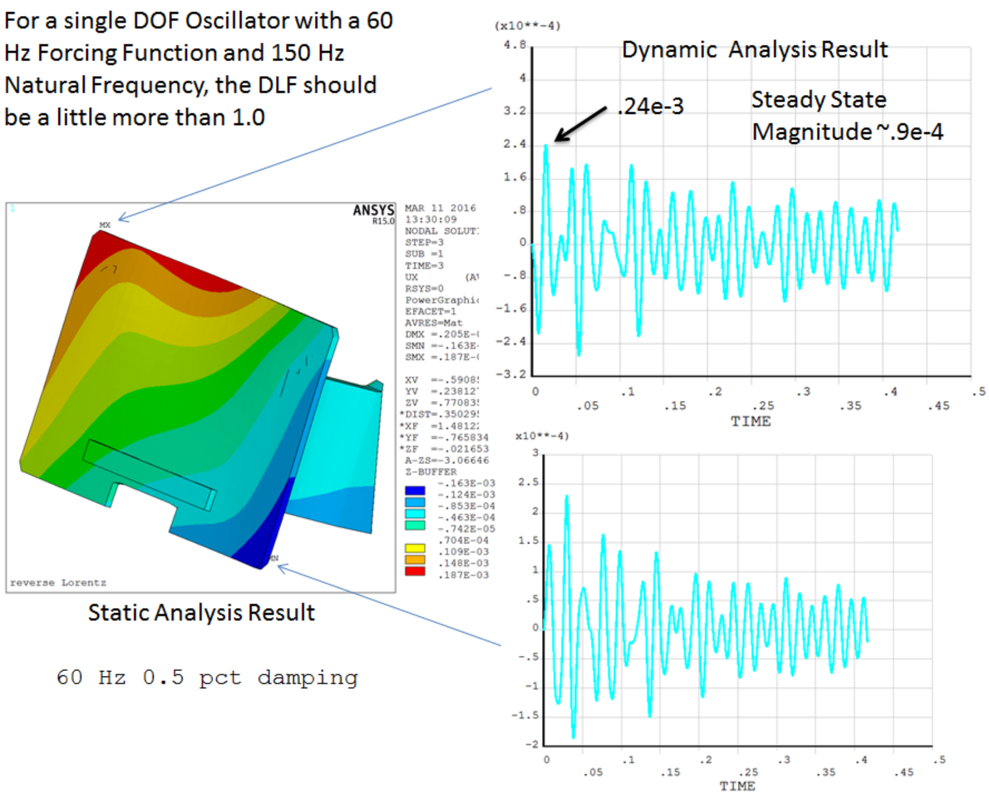

Figure 11.1.2 -1 Dynamic Response with 60, Hz Forcing Functions, l

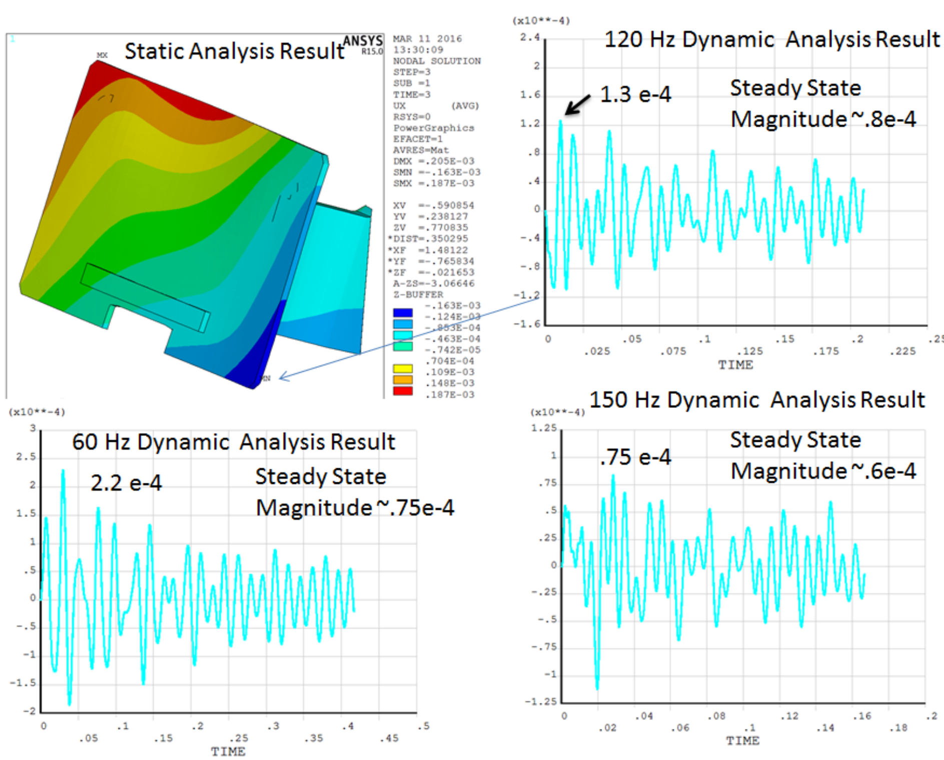

Figure 19.2 -2 Dynamic Response with 60, 120,and 150 Hz Forcing Functions, Lower Right Corner

192.1 Alternating Coils Operating with 3kA 60Hz

19.2 Static Disruption Simulation Based on the Global EMAG Model

19.3 Leads and Feedthroughs

NCC Coil Feedthru – In Vessel

- Minimum coil bend radius
- Minimum distance between bends
- Horizontal feedthru port or perpendicular port
- About 10 feet coil run as shown
- 5” port as shown
- To remove coil inside vessel, secondary passivation plate and tiles and primary tiles need to be removed
- Other potential interferences

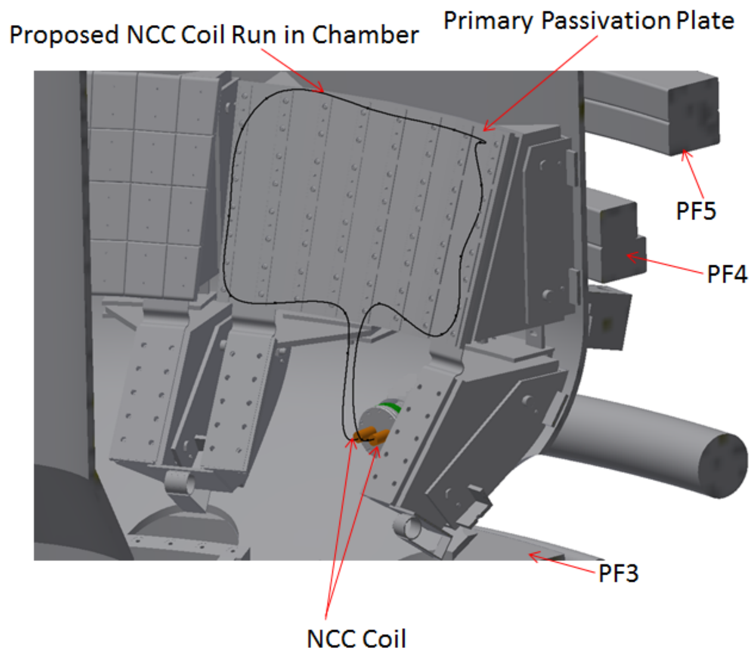

10.2.1 Moly Shield

Again, no shield is being installed at initial start-up of the Upgrade. The following calculations are being included for future reference.

19.0 Cryo-Divertor

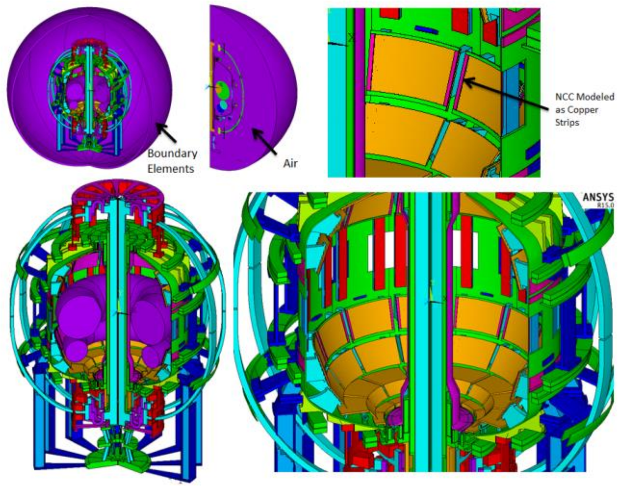

Figure `19.0-1 Electromagnetic Model

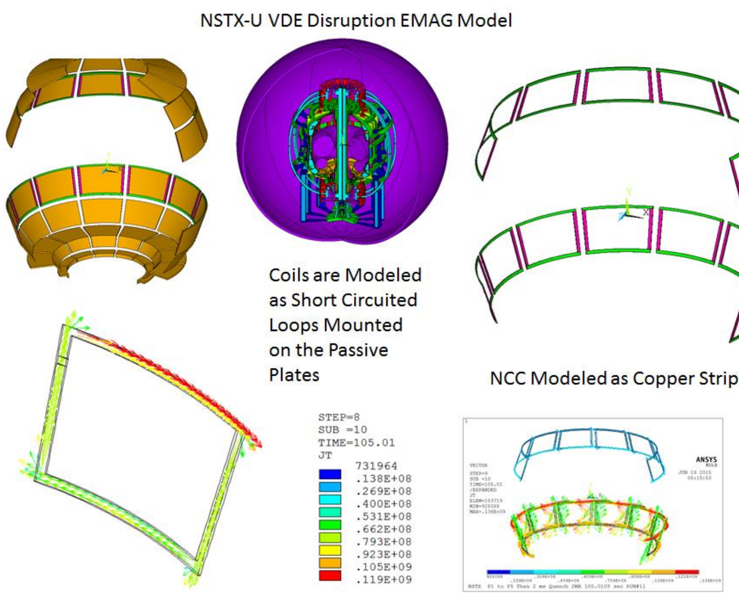

Figure 16.1-1.

19.1 Disruption Induced Currents and Voltages

An estimate of the current induced in the NCC coils in a disruption is 23 kA. This is for a self consistent full global EMAG model with the coils modeled as loops. The vector potential boundary condition sub model typically produces larger values. This was used as a basis for scaling the vector potential results. The NC coils power supplies are modeled as a short circuit. The consequences of the voltage applied to the power supplies has not been qualified. The 23kA is quite a bit larger than the 3kA nominal current.

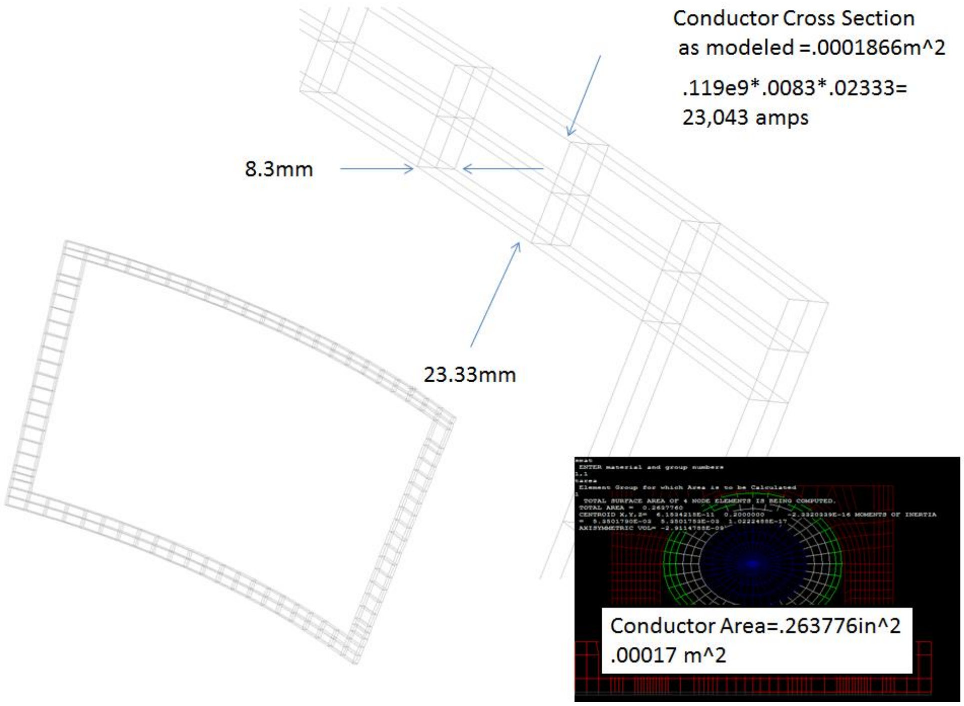

Figure 13.1-2 Induced Coil Current during a Disruption.

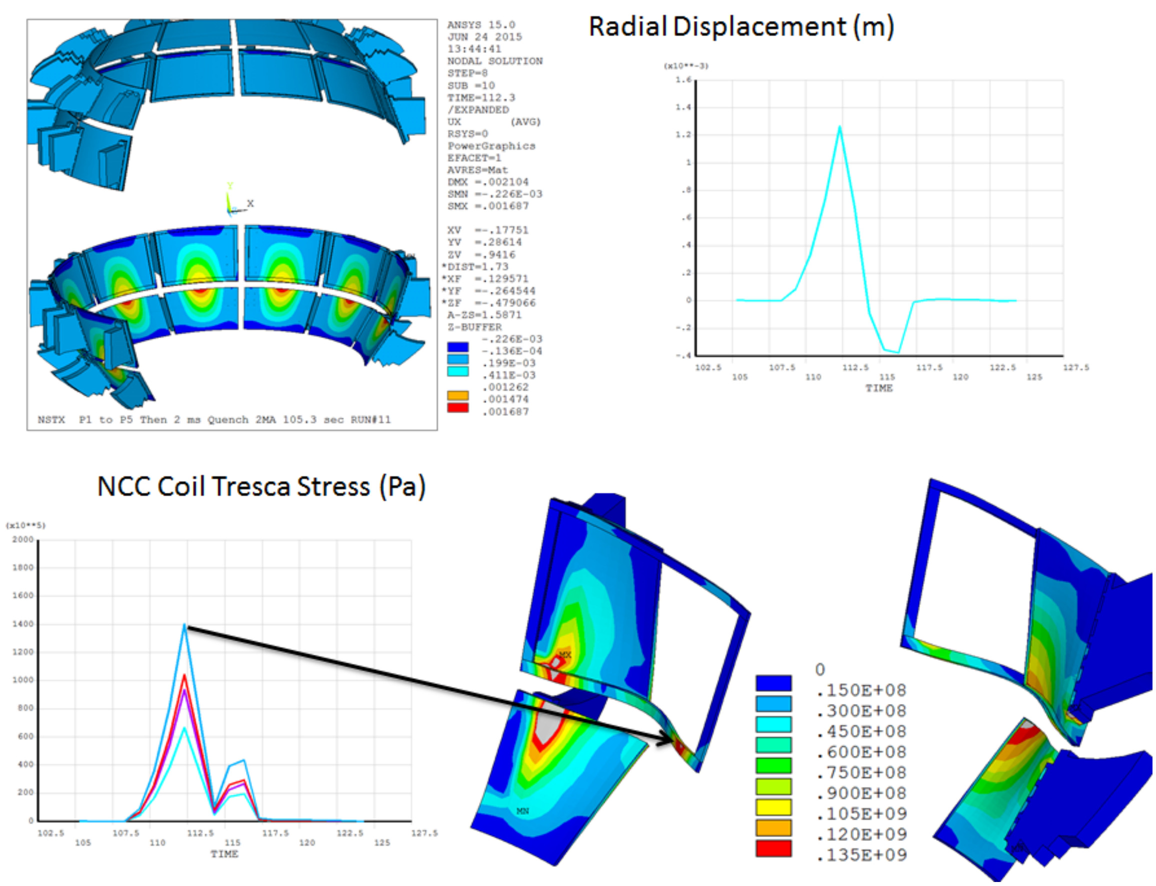

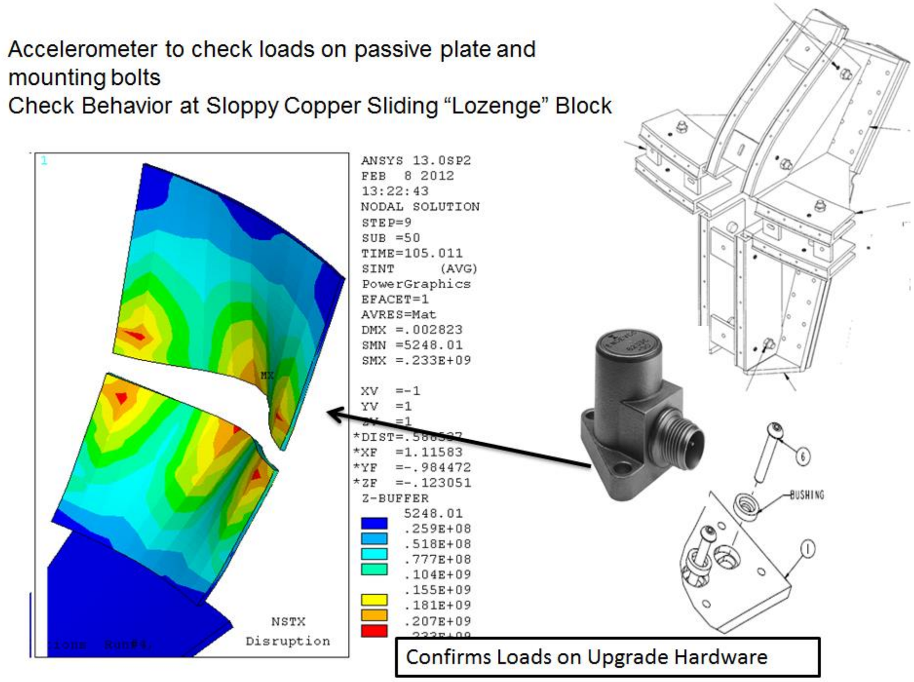

Figure 16.0-5 Passuive Plate Accelerometer Location

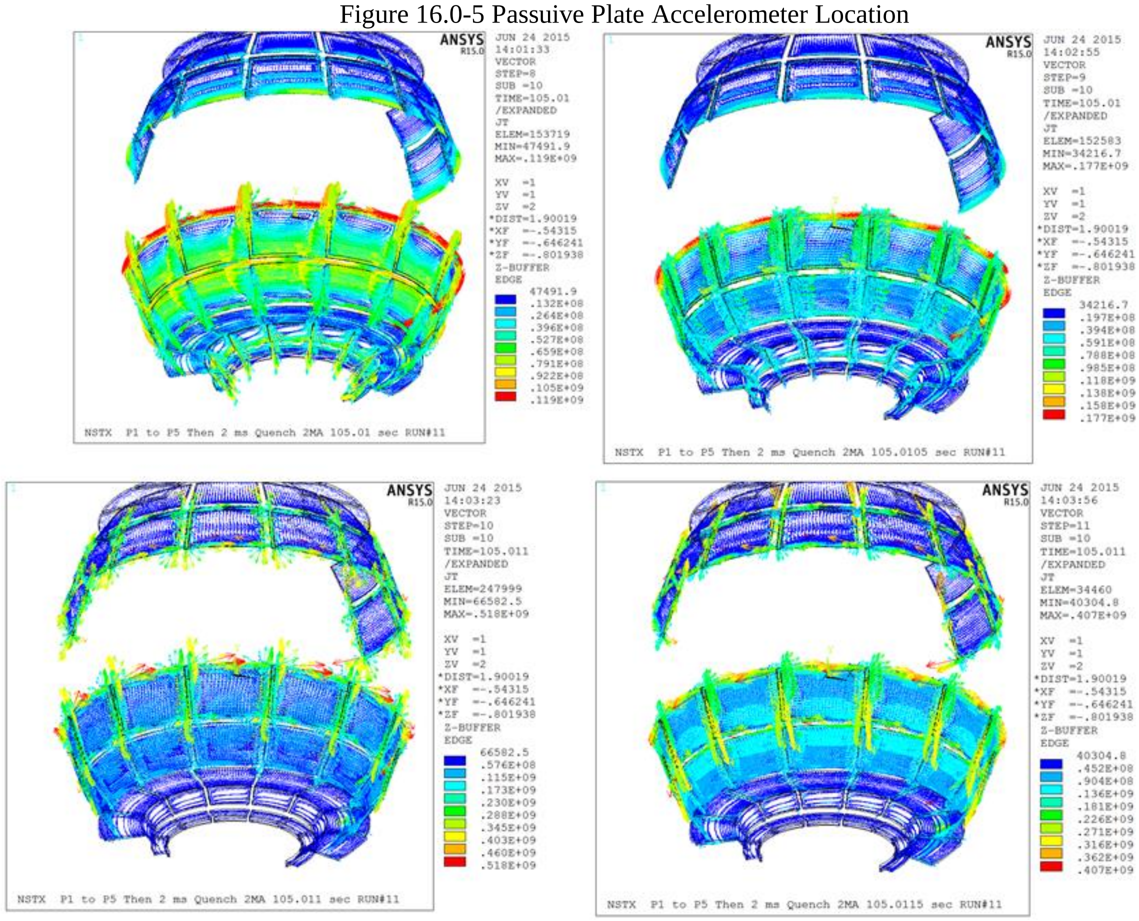

Figure 16.0-6

17.5 NCC Coil Frequency and Dynamic Load Factors

The NCC coils are excited with alternating currents as well as direct current. It is important that resonances are avoided. In the passive plate dynamic analysis, a natural frequency can be inferred from the vibrations induced by the disruption, after the disruption loading ceases.

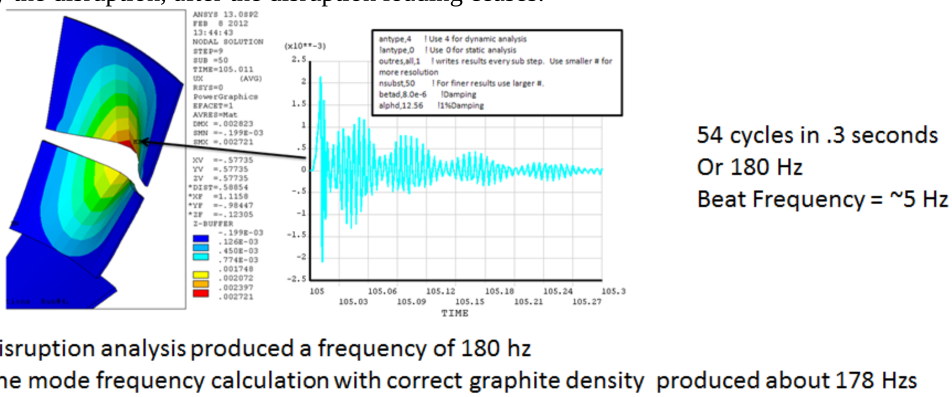

Figure 16.0-1 Transient Response to a Disruption

The natural frequency of the free vibration of the passive plates after being hit with a disruption, is 180 Hz. This is compared with a mode-frequency analysis of a similar model that produced 178 Hz. The March 2016 model produces a first mode natural frequency of 102 Hz. For a mode shape unlike the Disruption loading displaced shape. The first mode from the March 2016 model that would have a significant participation factor with respect to the disruption load vector is mode 4 which has a frequency of 150 Hz.

*** FREQUENCIES FROM BLOCK LANCZOS ITERATION **

MODE	FREQUENCY (HERTZ)	MODE	FREQUENCY (HERTZ)
1	102.2992177716	26	413.5604746133
2	125.3377113582	27	416.0699088934
3	149.2941074407	28	418.1962143721
4	150.1831224353	29	419.8462549718
5	180.8313673552	30	432.7760988058
6	193.4630716752	31	434.4536628572
7	197.8147607743	32	453.5461456329
8	216.8837237584	33	462.9975700338
9	224.3131097182	34	474.3336620202
10	231.6380656735	35	481.3803803941
11	250.3953135053	36	487.4622898946
12	269.9654017797	37	491.2348033066
13	287.9451990936	38	495.6887566049
14	311.1288475549	39	501.3666223354
15	312.8238362314	40	506.1222786130
16	319.5156399463	41	509.7167185027
17	320.0148979155	42	513.5216425535
18	327.7343734282	43	534.8906305992
19	333.5832284982	44	535.3772576591
20	335.5831695279	45	545.0027287839
21	340.5953642824	46	566.3732616966
22	379.2453436331	47	568.9447043289
23	387.5423176890	48	571.2463352274
24	400.6831177791	49	574.9149550725
25	413.0217146923	50	579.1521536045

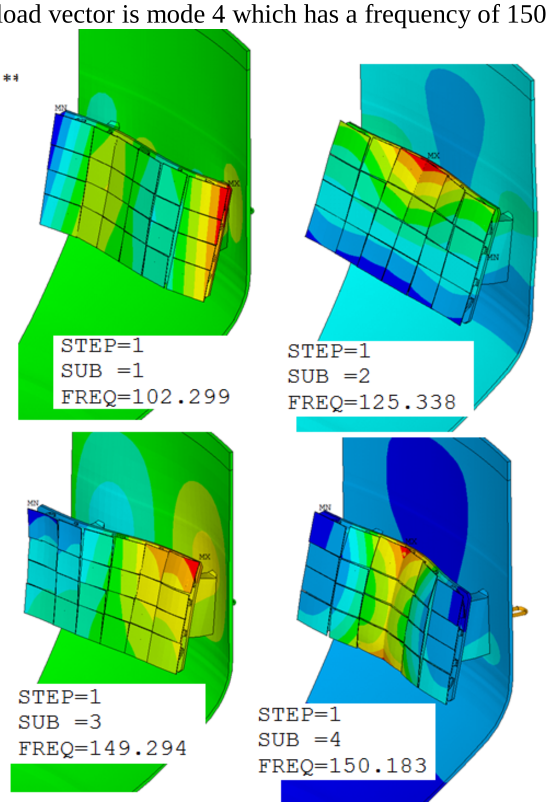

Figure 16.0-2 Mode-Frequency Analysis of the NCC coils

Looking at the mode shapes in Figure 14.0-2, mode 3 would have some significant coupling with the normal operating loads and deflected shapes. The frequency of mode 3 is 149 Hz, well away from the 66 Hz

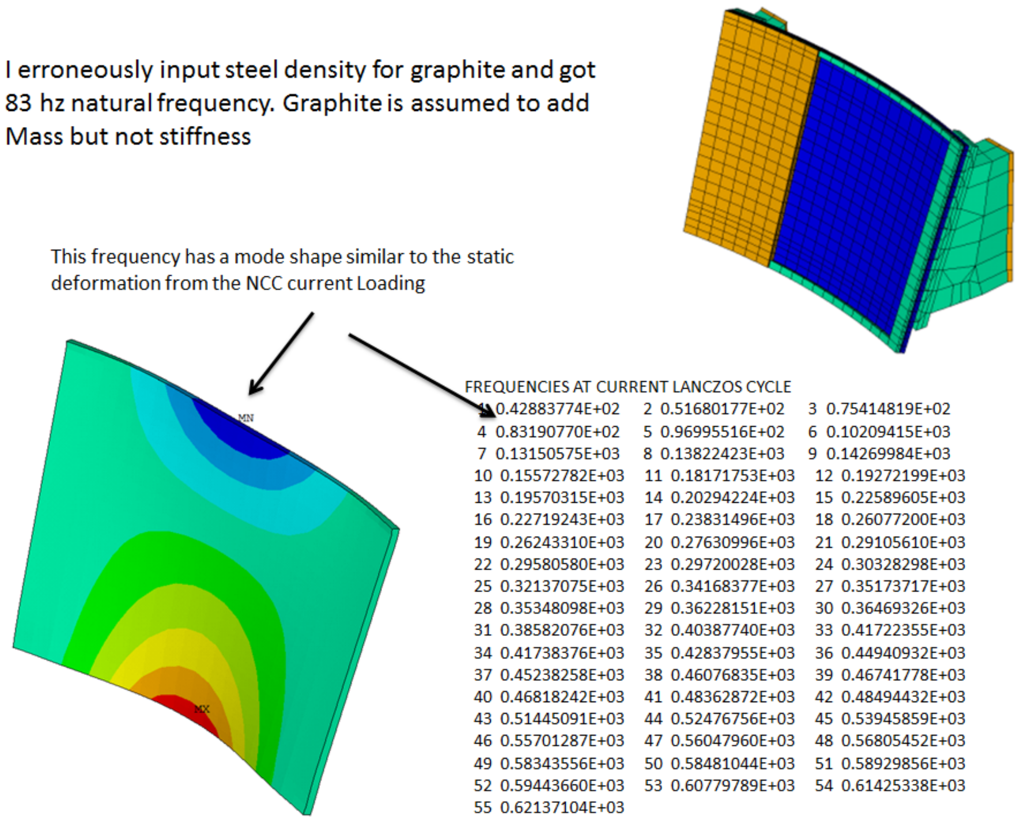

Figure 16.0-3 Mode-Frequency Analysis of the NCC coils witgh Steel Density for the Tiles

NCC 83 Hz forcing function, .5% damping

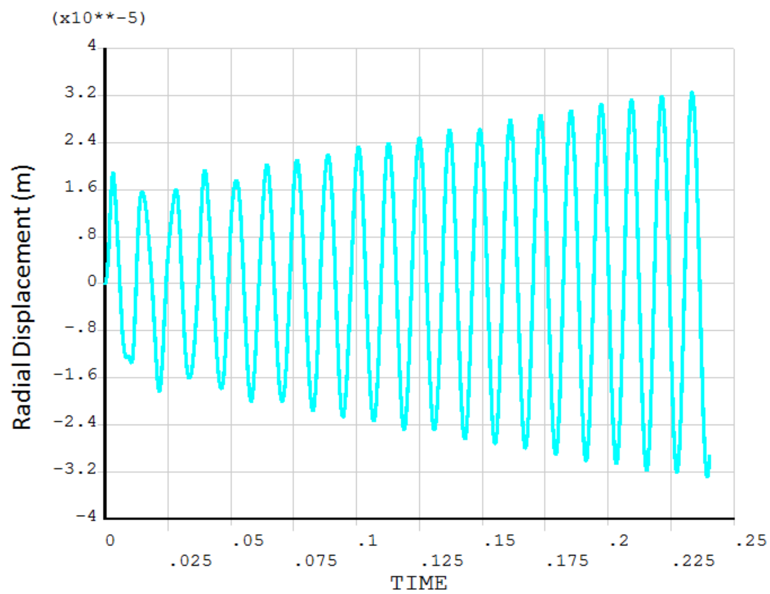

With the wrong natural frequency I got amplification

Figure 16.0-4 Transient Analysis of the NCC coils with a 83 Hz Forcing Function

With graphite density corrected I got No Resonance

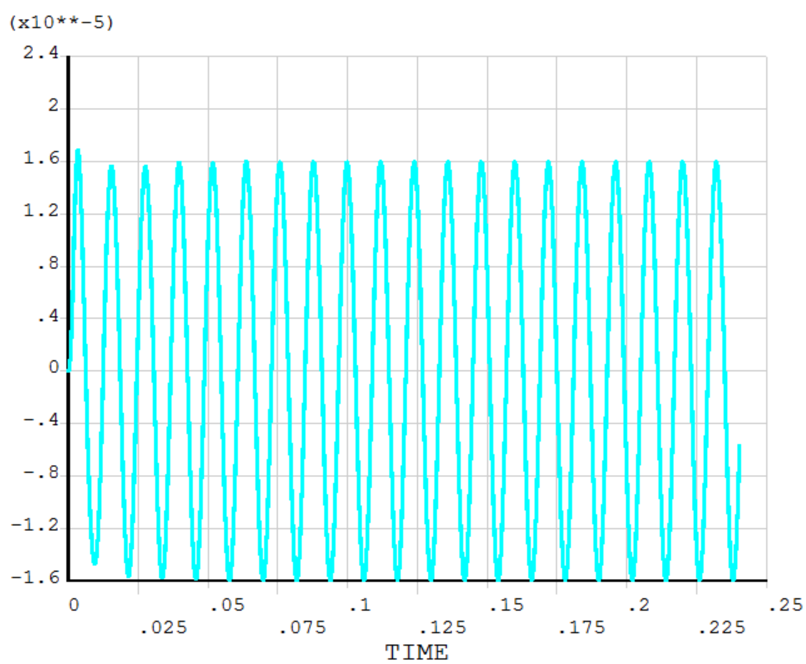

Max PF and TF on the NCC Coil 83 Hz 5 pct damping

Figure 14.0-5 Transient Analysis with Proper Graphite Tile Density, at 83 Hz Forcing Function

20.0 Cryo-Divertor Analysis

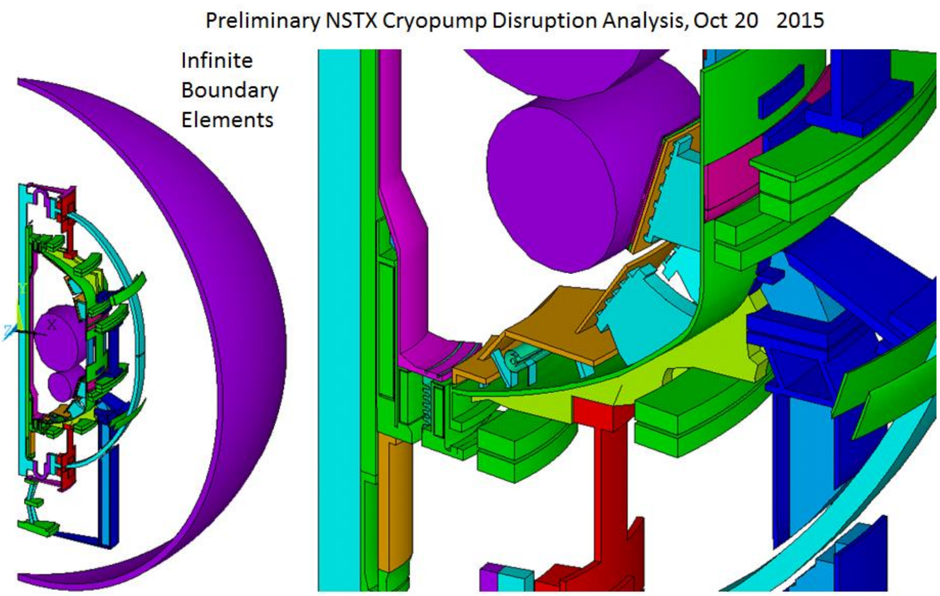

Figure 20.0-1

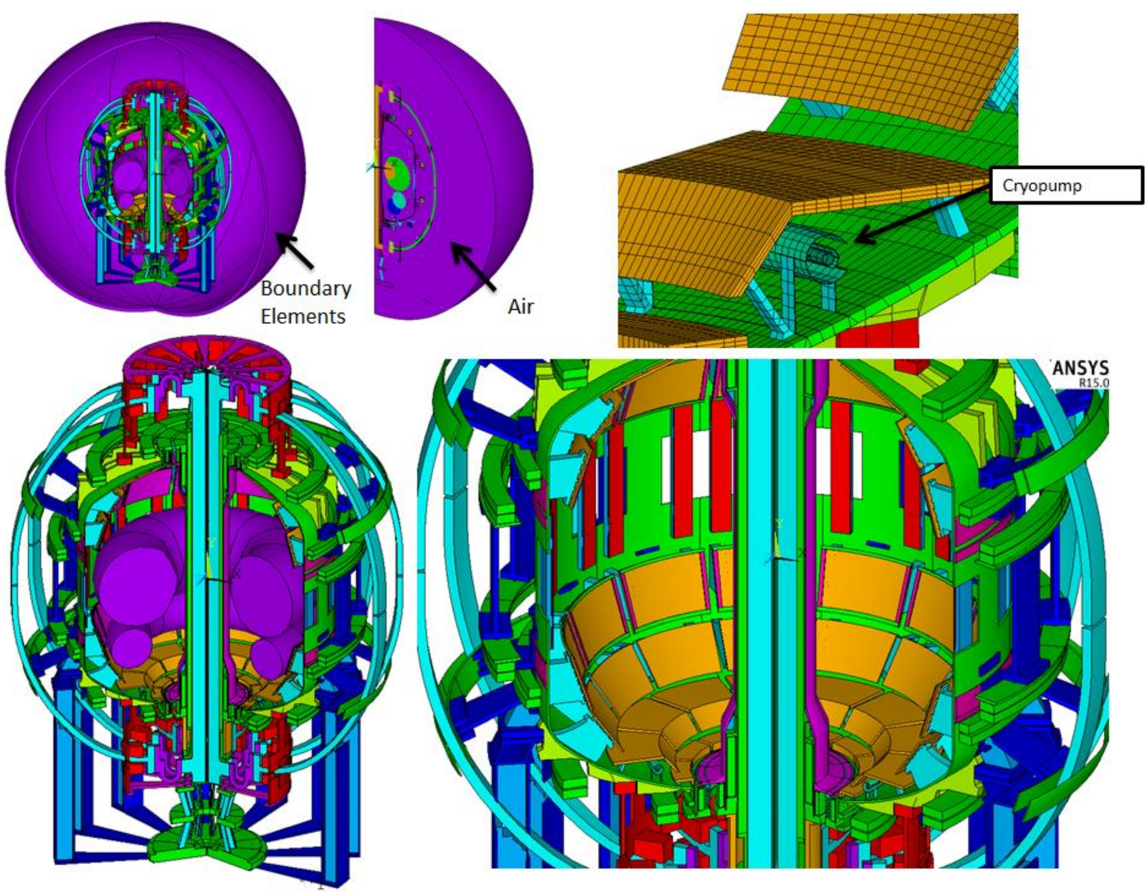

Figure 20.2 More of the Cryopump Electromagnetic Model

Figure 20.0-2 Displacement Compatibility at the Termination

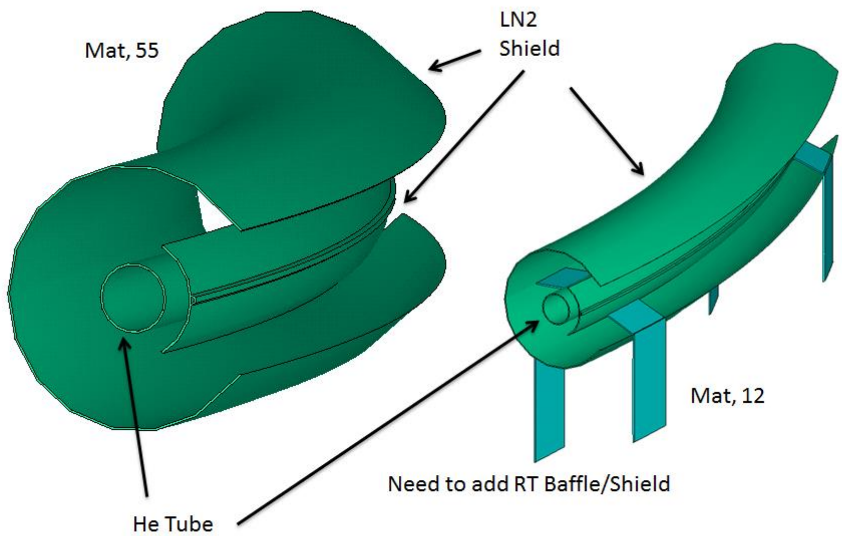

Figure 17.0-3 Bake-Out Stress at the Termination

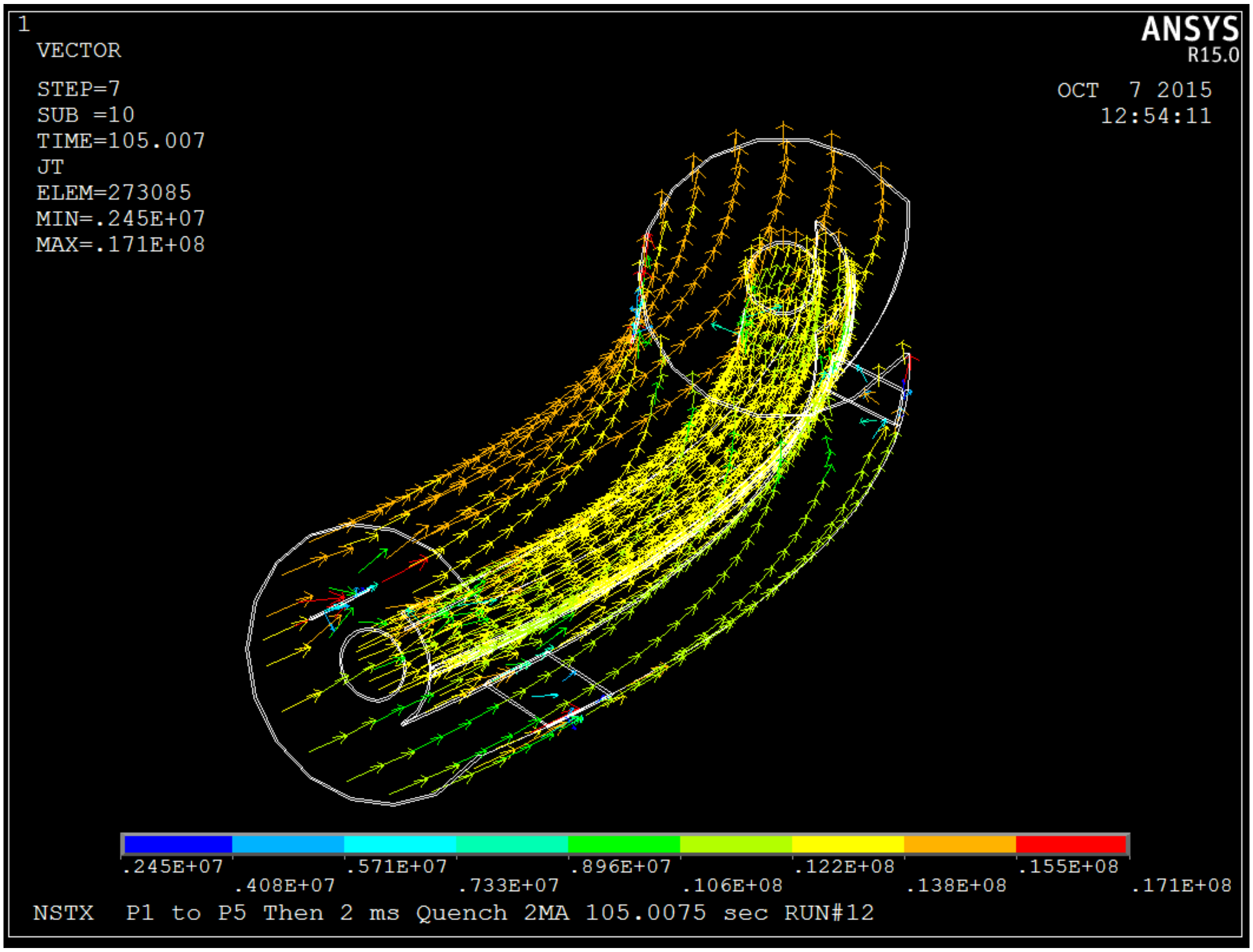
1
VECTOR
STEP=7
SUB =10
TIME=105.007
JT
ELEM=273085
MIN=.245E+07
MAX=.171E+08
ANSYS
R15.0
OCT 7 2015
12:54:11
.245E+07
.408E+07
.571E+07
.733E+07
.896E+07
.106E+08
.122E+08
.138E+08
.155E+08
.171E+08
NSTX P1 to P5 Then 2 ms Quench 2MA 105.0075 sec RUN#12

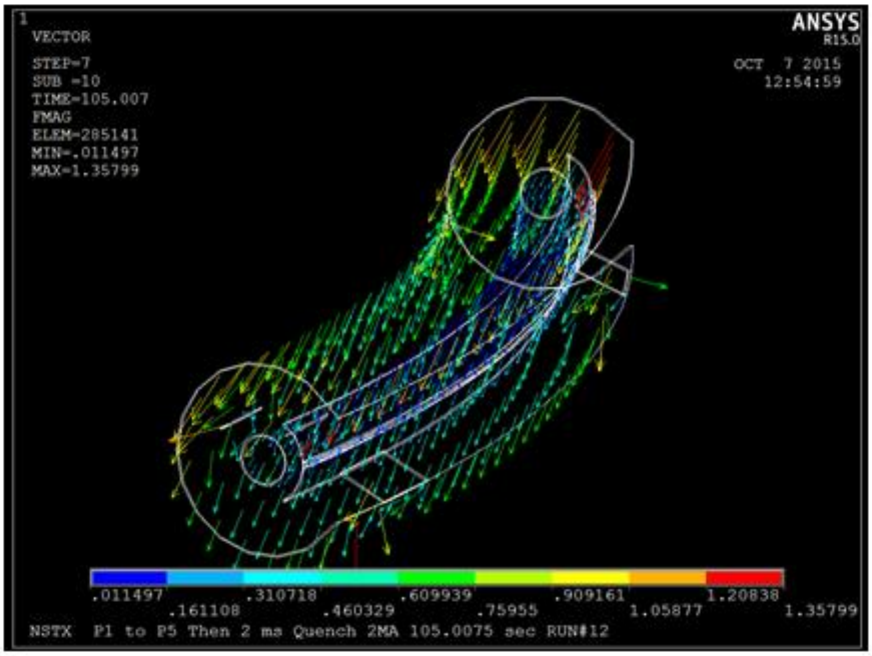
ANSYS
R15.0
VECTOR
STEP=7
SUB =10
TIME=105.007
FMAG
ELEM=285141
MIN=.011497
MAX=1.35799
OCT 7 2015
12:54:59
.011497
.161108
.310718
.460329
.609939
.75955
.909161
1.05877
1.20838
1.35799
NSTX P1 to P5 Then 2 ms Quench 2MA 105.0075 sec RUN#12

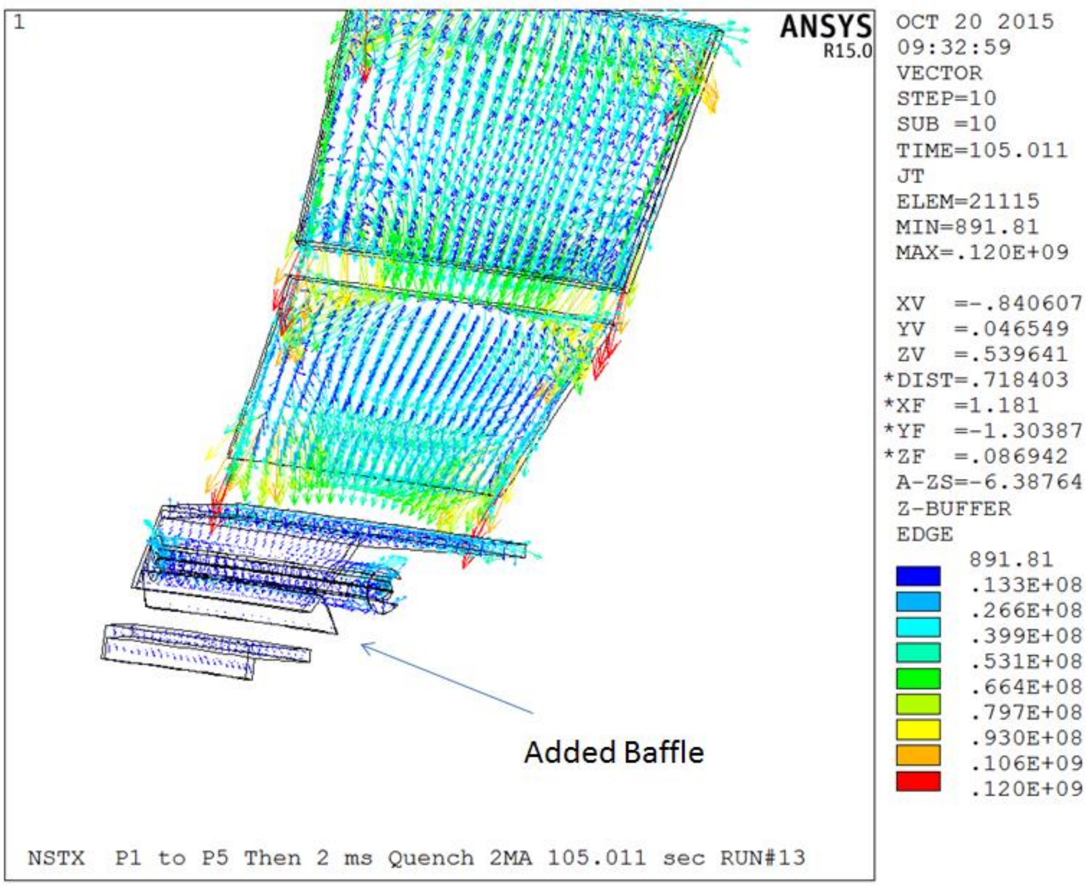
ANSYS
R15.0
OCT 20 2015
09:32:59
VECTOR
STEP=10
SUB =10
TIME=105.011
JT
ELEM=21115
MIN=891.81
MAX=.120E+09
XV =-.840607
YV =.046549
ZV =.539641
*DIST=.718403
*XF =1.181
*YF =-1.30387
*ZF =.086942
A-ZS=-6.38764
Z-BUFFER
EDGE
891.81
.133E+08
.266E+08
.399E+08
.531E+08
.664E+08
.797E+08
.930E+08
.106E+09
.120E+09
Added Baffle
NSTX P1 to P5 Then 2 ms Quench 2MA 105.011 sec RUN#13

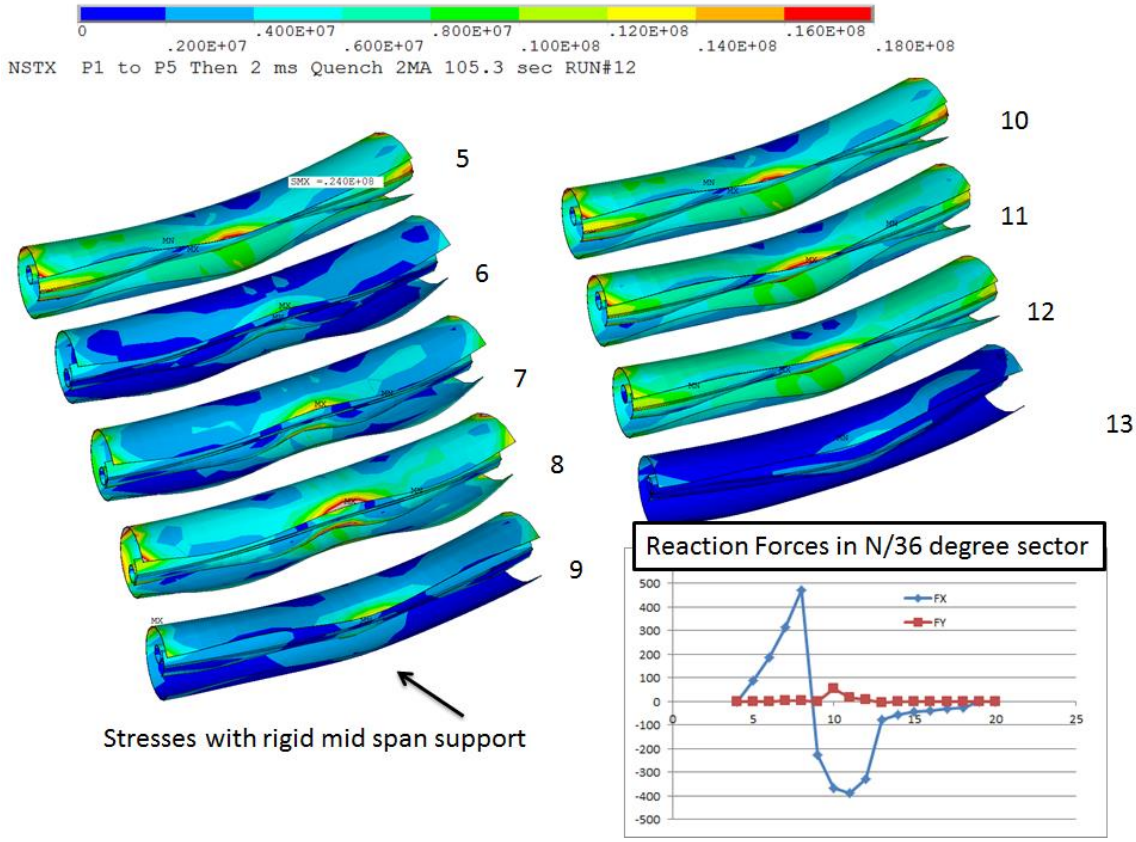
0
.200E+07
.400E+07
.600E+07
.800E+07
.100E+08
.120E+08
.140E+08
.160E+08
.180E+08
NSTX P1 to P5 Then 2 ms Quench 2MA 105.3 sec RUN#12
SMX =.240E+08
5
6
7
8
9
10
11
12
13
Stresses with rigid mid span support
Reaction Forces in N/36 degree sector
FX
FY
500
400
300
200
100
0
-100
-200
-300
-400
-500
0
5
10
15
20
25

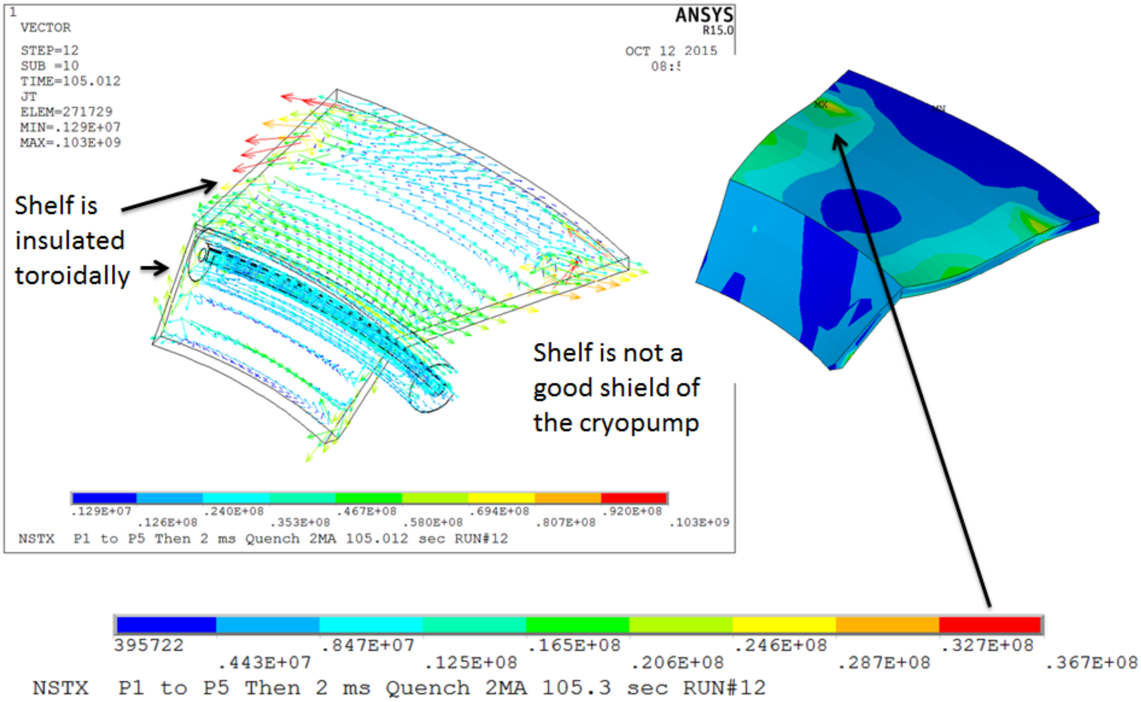

21.0 Copper Divertor Tubes (Pre-Recovery)

In the vintage of the Cryo-Divertor studies, the copper tubes in the divertor flange were also modeled. These tubes will be replaced with Inconel tubes, so the induced eddy currents will be much less than calculated here

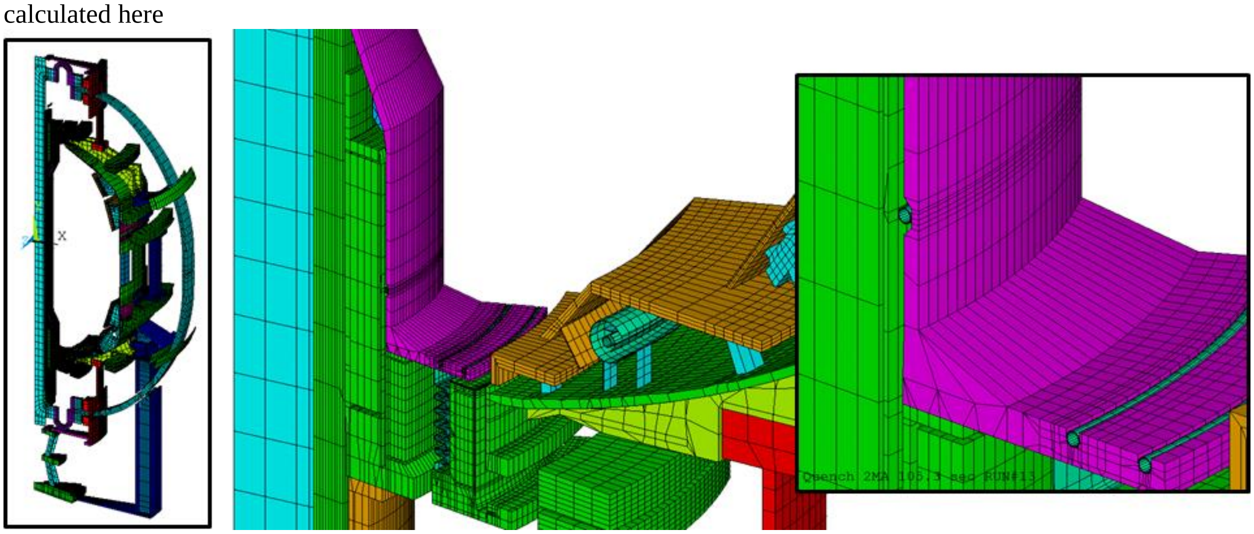

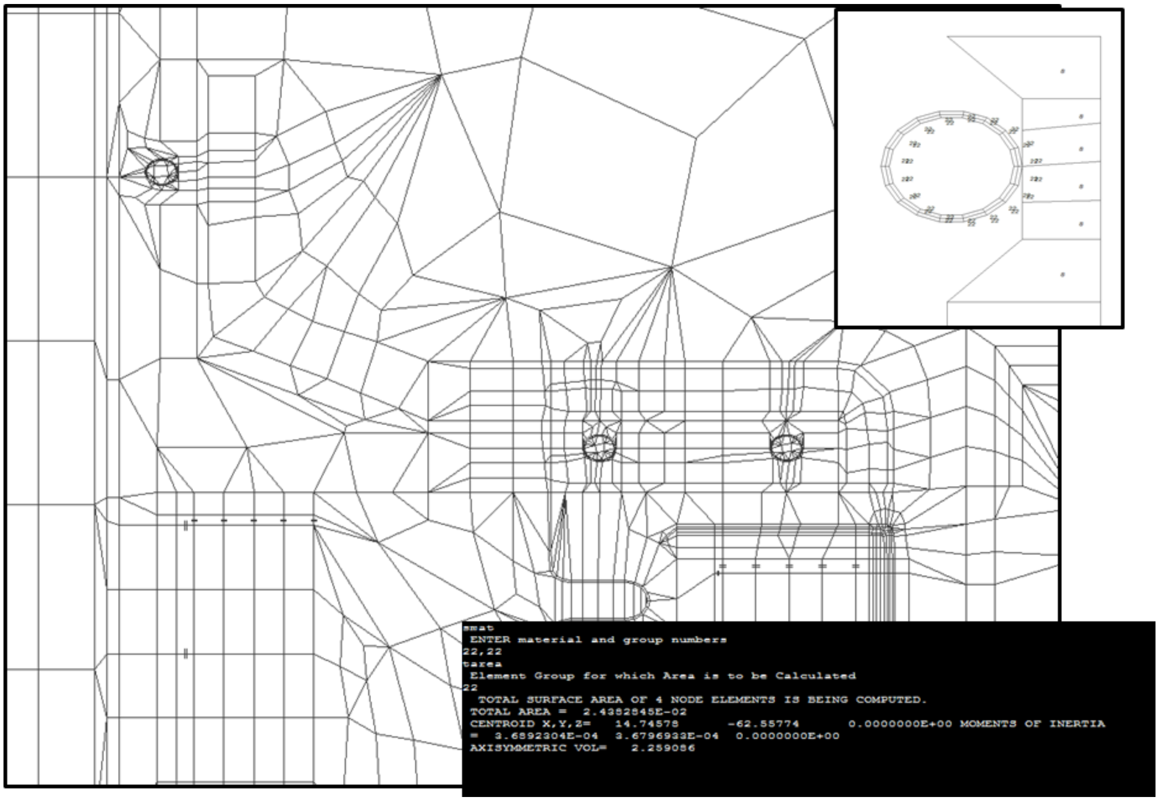

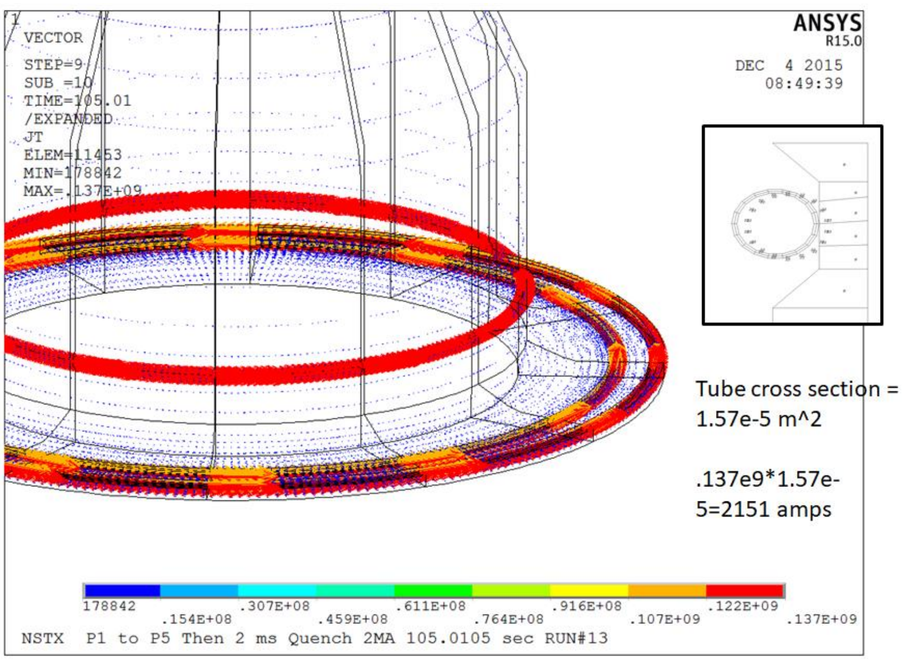

22.0 PF1c Case Disruption Currents (Pre Recovery)

Prior to the deletion of the CHI capability in NSTXU, there was a potential for plasma to enter the CHI gap and heat the PF1c case. This overheated the case. Various shields were investigated including a moly shield. This would have the potential of picking up significant eddy currents. Disruption loads on the PF1c case were calculated with an analysis and model developed for the passive plate simulation, [ref 3 Appendix I]. Only the lower PF1c case was modeled (See section 7.0) A downward VDE was modeled, so the lower case needed to be detailed, but the results are representative for an upper PF1c and VDE. The molybdenum thermal shield might have been interesting in terms of disruption response. The disruption model was re-run with only the stainless steel casing. The peak stress was about one MPa

Figure 22.0-4 Results for a stainless steel PF1c Case

The thermal performance of the PF1c case and thermal shield is analyzed using a True Basic code that is included in appendix E. Results of this program are tabulated below:

Figure 22-1 Results with the Thermal Shield

Appendix E is set up to produce the upper plot in figure 10.0-1

Figure 22-2

Figure 22-3

22.2 With Thermal Shield

Len Myatt recommended an 1/8 inch outer shell. – This leaves the design with 1/8th of an inch for a thermal shield. The first option investigated was a 1/16 inch of moly and a few layers of SST shim stock like was used on the C-Mod outer divertor. This is geometrically tight. The shield is also the electrode for the CHI so the shield design may be challenging. It is not needed early in the operation of the machine, but may be needed later.

Figure 10.2-1 Thermal Shield Concept

Appendix A

Appendix B

Appendix C

True Basic Program to Compute Force Densities from Nodal Forces

```
dim d$(20),dd(20)
dim nn(350000),nx(350000),ny(350000),nz(350000)
dim n1(350000),n2(350000),n3(350000),n4(350000),n5(350000),n6(350000),n7(350000),n8(350000)
dim fx(350000),fy(350000),fz(350000)


for iload=1 to 9
let innfile$="nlist.lis"
let inefile$="elist.lis"

let inffile$="q1flist0"&str$(iload)&".lis"
let outfile$="f10"&str$(iload)&".txt"
let cloudfile$="c10"&str$(iload)&".txt"
OPEN #1: name innfile$, create old
OPEN #2: name inefile$, create old
OPEN #3: name inffile$, create old
when error in
unsave outfile$
use
end when
when error in
unsave cloudfile$
use
end when
OPEN #4: name outfile$, create new
OPEN #5: name cloudfile$, create new
!when error in
do while more #1
line input #1: line$
!print line$
CALL comint(" ",line$,d$(),dd())
if dd(1)>0 then
let n=n+1
print dd(1);",";dd(2);",";dd(3);",";dd(4)
print#4: "n"
print#4: dd(1);",";dd(2);",";dd(3);",";dd(4)
let nn(dd(1))=dd(1)
let nx(dd(1))=dd(2)
let ny(dd(1))=dd(3)
let nz(dd(1))=dd(4)
end if
loop

do while more #2
line input #2: line$
!print line$
CALL comint(" ",line$,d$(),dd())
if dd(1)>0 then
let e=e+1
!print dd(7);",";dd(8);",";dd(9);",";dd(10)
print#4: "mat"
```

```
print#4: dd(2)
print#4: "e"
print#4: dd(7);",";dd(8);",";dd(9);",";dd(10);",";dd(11);",";dd(12);",";dd(13);",";dd(14)
let n1(e)=dd(7)
let n2(e)=dd(8)
let n3(e)=dd(9)
let n4(e)=dd(10)
let n5(e)=dd(11)
let n6(e)=dd(12)
let n7(e)=dd(13)
let n8(e)=dd(14)

end if
loop

do while more #3
line input #3: line$
!print line$
CALL comint(" ",line$,d$(),dd())
if dd(1)>0 then
print#4: "f"
print#4: dd(1);",";dd(2);",";dd(3);",";dd(4)
!let nn(dd(1))=dd(1)
let fx(dd(1))=dd(2)
let fy(dd(1))=dd(3)
let fz(dd(1))=dd(4)
end if
loop

!let line$=ucase$(trim$(line$))
!let b$=line$
!  DO    ! loop which splits up input by $
!   LET pcs=pos(b$,"$")
!   IF pcs=0 then LET a$=b$
!   IF pcs>0 then LET a$=b$[1:pcs-1]
!   IF pcs>0 then LET b$=b$[pcs+1:80]
!   CALL comint(",",a$,d$(),dd())
!
!
!print line$
!let l=len(a$)
!if d$(1)="N"  then
!print "n"
!print a$[3:l]
!print#1: "n"
!print#1: a$[3:l]
!print#1: dd(2);",";dd(3);",";dd(4);",";dd(5)
!end if
!if d$(1)="F"then
!F, 1,FX, -.28809E+07 $F, 1,FY, .18805E-01 $F, 1,FZ, .25462E+06
!print#1: "fa  "
!if d$(3)="FX" then print#1: dd(2);",";dd(4);",0,0"
!if d$(3)="FY" then print#1: dd(2);",0,";dd(4);",0"
!if d$(3)="FZ" then print#1: dd(2);",0,0,";dd(4)
!end if
```

```
!if d$(1)="E"then
!print#1: "e"
!print#1: a$[3:l]&",0,0,0,0,0,0"
!print#1: dd(2);",";dd(3);",";dd(4);",";dd(5);",";dd(6);",";dd(7);",";dd(8);",";dd(9)
!print a$[3:l]&",0,0,0,0,0,0"
!end if
!
!if d$(1)="MAT" then
!print#1: "mat"
!print#1: dd(2)
!end if
!
!if d$(1)="REAL" then
!print#1: "real"
!print#1: dd(2)
!end if
!
!if d$(1)="TYPE" then
!print#1: "type"
!print#1: dd(2)
!end if
!if pcs=0 then exit do

for i=1 to e
call evol(i,n1(),n2(),n3(),n4(),n5(),n6(),n7(),n8(),nx(),ny(),nz(),vol)
let xave=(nx(n1(i))+nx(n2(i))+nx(n3(i))+nx(n4(i))+nx(n5(i))+nx(n6(i))+nx(n7(i))+nx(n8(i)))/8
let yave=(ny(n1(i))+ny(n2(i))+ny(n3(i))+ny(n4(i))+ny(n5(i))+ny(n6(i))+ny(n7(i))+ny(n8(i)))/8
let zave=(nz(n1(i))+nz(n2(i))+nz(n3(i))+nz(n4(i))+nz(n5(i))+nz(n6(i))+nz(n7(i))+nz(n8(i)))/8
let fxave=(fx(n1(i))+fx(n2(i))+fx(n3(i))+fx(n4(i))+fx(n5(i))+fx(n6(i))+fx(n7(i))+fx(n8(i)))/8/vol
let fyave=(fy(n1(i))+fy(n2(i))+fy(n3(i))+fy(n4(i))+fy(n5(i))+fy(n6(i))+fy(n7(i))+fy(n8(i)))/8/vol
let fzave=(fz(n1(i))+fz(n2(i))+fz(n3(i))+fz(n4(i))+fz(n5(i))+fz(n6(i))+fz(n7(i))+fz(n8(i)))/8/vol
print#5: -xave;",";yave;",";-zave;",";-fxave;",";fyave;",";-fzave        ! This was to rotate 180Deg
next i
!use
print#4:"exit"
print#4:"exit"
close #1
close #2
close #3
close #4
close #5
next iload

for iload=10 to 20
let innfile$="nlist.lis"
let inefile$="elist.lis"

let inffile$="q1flist"&str$(iload)&".lis"
let outfile$="f1"&str$(iload)&".txt"
let cloudfile$="c1"&str$(iload)&".txt"
OPEN #1: name innfile$, create old
OPEN #2: name inefile$, create old
OPEN #3: name inffile$, create old
when error in
unsave outfile$
```

```
use
end when
when error in
unsave cloudfile$
use
end when
OPEN #4: name outfile$, create new
OPEN #5: name cloudfile$, create new
!when error in
do while more #1
line input #1: line$
!print line$
CALL comint(" ",line$,d$(),dd())
if dd(1)>0 then
let n=n+1
print dd(1);",";dd(2);",";dd(3);",";dd(4)
print#4: "n"
print#4: dd(1);",";dd(2);",";dd(3);",";dd(4)
let nn(dd(1))=dd(1)
let nx(dd(1))=dd(2)
let ny(dd(1))=dd(3)
let nz(dd(1))=dd(4)
end if
loop

do while more #2
line input #2: line$
!print line$
CALL comint(" ",line$,d$(),dd())
if dd(1)>0 then
let e=e+1
!print dd(7);",";dd(8);",";dd(9);",";dd(10)
print#4: "mat"
print#4: dd(2)
print#4: "e"
print#4: dd(7);",";dd(8);",";dd(9);",";dd(10);",";dd(11);",";dd(12);",";dd(13);",";dd(14)
let n1(e)=dd(7)
let n2(e)=dd(8)
let n3(e)=dd(9)
let n4(e)=dd(10)
let n5(e)=dd(11)
let n6(e)=dd(12)
let n7(e)=dd(13)
let n8(e)=dd(14)

end if
loop

do while more #3
line input #3: line$
!print line$
CALL comint(" ",line$,d$(),dd())
if dd(1)>0 then
print#4: "f"
print#4: dd(1);",";dd(2);",";dd(3);",";dd(4)
```

```
!let nn(dd(1))=dd(1)
let fx(dd(1))=dd(2)
let fy(dd(1))=dd(3)
let fz(dd(1))=dd(4)
end if
loop

!let line$=ucase$(trim$(line$))
!let b$=line$
!  DO    ! loop which splits up input by $
!   LET pcs=pos(b$,"$")
!   IF pcs=0 then LET a$=b$
!   IF pcs>0 then LET a$=b$[1:pcs-1]
!   IF pcs>0 then LET b$=b$[pcs+1:80]
!   CALL comint(",",a$,d$(),dd())
!
!
!print line$
!let l=len(a$)
!if d$(1)="N"  then
!print "n"
!print a$[3:l]
!print#1: "n"
!print#1: a$[3:l]
!print#1: dd(2);",";dd(3);",";dd(4);",";dd(5)
!end if
!if d$(1)="F"then
!F, 1,FX, -.28809E+07 $F, 1,FY, .18805E-01 $F, 1,FZ, .25462E+06
!print#1: "fa  "
!if d$(3)="FX" then print#1: dd(2);",";dd(4);",0,0"
!if d$(3)="FY" then print#1: dd(2);",0,";dd(4);",0"
!if d$(3)="FZ" then print#1: dd(2);",0,0,";dd(4)
!end if
!if d$(1)="E"then
!print#1: "e"
!print#1: a$[3:l]&",0,0,0,0,0,0"
!print#1: dd(2);",";dd(3);",";dd(4);",";dd(5);",";dd(6);",";dd(7);",";dd(8);",";dd(9)
!print a$[3:l]&",0,0,0,0,0,0"
!end if
!
!if d$(1)="MAT" then
!print#1: "mat"
!print#1: dd(2)
!end if
!
!if d$(1)="REAL" then
!print#1: "real"
!print#1: dd(2)
!end if
!
!if d$(1)="TYPE" then
!print#1: "type"
!print#1: dd(2)
!end if
!if pcs=0 then exit do
```

```
for i=1 to e
call evol(i,n1(),n2(),n3(),n4(),n5(),n6(),n7(),n8(),nx(),ny(),nz(),vol)
let xave=(nx(n1(i))+nx(n2(i))+nx(n3(i))+nx(n4(i))+nx(n5(i))+nx(n6(i))+nx(n7(i))+nx(n8(i)))/8
let yave=(ny(n1(i))+ny(n2(i))+ny(n3(i))+ny(n4(i))+ny(n5(i))+ny(n6(i))+ny(n7(i))+ny(n8(i)))/8
let zave=(nz(n1(i))+nz(n2(i))+nz(n3(i))+nz(n4(i))+nz(n5(i))+nz(n6(i))+nz(n7(i))+nz(n8(i)))/8
let fxave=(fx(n1(i))+fx(n2(i))+fx(n3(i))+fx(n4(i))+fx(n5(i))+fx(n6(i))+fx(n7(i))+fx(n8(i)))/8/vol
let fyave=(fy(n1(i))+fy(n2(i))+fy(n3(i))+fy(n4(i))+fy(n5(i))+fy(n6(i))+fy(n7(i))+fy(n8(i)))/8/vol
let fzave=(fz(n1(i))+fz(n2(i))+fz(n3(i))+fz(n4(i))+fz(n5(i))+fz(n6(i))+fz(n7(i))+fz(n8(i)))/8/vol
print#5: -xave;",";yave;",";-zave;",";-fxave;",";fyave;",";-fzave        ! This was to rotate 180Deg
next i
!use
print#4:"exit"
print#4:"exit"
close #1
close #2
close #3
close #4
close #5
next iload


!print#1:"exit"
!close #1
!close #2
!end when
END

 SUB comint(del$,a$,d$(),dd())
  FOR q=1 TO 12
   LET D$(Q)=""
   LET dd(q)=0
  NEXT Q
  LET a$=ucase$(a$)
  IF del$=" " then
   DO
   LET lbs=len(a$)
   LET pob=pos(a$,"  ")
   IF pob>0 then LET a$=a$[1:pob]&a$[pob+2:lbs]
   LOOP while pob>0
   LET lbs=len(a$)
   IF a$[1:1]=" " then LET a$=a$[2:lbs]
  END IF
  LET i=0
  DO
   LET i=i+1
   IF pos(a$,del$)=0 then EXIT DO
   LET pc=pos(a$,del$)
   LET d$(i)=a$[1:pc-1]
   LET a$=a$[pc+1:100)
  LOOP
  LET d$(i)=a$
  Let t=i
  for i=1 to t
  let d$(i)=trim$(d$(i))
```

```
when error in
  let dd(i)=val(d$(i))
use
  let dd(i)=0
end when
  next i
  ! End of data parsing
 END SUB

sub evol(i,n1(),n2(),n3(),n4(),n5(),n6(),n7(),n8(),nx(),ny(),nz(),vol)
call tetvol(n2(i),n4(i),n5(i),n1(i),nx(),ny(),nz(),vol1)
call tetvol(n2(i),n5(i),n7(i),n6(i),nx(),ny(),nz(),vol2)
call tetvol(n4(i),n7(i),n5(i),n8(i),nx(),ny(),nz(),vol3)
call tetvol(n4(i),n2(i),n7(i),n3(i),nx(),ny(),nz(),vol4)
call tetvol(n5(i),n2(i),n7(i),n4(i),nx(),ny(),nz(),vol5)
let vol=vol1+vol2+vol3+vol4+vol5
end sub

sub tetvol(p1,p2,p3,p4,nx(),ny(),nz(),vol)
let ax=nx(p2)-nx(p1)
let ay=ny(p2)-ny(p1)
let az=nz(p2)-nz(p1)
let BQX=nx(p3)-nx(p1)
let bqy=ny(p3)-ny(p1)
let bqz=nz(p3)-nz(p1)
let cx=nx(p4)-nx(p1)
let cy=ny(p4)-ny(p1)
let cz=nz(p4)-nz(p1)

call cross(ax,ay,az,BQX,bqy,bqz,dx,dy,dz)
call mag(magd,dx,dy,dz)
call dotp(dx,dy,dz,cx,cy,cz,dp)
!let vol=abs(dp/6/magd)
let vol=abs(dp/6)
end sub

sub dotp(ax,ay,az,BQX,bqy,bqz,dp)
let dp=ax*BQX+ay*bqy+az*bqz
end sub

sub cross(ax,ay,az,BQX,bqy,bqz,cx,cy,cz)
let cx=ay*bqz-az*bqy
let cy=az*BQX-ax*bqz
let cz=ax*bqy-ay*BQX
end sub

sub mag(magv,ax,ay,az)
let magv=(ax^2+ay^2+az^2)^.5
end sub
```

Appendix D